



Swansea University
Prifysgol Abertawe



Swansea University E-Theses

Synthesis, complexation and electrochemistry of novel ferrocenyl chalcogenide ligands.

Jing, Su

How to cite:

Jing, Su (2006) *Synthesis, complexation and electrochemistry of novel ferrocenyl chalcogenide ligands..* thesis, Swansea University.

<http://cronfa.swan.ac.uk/Record/cronfa42493>

Use policy:

This item is brought to you by Swansea University. Any person downloading material is agreeing to abide by the terms of the repository licence: copies of full text items may be used or reproduced in any format or medium, without prior permission for personal research or study, educational or non-commercial purposes only. The copyright for any work remains with the original author unless otherwise specified. The full-text must not be sold in any format or medium without the formal permission of the copyright holder. Permission for multiple reproductions should be obtained from the original author.

Authors are personally responsible for adhering to copyright and publisher restrictions when uploading content to the repository.

Please link to the metadata record in the Swansea University repository, Cronfa (link given in the citation reference above.)

<http://www.swansea.ac.uk/library/researchsupport/ris-support/>

Synthesis, Complexation and
Electrochemistry of Novel
Ferrocenyl Chalcogenide Ligands

By

Su Jing

A Thesis Submitted for the Degree of Doctor of Philosophy

Department of Chemistry
Swansea University

2006

ProQuest Number: 10801723

All rights reserved

INFORMATION TO ALL USERS

The quality of this reproduction is dependent upon the quality of the copy submitted.

In the unlikely event that the author did not send a complete manuscript and there are missing pages, these will be noted. Also, if material had to be removed, a note will indicate the deletion.



ProQuest 10801723

Published by ProQuest LLC (2018). Copyright of the Dissertation is held by the Author.

All rights reserved.

This work is protected against unauthorized copying under Title 17, United States Code
Microform Edition © ProQuest LLC.

ProQuest LLC.
789 East Eisenhower Parkway
P.O. Box 1346
Ann Arbor, MI 48106 – 1346

DECLARATION

This work has not previously been accepted in substance for any degree and is not being concurrently submitted in candidature for any degree.

Signed..... (candidate)

Date 2006-09-18

STATEMENT 1

This thesis is the result of my own investigations, except where otherwise stated. Where correction services have been used, the extent and nature of the correction are clearly marked in a footnote(s).

Other sources are acknowledged by footnotes giving explicit references. A bibliography is appended.

Signed..... (candidate)

Date 2006-09-18

STATEMENT 2

I hereby give consent for my thesis, if accepted, to be available for photocopying and for interlibrary loan, and for the title and summary to be made available to outside organizations.

Signed..... (candidate)

Date 2006-09-18



Presentations and Publications

Aspects of the work reported in this thesis have been presented previously in the following formats:

Peer reviewed papers:

1. **Electrochemical and NMR Spectroscopic Studies of Selenium- and Tellurium-substituted Ferrocenes II: Diferrocenyl Chalcogenides, Fc_2E , Diferrocenyl Dichalcogenides, Fc_2E_2 , and Bis(ferrocenylchalcogeno)alkanes, $\text{FcE}(\text{CH}_2)_n\text{E}'\text{Fc}$ ($\text{E}, \text{E}' = \text{Se}: n = 1, 2, 3; \text{E}, \text{E}' = \text{Te}: n = 1, 3; \text{E} = \text{Se}, \text{E}' = \text{Te}: n = 3$; $\text{Fc} = [\text{Fe}(\eta^5\text{-C}_5\text{H}_5)(\eta^5\text{-C}_5\text{H}_4)]$), M. R. Burgess, S. Jing, C. P. Morley, *J. Organomet. Chem.*, 2006, **691**, 3484-3489.**
2. **Synthesis and Characterization of Palladium and Platinum Complexes of 1,3-Bis(ferrocenylchalcogeno)propanes: X-ray Crystal Structures of $\text{FcSe}(\text{CH}_2)_3\text{SeFc}$ and $[\text{M}\{\text{FcE}(\text{CH}_2)_3\text{E}'\text{Fc}\}_2](\text{PF}_6)_2$ ($\text{M} = \text{Pd}, \text{Pt}; \text{E}, \text{E}' = \text{Se}, \text{Te}; \text{Fc} = [\text{Fe}(\eta^5\text{-C}_5\text{H}_5)(\eta^5\text{-C}_5\text{H}_4)]$), S. Jing, C. P. Morley, C. A. Webster, M. Di Vaira, *Dalton Trans.*, 2006, 4335-4332.**
3. **Reactions of Diferrocenyl Dichalcogenides with $[\text{W}(\text{CO})_5(\text{THF})]$: X-ray Crystal Structures of Fc_2Te_2 and $[\text{W}_2(\mu\text{-SeFc})_2(\text{CO})_8]$ ($\text{Fc} = [\text{Fe}(\eta^5\text{-C}_5\text{H}_5)(\eta^5\text{-C}_5\text{H}_4)]$), M. R. Burgess, S. Jing, C. P. Morley, C. Thöne, *J. Organomet. Chem.*, published online 24 August 2006.**

Oral Presentation:

1. **Bis(ferrocenylchalcogeno)propanes: A Synthetic, Coordination and Electrochemical Study**, S. Jing, C. P. Morley, 11th Asian Chemical Congress, 24-26 August 2005, Korea.

Poster Presentations:

1. **Synthesis, Complexation and Electrochemistry Study of Bis(ferrocenylchalcogeno)alkanes**, S. Jing, C. P. Morley, M. Di Vaira, RSC Coordination Chemistry Discussion Group Meeting, 11-12 July 2005, United Kingdom.

2. **A New Kind of Electrochemical Sensor Based on Bis(ferrocenylchalcogeno)propanes**, S. Jing, C. P. Morley, M. Di Vaira, Dalton Discussion 9: Functional Molecular Assemblies, 19-21 April 2006, United Kingdom.

Acknowledgements

I would like to express my deepest thanks to my supervisor, Dr. Chris Morley, for his instructive guidance, patience, encouragement and endless support during my research and time here. I would also like to thank him for his constant help towards improving my English.

I would like to give my gratitude to Professor Massimo Di Vaira of the University of Florence for his work on the X-ray crystal structures that appear in this thesis. My thanks also go to Chris Webster for his help in the lab, especially in the first year when he provided me with much help and advice towards getting started. I would also like to thank him for solving several crystal structures during his stay in Italy.

I would like to extend my gratitude to the staff of the EPSRC Mass Spectrometry Centre, Swansea, for their time and effort in producing mass spectrometric data, I made them quite busy. Thanks also, to the assistance provided by the technicians, especially Ian for his work on the NMR spectrometry. Thanks must also be given to Dr. Suzi Kean for her support on the NMR spectrometry.

I would like to thank all the academic, secretarial staff in the chemistry department, for all the help and advice they have given me during these three years.

I would like to acknowledge Swansea University and the China Scholarship Council for financial support. I also wish to thank Johnson Matthey plc for their generous loan of palladium and platinum salts.

Sincere thanks are also extended to all my kindly friends in the department, who have made it a happy place to work, particularly Rachel, Karen, Vicky, Stephen, Lee and Jeremy.

Many thanks also go to my friends, who helped me adjust to life in UK, particularly Shuying Cheng, Yan Hu, Bowen Wang, Shujing Ding, Xiaojing Mu, Min Yang, Xiaolin Cui, Xin Ma and Wei Li.

Finally and most importantly, I would like to express my infinite thanks to my parents for taking care of my son and providing emotional support during my studies. Huge thanks go to my husband and son, Jingsong Ding and Jing Ding, for their unconditional support, understanding and encouragement, which is so important to me.

Summary

The aim of this work was the synthesis of novel ferrocenyl chalcogenide ligands and their late transition metal complexes, and the study of relevant electrochemistry to provide information for exploring their potential application in a new type of electrochemical sensor.

The introduction reviews four sections of the literature. Group 6 metal carbonyl and palladium, platinum complexes of neutral chalcogenoether ligands are briefly introduced. The electrochemistry of linked ferrocenes is explored. Finally, the use of ferrocene in the design of electrochemical sensors is described.

Subsequent chapters describe the synthesis and characterisation of novel ferrocenyl chalcogenide compounds, which can be divided into three categories: (1) Four series of ferrocenyl chalcogenide compounds with flexible saturated hydrocarbon chains: bidentate, linear tridentate, tripodal or tetradentate ligands; (2) Two macrocyclic ferrocenyl selenide compounds with four Se donor atoms; (3) Three ferrocenyl chalcogenide compounds with a rigid chain. Four compounds' structures have been determined by X-ray crystallography: $\text{FcSe}(\text{CH}_2)_3\text{SeFc}$, $\text{FcSe}(\text{CH}_2)_3\text{Se}(\text{CH}_2)_3\text{SeFc}$, difeSe_4 and $\text{FcSeCH}_2\text{C}_6\text{H}_4\text{CH}_2\text{SeFc}$.

The coordination chemistry of ferrocenyl chalcogenide compounds was then systematically studied. New compounds include: (1) Palladium and platinum complexes of the ligands with flexible saturated hydrocarbon chains; (2) Group 6 metal carbonyl complexes of bis(ferrocenylchalcogeno)propanes; (3) Palladium and platinum complexes of the macrocyclic ligands; (4) The platinum complex of $\text{FcSeCH}_2\text{C}_6\text{H}_4\text{CH}_2\text{SeFc}$. Techniques used to characterize these compounds include: multinuclear NMR spectroscopy; mass spectrometry; UV-vis and IR spectroscopy. Eighteen complexes' structures have been determined by X-ray crystallography: $[\text{M}\{\text{FcE}(\text{CH}_2)_3\text{E}'\text{Fc}\}_2](\text{PF}_6)_2$ ($\text{M} = \text{Pd}$ or Pt ; $\text{E}, \text{E}' = \text{Se}$ or Te), $[\text{MCl}_2(\text{FcSeCH}_2\text{SeFc})_2]$ ($\text{M} = \text{Pd}$ or Pt), $[\text{MCl}_2(\text{FcTeCH}_2\text{TeFc})]$ ($\text{M} = \text{Pd}$ or Pt), $[\text{PdCl}_2(\text{FcSeCH}_2\text{CH}_2\text{SeFc})]$, $[\text{PtCl}\{\text{FcSe}(\text{CH}_2)_3\text{Se}(\text{CH}_2)_3\text{SeFc}\}]\text{PF}_6$, $[\text{Cr}(\text{CO})_4\{\text{FcTe}(\text{CH}_2)_3\text{TeFc}\}]$, $[\text{Mo}(\text{CO})_4\{\text{FcE}(\text{CH}_2)_3\text{E}'\text{Fc}\}]$ ($\text{E}, \text{E}' = \text{Se}$ or Te), $[\text{W}(\text{CO})_4\{\text{FcTe}(\text{CH}_2)_3\text{TeFc}\}]$, and the supramolecular complex $[\text{Pt}_2\text{Cl}_2\{\text{FcSeCH}_2\text{C}_6\text{H}_4\text{CH}_2\text{SeFc}\}_3](\text{PF}_6)_2$ with an unusual dinuclear triple helical geometry.

The electrochemistry study of the above compounds by cyclic voltammetry and differential pulse voltammetry proved that the communication between ferrocene units occurs via a through bond mechanism, and it is tentatively concluded that the interaction between ferrocene units can only happen when they occupy inequivalent positions.

List of Abbreviations

ⁿ Bu	<i>n</i> -butyl
ⁱ Bu	<i>iso</i> -butyl (2-methylpropyl)
^t Bu	<i>tert</i> -butyl (1,1-dimethylethyl)
Cp	η ⁵ -cyclopentadienyl
Cp*	η ⁵ -pentamethylcyclopentadienyl
CT	charge transfer
CV	cyclic voltammetry
difcSe ₄	1,5,16,21-tetraselena[5.5]ferrocenophane
difcSe ₄ -p-Xylene	1,10,22,31-tetraselena[2]-p-cyclo[2](1,1')ferroceno- -[2]paracyclo[2](1,1')ferrocenophane
DPV	differential pulse voltammetry
EI/CI MS	electron impact/chemical ionisation mass spectrometry
ES MS	electrospray mass spectrometry
Et	ethyl
FAB MS	fast atom bombardment mass spectrometry
MALDI	matrix-assisted laser desorption/ionization
fc	1,1'-ferrocenediyl
Fc	ferrocenyl
FcH ⁺	ferrocenium
fc[Se(CH ₂) ₃ Br] ₂	1,1'-bis(3-bromopropylseleno)ferrocene
fcSe ₄	1,5,9,12-tetraselena[12]ferrocenophane
Fv	fulvalene
Hex	hexyl
HOMO	highest occupied molecular orbital
IR	infrared
LUMO	lowest unoccupied molecular orbital
L	ligand
Me	methyl
nbd	norbornadiene
NMR	nuclear magnetic resonance
Oct	octyl
Pent	pentyl

Ph	phenyl
Pr	propyl
THF	tetrahydrofuran
TMEDA	N, N, N', N' -tetramethylethylenediamine
TMPDA	N, N, N', N' -tetramethylpropylenediamine
UV-vis	ultraviolet-visible

Contents

Chapter One Introduction	1
1.1 Background	2
1.2 Cr, Mo, W carbonyl complexes with neutral chalcogenoether ligands	4
1.2.1 Monodentate ligands	4
1.2.2 Bidentate ligands	7
1.3 Pd and Pt complexes with neutral chalcogenoether ligands	10
1.3.1 Monodentate ligands	10
1.3.2 Bidentate ligands	12
1.3.3 Polydentate ligands	18
1.3.4 X-Ray structure data	21
1.4 Electrochemistry of linked ferrocenes	23
1.4.1 Fulvalene complexes	24
1.4.2 Ferrocenes linked by carbon bridges	25
1.4.3 Ferrocenes linked through heteroatoms	30
1.5 Ferrocene in the design of electrochemical sensors	36
1.5.1 s-Block cations	36
1.5.2 Anions	38
1.5.3 Transition metal cations	41
1.6 References for Chapter One	46
Chapter Two Synthesis of Novel Ferrocenyl Chalcogenide Compounds	56
2.1 Background to synthesis and characterisation of ferrocenylchalcogenide compounds	
2.1.1 Chalcogenaferrocenophanes	57
2.1.1.1 Chalcogena[1]ferrocenophanes	57
2.1.1.2 Chalcogena[3]ferrocenophanes	59
2.1.2 Compounds with ferrocenyl chalcogenide or 1,1'-ferrocenylene dichalcogenide groups	66
2.1.2.1 Compounds with ferrocenyl chalcogenide groups	66
2.1.2.2 Compounds with 1, 1'-ferrocenylene dichalcogenide groups	

	68
2.1.2.3 Chalcogeno-esters	70
2.1.2.4 Ferrocenylamine selenide compounds	71
2.1.3 Diferrocenyl dichalcogenides and their derivatives	73
2.1.3.1 Diferrocenyl dichalcogenides	73
2.1.3.2 Bis[2-(dimethylaminomethyl)ferrocenyl] dichalcogenides	75
2.1.3.3 Chiral diferrocenyl dichalcogenides	75
2.1.4 Chalcogen-bridged ferrocene oligomers and polymers	77
2.1.4.1 Trinuclear and tetranuclear chalcogen-bridged ferrocenes	77
2.1.4.2 Poly(ferrocenyl selenide)	77
2.2 Synthesis and characterization of new ferrocenyl chalcogenide compounds	78
2.2.1 Ferrocenyl chalcogenide compounds with a flexible hydrocarbon chains	
2.2.1.1 Synthesis	78
2.2.1.2 Crystal structures	85
2.2.1.3 ^1H and ^{13}C NMR spectroscopy	93
2.2.1.4 ^{77}Se and ^{125}Te NMR spectroscopy	96
2.2.1.5 Electronic absorption spectroscopy	100
2.2.2 Macrocyclic ferrocenyl selenide ligands	103
2.2.2.1 Synthesis	104
2.2.2.2 Crystal structure of difeSe_4	108
2.2.3 Ferrocenyl chalcogenide compounds with a rigid chain	112
2.3 References for Chapter Two	118
Chapter Three Coordination Chemistry of Ferrocenyl Chalcogenides	124
3.1 Background to coordination chemistry of ferrocenyl chalcogenides	125
3.1.1 Monodentate ferrocenyl chalcogenide complexes	125
3.1.2 Complexes of bidentate ferrocenyl chalcogenide ligands	125
3.1.3 Tetradentate ligands	133
3.2 Pd and Pt complexes of ferrocenyl chalcogenide compounds with a flexible hydrocarbon chain	135
3.2.1 Pd and Pt complexes of $\text{FcE}(\text{CH}_2)_3\text{E}'\text{Fc}$ (E, E' = Se, Te)	135
3.2.1.1 Synthesis	135
3.2.1.2 Structure	136

3.2.1.3 Electronic spectra	152
3.2.2 Pd and Pt complexes of $\text{FcE}(\text{CH}_2)_n\text{EFc}$ ($n = 1, E = \text{Se or Te}; n = 2, E = \text{Se}$)	154
3.2.2.1 Synthesis	154
3.2.2.2 Structures	154
3.2.3 Pd and Pt complexes of $\text{FcE}(\text{CH}_2)_3\text{E}'(\text{CH}_2)_3\text{EFc}$ ($E, E' = \text{Se or Te}$)	170
3.2.3.1 Synthesis	170
3.2.3.2 Structure of $[\text{PtCl}\{\text{FcSe}(\text{CH}_2)_3\text{Se}(\text{CH}_2)_3\text{SeFc}\}](\text{PF}_6)$	172
3.2.4 Pd and Pt complexes of $\text{FcE}(\text{CH}_2)_3\text{Se}(\text{CH}_2)_3\text{Se}(\text{CH}_2)_3\text{EFc}$ ($E = \text{Se or Te}$)	176
3.3 Group 6 carbonyl complexes of $\text{FcE}(\text{CH}_2)_3\text{E}'\text{Fc}$ ($E, E' = \text{Se, Te}$)	177
3.3.1 Synthesis and NMR spectra	177
3.3.2 Structures of $[\text{M}(\text{CO})_4\{\text{FcE}(\text{CH}_2)_3\text{E}'\text{Fc}\}]$ ($\text{M} = \text{Cr}, E = E' = \text{Te}; \text{M} = \text{Mo}, E, E' = \text{Se or Te}; \text{M} = \text{W}, E = E' = \text{Te}$)	180
3.3.3 Comparison of ligand properties	193
3.4 Pd and Pt complexes of macrocyclic ferrocenyl chalcogenide ligands	197
3.5 Pt complex of $\text{FcSeCH}_2\text{C}_6\text{H}_4\text{CH}_2\text{SeFc}$	200
3.6 References for Chapter Three	206

Chapter Four Electrochemistry Study of Novel Ferrocenyl Chalcogenide Compounds and Metal Complexes 211

4.1 Background	212
4.1.1 Electrochemistry of chalcogenaferrocenophanes	212
4.1.2 Electrochemistry of ferrocenyl alkyl chalcogenides	214
4.1.3 Electrochemistry of poly-ferrocenes linked by selenium and tellenium bridges	215
4.1.4 Electrochemistry of transition metal complexes	217
4.2 Electrochemistry of novel ferrocenyl chalcogenide compounds	218
4.2.1 $\text{FcE}(\text{CH}_2)_n\text{E}'\text{Fc}$ ($E, E' = \text{Se or Te}; n = 0, 1, 2, 3$)	218
4.2.2 Other ferrocenyl chalcogenide ligands	227
4.2.2.1 $\text{FcE}(\text{CH}_2)_3\text{E}'(\text{CH}_2)_3\text{EFc}$	227
4.2.2.2 $\text{FcECH}_2\text{C}_6\text{H}_4\text{CH}_2\text{EFc}$ ($E = \text{Se or Te}$)	228
4.2.2.3 fcSe_4 and difcSe_4	228

4.3 Electrochemistry of transition metal complexes	229
4.3.1 $[M\{FcE(CH_2)_3E'Fc\}_2](PF_6)_2$ (M = Pd or Pt, E, E' = Se or Te)	229
4.3.2 $[MCl\{FcE(CH_2)_3E'(CH_2)_3EFc\}]PF_6$ (M = Pd or Pt, E, E' = Se or Te)	234
4.3.3 $[M\{FcE(CH_2)_3Se(CH_2)_3Se(CH_2)_3EFc\}](PF_6)_2$ (M = Pd or Pt, E = Se or Te)	240
4.3.4 $[M(fcSe_4)](PF_6)_2$ and $[M(difcSe_4)](PF_6)_2$ (M = Pd or Pt)	242
4.3.5 $[Pt_2Cl_2\{FcSeCH_2C_6H_4CH_2SeFc\}_3](PF_6)_2$	244
4.3.6 $[M(CO)_4\{FcE(CH_2)_3E'Fc\}]$ (M = Cr, E = E' = Te; M = Mo, E, E' = Se or Te; M = W, E = E' = Te)	245
4.4 References for Chapter Four	247
Chapter Five Rhodium Complexes of Novel Ferrocenyl Chalcogenide Ligands	249
5.1 Background	250
5.1.1 Monodentate ligands	250
5.1.2 Bidentate ligands	251
5.1.3 Polydentate ligands	251
5.2 Rh(III) complexes of $FcE(CH_2)_3E'Fc$ (E, E' = Se or Te)	254
5.2.1 Synthesis	254
5.2.2 Electronic spectra	254
5.2.3 Electrochemistry	256
5.3 Other rhodium(III) complexes	260
5.4 References for Chapter Five	261
Chapter Six Miscellaneous Reactions	262
6.1 Attempted reactions	263
6.2 References for Chapter Six	267
Chapter Seven Experimental	268
7.1 General	269
7.2 Preparation of starting materials	270
7.2.1 Fc_2E_2 (E = Se or Te)	270

7.2.2 Fc ₂ E (E = Se or Te)	271
7.2.3 fcSe ₃	272
7.2.4 MeC(CH ₂ Br) ₃	273
7.2.5 NCS _e CH ₂ CH ₂ CH ₂ SeCN	273
7.2.6 Other starting materials	274
7.3 Synthesis of new ferrocenyl chalcogenide ligands	275
7.3.1 FcE(CH ₂) _n E'Fc (n = 1, E = E' = Se or Te; n = 2, E = E' = Se; n = 3, E & E' = Se or Te), FcE(CH ₂) ₃ X (E = Se, X = Br or I; E = Te, X = Br)	275
7.3.2 FcE(CH ₂) ₃ E'(CH ₂) ₃ EFc (E, E' = Se or Te)	281
7.3.3 CH ₃ C(CH ₂ EFc) ₃ (E = Se or Te)	283
7.3.4 FcE(CH ₂) ₃ Se(CH ₂) ₃ Se(CH ₂) ₃ EFc (E = Se or Te)	284
7.3.5 fc[Se(CH ₂) ₃ Br] ₂	285
7.3.6 difcSe ₄	286
7.3.7 fcSe ₄	286
7.3.8 FcECH ₂ C ₆ H ₄ CH ₂ EFc (E = Se or Te)	289
7.3.9 difcSe ₄ -p-Xylene	290
7.4 Synthesis of transition metal complexes with ferrocenyl chalcogenide ligands	292
7.4.1 [M{FcE(CH ₂) ₃ E'Fc} ₂](PF ₆) ₂ (M = Pd or Pt; E, E' = Se or Te)	292
7.4.2 [MCl ₂ {FcE(CH ₂) _n EFc}] (M = Pd or Pt, n = 1, E = Se or Te; M = Pt, n = 2, E = Se)	293
7.4.3 [M(CO) ₄ {FcE(CH ₂) ₃ E'Fc}] (M = Cr or W, E = E' = Te; M = Mo, E, E' = Se or Te)	294
7.4.4 [MCl{FcE(CH ₂) ₃ E'(CH ₂) ₃ EFc}](PF ₆) (M = Pd or Pt; E & E' = Se or Te)	296
7.4.5 [M{FcE(CH ₂) ₃ Se(CH ₂) ₃ Se(CH ₂) ₃ EFc}](PF ₆) ₂ (M = Pd or Pt; E = Se or Te)	300
7.4.6 [Pt ₂ Cl ₂ (FcSeCH ₂ C ₆ H ₄ CH ₂ SeFc) ₃](PF ₆) ₂	301
7.4.7 [M(difcSe ₄)](PF ₆) ₂ (M = Pd or Pt)	301
7.4.8 [M(fcSe ₄)](PF ₆) ₂ (M = Pd or Pt)	302
7.5 Rhodium complexes	306
7.6 Other attempted reactions	308
7.7 References for Chapter Seven	311

CHAPTER ONE

Introduction

1.1 Background

Selenium and tellurium are the two heavier members of Group 16. Like their congeners oxygen and sulfur, they have two p electrons less than the next following noble gases. Selenium and tellurium are comparatively rare elements, comprising only 0.05 ppm for Se and 0.002 ppm for Te of the earth's crust.¹

Selenium was isolated in 1817 by Swedish chemists J. J. Berzelius and J. G. Gahn, and named from the Greek *selene*, the moon. Selenium has six isotopes from mass 74 to 82. The most abundant isotope is ⁸⁰Se (49.6%), which means that fragments containing selenium generated in mass spectrometry form broad clusters. All these isotopes have zero nuclear spin except ⁷⁷Se (I = ½, 7.6% abundance).

Tellurium was discovered in 1782 by the Austrian chemist F. J. Müller von Reichenstein. Tellurium means earth in Latin (*tellus*). Of the eight naturally occurring stable isotopes, ¹³⁰Te (33.8%) and ¹²⁸Te (31.7%) are the most abundant, and only ¹²³Te (0.91%) and ¹²⁵Te (7.14%) are NMR active.

Organoselenium and -tellurium compounds have been known from the early nineteenth century, but they were largely ignored for most of the succeeding time, probably due to the commercial non-availability of a wide variety of them and the misconception that they are all air-sensitive, foul-smelling and toxic. The situation was changed dramatically after the discovery of the selenoxide *syn*-elimination reaction route to alkenes.² Since then, many publications devoted to these compounds have appeared in the literature. There has been more and more interest in both the synthesis of new classes of organochalcogen compounds and finding new synthetic applications of existing organochalcogen compounds. There have been several reviews published on this subject. In the 1980s two reviews about chalcogenides in transition metal complexes were published.^{3, 4} Then the ligand chemistry of polydentate organoselenium and -tellurium ligands was reviewed in 1992.⁵ That of selenoether and telluroether ligands was reviewed by Levason and co-workers in 1993 and 2000.^{6, 7} The ligand chemistry of the polytelluride ion was reviewed in 1994 covering the literature up to early 1993.⁸ Metal carbonyls containing bridging tellurium ligands have also been reviewed.⁹ At the end of the 20th century, a full review of the ligand chemistry of tellurium during the last decade was published by Singh and Sharma.¹⁰ The synthetic methods for introducing Group 16 elements into organic molecules were summarized by Ogawa.¹¹ Recently there have been some

reviews concerning specific organochalcogen ligands: Silvestru and Drake focused on $(XPR_2)(YPR'_2)NH$ acids ($X, Y = O, S, Se$; $R, R' = \text{alkyl, aryl, alkoxy}$) and their main group metal derivatives;¹² Kawashima reviewed the synthesis of four-membered heterocyclic compounds containing tetracoordinate selenium or tetracoordinate tellurium.¹³

As part of a wide-ranging study of organoselenium and -tellurium compounds, ferrocenylselenides and -tellurides have attracted more and more interest. Following the discovery of ferrocene in the 1950s,^{14,15} it was found to be unusually stable, and its structure and bonding defied conventional bonding descriptions. The sandwich structure of ferrocene was first predicted from its IR and NMR spectra and then confirmed by X-ray crystallography in 1954. The fascinating structural properties of ferrocene and its derivatives have been the subject of increasing attention in all fields of organometallic chemistry.¹⁶ One of the most interesting features of ferrocene-based ligands in coordination chemistry is their flexibility, possibly due to the organometallic "ball-joint". The skeletal flexibility of these metalligands confers the ability to stabilize complexes having varied metal geometry and a variety of coordinative bonding. They have been used as homogeneous catalysts for various processes,¹⁶ molecular sensors,¹⁷ molecular magnetic¹⁸ and non-linear optical materials.¹⁹ More and more papers concerning ferrocenylselenide and -telluride ligands have been published from the 1990s onward.

Before the detailed elaboration of my work, the literature work relating to chalcogenoether ligands will be considered. This has been divided as follows: firstly, Cr, Mo, W carbonyl complexes with neutral chalcogenoether ligands; secondly, Pd and Pt complexes with neutral chalcogenoether ligands. Discussion of chalcogen-based ligands which contain ferrocenyl groups will be deferred until Chapter Three. The third section summarizes the electrical communication between bridged ferrocenyl groups. In the last section, there is a brief introduction to the use of ferrocene derivatives in the design of electrochemical sensors.

1.2 Cr, Mo, W carbonyl complexes with neutral chalcogenoether ligands

Most seleno- or telluroether complexes of Group 6 metal carbonyls are M(0) complexes. It appears that polydentate ligands do not form stable complexes of this type, so the introduction below covers first monodentate ligands, then bidentate ligands.


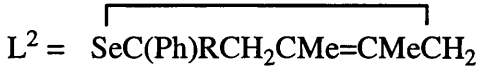
1.2.1 Monodentate ligands

The metal carbonyl complexes of monodentate ligands may be generally formulated as $[M(CO)_5L]$ (M = Cr, Mo, W), and are summarized in Table 1.1.

Table 1.1 Literature work concerning $[M(CO)_5L]$ complexes (M = Cr, Mo, W)

M	L	Bond length (Å)	Ref.
Cr	TeEt ₂		20
Cr, Mo, W	SeEt ₂		21
W	Se (CH ₂ SiMe ₃) ₂		22
Cr, Mo, W	Me ₃ SiCH ₂ SeSeCH ₂ SiMe ₃		22
Cr, Mo, W	MeSeCH ₂ SeMe, MeSCH ₂ SeMe		23-25
W	Te[η ¹ -(Me ₃ Si) ₃ C ₅ H ₂] ₂	W-Te = 2.8385(6)	26
W	Se(C ₅ Me ₅)Me		27
Mo	L ¹	Mo-Te = 2.814(1), 2.820(2)	28
W	TePh ₂	W-Te = 2.809(1)	29
W	L ²	W-Se = 2.674(1)	30
Cr, Mo, W	E(<i>p</i> -C ₆ H ₄ OCH ₃) ₂ (E = Se, Te)	Cr-Te = 2.684 (1)	31, 32
Cr	Te (<i>o</i> -C ₆ H ₄ CH ₂ NMe ₂) ₂	Cr-Te = 2.6665 (9)	33

Note:

L¹ =  L² = 

The synthetic routes can be divided into four types.

The first is a substitution reaction, which starts from the thermally labile THF complex $[\text{M}(\text{CO})_5(\text{THF})]$; THF can then be replaced by chalcogenoether ligands under mild conditions (Fig. 1.1).

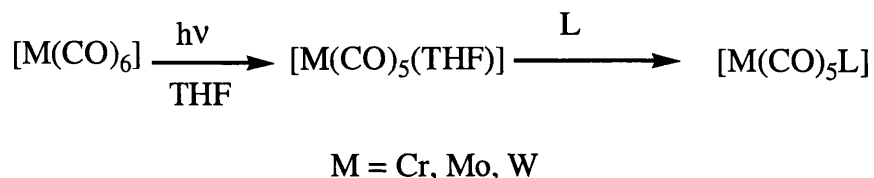


Fig. 1.1 Synthetic route starting from $[\text{M}(\text{CO})_5(\text{THF})]$

The second route involves electrophilic alkylation of a coordinated chalcogen (example shown in Fig. 1.2).^{20, 21}

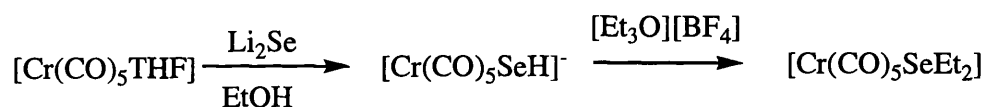


Fig. 1.2 Synthetic route involving alkylation of coordinated chalcogen

The third is the reaction of the pentacarbonyl(selenoketone) complex $[\text{W}(\text{CO})_5\{\text{Se}=\text{C}(\text{Ph})\text{R}\}]$ ($\text{R} = \text{H, Ph}$) with 2,3-dimethyl-1,3-butadiene by [4 + 2]-cycloaddition to give a metal-coordinated selenacycle (Fig. 1.3).³⁰

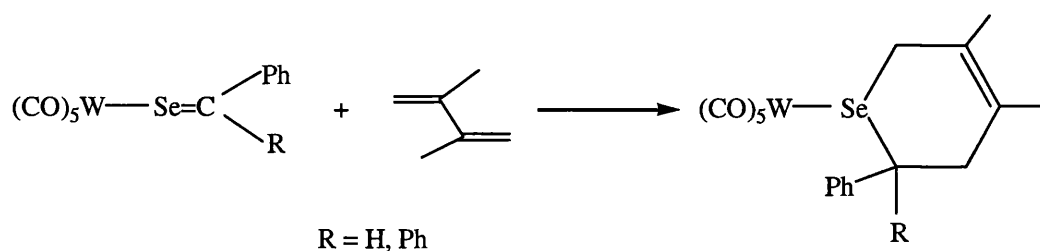
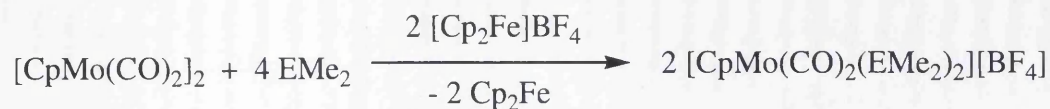


Fig. 1.3 Synthetic route by [4 + 2]-cycloaddition

The fourth route uses the ferrocenium cation $[\text{Cp}_2\text{Fe}]^+$ as a one-electron oxidizing agent to break the metal-metal bond in a dinuclear organometallic complex, which then reacts to form the corresponding cationic compound.^{34, 35}



E = Se, Te

Fig. 1.4 Synthetic route using ferrocenium cation $[\text{Cp}_2\text{Fe}]^+$

The known crystal structures of $[\text{M}(\text{CO})_5\text{L}]$ complexes are quite similar; an example²⁶ is shown in Fig. 1.5. The coordination geometry at M is only slightly distorted from regular octahedral. The relative shortening of the M-CO(*trans*) bond compared to the mean of the M-CO(*cis*) bonds indicates good donor properties of the chalcogen atom.

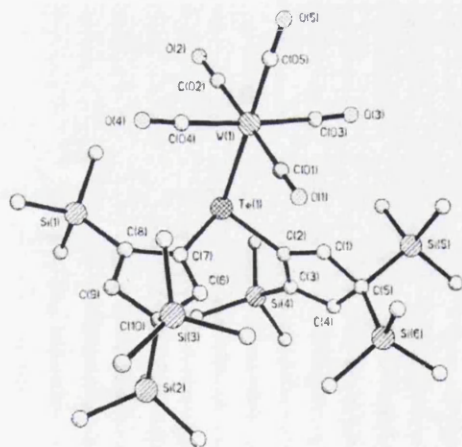


Fig. 1.5 Structure of $[\text{W}(\text{CO})_5\{\text{Te}(\eta^1\text{-(Me}_3\text{Si)}_3\text{C}_5\text{H}_2)_2\}]$

Although most reactions with REER involve the cleavage of the E-E bond with the formation of terminal or bridging ER^- ligands, in the complex $[\text{M}(\text{CO})_5(\text{Me}_3\text{SiCH}_2\text{SeSeCH}_2\text{SiMe}_3)]$ (M = Cr, Mo, W),²² there is the coordination of an intact RSeSeR ligand. ^1H NMR spectroscopy shows that at higher temperature, there is a 1, 2-metal shift between the two chalcogen atoms of the diselenide.

Some bidentate ligands, such as $\text{MeSeCH}_2\text{SeMe}$, $\text{MeSCH}_2\text{SeMe}$, can only coordinate

via one donor atom due to the small bite angle for chelation.²³⁻²⁵

Reaction of 1,3-dihydrobenzo[*c*]tellurophene and $[\text{Mo}(\text{CO})_4(\text{nbd})]$ yielded a disubstituted molybdenum(0) carbonyl species $[\text{Mo}(\text{CO})_4\text{L}_2]$ with C_{2v} geometry. The crystal structure confirms that the telluroethers occupy mutually *cis* positions in the distorted octahedral molecule, with Mo–Te(1) 2.814(1) Å, Mo–Te(2) 2.820(2) Å; the Mo–CO distances *trans* to the telluroether ligands are shorter than the *cis* ones.²⁸ A similar complex $[\text{Cr}(\text{CO})_4(\text{SeEt}_2)]$ has also been obtained.²¹

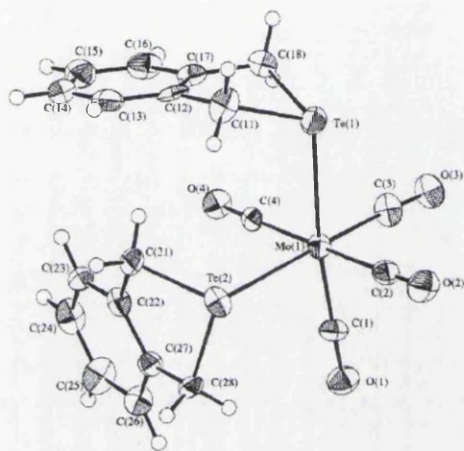


Fig.1.6 The structure of $[\text{Mo}(\text{CO})_4(\text{Te} \begin{array}{c} \diagup \\ \diagdown \end{array} \text{C}_6\text{H}_4)_2]$

The reaction between $[\text{Cr}(\text{CO})_5\text{THF}]$ and L (L = Me_2Se , Et_2Se) may yield $[\text{Cr}(\text{CO})_5]_2\text{L}$, in which the ligand bridges two metal centres.³⁶

1.2.2 Bidentate ligands

The syntheses of the complexes $[\text{M}(\text{CO})_4(\text{L-L})]$ are straightforward, by reaction of the bidentate ligand with $[\text{M}(\text{CO})_4(\text{nbd})]$ (M = Cr, Mo), $[\text{M}(\text{CO})_4(\text{piperidine})_2]$ (M = Mo, W) or $[\text{W}(\text{CO})_4(\text{TMPDA})]$ in a suitable solvent. Literature work is summarized in Table 1.2.

Table 1.2 Literature work concerning $[M(CO)_4(L-L)]$ complexes ($M = Cr, Mo, W$)

M	L	M-E bond length (Å)	Ref.
Cr	MeSeCH ₂ CH ₂ SeMe		37
Cr, Mo, W	¹ PrSeCH ₂ CH ₂ Se ¹ Pr		38, 39
Cr, Mo, W	MeSeCH ₂ CMe ₂ CH ₂ SeMe		40
Cr, Mo, W	MeSe(CH ₂) ₃ SeMe	Cr-Se = 2.517(1), 2.520(2)	41
	MeSe(CH ₂) ₂ SeMe		
	MeTe(CH ₂) ₃ TeMe		
	<i>o</i> -C ₆ H ₄ (EMe) ₂ (E = Se, Te)		
	PhTe(CH ₂) ₃ TePh		
Mo, W	<i>o</i> -C ₆ H ₄ (CH ₂ TeMe) ₂	W-Te = 2.7907(8), 2.792(8)	42
Mo	η^2 -MeC(CH ₂ SeMe) ₃		43
Cr, Mo, W	[8]aneSe ₂	W-Se = 2.650(1)	44

These complexes are *cis*-tetracarbonyls $[M(CO)_4(L-L)]$. An example crystal structure is shown in Fig. 1.7. The structure of $[Cr(CO)_4\{MeSe(CH_2)_3SeMe\}]$ ⁴¹ reveals that in the solid state the ligand adopts the *DL* conformation, Cr-Se = 2.517(1), 2.520(2) Å, and Cr-C_{*cis*} bond lengths are longer than those of Cr-C_{*trans*} due to back-donation.

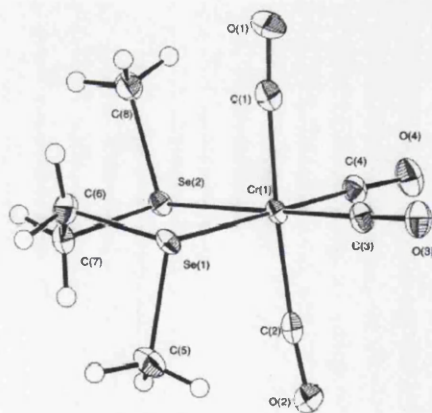


Fig. 1.7 Crystal structure of $[Cr(CO)_4\{MeSe(CH_2)_3SeMe\}]$

The tripodal ligand MeC(CH₂EMe)₃ (E = Se, Te) behaves as a bidentate ligand in *cis*- $[Mo(CO)_4\{\eta^2\text{-MeC(CH}_2\text{EMe)}_3\}]$.⁴³

Although neutral chalcogen ligands are usually found in combination with low valent metal carbonyl complexes, an unusual Mo(V) complex, *fac*-[MoOCl₃{MeSe(CH₂)₃SeMe}], was reported in 1982. MeSe(CH₂)₃SeMe yields this six-coordinate complex on reaction with MoOCl₃ or [MoOCl₃(THF)] (Fig. 1.8).⁴⁵

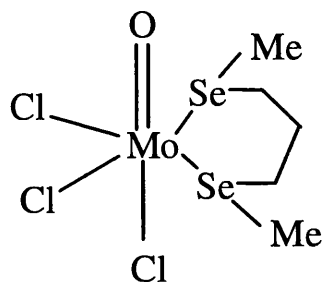


Fig. 1.8 Structure of *fac*-[MoOCl₃{MeSe(CH₂)₃SeMe}]

1.3 Pd and Pt complexes with neutral chalcogenoether ligands

This is an extensively studied field, and a lot of work has been reported. It will be covered in the order monodentate, bidentate and polydentate ligands. A summary of M-E bond lengths from crystal structures is also included.

1.3.1 Monodentate ligands

Since the synthesis of ER_2 (R = alkyl or aryl), many complexes $[MX_2L_2]$ (M = Pd or Pt; X = Cl, Br, I or SCN; L = monodentate chalcogen ligand) have been reported.⁴⁶

There are two synthetic routes: from $[MX_4]^{2-}$ or $[MX_2L_2]$ (L = PhCN or MeCN) with the ligand in a 1:2 ratio. The relevant literature is summarized in Table 1.3.

Many $[MX_2(ER_2)_2]$ complexes exist in the *trans* form in the solid, as confirmed by their crystal structures (example shown in Fig.1.9). Only $[PtX_2(SeR_2)_2]^{46}$ and $[PtCl_2L_2]$ (L = $\overline{Te(CH_2)_4}$)⁵⁵ exist as a mixture of *cis* and *trans* isomers in the solid.

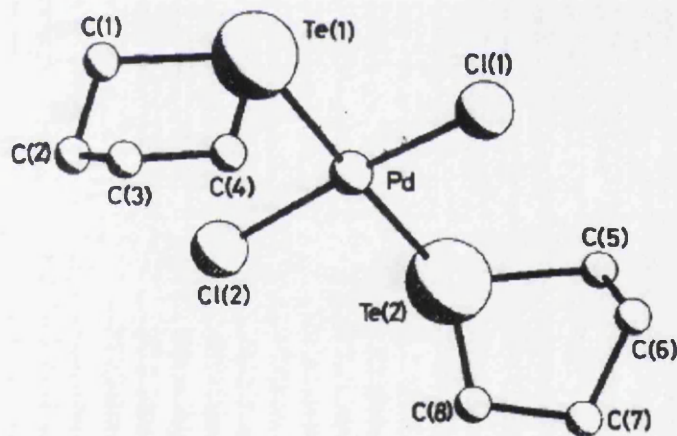
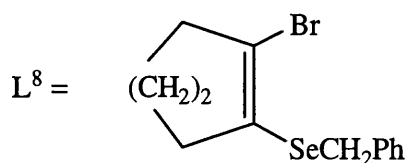
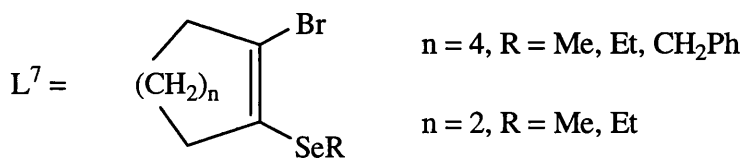
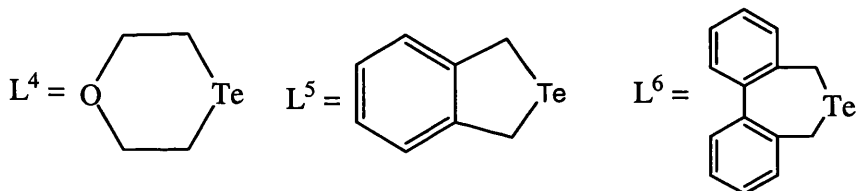


Fig. 1.9 The molecular structure of $[PdCl_2\{\overline{Te(CH_2)_4}\}_2]$

Table 1.3 Literature work concerning $[MX_2L_2]$ complexes

M	X	L	Ref.
Pd, Pt	Cl, Br, I	Me_2Se	46
Pt	Cl	$Te(CH_2Ph)_2$	47
Pt	Cl, SCN	$Te(CH_2CH_2Ph)_2$	48, 49
Pd, Pt	Cl	$Me_3M'CH_2SeR$ ($M' = Si, Ge; R = Me, Ph$)	50
Pd	Cl, Br, I	L^1, L^2	51
Pd, Pt	Cl, Br, I	$TeMe_2, TePh_2, TeMePh$	52
Pd, Pt	Cl	$MeE(C_4H_3S), MeE(C_4H_3O)$	53, 54
Pd, Pt	Cl, Br, I	L^3	55
Pt	Cl	L^4	56
Pd, Pt	Cl	L^5	57
Pd	Cl	L^6	58
Pt	Cl	L^7	59
Pd	Cl	L^8	
Pd, Pt	Cl	$RSeCH_2SeR, R = Me, Ph$	60
Pt	Br	1,4-oxaselenan	61

Note : $L^1 = \overline{Se(CH_2)_n}$ ($n = 4, 5, 6$) $L^2 = \overline{SeCHCMe_2CH_2}$ $L^3 = \overline{Te(CH_2)_4}$



It has been proved by multinuclear (^1H , ^{77}Se or ^{125}Te) NMR spectroscopies that in solution these complexes undergo *cis-trans* isomerisation and intermolecular ligand exchange processes.^{6, 46}

The M(IV) complexes, such as $[\text{R}_4\text{N}][\text{PdX}_5(\text{SeMe}_2)]^{62}$ and $[\text{PtCl}_4(\text{SeMe}_2)_2]^{63}$, have been prepared by oxidation of their M(II) analogues by X_2/CCl_4 .

RSeCH_2SeR ($\text{R} = \text{Me}, \text{Ph}$) can only act as monodentate ligands to form the complexes $[\text{MCl}_2\text{L}_2]$ ($\text{M} = \text{Pd}, \text{Pt}$). IR spectra show that the palladium complexes are *trans* and the platinum complexes *cis* in the solid state. The analogous Te ligands RTeCH_2TeR ($\text{R} = \text{Me}, \text{Ph}$) afford insoluble products which maybe the polymers $[(\text{MCl}_2\text{L})_n]$.⁶⁰

1.3.2 Bidentate ligands

In the 1980s, Abel and his coworkers studied extensively trimethylplatinum(IV) chalcogenoether complexes using dynamic NMR spectroscopy. The reaction of $[(\text{PtXMe}_3)_4]$ ($\text{X} = \text{Br}, \text{I}$) and $\text{MeSe}(\text{CH}_2)_n\text{SeMe}$ ($n = 0, 1$) (Fig. 1.10) gives the complex $[(\text{PtXMe}_3)_2(\text{L-L})]$, containing a bridging diorganodiselenide ligand. The structure has been confirmed by X-ray crystallographic study of $[(\text{PtXMe}_3)_2(\text{MeSeSeMe})]$ ($\text{X} = \text{Br}, \text{I}$).⁶⁴⁻⁶⁶ In the structure of $[(\text{PtI Me}_3)_2(\text{MeSeSeMe})]$ (shown in Fig. 1.11), the platinum atoms in the molecule are held together by three bridging groups, two iodide bridges, and one diselenium bridge: the platinum-platinum non-bonded distance is 3.901(2) Å (3.740 Å in the bromide analogue); the torsional angle C-Se-Se-C is 129° (127° for the bromo complex) and the Se-Se bond distance is 2.358(4) Å (2.36(1) Å for the bromo complex). The interaction of PhEPh ($\text{E} = \text{Se}$ or Te) with $[(\text{PtXMe}_3)_4]$ can also afford binuclear complexes $[(\text{PtXMe}_3)_2(\text{PhEPh})]$ ($\text{X} = \text{Br}, \text{I}$).⁶⁷

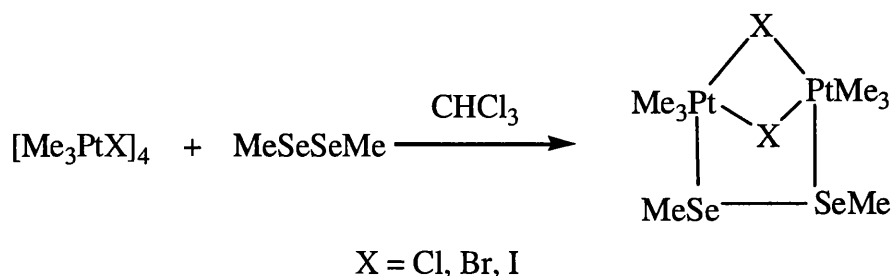


Fig. 1.10 Synthetic scheme for $[(\text{PtXMe}_3)_2(\text{L-L})]$

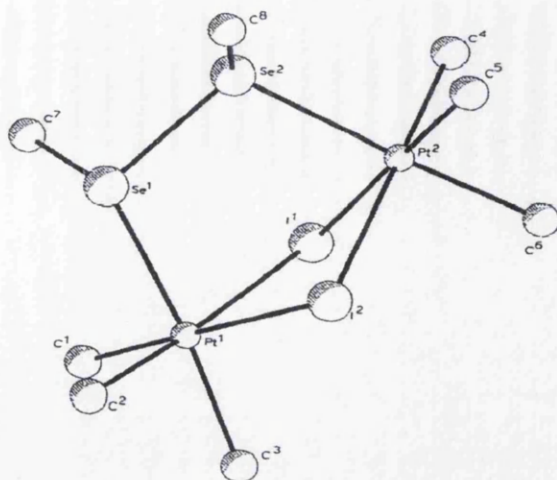


Fig. 1.11 Crystal structure of $[(PtIme_3)_2(MeSeSeMe)]$

A dynamic NMR study of these complexes revealed two different modes of fluxionality. The lower energy process has been ascribed to the concerted/correlated double inversion of the coordinated chalcogen atoms and the higher energy fluxion is attributed to an intermetallic ligand commutation of the two chalcogen atoms between the two platinum atoms, leading to exchange of the three platinum methyl environments. The order of inversion energies is sulphur < selenium < tellurium for this kind of complex.⁶⁷⁻⁶⁹

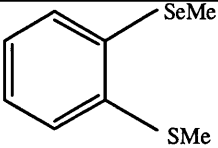
In contrast, the mononuclear complexes $[PtXMe_3(L-L)]$ are formed from the reaction of $[(PtXMe_3)_4]$ ($X = Cl, Br, I$) and $MeSe(CH_2)_nSeMe$ ($n = 2, 3$), $MeSZSeMe$ ($Z = (CH_2)_2, o-C_6H_4$) or $MeSeCH=CHSeMe$.^{65, 70, 71} The Te analogues $[PtIme_3(L-L)]$ ($L-L = RTe(CH_2)_3TeR$ and $o-C_6H_4(TeMe)_2$) were also prepared in the 1990s.⁷² There are four possible isomers, *meso*-1, *meso*-2, *DL*-1 and *DL*-2 (N.B. The two *DL* forms will be degenerate for homochalcogen complexes). Dynamic NMR study showed in these mononuclear complexes that the chalcogen atoms invert independently and all possible invertomers were detected at low temperatures.⁷⁴ The ligand backbone and halogen size affect invertomer populations and chalcogen inversion energy.⁷⁰⁻⁷⁴ The pyramidal inversion barriers decrease in the order $Te > Se > S$ for analogous complexes.⁷²

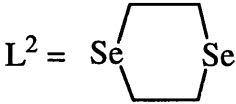
In the 1920s the first Pd(II) and Pt(II) complexes with the bidentate ligand $EtSeCH_2CH_2SeEt$ were reported as $[MCl_2(L-L)]$.^{75, 76} Since then, a series of this class

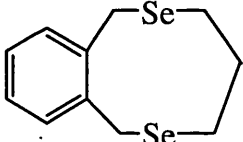
has been synthesized by a route similar to that used for monodentate ligands. The literature work is summarized in Table 1.4.

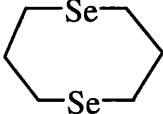
Table 1.4 Literature work concerning [MX₂(L-L)]

M	X	L-L	Ref.
Pd, Pt	Cl	EtSe(CH ₂) ₃ SeEt	75, 76
Pd	Cl	MeSe(CH ₂) _n SeMe, n = 2, 3	77
Pd, Pt	Cl, Br	¹ PrSe(CH ₂) ₂ SePr ¹	78-82
Pd	Cl	L ¹	83
Pd, Pt	Cl, Br	L ²	84
Pd, Pt	Cl, Br, I	MeSeCH ₂ CH ₂ SeMe, PhSeCH ₂ CH ₂ SePh, <i>o</i> -C ₆ H ₄ (SeMe) ₂ , <i>cis</i> -MeSeCH=CHSeMe, or MeSeCH ₂ CH ₂ CH ₂ SeMe	85
Pd, Pt	Cl	L ³	86
Pd, Pt	Cl	MeC(CH ₂ SeMe) ₃ , (MeSeCH ₂ CH ₂ CH ₂) ₂ Se	87
Pd	Cl	(MeSeCH ₂ CH ₂ CH ₂) ₂ Se	87
Pd	SCN, Cl, Br	<i>o</i> -C ₆ H ₄ (SeMe)(PPh ₂)	88, 89
Pd, Pt	Cl, Br	<i>o</i> -C ₆ H ₄ (SeMe)(AsMe ₂)	88
Pt	Cl, Br, I	MeSeCH ₂ CH ₂ CH=CH ₂ , CH ₂ =CHCH ₂ CH ₂ SeCH ₂ CH ₂ CH=CH ₂	90, 91
Pd, Pt	Cl, Br, I	RTe(CH ₂) ₃ TeR, R = Me, Ph	92, 93
Pd, Pt	Cl, Br	(<i>p</i> -EtOC ₆ H ₄)Te(CH ₂) _n Te(<i>p</i> -C ₆ H ₄ OEt) (n = 6-10)	94
Pd	Cl	(<i>p</i> -MeOC ₆ H ₄ Te) ₂ CH ₂	95
Pd, Pt	Cl	L ⁴	96

Note : L¹ = 

L² = 

L³ = 

L⁴ = 

NMR spectroscopies show that the complexes are present as two invertomers in solution, having *meso* and *DL* geometries (Fig. 1.12), which interconvert by pyramidal inversion at the heteroatoms,⁸⁵ but most of these compounds are poorly soluble and thermally unstable, precluding investigations of any dynamic processes.

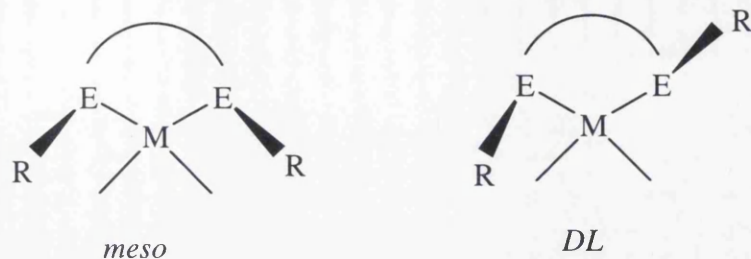


Fig. 1.12 Structures of *meso* and *DL* invertomers

In the solid state, the expected square planar geometry around the Pd or Pt is found, with the ligand forming a chelate ring (example shown in Fig. 1.13).

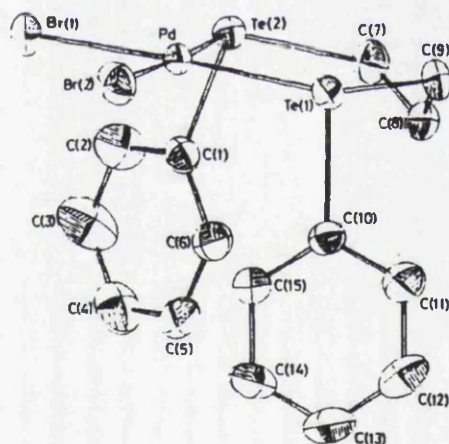


Fig. 1.13 Crystal structure of $[\text{PdBr}_2\{\textit{meso}\text{-PhTe}(\text{CH}_2)_3\text{TePh}\}]^{92}$

Only the Pt(II) diselenoether complexes can be readily oxidised by X_2/CCl_4 to Pt(IV). The crystal structure of *meso*- $[\text{PtCl}_4\{o\text{-C}_6\text{H}_4(\text{SeMe})_2\}]$ is shown in Fig. 1.14. NMR studies show that its predominant invertomer in solution is the *meso* isomer.⁶⁴

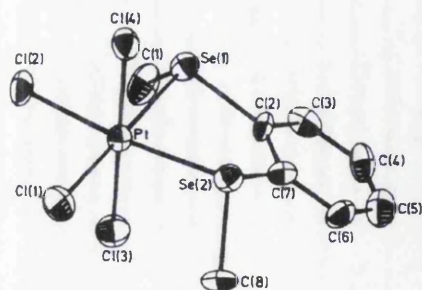


Fig. 1.14 Crystal structure of *meso*-[PtCl₄{*o*-C₆H₄(SeMe)₂}]

A kind of novel tetramer has been obtained from a DMSO solution of [PdI₂{*o*-C₆H₄(TeMe)₂}]. There are three different Pd-Te distances: 2.55 Å (the bond to the methylated Te atom), 2.52 Å (the bond to the demethylated Te atom in the ligand carbon framework) and 2.60 Å (the remaining Pd to demethylated Te atom distance).⁹⁷

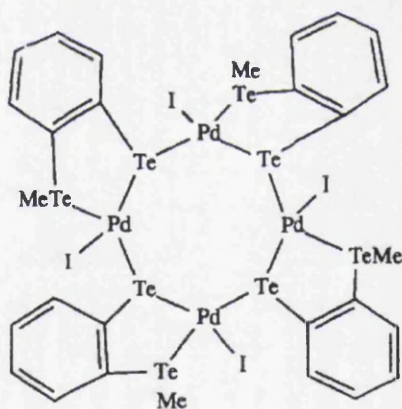


Fig. 1.15 The structure of the tetramer obtained from a DMSO solution of [PdI₂{*o*-C₆H₄(TeMe)₂}]

The reaction of [MCl₂(MeCN)₂] (M = Pd, Pt) with L-L and TIPF₆ in a 1:2:2 ratio yields planar [M(L-L)₂][PF₆]₂, which has a much better solubility than [MX₂(L-L)]. L-L include MeSe(CH₂)₃SeMe,⁹⁸ RTe(CH₂)₃TeR (R = Me or Ph), *o*-C₆H₄(TeMe)₂, *o*-C₆H₄(CH₂TeMe)₂,^{102, 103} [8]aneSe₂.⁹⁶ The example cation structure of the complex [Pt{MeSe(CH₂)₃SeMe}₂](PF₆)₂·2MeCN (Fig. 1.16)⁹⁶ shows that the Pt atom occupies a crystallographic inversion centre and is coordinated to a square planar

array of four Se donor atoms. The coordinated diselenoether ligands both adopt the *DL* configuration. The angles around the central Pt are all nearly 90 or 180° reflecting the good match of the six-membered chelate rings formed by the diselenoether and the *cis*-angles required for the square planar geometry.

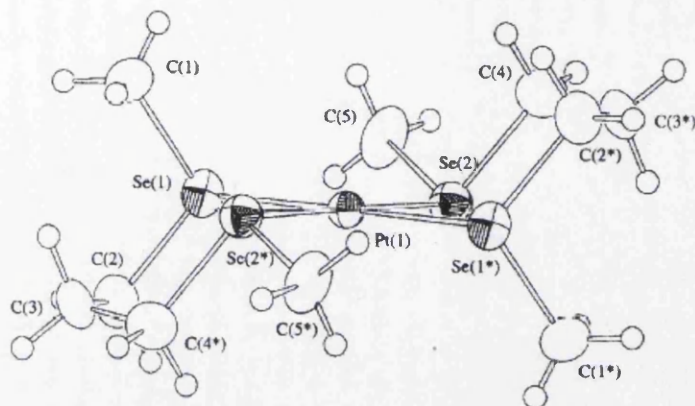


Fig. 1.16 Structure of the cation $[\text{Pt}\{\text{MeSe}(\text{CH}_2)_3\text{SeMe}\}_2]^{2+}$

In combination with Pd(II) and Pt(II), the tripodal ligands $\text{MeC}(\text{CH}_2\text{SeMe})_3$ ($\text{E} = \text{Se}$ or Te) and $\text{MeC}(\text{CH}_2\text{TePh})_3$ behave as bidentate ligands with one free donor atom.¹⁰¹ The crystal structure of $[\text{Pt}\{\text{MeC}(\text{CH}_2\text{SeMe})_3\}_2][\text{PF}_6]_2$ (Fig. 1.17) shows Pt coordinated to four Se atoms to form a distorted square plane. The methyl groups on both ligands are in a *DL* configuration and the uncoordinated arm of each tripod is pointing away from the Pt(II) centre. Disorder in the crystal structure was observed due to the very flexible nature of the uncoordinated arms.

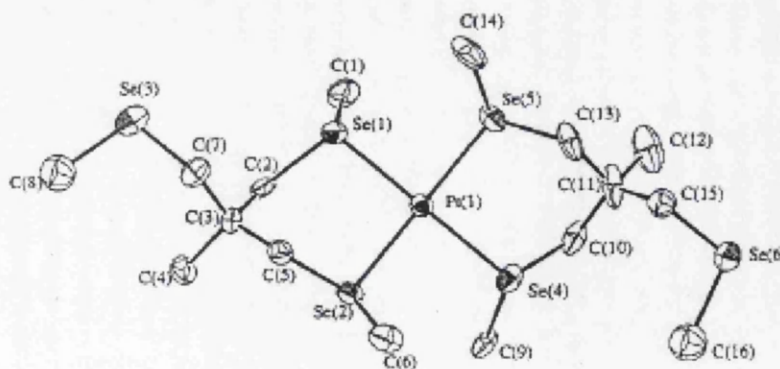


Fig. 1.17 Structure of the cation $[\text{Pt}\{\text{MeC}(\text{CH}_2\text{SeMe})_3\}_2]^{2+}$

1.3.3 Polydentate ligands

The linear tetradentate ligand $\text{MeSe}(\text{CH}_2)_2\text{Se}(\text{CH}_2)_3\text{Se}(\text{CH}_2)_2\text{SeMe}$ was prepared in 1976 by Levason *et al.*; the complexes $[\text{Pd}_2\text{X}_4(\text{L-L-L-L})]$ ($\text{X} = \text{Cl}, \text{Br}, \text{I}$) were synthesized with characteristic terminal *cis*- PdCl_2 groups (Fig. 1.18).¹⁰²

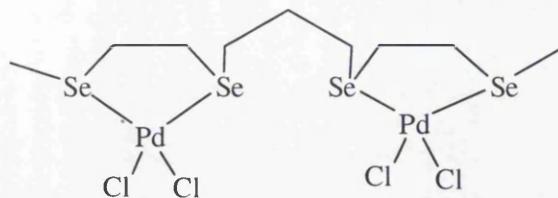


Fig. 1.18 Complex $[\text{Pd}_2\text{Cl}_4(\text{L-L-L-L})]$

Linear 2, 5, 8-triselenanonane, NaBF_4 , and $[\text{Pt}(\text{Me})_3]_4$ afford the Pt(IV) complex *fac*- $[\text{PtMe}_3(\text{MeSeCH}_2\text{CH}_2\text{SeCH}_2\text{CH}_2\text{SeMe})][\text{BF}_4]$.^{103, 104} Variable temperature ^1H NMR studies have shown that pyramidal inversion takes place only at the terminal chalcogen atoms.

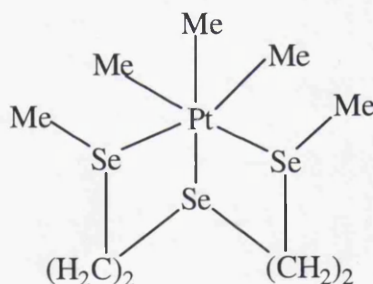


Fig. 1.19 Cation of complex *fac*- $[\text{PtMe}_3(\text{MeSeCH}_2\text{CH}_2\text{SeCH}_2\text{CH}_2\text{SeMe})][\text{BF}_4]$

As mentioned in Table 1.4, the linear ligand $\text{Se}(\text{CH}_2\text{CH}_2\text{CH}_2\text{SeMe})_2$ has been observed to bind in a *cis*-bidentate manner to Pd or Pt centres; it can also act in a tridentate manner to form $[\text{PtCl}(\text{L-L-L})]\text{PF}_6$.⁸⁷ The same kind of complex can form from $\text{Te}(\text{CH}_2\text{CH}_2\text{TeR})_2$ ($\text{R} = \text{Me}$ or Ph).¹⁰⁵ The mixed donor ligand $\text{MeS}(\text{CH}_2)_3\text{Te}(\text{CH}_2)_3\text{SMe}$ yields analogous Pd or Pt complexes.¹⁰⁶ The structure of $[\text{PtCl}\{\text{MeS}(\text{CH}_2)_3\text{Te}(\text{CH}_2)_3\text{SMe}\}]\text{PF}_6$ revealed two independent cations and anions in the asymmetric unit, with one of the PF_6 groups disordered (Fig. 1.20).

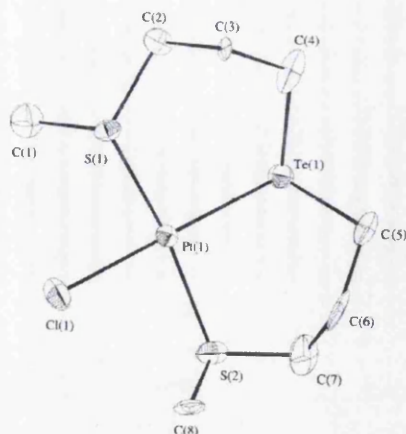


Fig.1.20 A view of one of the independent cations in
 $[\text{PtCl}\{\text{MeS}(\text{CH}_2)_3\text{Te}(\text{CH}_2)_3\text{SMe}\}]\text{PF}_6$

The tetraselenoether [16]aneSe₄ forms $[\text{M}(\{16\}\text{aneSe}_4)](\text{PF}_6)_2$ (M = Pd or Pt); single crystal X-ray studies reveal a planar metal geometry with the ligand in the *up, up, down, down* conformation (Fig. 1.21).⁹⁸ But it seems the type of anion affects the conformation: the structure of $[\text{Pd}(\{16\}\text{aneSe}_4)](\text{BF}_4)_2$ shows the macrocycle in the *all up* conformation (Fig. 1.22), which may due to the smaller and more polarising anions; the same is true for the complex $[\text{Pd}(\{16\}\text{aneSe}_4)]\text{Cl}(\text{BF}_4)$.¹⁰⁷ The $[\text{Pt}(\{16\}\text{aneSe}_4)](\text{PF}_6)_2$ complex can be oxidized by Cl₂ or Br₂ to Pt(IV) in *trans*- $[\text{PtX}_2(\{16\}\text{aneSe}_4)](\text{PF}_6)_2$, and the X-ray structure of the complex *trans*- $[\text{PtCl}_2(\{16\}\text{aneSe}_4)](\text{PF}_6)_2$ shows the same ligand conformation as in the Pt(II) starting material.¹⁰⁸ In contrast to the planar M(II) complexes, the octahedral Pt(IV) complex has only one macrocycle conformation in solution (*up, up, down, down*).

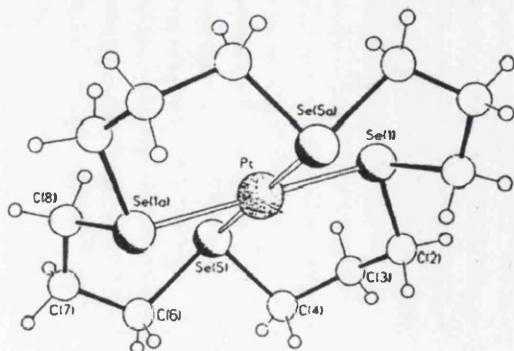


Fig. 1.21 Crystal structure of $[\text{Pt}(\{16\}\text{aneSe}_4)]^{2+}$ (PF_6^- salt)

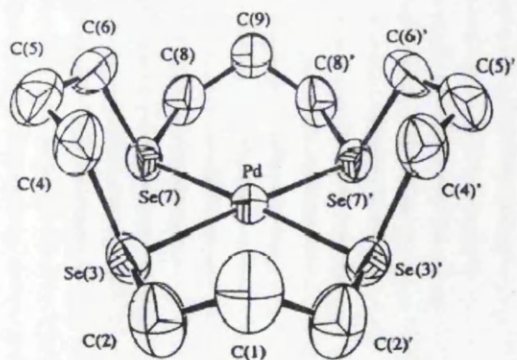


Fig. 1.22 Crystal structure of $[\text{Pd}([\text{16]aneSe}_4)]^{2+}$ (BF_4^- salt)

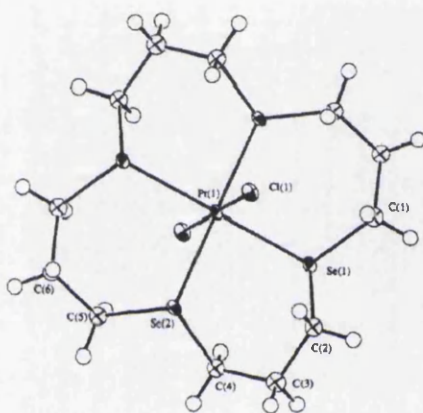


Fig. 1.23 View of the X-ray structure of $[\text{PtCl}_2([\text{16]aneSe}_4)]^{2+}$

The potentially hexadentate $[\text{24]aneSe}_6$ reacts with PdCl_2 in MeCN to form $[\text{Pd}_2\text{Cl}_2([\text{24]aneSe}_6)](\text{BF}_4)_2$ which contains two planar PdSe_3Cl units (Fig. 1.24).¹⁰⁷

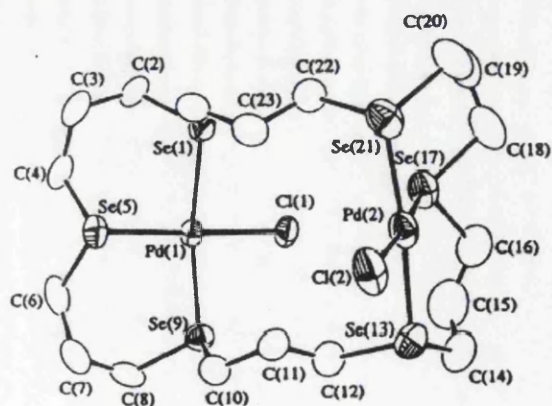


Fig. 1.24 Crystal structure of $[\text{Pd}_2\text{Cl}_2([\text{24]aneSe}_6)]^{2+}$

1.3.4 X-Ray structural data

The available X-ray studies of Pd or Pt complexes of neutral selenoethers and telluroethers are summarized in Table 1.5 for Pt(IV) and Table 1.6 for M(II). The structures show that the coordinated chalcogenoethers have pyramidal geometries, and all have ER₂ groups coordinated to a single metal centre. The bond lengths are similar to, or slightly shorter than, those expected for single bonds on the basis of the appropriate covalent radii. This is consistent with the ligands behaving as σ donors, with small or negligible π components.

The *trans* influences of SeR₂ or TeR₂ ligands are less than that of PR₃, but greater than that of Cl⁻. The Pd-Te bond lengths in [$\text{Pd}(o\text{-C}_6\text{H}_4(\text{TeMe})\text{Te})\text{I}$]₄ are consistent with a *trans* influence order RTe > R₂Te.⁹⁷

Table 1.5 Structural data for Pt(IV) complexes

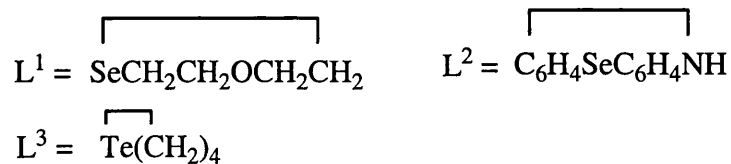
Complex	M-E	Bond Length(s) (Å)	Ref.
[PtClMe ₃ (MeSeCH=CHSeMe)]	Pt-Se	2.532(4), 2.525(4)	70
[PtIme ₃ (MeSeCH=CHSeMe)]	Pt-Se	2.531(2), 2.535(3)	70
[PtCl ₄ { <i>o</i> -C ₆ H ₄ (SeMe) ₂ }]	Pt-Se	2.432(2), 2.431(1)	63
[{PtClMe ₃] ₂ {(SeC ₆ H ₂ (OMe) ₂) ₂ }]	Pt-Se	2.569(1), 2.620(1)	99
[(PtBrMe ₃) ₂ (MeSeSeMe)]	Pt-Se	2.598(7), 2.590(7)	64
[(PtIme ₃) ₂ (MeSeSeMe)]	Pt-Se	2.564(3), 2.563(3)	66

Table 1.6 Structure data for M(II) complexes

Complex	M-E	Bond Length(s) (Å)	Ref.
<i>trans</i> -[PdCl ₂ (SeEt ₂) ₂]	Pd-Se	2.424(7)	110
[PdCl ₂ (Me ₃ SiCH ₂ SeMe) ₂]	Pd-Se	2.429(1)	50
[PdCl ₂ (Me ₃ GeCH ₂ SeMe) ₂]	Pd-Se	2.418(2)	50
[PdCl ₂ {(C ₄ H ₃ S)SeCH ₃ }] ₂	Pd-Se	2.439(2)	53
[PtBr ₂ (L ¹) ₂]	Pt-Se	2.430(2)	61
[PtCl ₂ (L ²) ₂]	Pt-Se	2.376(2), 2.400(2)	111
[PtCl ₂ {(MeO) ₂ C ₆ H ₂ Se ₂ C ₆ H ₂ (OMe) ₂ }]	Pt-Se	2.374(5), 2.384(2)	109
[PtCl ₂ {(C ₄ H ₃ S)SeMe}] ₂	Pt-Se	2.411(4)	53
[PdCl ₂ (L ³) ₂]	Pd-Te	2.593(3)	55

[Pd(SCN) ₂ {Te(CH ₂ CH ₂ CH ₂ SiMe ₃) ₂ }] ₂	Pd-Te	2.606(1)	49
[PdCl ₂ {(C ₄ H ₃ S)TeMe}] ₂	Pd-Te	2.538(1), 2.546(1)	53
[PdCl ₂ {(C ₄ H ₃ O)TeMe}] ₂	Pd-Te	2.530(1)	53
[PtI ₂ (PhTeMe)] ₂	Pt-Te	2.578(1), 2.586(1)	63
[PtCl ₂ (<i>p</i> -EtOC ₆ H ₄ TeCH ₂ CH ₂ SMe)]	Pt-Te	2.514(1)	112
[PdCl ₂ (¹ PrSeCH ₂ CH ₂ Se ¹ Pr)]	Pd-Se	2.40(1), 2.36(1)	113
[Pt{MeSe(CH ₂) ₃ SeMe}] ₂ (PF ₆) ₂	Pt-Se	2.414(2), 2.421(2)	96
[PdCl ₂ ([8]aneSe ₂)]	Pd-Se	2.3647(8), 2.3693(8)	96
[Pt{MeC(CH ₂ SeMe) ₃ }] ₂ {PF ₆ }] ₂	Pt-Se	2.426(2), 2.430(2), 2.425(2), 2.435(2)	101
[Pt([16]aneSe ₄)](PF ₆) ₂	Pt-Se	2.420(3), 2.417(3)	98
[Pd([16]aneSe ₄)](PF ₆) ₂	Pd-Se	2.435(2), 2.428(1)	98
[Pd([16]aneSe ₄)](BF ₄) ₂	Pd-Se	2.423(1), 2.432(1)	107
[Pd([16]aneSe ₄)Cl](BF ₄)	Pd-Se	2.4560(7), 2.4395(7), 2.4583(7), 2.4330(7)	107
[Pd ₂ Cl ₂ ([24]aneSe ₆)]{BF ₄ }] ₂	Pd-Se	2.428(1), 2.372(1), 2.428(1), 2.428(1), 2.364(1), 2.421(1)	107
[PtCl ₂ ([16]aneSe ₄)](PF ₆) ₂	Pt-Se	2.5015(6), 2.4957(7)	107
[Pd(benzo-[15]aneSe ₂ O ₃) ₂](PF ₆) ₂	Pd-Se	2.4191(5), 2.4183(5)	114
[PdBr ₂ (PhTeCH ₂ CH ₂ CH ₂ TePh)]	Pd-Te	2.528(1), 2.525(1)	92
[{Pd(<i>o</i> -C ₆ H ₄ (TeMe)Te)I}] ₄	Pd-Te	2.540(2), 2.593(2), 2.521(2), 2.554(2), 2.599(2), 2.513(2), 2.602(2), 2.608(2), 2.549(2), 2.542(2), 2.519(2), 2.521(2)	97
[PdCl ₂ {(<i>p</i> -MeOC ₆ H ₄ Te) ₂ CH ₂ }]	Pd-Te	2.529(2), 2.527(2)	95
[Pd{ <i>o</i> -C ₆ H ₄ (TeMe) ₂ }] ₂ [PF ₆]] ₂	Pd-Te	2.5716(4), 2.5789(5)	109
[PtCl ₂ {MeSCH ₂ CH ₂ Te(<i>p</i> -C ₆ H ₄ OEt)}]	Pt-Te	2.514(1)	112
[PdCl ₂ {EtSCH ₂ CH ₂ Te(<i>p</i> -C ₆ H ₄ OMe)}]	Pd-Te	2.492(13)	115
[PtCl{MeS(CH ₂) ₃ Te(CH ₂) ₃ SMe}]PF ₆	Pt-Te	2.5258(11), 2.5191(12)	106

Note:



1.4 Electrochemistry of linked ferrocenes

Since its discovery in 1951, the electrochemical study of ferrocene has attracted wide interest. Acting as a reversible one-electron redox couple, it can be used as a reference for electrochemistry in organic solvents.¹⁶ From the 1970s, a series of biferrocenes,^{116, 117} bridged-biferrocenes¹¹⁷⁻¹²⁸ and poly(vinylferrocene)s¹²⁹⁻¹³³ have been synthesized. These linked ferrocenes can be divided into eight types, based on the different cyclopentadienyl derivatives from which they are derived, as shown in Fig. 1.25.¹³⁴

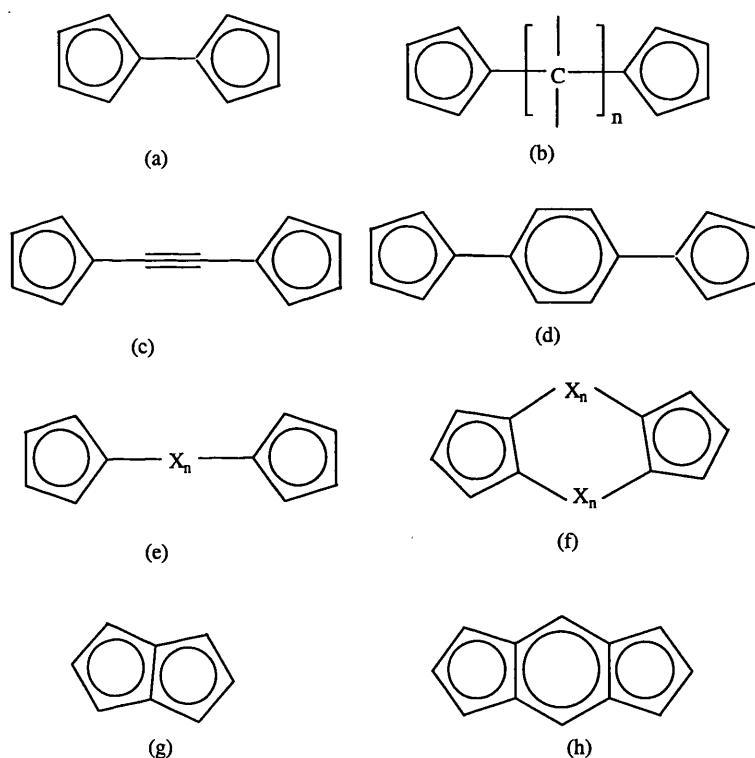


Fig.1.25 Examples of different types of linked cyclopentadienyl systems:

- (a) fulvalene
- (b) – (d) carbon-bridged non-fused ring systems
- (e) – (f) heteroatom-bridged systems (X: noncarbon atom)
- (f) – (h) fused ring systems

Much of the interest in compounds composed of more than one ferrocenyl unit has focused on phenomena associated with interactions between the iron centres. Of the various types of techniques used to study them, electrochemical techniques

(commonly cyclic voltammetry) have been among the most widely used tools to investigate iron-iron interactions. This may be due to the fact that one can use the most chemically stable member of a redox series, whereas use of other techniques may require isolation of oxidized or reduced species, which may be chemically very sensitive. Also the equipment and the experiment are relatively simple.

The ferrocenyl unit can be easily oxidized and used to understand multiple-electron-transfer reactions. The potential separation, $\Delta E_{1/2}$, between the oxidations of two ferrocenyl units provides a measurement of charge interaction between the two reaction sites. The separation (or the interaction between the ferrocenyl moieties) can be affected by many factors.

Poly(ferrocenyl) compounds containing each of the types of linked cyclopentadienyl groups, except fused ring systems, are next considered in turn. Discussion of Se and Te bridged compounds will be deferred until Chapter Four.

1.4.1 Fulvalene complexes

The cyclic voltammograms of polyferrocenes (Fig. 1.26) show that the number of waves observed is equal to the number of ferrocenyl groups in the polymer unit.

Biferrocene ($n = 0$) is two ferrocenes linked by a single bond. Its cyclic voltammogram in acetonitrile shows two oxidations with a separation of 330 mV.¹¹⁷ Little variation is observed between the values of $\Delta E_{1/2}$ for various biferrocene derivatives, indicating very similar levels of metal-metal interaction.

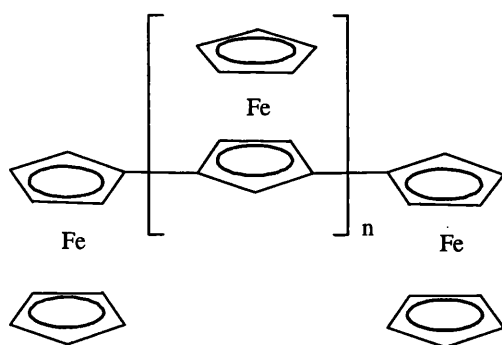


Fig. 1.26 Polyferrocene ($n = 0, 1, 2$)

Terferrocene ($n = 1$) has been shown to undergo three one-electron oxidations, separated by 220 and 370 mV. The rather small separation between the first two

oxidations suggests that the terminal ferrocene undergoes oxidation first. Quaterferrocene ($n = 2$) shows four oxidations separated by 200, 250, 280 mV. Because the ferrocene substituent of an oxidized ferrocene stabilizes the cation by donating electron density, the first oxidation potentials of these species decrease with increasing oligomerization, and are -90 ($n = 0$), -180 ($n = 1$), and -240 ($n = 2$) mV relative to ferrocene.¹²²

The bis(fulvalene)diiron system, Fv_2Fe_2 (Fig. 1.27), shows an even more negative first oxidation potential shift (-280 mV relative to ferrocene) and a larger separation between the first and second oxidations ($\Delta E_{1/2} = 590$ mV) than that of biferrocene.¹¹⁷

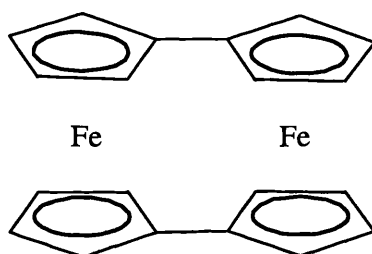


Fig. 1.27 bis(fulvalene)diiron

1.4.2 Ferrocenes linked by carbon bridges

Saturated carbon bridges

Compared to bimetalloenes, linked ferrocenes with a single saturated carbon bridge show weaker metal-metal interactions. For example, the two oxidation potentials of diferrocenylmethane, $FcCH_2Fc$, are separated by only 170 mV; the first oxidation potential is shifted a little negatively compared to that of ferrocene.¹¹⁷ Longer saturated bridges lead to almost unresolved separations between oxidations. No separation was observed between the two oxidations of $FcCH_2CH_2Fc$ in acetonitrile,^{117, 118} but a value of 80 mV has been reported for $Fc(CMe_2)_2Fc$ in dichloromethane.¹³⁵ The electrochemistry of the high molecular weight polymers $[Fe\{(C_5H_3Me)_2(CH_2)_2\}]_n$ (Fig.1.28) shows two reversible waves separated by 60 mV, corresponding to initial oxidation of alternate iron centres, followed by oxidation of the intervening ferrocenes.^{136, 137}

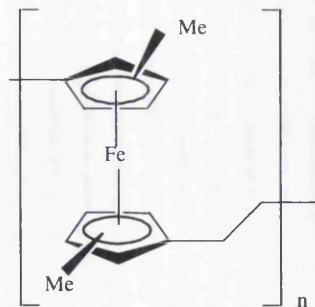


Fig.1.28 High molecular weight polymers $[\text{Fe}\{(\text{C}_5\text{H}_3\text{Me})_2(\text{CH}_2)_2\}]_n$

Poly(vinylferrocene) (Fig.1.29) has three saturated carbon atoms between each ferrocene. A single oxidation wave is observed, indicating negligible metal-metal interactions in this system.^{130, 138}

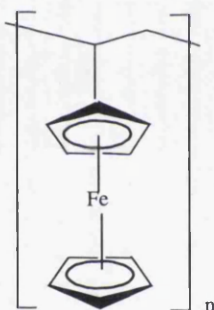


Fig.1.29 Poly(vinylferrocene)

Stronger electrochemical metal-metal interactions occur when two linkages are made between two ferrocenes and the metals are brought into closer proximity. The [1,1]ferrocenophanes in Fig. 1.30 showed $\Delta E_{1/2}$ in 90% aqueous ethanol of 190, 200 and 300 mV, respectively, and under the same conditions, $\Delta E_{1/2}$ of only 100 mV was obtained for Fc_2CHMe ¹³⁹.

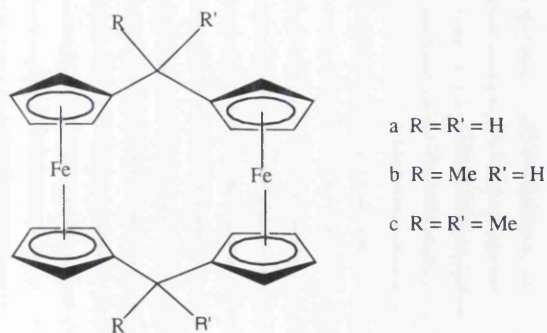


Fig.1.30 [1,1]ferrocenophanes

Köhler and co-workers have designed a kind of ferrocene in which two cyclopentadienyl groups are held at a fixed angle by a rigid insulating bridge.¹⁴⁰ The intramolecular iron-iron distances are 6.11 Å (*syn,syn*, Fig. 1.31a) and 5.34 Å (*syn,anti*, Fig. 1.31b), with $\Delta E_{1/2}$ values of 160 and 140 mV respectively in THF. Greater interactions are observed in the species with the larger Fe-Fe separation. The similar trimetallic species (Fig. 1.31c) shows three waves in THF separated by 190 and 100 mV, similar to those of the terferrocene, $[\text{Fe}(\text{C}_5\text{H}_4\text{CMe}_2\text{Fc})_2]$.

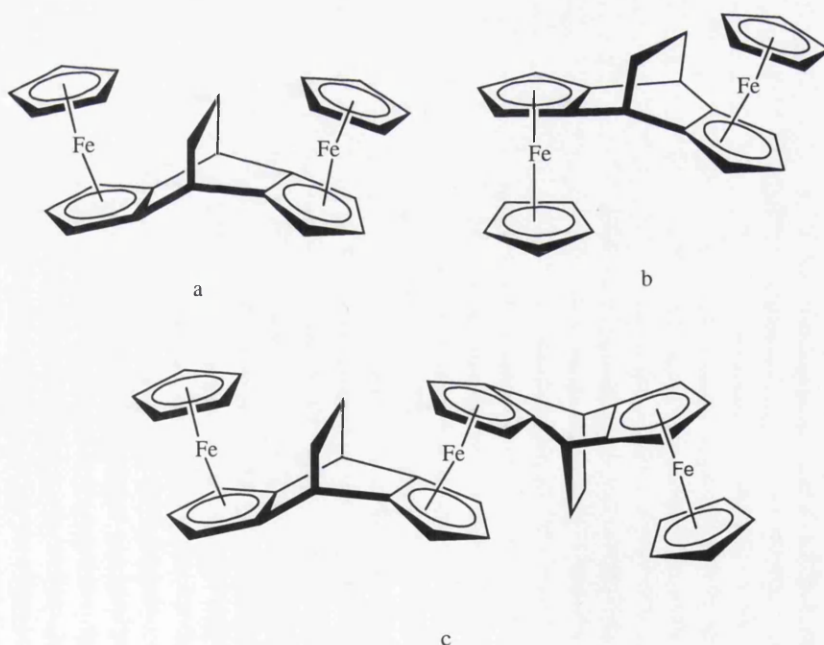


Fig.1.31 Ferrocenes with two cyclopentadienyl groups held at a fixed angle by a rigid insulating bridge

Unsaturated carbon bridges

Ferrocenes linked by olefinic bridges show slightly larger metal-metal interactions than those with analogous saturated bridges. The *cis* and *trans* isomers of $(C_5H_4Et)Fe(C_5H_4CMe=CMeC_5H_4)Fe(C_5H_4Et)$ show two one-electron oxidation waves with $\Delta E_{1/2} = 150$ mV.¹⁴¹ The series of polyene-bridged biferrocenes $Fe(CH=CH)_nFe$ (all *trans*) show $\Delta E_{1/2}$ of 170, 129, and 100 mV for $n = 1, 2$ and 3 respectively, and unresolved separations for $n = 4 - 6$.¹⁴² Chen proved that a different conformation affects the interaction, with $\Delta E_{1/2} = 159, 170$ and 172 mV for the compounds shown in Fig. 1.32a, 1.32b and 1.32c respectively, which is consistent with the Fe-Fe interatomic distance.¹²⁷

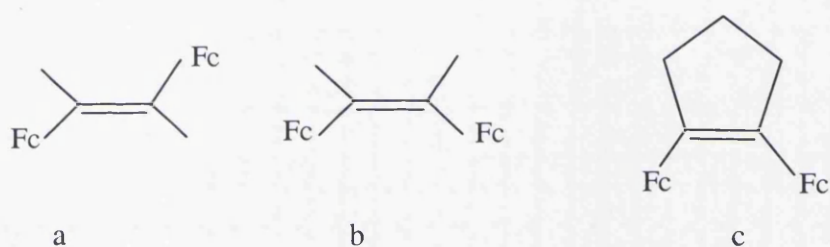


Fig.1.32 Different alkene-bridged biferrocenes

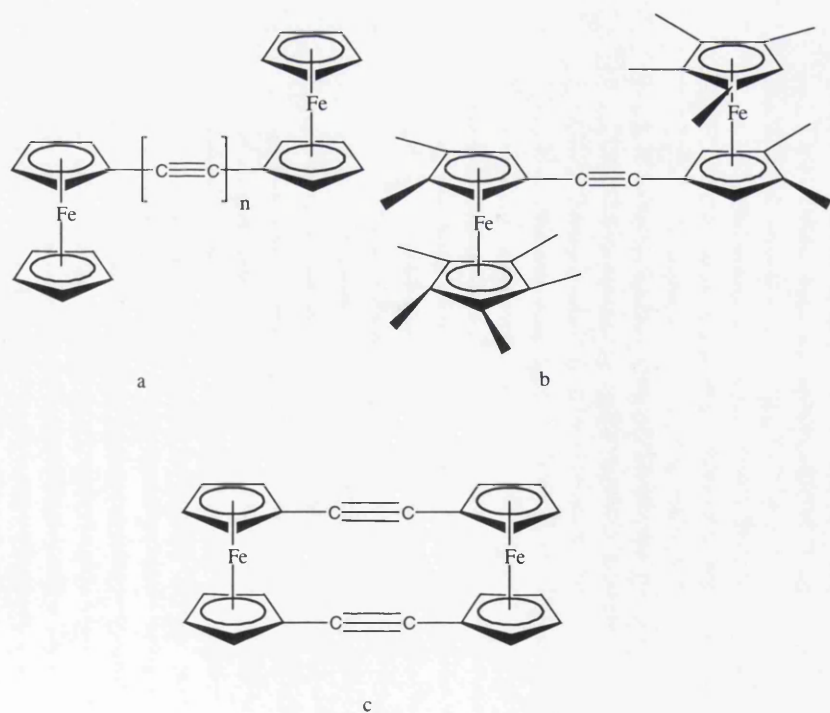


Fig.1.33 Diferrocenyl alkynes

In the diferrocenyl alkynes, the metal-metal interactions were found to be similar to those in C=C-bridged systems (Fig.1.33). For the compounds shown in Fig. 1.33a, when $n = 1$ the two oxidations are separated by 130 mV in dichloromethane, and only 100 mV when $n = 2$.¹¹⁶ For the compound shown in Fig. 1.33b, $\Delta E_{1/2}$ is 160 mV.¹⁴⁴ However [2.2]ferrocenophane-1,13-diyne (Fig. 1.33c) has the $\Delta E_{1/2} = 355$ mV.¹¹⁶

The phenylene-bridged metallocenes, $\{\text{Cp}^*\text{Fe}(\text{C}_5\text{H}_2\text{Me}_2)\}_2\text{-}p\text{-C}_6\text{H}_4$ and $\{\text{Cp}^*\text{Fe}(\text{C}_5\text{Me}_4)\}_2\text{-}p\text{-C}_6\text{H}_4$ (Fig. 1.34) showed two reversible oxidations separated by 120 mV, but for the biphenylene-bridged species there was no separation.¹⁴³ In the *m*-phenylene-bridged isomers the separation is only 60 mV, which means that the *para* isomers display a stronger interaction despite the increased iron-iron distance.¹⁴⁴ Only a single oxidation was observed for $\text{FcCH}=\text{CHC}_6\text{H}_4\text{CH}=\text{CHFc}$ due to the length of the bridge.¹¹⁷

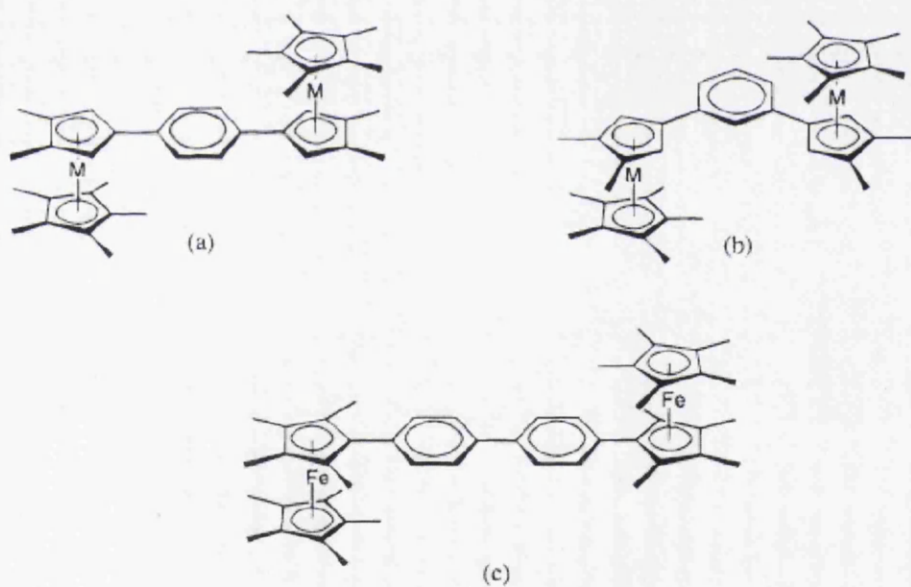


Fig. 1.34 Phenylene-bridged ferrocenes

In “face-to-face” diferrocenes the iron-iron interaction takes place through the Cp ring of one ferrocene being cofacial with that of another ferrocene.¹⁴⁵ The naphthalene-bridged ferrocene shown in Fig. 1.35 has a first oxidation which occurs at significantly lower potential than in the biferrocene, indicating some delocalization of charge in the partially oxidized species via interaction of the cofacial π -orbitals of adjacent ferrocenes.

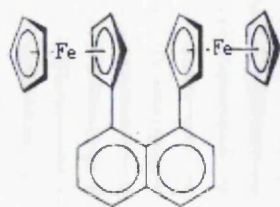


Fig. 1.35 A “face-to-face” diferrocenes

1.4.3 Ferrocenes linked through heteroatoms

Silicon bridges

Lots of silicon-bridged ferrocenes have been synthesized and studied by electrochemistry.

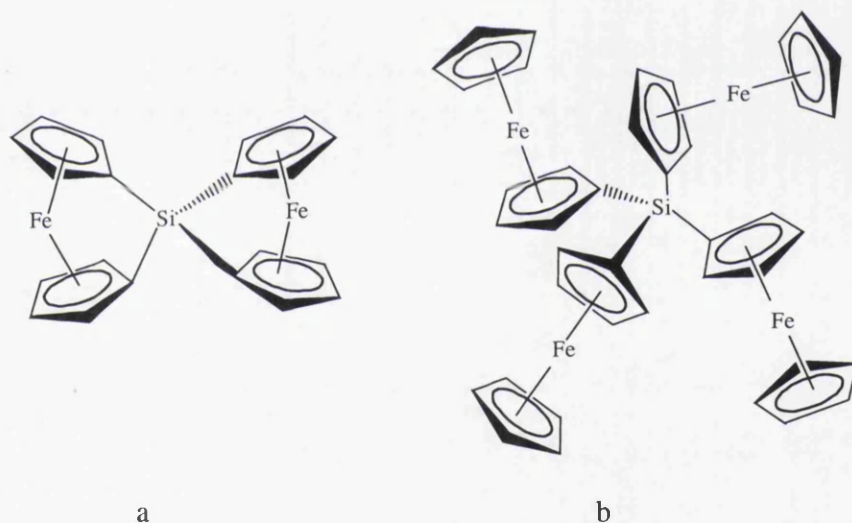


Fig.1.36 a) Spirocyclic [1]silaferrocenophane; b) Tetraferrocenylsilane

The CV of the spirocyclic [1]silaferrocenophane (Fig. 1.36a) showed two oxidations with a large separation of 370 mV, indicating a significant Fe-Fe interaction between the two ferrocenophane units. Cyclic voltammetry of tetraferrocenylsilane (Fig. 1.36b) in benzonitrile resolved four reversible oxidations with separations of 180, 140 and 100 mV.¹⁴⁶

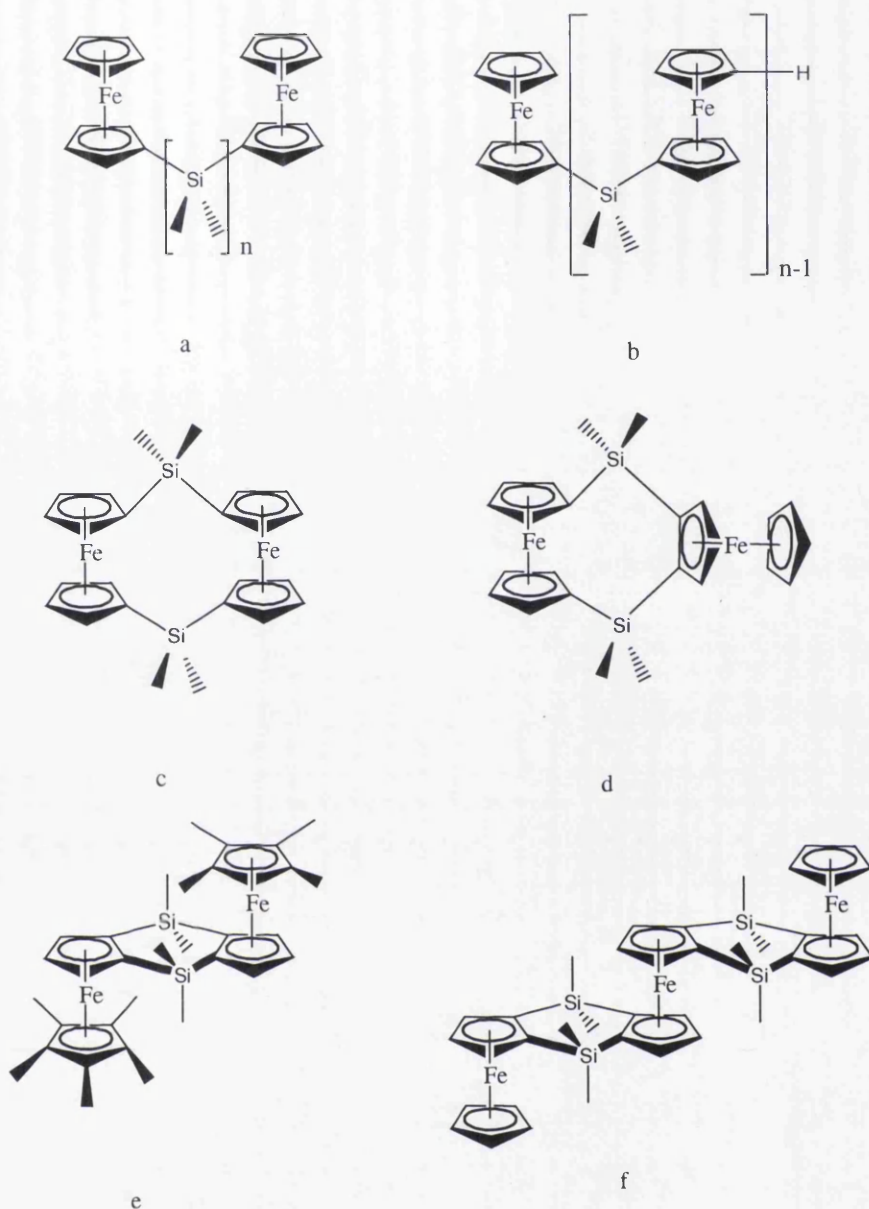


Fig.1.37 Ferrocenes linked with SiMe_2 Bridges

In the series $\text{Fc}_2(\text{SiMe}_2)_n$ (Fig. 1.37a), $\Delta E_{1/2}$ is 150, 110, 80, and 0 mV for $n = 1, 2, 3$ and 6 respectively; These values are greater than for the carbon-bridged analogues despite the longer metal-metal distances due to the greater length of C-Si and Si-Si bonds.¹⁴⁷ This proves the existence of through-bond metal-metal communication.

The series $\text{Fc}(\text{SiMe}_2\text{C}_5\text{H}_4\text{FeC}_5\text{H}_4)_{n-1}\text{H}$ was synthesized and studied by Manners' group.¹⁴⁸ When $n = 3$, two waves were observed in a 2:1 ratio with $\Delta E_{1/2} = 260$ mV. This can be explained by presuming that the two terminal ferrocenes are too far apart to interact, and have the same oxidation potential. The large value of $\Delta E_{1/2}$ means the

third electron must be removed from a site adjacent to two cations. Similarly the members of the series with $n = 4$ and $n = 8$ have three waves in the ratio 2:1:1 and 4:1:3 respectively. A study of poly-[Fe(C₅H₄)₂SiR₂] (R = Me, Et, Bu, *n*-hexyl) showed both steric and electronic factors affect the $\Delta E_{1/2}$ value.¹⁴⁹⁻¹⁵¹ The compounds shown in Fig. 1.37c-f behave similarly.¹⁵²⁻¹⁵³

Germanium, tin and lead bridges

The CV of [1]germaferrocenophane also showed two oxidations in dichloromethane, with a smaller $\Delta E_{1/2}$ value (250 mV) than that of the silicon analogue (Fig.1.36a), implying a larger Fe-Fe interaction for the Si bridge compared to that for Ge. The longer through bond Fe...Fe distances (7.94 Å, compared to 7.78 Å in silicon analogue) also give the evidence for metal-metal interactions.¹⁴⁶ The first oxidation potential is positive versus ferrocene.

The CV of the GeMe₂-bridged ferrocene polymer in dichloromethane showed two oxidations separated by 200 mV, similar to the 210 mV for the SiMe₂ polymer.¹⁴⁹ GeR₂-bridged polymers (R = Et or ⁿBu) show similar results with potentials slightly higher than the Si analogues, and the introduction of the *n*-butyl group onto the group 14 bridge significantly increases the difference between the first and second oxidation potentials.¹⁵⁶

A soluble SnⁿBu₂-bridged ferrocene polymer has been found to have two oxidations separated by 240 mV, compared to 290 mV for the SiⁿBu₂-bridged polymer. It seems that the d- π overlap of tin atoms and the cyclopentadienyl rings plays an important role.¹⁴⁹ The SnⁿBu₂-bridged [1,1]ferrocenophane showed two reversible oxidations separated by 200 mV, shifted positively versus ferrocene.¹⁵⁷

The lead-bridged species Fc₂PbPh₂, (FcPbPh₂C₅H₄)Fe(C₅H₄PbPh₃) and [(C₅H₄)₂PbPh₂]₂Fe₂ have $\Delta E_{1/2}$ values of 165, 136 and 279 mV by CV studies in dichloromethane.¹⁵⁸

Boron bridges

In [BFc₄]⁻, four reversible redox processes were observed with $\Delta E_{1/2}$ values of 270, 200 and 120 mV, which reflects the close proximity of all four iron centres.¹⁵⁹

Nitrogen and phosphorus bridges

In the N,N'-diferrocenyldiazabutadiene series (Fig. 1.38) sequential oxidations of the two ferrocenyl units occur at potential values differing by 60 mV ($X = H$), 80 ($X = Si(CH_3)_3$) and 90 ($X = Si(CH_3)_2^cHex$), whereas in $Fc(CH=CH)_2Fc$ they are separated by about 130 mV; the poor conjugation of nitrogen atoms with respect to carbon atoms is hence reflected in less, if any, electronic communication between the ferrocenyl units. The oxidation potential shifts a little positively with respect to ferrocene.¹²⁶

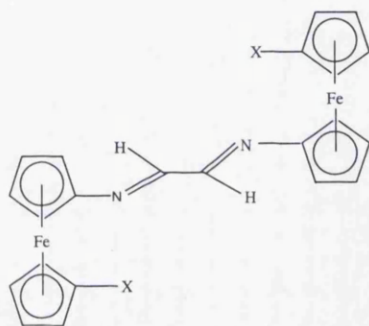


Fig.1.38 N,N'-Diferrocenyldiazabutadiene series

Two waves with $\Delta E_{1/2} = 190$ mV are observed for poly- $[Fe(C_5H_3^nBu)(C_5H_4)PPh]$.¹⁶⁰

Sulphur bridges

Diferrocenyl sulphide (Fc_2S) has two oxidations with $\Delta E_{1/2} = 290$ mV in dichloromethane,¹⁶¹ a greater value than that observed for similar carbon- and silicon-bridged species and near that for the unbridged biferrocene (330 mV in CH_2Cl_2).¹⁶² The electron-withdrawing group, sulphur, results in a higher oxidation potential with respect to ferrocene.¹⁶¹

The trinuclear sulphur-bridged ferrocenes $Fc-S-fc-S-Fc$ (Fig. 1.39) shows two closely spaced oxidation steps and another one at higher potential. The different separations, $\Delta E_{1/2}(1) = 90$ mV and $\Delta E_{1/2}(2) = 390$ mV, mean the first two-electron step corresponds to almost simultaneous electron removal from the terminal, non-interacting ferrocenyl units, whereas the second process is centred on the central ferrocene. Tetranuclear $Fc-S-fc-SS-fc-S-Fc$ behaves similarly: oxidation occurs through a single two-electron process centred on the terminal ferrocenyl units, followed by two

separate one-electron steps centred on the inner sulphur-bridged diferrocene unit, $\Delta E_{1/2}(1) = 290$ mV and $\Delta E_{1/2}(2) = 120$ mV (Fig. 1.40).¹³¹

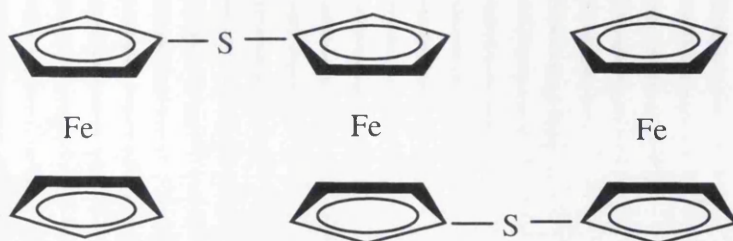


Fig. 1.39 Fc-S-fc-S-Fc

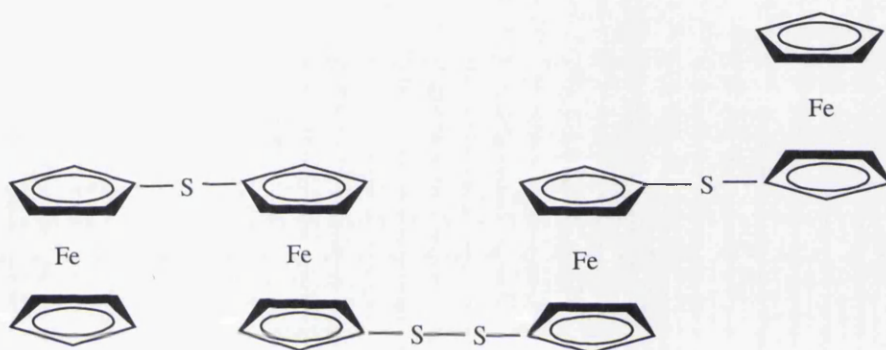


Fig. 1.40 Fc-S-fc-SS-fc-S-Fc

There are two waves in the CVs of the soluble polymers poly-[Fe(C₅H₃ⁿBuS)(C₅H₄S)] ($\Delta E_{1/2} = 319$ mV), poly-[2-Fe(C₅H₃^tBuS)(C₅H₄S)] and poly-[2,3'-Fe(C₅H₃^tBuS)₂] ($\Delta E_{1/2} = 290$ mV), as found for poly(ferrocenylsilane)s, poly(ferrocenylgermane)s and poly(ferrocenylphosphine)s.¹⁶³⁻¹⁶⁵ These values are similar to those for Fc₂S, so the effect of the longer bridge is evidently balanced by the fact that the second oxidation involves making a cation next to two other cations in the polymer, rather than one as in diferrocenyl sulphide.

Cyclic voltammetric studies of poly(dimethylferrocenyl sulfide) in THF showed the presence of two reversible oxidation waves with $\Delta E_{1/2}$ ca. 320 mV, which is consistent with the presence of significantly stronger M...M interactions compared to those present in other ring-opened poly(ferrocene)s derived from [1]ferrocenophanes.¹⁴⁸

Mercury bridge

Fc_2Hg has only one oxidation wave corresponding to a two-electron process, indicating no metal-metal interaction. The oxidation potential shifts negatively relative to ferrocene by 130 mV, more than for carbon-bridged diferrocenes.¹¹⁷

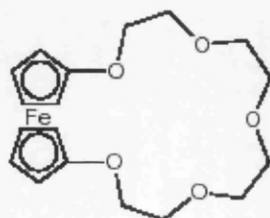
1.5 Ferrocene in the design of electrochemical sensors

Electrochemical molecular recognition has become a fashionable research area with its combination of electrochemistry and supramolecular chemistry. To design highly selective and sensitive electrochemical sensors for charged or neutral target guest species is the main target in this area. The heart of a sensor is a receptor, which has a binding site and a reporter capable of signaling after the receptor-substrate interaction. Sensor efficiency can be compared as follows: (i) the selectivity of the binding tendencies; and (ii) ease and simplicity of detecting and measuring the displayed signal.^{166, 167}

From the first report in the late 1970s of the synthesis and complexation of metallocene-containing macrocyclic ligands capable of electrochemical detection of a metal cation,¹⁶⁸ ferrocene derivatives have been widely employed in the study of redox-active ligands in molecular recognition processes whereby complexation of a guest species (e.g. a metal ion) in solution leads to a change in the electrochemical response of the host molecule. Different types of sensors including the ferrocene unit have been designed and studied for three main target guests: s-block cations; anions; transition metal cations. The brief introduction below is organized accordingly.

1.5.1 s-Block cations

Some ferrocene-functionalised crown ethers were first reported to recognize s-block cations.¹⁶⁹ On addition of sodium cations to a ligand solution, a new wave at a higher positive potential appeared corresponding to the complexed species (Fig. 1.41). The oxidised ferrocene crown ether has a lower binding constant with sodium than the unoxidised receptor due to the electrostatic repulsion of the ferrocenium positive charge and the guest alkali metal cation; this property can be used to transport alkali metal cations across liquid membranes containing **1** as a carrier.¹⁷⁰



1

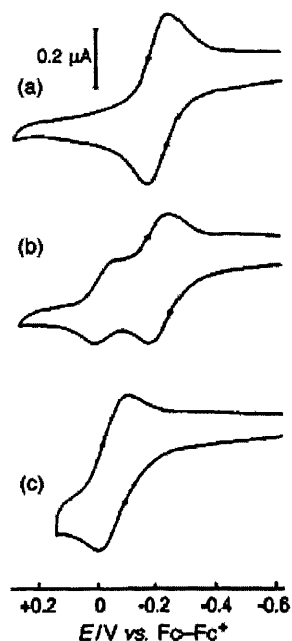


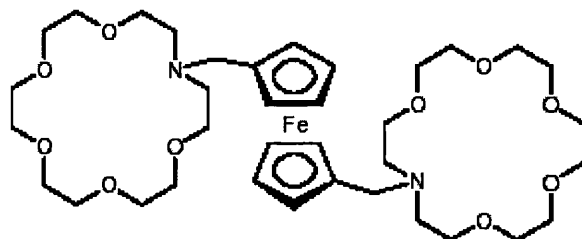
Fig.1.41 Cyclic voltammograms for 0.2 mmol dm^{-3} compound **1** (in the presence of 0.1 mol dm^{-3} $n\text{-Bu}_4\text{NPF}_6$ in CH_2Cl_2 , scan rate 40 mV s^{-1})

(a) in the absence of NaClO_4 ;

(b) in the presence of 1 mmol dm^{-3} NaClO_4 , after stirring the solution for 5 min;

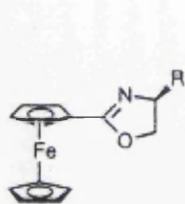
(c) in the presence of 1 mmol dm^{-3} NaClO_4 , after stirring the solution for 1 h.

The receptor, **2**, can asymmetrically complex and electrochemically recognize two different Group 2 metal cations (Ba^{2+} , Mg^{2+}) simultaneously in acetonitrile solution. Three waves are observed, which are shifted anodically from free **2** by 150, 395 and 275 mV respectively, corresponding to the three complexes $2 \cdot 2\text{Ba}^{2+}$, $2 \cdot 2\text{Mg}^{2+}$ and $2 \cdot \text{Ba}^{2+} \cdot \text{Mg}^{2+}$.¹⁷¹

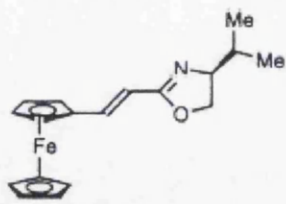


2

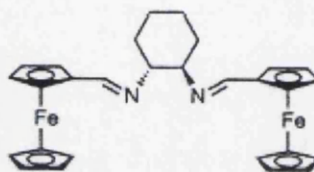
More recently, non-macrocyclic functional groups which act as cation binding sites have provided new voltammetric sensors. For example, Bryce reported that certain ferrocenyl oxazoline and imine derivatives, such as **3**, **4** and **5**, display remarkably high selectivities for Mg^{2+} and Ca^{2+} ions with no interference from a large excess of other metal salts.¹⁷²⁻¹⁷⁴



3 (R = H, ⁱPr)



4

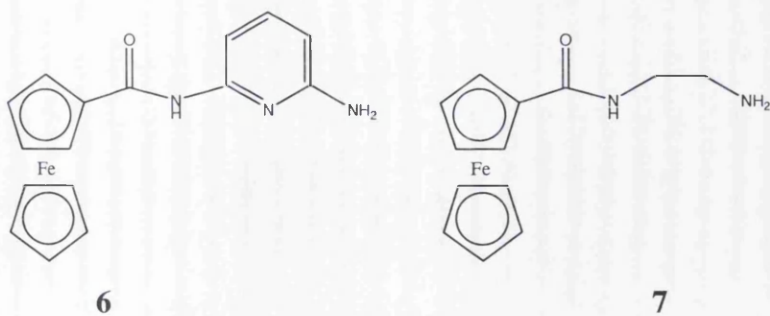


5

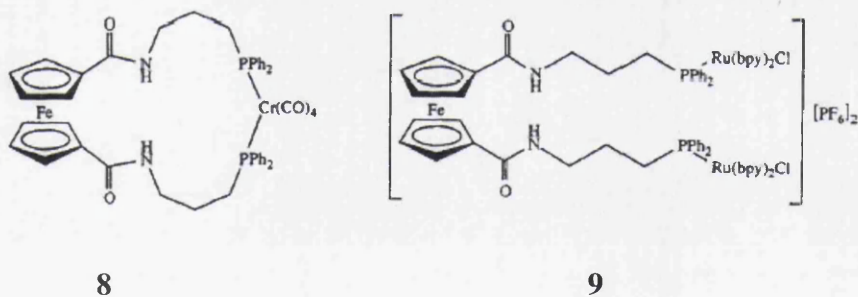
1.5.2 Anions

Anions play numerous indispensable roles in biological and chemical processes and the detection/extraction of anionic pollutants such as phosphate and nitrate, excess amounts of which may destroy aquatic life cycles, is of great importance. The development of responsive ligand systems for anionic guest species has been realized. Many ferrocene-based host molecules have been synthesized.¹⁷⁵ These neutral receptors have no inherent electrostatic attraction with anions and consequently stability constants are much lower in magnitude than for the analogous positively charged cobaltocenium systems.

By appending ferrocene units with secondary amides, some neutral receptors were obtained (e.g. **6** and **7**), which exhibit an interesting electrochemical anion recognition effect.¹⁷⁶ Compound **6** can detect H_2PO_4^- anions in the presence of a 10-fold excess of HSO_4^- and Cl^- ions, but receptor **7** displays the reverse selectivity, binding HSO_4^- selectively in the presence of H_2PO_4^- . This novel anion selectivity is due to the presence of the basic amine functionality, which is protonated by the acidic hydrogen sulfate anion. This protonated receptor then shows a high binding affinity for the di-negative sulfate anions produced.



Beer *et al.* have proved that the combination of transition metal and ferrocene amide moieties enhances the strength of anion binding. Neutral and charged transition metal-coordinated ferrocene phosphine amide receptors, such as **8** and **9**, can electrochemically recognise anions via significant cathodic perturbations of the respective ferrocene and transition metal oxidation waves (Fig. 1.42). The positively charged ruthenium receptor **9** has the greatest strength of anion binding, which indicates that attractive electrostatic forces are of significant importance to the anion recognition process.¹⁷⁷



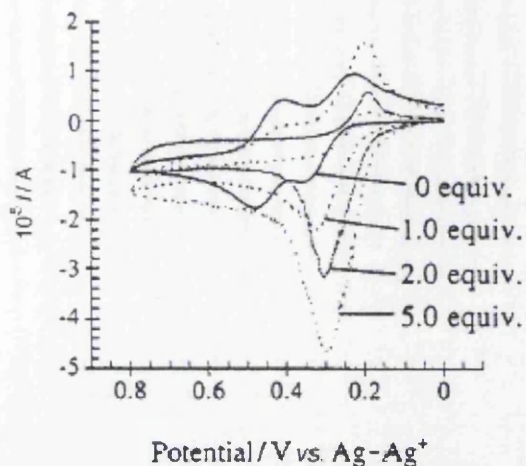
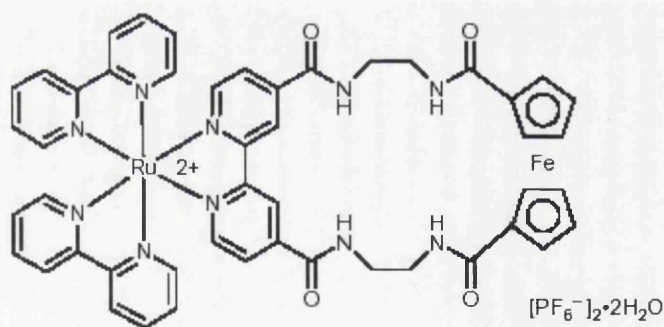


Fig.1.42 Cyclic voltammograms of compound **8** in the presence of increasing amounts of H_2PO_4^- in 1:1 acetonitrile–dichloromethane

Receptor **10** contains multiple redox centres: a redox-active ruthenium bipyridyl moiety and a ferrocene group. The combination of a transition metal fragment with the ferrocene amide group enhances the strength of anion binding. In the presence of chloride anions the amide-substituted bipyridyl reduction wave is shifted cathodically by 40 mV whereas the ferrocene–ferrocenium redox couple is shifted cathodically by 60 mV. The cathodic shift is therefore observed for both redox centres.¹⁷⁸



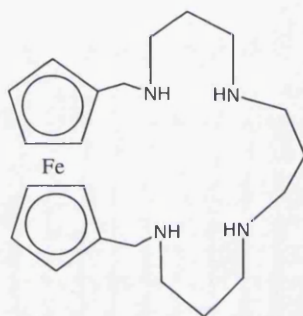
10

Some dendrimers containing three, nine or eighteen ferrocene units show a dendritic effect in anion recognition, and lower poly-ferrocene-substituted calixarenes have been proven to bind and electrochemically to sense anions with large perturbations.¹⁷⁹

1.5.3 Transition metal cations

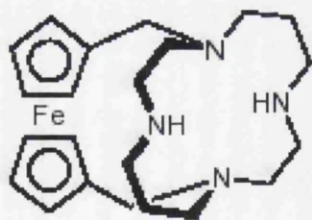
Transition metal cations are important in life processes, playing crucial roles at the active sites of many enzymes, with natural systems exhibiting exquisite control of metal-ion uptake, transport and storage. The development of electrochemical sensors for transition metal cationic guests is currently of considerable interest for a range of biologically important substrates.

The polyaza ferrocene macrocyclic ligand **11** can electrochemically sense various transition metal cations in polar organic solvents and in water at high pH values.¹⁸⁰



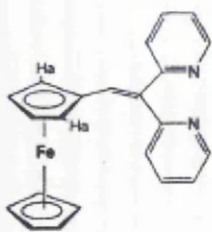
11

A ferrocene-bridged cyclam **12** exhibits large changes in redox properties in the presence of transition metal cations by through space electrostatic interactions.¹⁸¹

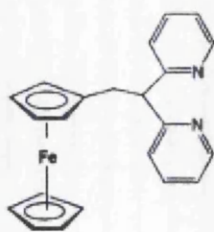


12

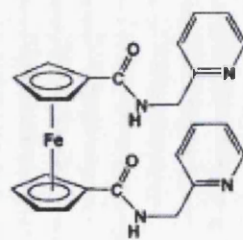
Tucker and co-workers have attached pyridine ligands to ferrocene derivatives **13-15** and monitored their complexation with Mo(0), Pt(II), especially Cu(I) and Zn(II) ions.^{182, 183}



13

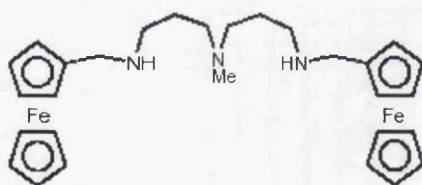


14

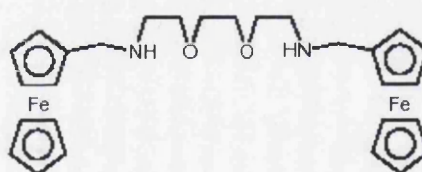


15

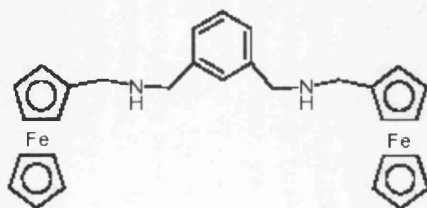
Several complexes containing two ferrocenyl moieties have been synthesized to investigate the effectiveness of the bridging groups between the redox nuclei in facilitating an internuclear interaction. When two ferrocenyl moieties interact electronically with each other, their redox potentials are not identical, and the difference between the two can be used to evaluate the magnitude of the interaction. Beer and Smith have produced a series of acyclic ferrocene receptors, **16-19**, and studied the effects of adding transition metal cations (Ni^{2+} , Cu^{2+} , Zn^{2+} , Ca^{2+} , Pb^{2+}) to solutions of the receptors.¹⁸⁴ The type of electrochemical response fell into two classes, either protonation or metal-ion coordination. Coordination and protonation compete for this type of receptor in acetonitrile solution, and the affinity of the receptor and observed redox response are directly tunable (Fig. 1.43 and Fig. 1.44).



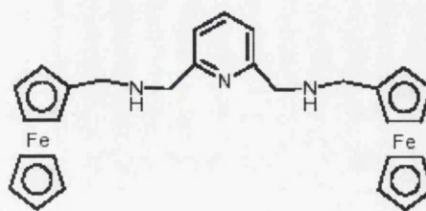
16



17



18



19

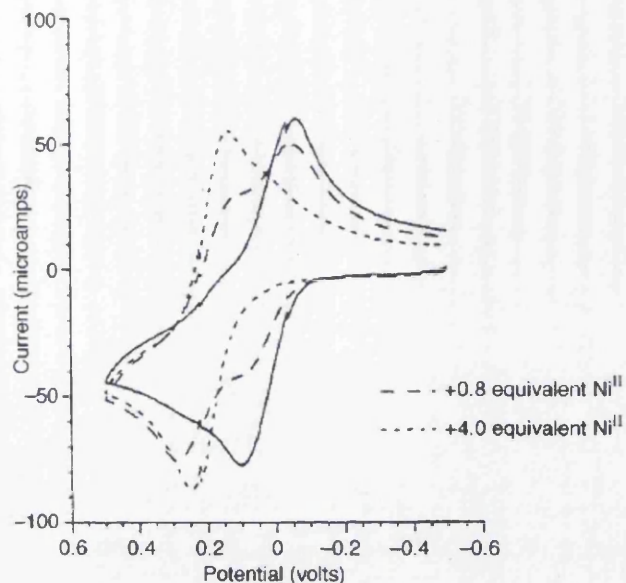


Fig. 1.43 Cyclic voltammogram of receptor **18** and the effect of nickel (II) perchlorate addition (protonation-type response)

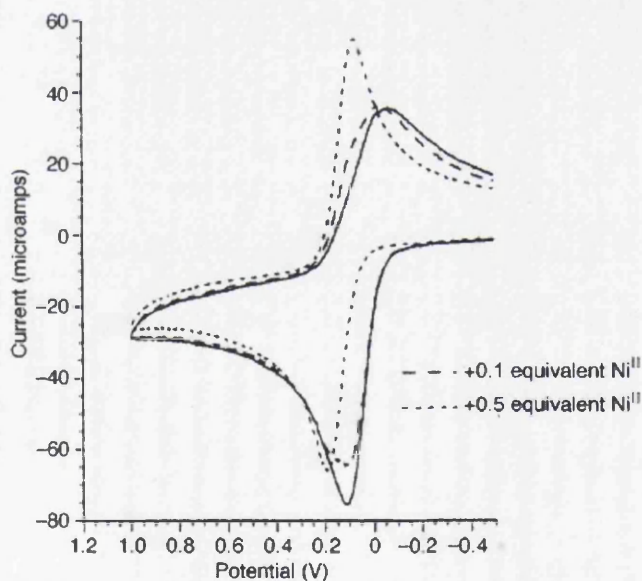
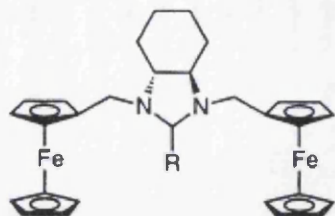


Fig. 1.44 Cyclic voltammogram of receptor **19** and the effect of nickel(II) perchlorate addition (coordination-type response)

Bryce reported that bis(ferrocenyl) derivatives, **20**, containing an imidazoline unit act as efficient voltammetric sensors. Sensors **20a**, **20c** and **20d** respond to Mg^{2+} and Zn^{2+} ions in acetonitrile solution and a new positively shifted redox peak appears (Fig.

1.45). Compounds **20b** and **20e** are selective for Zn^{2+} and Mg^{2+} ions, respectively, whilst **20d** is selectively responsive to Ca^{2+} ions in the presence of several other metal salts.¹⁸⁵



20a (R = H); **20b** (R = CO_2Et); **20c** (R = 2-salicyl);

20d (R = 2-pyridyl); **20e** (R = CH_2OH)

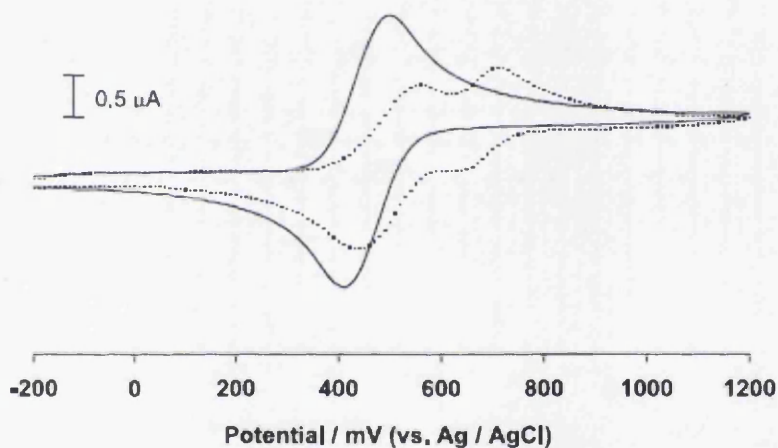
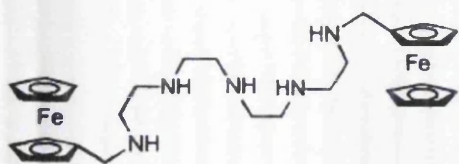
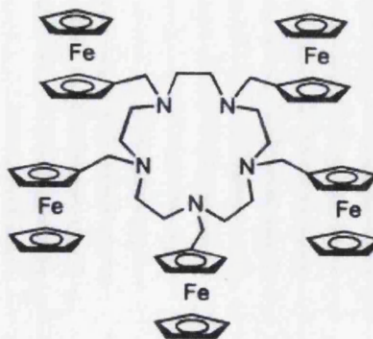


Fig. 1.45 Cyclic voltammograms of **20a** in MeCN (—) and after the addition of $\text{Zn}(\text{ClO}_4)_2$ (0.6 equivalents) (----)

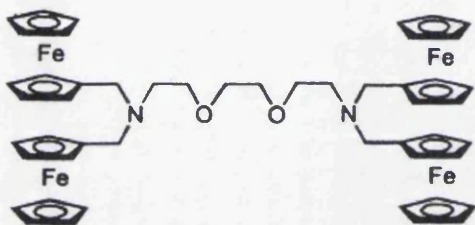
Martínez-Mañez has proved that a combination of coordination properties and suitable redox groups can be a good method strategically to design new receptors for the electrochemical recognition of the toxic heavy metal ions Hg^{2+} and Pb^{2+} in non-aqueous solution, including the selection of suitable binding sites such as aza-oxa derivatives and their functionalisation with ferrocenyl groups. For compounds **21** and **22**, there was a positive shift of the ferrocene oxidation wave in the presence of Ni^{2+} , Cu^{2+} , Zn^{2+} , Cd^{2+} , Hg^{2+} and Pb^{2+} . In contrast, **23** and **24** show two-wave behaviour in response to Pb^{2+} and Hg^{2+} .¹⁸⁶



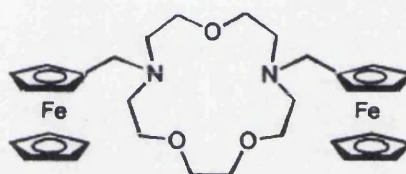
21



22



23



24

In these existing sensors, we can see that the binding atoms are all hard Lewis bases, nitrogen or oxygen, which will prefer to coordinate to hard Lewis acids. The CV experiments conducted so far show that two kinds of signals may appear after host-guest combination: the shift of a wave or the appearance of a new wave. The mechanism for these changes is not always clear.

Our objective is to attach donor atoms to ferrocene, such as Se and Te, which are soft Lewis bases, and prefer to bind soft Lewis acids, such as late transition metals, Pd, Pt, Rh, Hg, Ag and so on. The research aim of this thesis is thus to synthesize novel ferrocenyl chalcogenide ligands and their late transition metal complexes, and the study of relevant electrochemistry will provide information which may eventually lead to the development of a new type of electrochemical sensor.

1.6 References for Chapter One

1. N. N. Greenwood and A. Earnshaw (Eds.), *Chemistry of the Elements*, Pergamon, UK, 1984
2. H. J. Reich, I. L. Reich, J. M. Renga, *J. Am. Chem. Soc.*, 1973, **95**, 5813
3. H. J. Gysling, *Coord. Chem. Rev.*, 1982, **42**, 133
4. S. G. Murray, F. R. Hartley, *Chem. Rev.*, 1981, **81**, 365
5. A. K. Singh, S. Sharma, *Coord. Chem. Rev.*, 2000, **209**, 49
6. E. G. Hope, W. Levason, *Coord. Chem. Rev.*, 1993, **122**, 109
7. W. Levason, S. D. Orchard, G. Reid, *Coord. Chem. Rev.*, 2002, **225**, 159
8. M. G. Kanatzidis, S. P. Huang, *Coord. Chem. Rev.*, 1994, **130**, 509
9. P. Mathur, *Adv. Organomet. Chem.*, 1997, **41**, 243
10. A. K. Singh, S. Sharma, *Coord. Chem. Rev.*, 2000, **209**, 49
11. A. Ogawa, *J. Organomet. Chem.*, 2000, **611**, 463
12. C. Silvestru, J. E. Drake, *Coord. Chem. Rev.*, 2001, **223**, 117
13. T. Kawashima, *Coord. Chem. Rev.*, 2003, **244**, 137
14. T. J. Kealy, P. L. A. Pauson, *Nature*, 1951, **168**, 1039
15. S. A. Miller, J. F. Tebboth, J. F. Tremaine, *J. Chem. Soc.*, 1952, 632
16. A. Togni, T. Hayashi (Eds.), *Ferrocenes: Homogeneous catalysis-organic synthesis-materials science*, VCH, Weinheim, Germany, 1995
17. R. W. Wagner, P. A. Johnson, J. S. Lindsey, *J. Chem. Soc., Chem. Commun.*, 1991, 1463
18. J. S. Miller, A. J. Epstein, *Angew. Chem. Int. Ed. Engl.*, 1994, **33**, 385
19. (a) P. Nguyen, P. Gómez-Elipse, I. Manners, *Chem. Rev.*, 1999, **99**, 1515; (b) S. Barlow, D. O'Hare, *Chem. Rev.*, 1997, **97**, 637; (c) D. R. Kanis, M. A. Ratner, T. J. Marks, *Chem. Rev.*, 1994, **94**, 195; (d) N. J. Long, *Angew. Chem. Int. Ed. Engl.*, 1995, **34**, 21; (e) T. Verbiest, S. Houbrechets, M. Kaurann, K. Clays, A. Persoons, *J. Mater. Chem.*, 1997, **7**, 2175; (f) I. Cuadrado, M. Morán, C. M. Casado, B. Alonso, J. Losada, *Coord. Chem. Rev.*, 1999, **193**, 395; (g) G. G. A. Balavione, J.-C. Daran, G. Iftime, P. G. Lacroix, E. Manoury, J. A. Delaire, I. Maltey-Fanton, K. Nakatani, S. D. Bella, *Organometallics*, 1999, **18**, 21; (h) M. Blancharddesce, C. Runser, A. Fort, M. Barzoukas, J. M. Lehn, V. Alain, *Chem. Phys.*, 1995, **199**, 253
20. H. Hausmann, M. Hoefler, T. Kruck, H.W. Zimmermann, *Chem. Ber.*, 1981,

21. G. Bremer, P. Kluefers, T. Kruck, *Chem. Ber.*, 1985, **118**, 4224
22. E. W. Abel, S. K. Bhargava, P. K. Mittal, K. G. Orrell, V. Šik, *J. Chem. Soc., Dalton Trans.*, 1985, 1561
23. E. W. Abel, S. K. Bhargava, T. E. Mackenzie, P. K. Mittal, K. G. Orrel, V. Sik, *J. Chem. Soc., Chem. Commun.*, 1982, 983
24. E. W. Abel, T. E. Mackenzie, K. G. Orrel, V. Sik, *Polyhedron*, 1987, **6**, 1785
25. E. W. Abel, S. K. Bhargava, T. E. Mackenzie, P. K. Mittal, K. G. Orrel, V. Sik, *J. Chem. Soc., Dalton Trans.*, 1987, 757
26. G. Thaler, K. Wurst, F. Sladky, *Organometallics*, 1996, **15**, 4639
27. C. M. Bates, C. P. Morley, *J. Organomet. Chem.*, 1997, **533**, 197
28. W. Levason, G. Reid, V.-A. Tolhurst, *J. Chem. Soc., Dalton Trans.*, 1998, 3411
29. W. F. Liaw, M. H. Chiang, C.H. Lai, S. J. Chiou, G. H. Lee, S. M. Peng, *Inorg. Chem.*, 1994, **33**, 2493
30. H. Fischer, U. Gerbing, J. Reide, *J. Organomet. Chem.*, 1989, **364**, 155
31. J. K. Shen, Y. C. Gao, Q. Z. Schi, A. L. Rheingold, F. Basolo, *Inorg. Chem.* 1991, **30**, 1868
32. Y. Gao, X. Yang, Q. Shi, *Inorg. Chim. Acta*, 1995, **240**, 661
33. R. Kaur, H. B. Singh, R. J. Butcher, *Organometallics*, 1995, **14**, 4755
34. H. Schumann, *J. Organomet. Chem.*, 1986, **304**,
35. N. Kuhn, H. Schumann, E. Zauder, *J. Organomet. Chem.*, 1988, **354**, 161
36. G. Bremer, R. Boese, M. Keddo, T. Kruck, *Z. Naturforsch., B: Anorg. Chem. Org. Chem.*, 1986, **41**, 981
37. E. W. Abel, G. V. Hutson, *J. Inorg. Nucl. Chem.*, 1969, **31**, 3333
38. G. Hunter, R. C. Massey, *J. Chem. Soc., Dalton Trans.*, 1976, 2007
39. R. Donaldson, G. Hunter, R. C. Massey, *J. Chem. Soc., Dalton Trans.*, 1974, 288
40. G. Hunter, R. C. Massey, *J. Chem. Soc., Dalton Trans.*, 1975, 209
41. A. J. Barton, W. Levason, G. Reid, *J. Organomet. Chem.*, 1999, **579**, 235
42. W. Levason, B. Patel, G. Reid, A. J. Ward, *J. Organomet. Chem.*, 2001, **619**, 218
43. A. J. Barton, J. Connolly, W. Levason, A. Media-Jalon, S. D. Orchard, G. Reid, *Polyhedron*, 2000, **19**, 1373

44. M. K. Davis, M.C. Durrant, W. Levason, G. Reid, R. L. Richards, *J. Chem. Soc., Dalton Trans.*, 1999, 1077
45. C.A. McAuliffe, A. Werfalli, *Inorg. Chim. Acta*, 1982, **64**, L19
46. H.J. Gysling, in S. Patai and Z. Rappoport (Eds.), *The Chemistry of Organic Selenium and Tellurium Compounds*, Vol 1, Wiley, New York, 1986, 679
47. E. Fritzmann, *J. Russ. Phys. Chem. Soc.*, 1915, **47**, 588
48. H. J. Gysling, N. Zumbulyadis, J. A. Roberson, *J. Organomet. Chem.*, 1981, **209**, C41
49. H. J. Gysling, H. R. Luss, D. L. Smith, *Inorg. Chem.*, 1979, **18**, 2696
50. R. K. Chadha, J. M. Chehayber, J.E. Drake, *Inorg. Chem.*, 1986, **25**, 611
51. E. W. Abel, T. E. Mackenzie, K. G. Orrell, V. Sik, *J. Chem. Soc., Dalton Trans.*, 1986, 205
52. T. Kemmitt, W. Levason, *Inorg. Chem.*, 1990, **29**, 731
53. R. Oilunkaniemi, R.S. Laitinen, J. Pursiainen, M. Ahlgren, *Phosphorus Sulfur Silicon*, 1998, **136-138**, 577
54. R. Oilunkaniemi, J. Komulainen, R.S. Laitinen, M. Ahlgren, J. Pursiainen, *J. Organomet. Chem.*, 1998, **571**, 129
55. T. Kemmitt, W. Levason, R. D. Oldroyd, M. Webster, *Polyhedron*, 1992, **11**, 2165
56. A. K. Singh, M. Kadarkaraisamy, S. Husebye, K. W. Tornroos, *J. Chem. Res.*, 2000, **5**, 64
57. W. Levason, G. Reid, V.-A. Tolhurst, *J. Chem. Soc., Dalton Trans.*, 1998, 3411.
58. A. Z. Al-Rubaie, A. Al-Marzook, S. A. N. Al-Jadaan, *Rec. Trav. Chim. Pays-Bas*, 1996, **115**, 427
59. P. K. Khanna, C. P. Morley, *J. Organomet. Chem.*, 1993, **450**, 109
60. A. F. Chiffey, J. Evans, W. Levason, M. Webster, *J. Chem. Soc., Dalton Trans.*, 1994, 2835
61. J. C. Barnes, G. Hunter, M. W. Lown, *J. Chem. Soc., Dalton Trans.*, 1977, 458
62. D. J. Gulliver, W. Levason, *J. Chem. Soc., Dalton Trans.*, 1982, 1895
63. E. G. Hope, W. Levason, M. Webster, S. G. Murray, *J. Chem. Soc., Dalton Trans.*, 1986, 1003
64. E. W. Abel, A. R. Khan, K. Kite, K. G. Orell, V. Sik, T. S. Cameron, R. Cordes, *J. Chem. Soc., Chem. Commun.*, 1979, 713

65. E. W. Abel, A. R. Khan, K. Kite, K. G. Orell, V. Sik, *J. Chem. Soc., Dalton Trans.*, 1980, 1169
66. E. W. Abel, A. R. Khan, K. Kite, M. B. Hursthouse, K. M. A. Malik, M. A. Mazid, *J. Organomet. Chem.*, 1982, **235**, 121
67. E. W. Abel, M. A. Beckett, K. G. Orrell, V. Sik, D. Stephenson, H. B. Singh, N. Sudha, *Polyhedron*, 1988, **7**, 1169
68. E. W. Abel, A. R. Khan, K. Kite, K. G. Orell, V. Sik, *J. Chem. Soc., Dalton Trans.*, 1980, 2220
69. E. W. Abel, S. K. Bhargava, K.G. Orrell, *Prog. Inorg. Chem.*, 1984, **32**, 1
70. E. W. Abel, S. K. Bhargava, K. G. Orrell, A. W. G. Platt, V. Sik, T. S. Cameron, *J. Chem. Soc., Dalton Trans.*, 1985, 345.
71. E. W. Abel, S. K. Bhargava, K. Kite, K. G. Orrell, V. Sik, B. L. Williams, *J. Chem. Soc., Dalton Trans.*, 1982, 583
72. E. W. Abel, K. G. Orrell, S. P. Scanlan, D. Stevenson, T. Kemmitt, W. Levason, *J. Chem. Soc., Dalton Trans.*, 1991, 591.
73. E. W. Abel, A. R. Khan, K. Kite, K. G. Orrell, V. Sik, *J. Chem. Soc., Dalton Trans.*, 1980, 1175
74. K. G. Orrell, *Coord. Chem. Rev.*, 1989, **96**, 1
75. E. Fritzmann, *Z. Anorg. Allgem. Chem.*, 1924, 119
76. E. Fritzmann, *Z. Anorg. Allgem. Chem.*, 1924, 133
77. E. E. Aynsley, N. N. Greenwood, J. B. Leach, *Chem. Ind. (London)*, 1966, 379
78. N. N. Greenwood, G. Hunter, *J. Chem. Soc. (A)*, 1967, 1520
79. H. J. Whitfield, *J. Chem. Soc. (A)*, 1970, 113
80. G. Hunter, R. C. Massey, *Chem. Commun.*, 1973, 797
81. G. Hunter, R. C. Massey, *J. Chem. Soc., Dalton Trans.*, 1976, 2007
82. N. N. Greenwood, G. Hunter, *J. Chem. Soc. (A)*, 1969, 929
83. D. M. Roundhill, S. G. N. Roundhill, W. B. Beaulieu, U. Bagchi, *Inorg. Chem.*, 1980, **19**, 3365
84. P. J. Hendra, N. Sadasivan, *J. Chem. Soc.*, 1965, 2063
85. D. J. Gulliver, E. G. Hope, W. Levason, S. G. Murray, G. L. Marshall, *J. Chem. Soc., Dalton Trans.*, 1985, 1265
86. T. Kumagai, S. Akabori, *Chem. Lett.*, 1989, 1667
87. E. G. Hope, W. Levason, S. G. Murray, G. L. Marshall. *J. Chem. Soc., Dalton*

- Trans.*, 1985, 2185
88. S. K. Harbron, S. J. Higgins, E. G. Hope, T. Kemmitt, W. Levason, *Inorg. Chim. Acta*, 1987, **130**, 43
 89. D. M. Roundhill, S. G. N. Roundhill, W. B. Beaulieu, U. Bagchi, *Inorg. Chem.*, 1980, **19**, 3365
 90. S. K. Harbron, S. J. Higgins, E. G. Hope, T. Kemmitt, W. Levason, *Inorg. Chim. Acta*, 1987, **130**, 43
 91. E. W. Abel, D. G. Evans, J. R. Koe, V. Sik, P. A. Bates, M. B. Hursthouse, *J. Chem. Soc., Dalton Trans.*, 1989, 2315
 92. T. Kemmitt, W. Levason, M. Webster, *Inorg. Chem.*, 1989, **28**, 692
 93. T. Kemmitt, W. Levason, *Inorg. Chem.*, 1990, **29**, 731
 94. H. M. K. K. Pathirana, A. W. Downs, W. R. McWhinnie, P. Granger, *Inorg. Chim. Acta*, 1988, **143**, 161
 95. B. L. Khandelwal, A. Khalid, A. K. Singh, T. P. Singh, S. Karthikeyan, *J. Organomet. Chem.*, 1996, **507**, 65
 96. N. R. Champness, W. Levason, J. J. Quirk, G. Reid, C. S. Frampton, *Polyhedron*, 1995, **14**, 2753
 97. T. Kemmitt, W. Levason, M. D. Spicer, M. Webster, *Organometallics*, 1990, **9**, 1181
 98. N. R. Champness, P. F. Kelly, W. Levason, G. Reid, A. M. Z., Slawin, D. J. Williams, *Inorg. Chem.*, 1995, **34**, 651
 99. W. Levason, S. D. Orchard, G. Reid, V.-A. Tolhurst, *J. Chem. Soc., Dalton Trans.*, 1999, 2071
 100. W. Levason, B. Patel, G. Reid, A. J. Ward, *J. Organomet. Chem.*, 2001, **619**, 218
 101. W. Levason, S. D. Orchard, G. Reid, *Inorg. Chem.*, 2000, **39**, 3853
 102. W. Levason, C. A. McAuliffe, S. G. Murray, *J. Chem. Soc., Dalton Trans.*, 1976, 269
 103. E. W. Abel, K. Kite, P. S. Perkins, *Polyhedron*, 1986, **5**, 1459
 104. E. W. Abel, K. Kite, P. S. Perkins, *Polyhedron*, 1987, **6**, 549
 105. M. Hesford, W. Levason, S. D. Orchard, G. Reid, *J. Organomet. Chem.*, 2002, **649**, 214
 106. A. J. Barton, W. Levason, G. Reid, A. J. Ward, *Organometallics*, 2001, **20**, 3644

107. R. J. Batchelor, F. W. B. Einstein, I. D. Gay, J. Gu, B. M. Pinto, X. Zhou, *Inorg. Chem.*, 1996, **35**, 3667
108. W. Levason, J. J. Quirk, G. Reid, C. S. Frampton, *Inorg. Chem.*, 1994, **33**, 6120
109. U. Behrens, P. Berges, R. Bieganski, W. Hinrichs, C. Schiffing, G. Klar, *J. Chem. Res.(s)*, 1986, 326
110. P. E. Skakke, S. E. Rasmussen, *Acta Chem. Scand.*, 1970, **24**, 2634
111. A. R. Siedle, M. C. Retter, M. E. Jones, G. Filipovich, H. E. Mishmash, W. Bahmet, *Inorg. Chem.*, 1982, **21**, 2624
112. A. K. Singh, V. Srivastava, S. K. Dhingra, J. E. Drake, J. E. Bailey, *Acta Crystallogr. Sect. C*, 1992, **48**, 655
113. M. Romanov, A. V. Ablov, N. V. Gerbeleu, *Russ. J. Inorg. Chem.*, 1969, **14**, 196
114. C. Bornet, R. Amardeil, P. Meunier, J. C. Daran, *J. Chem. Soc., Dalton Trans.*, 1999, 1039
115. A. K. Singh, C. V. Amburose, M. Misra, R. J. Butcher, *J. Chem. Res. (S)*, 1999, 716
116. C. Levanda, K. Bechgaard., D. O. Cowan, *J. Org. Chem.*, 1976, **41**, 2700
117. W. H. Morrison, S. Krogsrud, D. N. Hendrickson, *Inorg. Chem.*, 1973, **12**, 1998
118. P. Shu, K. Bechgaard, D. Cowan, *J. Org. Chem.*, 1976, **41**, 1849
119. C. Levanda, D. Cowan, C. Leitch, K. Bechgaard, *J. Am. Chem. Soc.*, 1974, **96**, 6788
120. J. A. Kramer, F. H. Herbstein, D. H. Hendrickson, *J. Am. Chem. Soc.*, 1980, **102**, 2293
121. C. Levanda, K. Bechgaard, D. O. Cowan, M. D. Rausch, *J. Am. Chem. Soc.*, 1977, **99**, 2964
122. G. M. Brown, T. J. Meyer, D. O. Cowan, C. L. Vanda, F. Kaufman, P. V. Roling, Rausch M. D., *Inorg. Chem.*, 1975, **14**, 506
123. W. H. Morrison, E. Y. Ho, D. N. Hendrickson, *Inorg. Chem.*, 1975, **14**, 500
124. K. M. Kadish, Q. Y. Xu, J. M. Barbe, *Inorg. Chem.*, 1987, **26**, 2565
125. A. Ribou, J. Launay, M. L. Sachtleben, H. Li, C. W. Spangler, *Inorg. Chem.*, 1996, **35**, 3735
126. B. Bildstein, M. Malaun, H. Kopacka, M. Fontani, P. Zanello, *Inorg. Chim.*

Acta, 2000, **300-302**, 16

127. Y. J. Chen, D. Pan, C. Chiu, J. X. Su, S. J. Lin, K. S. Kwan, *Inorg. Chem.*, 2000, **39**, 953
128. S. Kumar, S. K. Tripathi, H. B. Singh, G. Wolmershäuser, *J. Organomet. Chem.*, 2004, **689**, 3046
129. J. B. Flanagan, S. Margel, A. J. Bard, F. Anson, *J. Am. Chem. Soc.*, 1978, **100**, 4248
130. T. W. Smith, J. Kuder, D. Wychick, *J. Polym. Sci., Polym. Chem. Ed.*, 1976, **A14**, 2433
131. P. Zanello, G. Opromolla, M. Herberhold, H. Brendel, *J. Organomet. Chem.*, 1994, **484**, 67
132. H. Atzkern, J. Hiermeier, B. Kanellakopoulos, F. H. Köhler, G. Müller, O. Steigelmann, *J. Chem. Soc., Chem. Commun.*, 1991, 997
133. H. Atzkern, J. Hiermeier, F. H. Köhler, A. Steck, *J. Organomet. Chem.*, 1991, **408**, 281
134. S. Barlow, D. O'Hare, *Chem. Rev.*, 1997, **97**, 637
135. H. Wadepohl, C. W. Vonderlieth, F. J. Paffen, H. Pritzkow, *Chem. Ber.*, 1995, **128**, 317
136. D. A. Foucher, C. H. Honeyman, J. M. Nelson, B. Z. Tang, I. Manners, *Angew. Chem. Int. Ed. Engl.*, 1993, **32**, 1709
137. J. M. Nelson, H. Rengel, I. Manners, *J. Am. Chem. Soc.*, 1993, **115**, 7035
138. J. B. Flanagan, S. Margel, A. J. Bard, F. C. Anson, *J. Am. Chem. Soc.*, 1978, **100**, 4248
139. J. E. Gorton, H. L. Lentzner, W. E. Watts, *Tetrahedron*, 1971, **27**, 4353
140. H. Atzkern, F. H. Köhler, R. Müller, *Z. Naturforsch. B: Chem. Sci.*, 1990, **45**, 329
141. T. Y. Dong, T. J. Ke, S. M. Peng, S. K. Yeh, *Inorg. Chem.*, 1989, **28**, 2103
142. A. Ribou, J. Launay, M. L. Sachtleben, H. Li, C. W. Spangler, *Inorg. Chem.*, 1996, **35**, 3735
143. E. Bunel, P. Campos, J. Ruz, L. Valle, I. Chadwick, M. S. Ana, G. Gonzalez, J. M. Manriquez, *Organometallics*, 1988, **7**, 474
144. J. M. Manriquez, M. D. Ward, J. C. Calabrese, P. J. Fagan, A. J. Epstein, J. S. Miller, *Mol. Cryst. Liq. Cryst.*, 1989, **176**, 527
145. M. T. Lee, B. M. Foxman, M. Rosenblum, *Organometallics*, 1985, **4**, 539

146. M. J. MacLachlan, A. J. Lough, W. E. Geiger, I. Manners, *Organometallics*, 1998, **17**, 1873
147. V. V. Dementev, F. Cervanteslee, L. Parkanyi, H. Sharma, K. H. Pannell, M. T. Nguyen, A. Dlaz, *Organometallics*, 1993, **12**, 1983
148. R. Rulkens, A. J. Lough, I. Manners, *J. Am. Chem. Soc.*, 1994, **116**, 797
149. D. A. Foucher, C. H. Honeyman, J. M. Nelson, B. Z. Tang, I. Manners, *Angew. Chem. Int. Ed. Engl.*, 1993, **32**, 1709
150. D. Foucher, R. Ziembinski, R. Petersen, J. Pudelski, M. Edwards, Y. Z. Ni, J. Massey, C. R. Jaeger, G. J. Vancso, I. Manners, *Macromolecules*, 1994, **27**, 3992
151. P. Nguyen, P. Gómez-Elipse, I. Manners, *Chem. Rev.*, 1999, **99**, 1515
152. D. L. Zechel, D. A. Foucher, J. K. Pudelski, G. P. A. Yap, A. L. Rheingold, I. Manners, *J. Chem. Soc., Dalton Trans.*, 1995, 1893
153. R. Petersen, D. A. Foucher, A. J. Lough, I. Manners, *Phosphorus Sulfur and Silicon and the Relat. Elem.*, 1994, **93**, 359
154. U. Siemeling, P. Jutzi, E. Bill, A. X. Trautwein, *J. Organomet. Chem.*, 1993, **463**, 151
155. H. Atzkern, P. Bergerat, M. Fritz, J. Hiermeier, P. Hudeczek, O. Kahn, B. Kanellakopulos, F. H. Köhler, M. Ruhs, *Chem. Ber.*, 1994, **127**, 277
156. R. N. Kapoor, G. M. Crawford, J. Mahmoud, V. V. Dementiev, M. T. Nguyen, A. F. Diaz, K. H. Pannell, *Organometallics*, 1995, **14**, 4944
157. T. Y. Dong, M. Y. Hwang, Y. S. Wen, W. S. Hwang, *J. Organomet. Chem.*, 1990, **391**, 377
158. G. Utri, K. E. Schwarzans, G. M. Allmaier, *Z. Naturforsch.*, 1990, **45B**, 755
159. D. O. Cowan, P. Shu, F. L. Hedberg, M. Rossi, T. J. Kistenmacher, *J. Am. Chem. Soc.*, 1979, **101**, 1304
160. C. H. Honeyman, D. A. Foucher, F. Y. Dahmen, R. Rulkens, A. J. Lough, I. Manners, *Organometallics*, 1995, **14**, 5503
161. D. C. O. Salazar, D. O. Cowan, *J. Organomet. Chem.*, 1991, **408**, 227
162. V. V. Dementev, F. Cervanteslee, L. Parkanyi, H. Sharma, K. H. Pannell, M. T. Nguyen, A. Dlaz, *Organometallics*, 1993, **12**, 1983
163. P. F. Brandt, T. B. Rauchfuss, *J. Am. Chem. Soc.*, 1992, **114**, 1926
164. D. L. Compton, T. B. Rauchfuss, *Organometallics*, 1994, **13**, 4367
165. D. L. Compton, P. F. Brandt, T. B. Rauchfuss, D. F. Rosenbaum, C. F.

- Zukoski, *Chem. Mater.*, 1995, **7**, 2342
166. P. D. Beer, P. A. Gale, Z. Chen, *Adv. Phys. Org. Chem.*, 1998, **31**, 1
167. L. Fabbrizzi, A. Poggi, *Chem. Soc. Rev.*, 1995, **24**, 197
168. G. Oepen, F. Vogtle, *Liebigs Ann. Chem.*, 1979, **8**, 1094
169. T. Saji, *Chem. Lett.*, 1986, **3**, 275
170. T. Saji, I. Kinoshita, *J. Chem. Soc., Chem. Commun.*, 1986, 716
171. P. D. Beer, Z. Chen, A. J. Pilgrim, *J. Chem. Soc., Faraday Trans.*, 1995, 4331
172. A. Chesney, M. R. Bryce, A. S. Batsanov, J. A. K. Howard, L. M. Goldenberg, *Chem. Commun.*, 1998, 677
173. O. B. Sutcliffe, A. Chesney, M. R. Bryce, *J. Organomet. Chem.*, 2001, **637-639**, 134
174. O. B. Sutcliffe, M. R. Bryce, A. S. Batsanov, *J. Organomet. Chem.*, 2002, **656**, 211
175. P. D. Beer, J. Cadman, *Coord. Chem. Rev.*, 2000, **205**, 131
176. P. D. Beer, A. R. Graydon, A. O. M. Johnson, D. K. Smith, *Inorg. Chem.*, 1997, **36**, 2112
177. J. E. Kingston, L. Ashford, P. D. Beer, M. G. B. Drew, *J. Chem. Soc., Dalton Trans.*, 1999, 251
178. P. D. Beer, F. Szemes, V. Balzani, C. M. Salà, M. G. B. Drew, S. W. Dent, M. Maestri, *J. Am. Chem. Soc.*, 1997, **119**, 11864
179. (a) C. Valerio, J. L., Fillaut, J. Ruiz, J. Guittard, J. C. Blais, D. Astruc, *J. Am. Chem. Soc.*, 1997, **119**, 2588; (b) P. A. Gale, Z. Chen, M. G. B. Drew, J. A. Heath, P. D. Beer, *Polyhedron*, 1998, **17**, 405
180. P. D. Beer, Z. Chen, M. G. B. Drew, A. O. M. Johnson, D. K. Smith, P. Spencer, *Inorg. Chim. Acta*, 1996, **246**, 143
181. H. Plenio, C. Aberle, *Chem. Commun.*, 1998, 2697
182. J. D. Carr, S. J. Coles, M. B. Hursthouse, J. H. R. Tucker, *J. Organomet. Chem.*, 2001, **637-639**, 304
183. M. E. Light, E. L. Munro, J. H. R. Tucker, J. Westwood, *Organometallics*, 2000, **19**, 3312
184. P. D. Beer, D. K. Smith, *J. Chem. Soc., Dalton Trans.*, 1998, 417
185. O. B. Sutcliffe, M. R. Bryce, A. S. Batsanov, *J. Organomet. Chem.*, 2002, **656**, 211
186. J. M. Lloris, R. Martínez-Máñez, J. Soto, T. Pardo, *J. Organomet. Chem.*,

CHAPTER TWO

Synthesis of Novel Ferrocenyl Chalcogenide Compounds

BACKGROUND, RESULTS AND DISCUSSION

2.1 Background to synthesis and characterisation of ferrocenylchalcogenide compounds

Existing ferrocenylchalcogenide compounds can be divided into four main categories: (1) Chalcogenaferrocenophanes; (2) Mono- and dichalcogenoferrocenes; (3) Diferrocenyl dichalcogenides and their derivatives; (4) Chalcogenide-bridged polyferrocenes. The relevant literature is summarized below.

2.1.1 Chalcogenaferrocenophanes

2.1.1.1 Chalcogena[1]ferrocenophanes

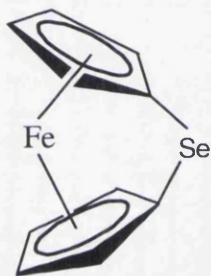


Fig. 2.1 Selena[1]ferrocenophane $[\text{Fe}\{(\eta\text{-C}_5\text{H}_4)_2\text{Se}\}]$

Since the first silicon-bridged [1]ferrocenophane was isolated in 1975 by Osborne and co-workers,¹ [1]ferrocenophanes with group 14 (E = Si, Ge, Sn), group 15 (E = P, As), and group 4 (E = Ti, Zr, Hf) bridging elements have been prepared and characterized.² The first reported chalcogen-bridged [1]ferrocenophane $[\text{Fe}\{(\eta\text{-C}_5\text{H}_4)_2\text{Se}\}]$ ³ (shown in Fig. 2.1) was obtained by the reaction of dilithioferrocene·TMEDA with selenium diethyldithiocarbamate $\text{Se}(\text{S}_2\text{CNET}_2)_2$ in 20-30% yields. Its molecular structure reveals a ring-tilt (α) of $26.4(3)^\circ$ (shown in Fig. 2.2), which reflects the strained structure and is substantially greater than that in the S analogue ($\alpha = 31.05(10)^\circ$). The ^1H NMR spectrum showed two pseudotriplets which were less separated than for the sulphur analogue. In the ^{13}C NMR spectrum, three resonances were observed for the Cp carbons: the signal for the *ipso*-carbon atom was found at 5.6 ppm, which is surprisingly further upfield than the analogous one bound to sulphur (14.3 ppm). The ^{77}Se NMR spectrum showed a singlet at 435 ppm, which is shifted slightly downfield from the resonance observed in diaryl

selenides such as Ph_2Se (402 ppm)⁴ and dramatically shifted downfield with respect to the ^{77}Se resonance of $\text{C}_5\text{H}_4\text{Se}$ in fcSe_3 (308 ppm).⁵

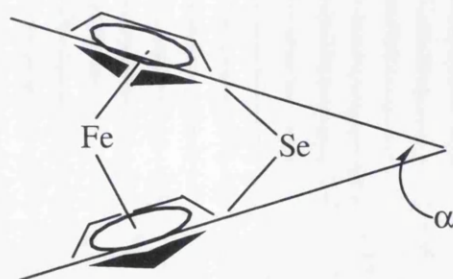


Fig. 2.2 Ring-tilt angle (α) in $[\text{Fe}\{(\eta\text{-C}_5\text{H}_4)_2\text{Se}\}]$

A substituted chalcogen-bridged [1]ferrocenophane (selena-2,2',4,4'-tetrakis(trimethylsilyl)[1]ferrocenophane) was obtained by the reaction of the dianion of bis[bis(trimethylsilyl)cyclopentadienyl]selane with FeCl_2 (shown in Fig. 2.3).⁶ There are only two singlets at 3.96 and 5.02 ppm in the ^1H NMR spectrum, assigned to the α and γ Cp protons. In the ^{13}C NMR spectrum, the resonance of the Cp-Se *ipso*-carbon appears at 11.5 ppm, a similar shift to that in other [1]ferrocenophanes, reflecting the structural distortion of these highly strained molecules. The molecular structure reveals a ring-tilt (α) of $26.9(2)^\circ$ (shown in Fig. 2.4), 0.5° larger than in the unsubstituted selena[1]ferrocenophane and 4.1° smaller than in thia[1]ferrocenophane.³

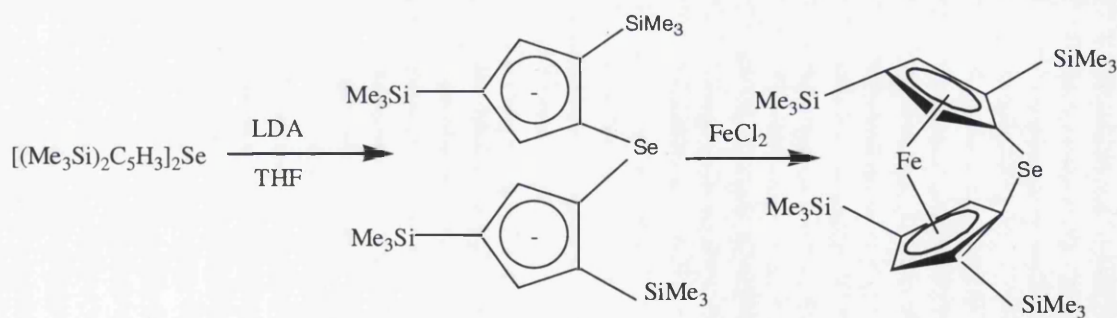


Fig. 2.3 Synthetic scheme for selena-2,2',4,4'-tetrakis(trimethylsilyl)[1]ferrocenophane

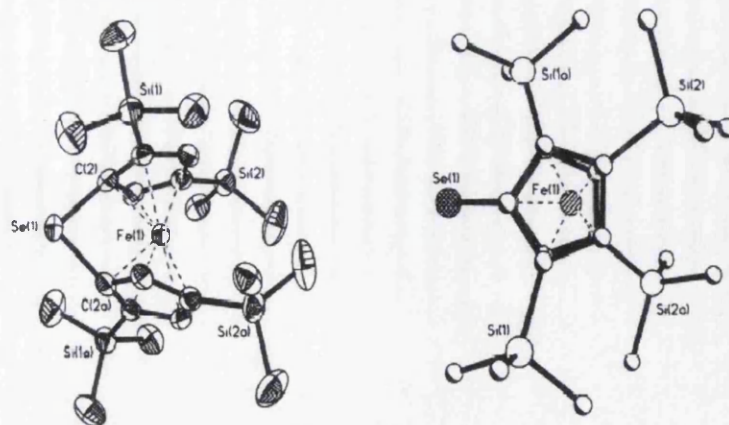


Fig. 2.4 Molecular structure of
seleno-2,2',4,4'-tetrakis(trimethylsilyl)[1]ferrocenophane

2.1.1.2 Chalcogena[3]ferrocenophanes $[\text{Fe}\{\eta\text{-C}_5\text{H}_4\text{E}\}_2\text{E}']$ (E = Se, Te)

2.1.1.2.1 E' = S, Se, Te

After the first 1,2,3-trichalcogena[3]ferrocenophane, fcS_3 ,⁷ was obtained in 1969, fcSe_3 and fcTe_3 were described in 1979 and 1990 respectively.^{8,9} 1,2,3-Trichalcogena[3]ferrocenophanes can be obtained through the method shown in Fig. 2.5, which involves insertion of the chalcogen E into the carbon-lithium bonds of fcLi_2 , and subsequent oxidation of the dilithium 1,1'-ferrocenylene dichalcogenolate, $\text{fc}(\text{ELi})_2$, by the chalcogen E' (E' = S, Se, Te). All nine 1,2,3-trichalcogena[3]ferrocenophanes have been obtained.¹⁰⁻¹⁹

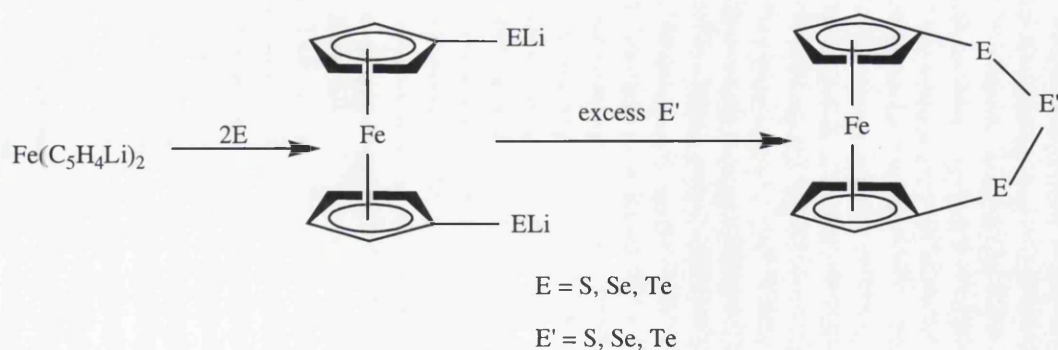


Fig. 2.5 Synthetic scheme for 1,2,3-trichalcogena[3]ferrocenophanes

The solid state structure of 1,2,3-trichalcogena[3]ferrocenophanes shows a lattice of molecules containing two almost coplanar and eclipsed cyclopentadienyl rings (see example in Fig. 2.6).^{9, 18}

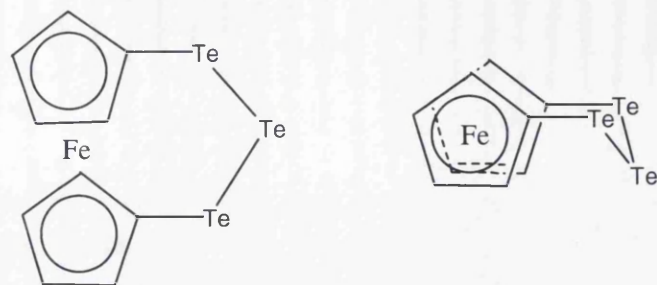


Fig. 2.6 Two representations of $fcTe_3$ in the solid state

The crystallographics of fcS_2Se ¹⁶ and $fcTe_3$ ⁹ show that the displacement of the ring-attached chalcogens E from their cyclopentadienyl ring plane is small: 22 pm in $fcTe_3$ and 4 pm in fcS_2Se . And the deviation of the rings from an exact parallel arrangement (“ring canting”) is also small: 4.6-5.0° for $fcTe_3$ and 2.9° for fcS_2Se .

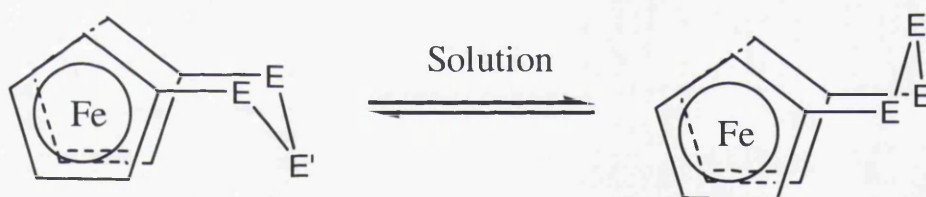


Fig. 2.7 Bridge reversal in [3]ferrocenophanes

The 1,2,3-trichalcogena[3]ferrocenophanes are non-rigid molecules in solution.^{7, 12, 14, 15, 19, 20} Abel and his coworkers^{14, 19, 20} have confirmed a hindered intramolecular motion (shown in Fig. 2.7) by temperature-dependent 1H and ^{13}C NMR spectroscopy. The calculations indicated that a transition state with a staggered conformation of the cyclopentadienyl rings might be energetically preferable to a transition state in which the $EE'E$ bridge becomes coplanar with the iron atom.²⁰ The free activation enthalpy, ΔG^\ddagger , of the “bridge-inversion” rearrangement decreases as the size of the chalcogen atoms in the bridge increases, such that fcS_3 (ΔG^\ddagger (298K) = 80.4 ± 0.2 kJ mol⁻¹) >

fcSe_3 (ΔG^\ddagger (298K) = 67.2 ± 0.1 kJ mol⁻¹) > fcTe_3 (ΔG^\ddagger (298K) = 51.8 ± 0.2 kJ mol⁻¹).^{14, 20}

The substituted compound, 1,2,3-triseleno-2,2',4,4'-tetrakis(trimethylsilyl)-[3]ferrocenophane, can be obtained in a similar way to seleno-2,2',4,4'-tetrakis(trimethylsilyl)[1]ferrocenophane (shown in Fig. 2.8).⁶ Due to the lower strain in this molecule than in [1]ferrocenophanes, the ¹H NMR spectrum shows the α and γ Cp protons less widely separated at 3.95 and 4.11 ppm and the ¹³C NMR shift of the *ipso*-C is 24.0 ppm. The structural data show the Cp rings are eclipsed and almost coplanar just like the other 1,2,3-trichalcogena[3]ferrocenophane series (shown in Fig. 2.9).⁹

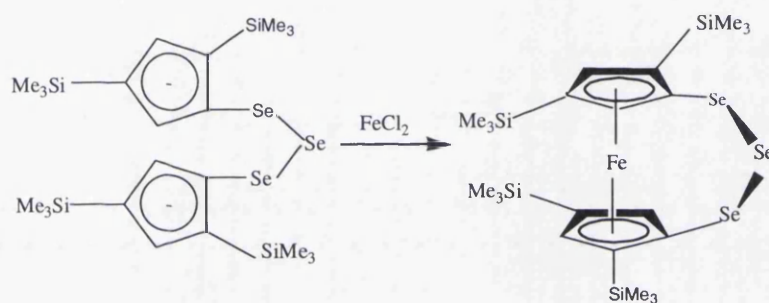


Fig. 2.8 Synthetic scheme for
1,2,3-triseleno-2,2',4,4'-tetrakis(trimethylsilyl)[3]ferrocenophane

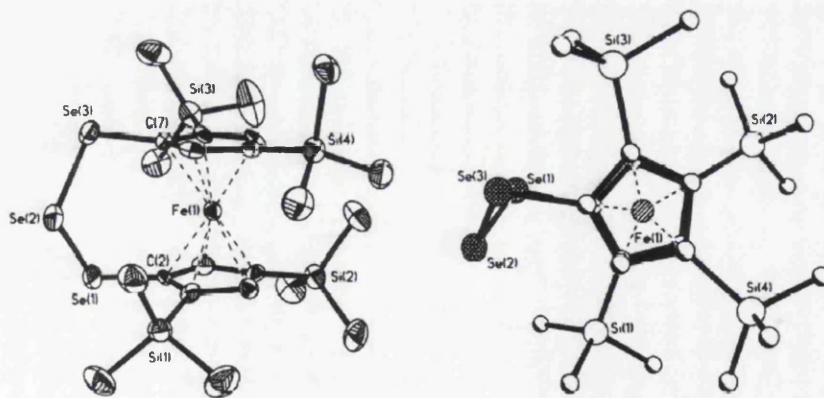


Fig. 2.9 Molecular structure of
1,2,3-triseleno-2,2',4,4'-tetrakis(trimethylsilyl)[3]ferrocenophane

2.1.1.2.2 E' is an element of Group 13, 14, 15

A large number of 1,3-trichalcogena[3]ferrocenophanes, fcE_2E' , has been obtained in which E' is an element of the main groups 13, 14, 15. The most general route is treating the 1,1'-dilithioferrocene intermediate $fcLi_2 \cdot TMEDA$ with chalcogen followed by the appropriate dihalide $E'X_2$. The other two routes, from 1,1'-ferrocenylene dichalcogenols, $fc(EH)_2$, or from 1,1'-bis(trimethylstannylchalcogeno)ferrocenes, $fc(ESnMe_3)_2$, were also used occasionally. All the relative literature work is summarized in Table 2.1.

Table 2.1 Literature references to 1,3-trichalcogena[3]ferrocenophanes

E'	E	
BNEt ₂	Se ²¹	Te ²¹
CH ₂	Se ^{13, 18, 22, 23}	Te ¹⁸
CPh ₂	Se ^{13, 23}	
SiMePh	Se ^{13, 23}	
SiMe ₂	Se ²³	Te ²¹
GeCl ₂	Se ²⁴	
SnCl ₂	Se ²⁴	
SnMe ₂	Se ^{23, 24}	Te ²⁵
SnPh ₂	Se ²³	
Pb	Se ²³	
PCl	Se ²¹	
PPh	Se ^{13, 26}	
P(S)Ph	Se ^{13, 26}	
P ^t Bu	Se ²¹	Te ²¹
AsPh	Se ²⁶	
As ^t Bu	Se ²¹	Te ²¹
Sb ^t Bu	Se ²¹	Te ²¹

Group 14 elements C, Si, Ge, Sn and Pb

Like 1,2,3-trichalcogena[3]ferrocenophanes, $[\text{Fe}\{(\eta\text{-C}_5\text{H}_4\text{E})_2\text{CH}_2\}]$ (E = Se, Te) are non-rigid molecules. From the ^{13}C NMR data, the shielding of the methylene carbon (CH_2) increased markedly when the two chalcogen atoms were changed from sulphur (52.7 ppm) to selenium (33.8 ppm) to tellurium (-25.2 ppm).¹⁸

Ferrocene-1,1'-diselenol reacted with tin dihalide reagents to afford good yields of $\text{SnR}_2(\text{Se}_2\text{fc})$ (R = CH_3 , C_6H_5), but the reaction with tin tetrachloride yielded a spiro compound, $\text{Sn}(\text{Se}_2\text{fc})_2$. The crystal structure of $\text{Sn}(\text{Se}_2\text{fc})_2$ shows the molecule is based on a pseudo-tetrahedral tin(IV) centre with angle Se-Sn-Se $108.6(1)^\circ$; the Sn-Se bond lengths are 2.516(1) and 2.539(1) Å, the Se-C bond lengths are 1.901(4) and 1.903(4) Å, with C-Se-Sn angles of $98.6(1)$ and $99.7(1)^\circ$ (shown in Fig. 2.10). Ferrocene-1,1'-diselenol reacted with lead(II) acetate in aqueous ethanol to give $\text{Pb}(\text{Se}_2\text{fc})$, which is an air-stable solid insoluble in all common organic solvents.²³

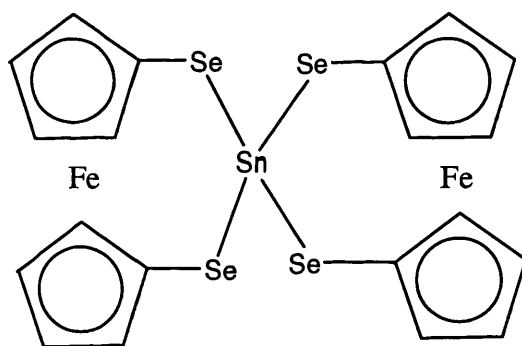


Fig. 2.10 The structure of $\text{Sn}(\text{Se}_2\text{fc})_2$

Herberhold and his coworkers also have synthesized some spiro compounds of the type $\text{Z}(\text{E}_2\text{fc})_2$ (Z = Si, Sn).^{21,18} The colour becomes deeper as the elements E and Z become heavier.^{9,21,24} All except $\text{Z}(\text{Te}_2\text{fc})_2$ are thermally stable, decomposing only above 200°C (Z = Si) or 250°C (Z = Ge, Sn).¹⁸ Different tin complexes can be obtained by the methods shown in Fig. 2.11.²⁵

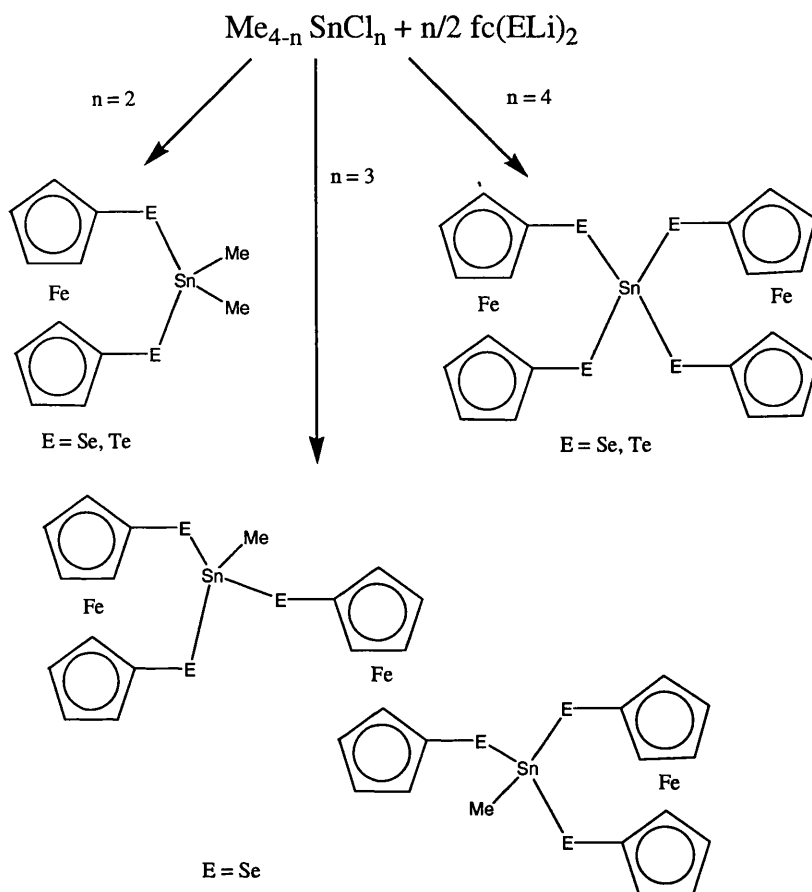


Fig. 2.11 Synthetic scheme for different tin complexes

Group 15 elements P, As, Sb

The reactions of MCl_3 ($\text{M} = \text{P, As, Sb}$) and 1,1'-bis(trimethylstannylchalcogeno)ferrocene, $\text{fc}(\text{ESnMe}_3)_2$, in the ratio 2:3, yield trinuclear products $\text{fc}(\text{EME}_2\text{fc})_2$ ($\text{E} = \text{Se, Te}$) (shown in Fig. 2.12).²¹ They can also be synthesized from $\text{fc}(\text{ELi})_2$ and MCl_3 . By oxidation with 3-chloroperbenzoic acid, the trinuclear phosphorus selenium compound will give $\text{fc}[\text{SeP}(\text{O})\text{Se}_2\text{fc}]_2$. Using PCl_3 will produce side-products: mononuclear $(\text{fcE}_2)\text{PCl}$ and binuclear $(\text{fcE}_2)\text{P}-\text{P}(\text{E}_2\text{fc})$.

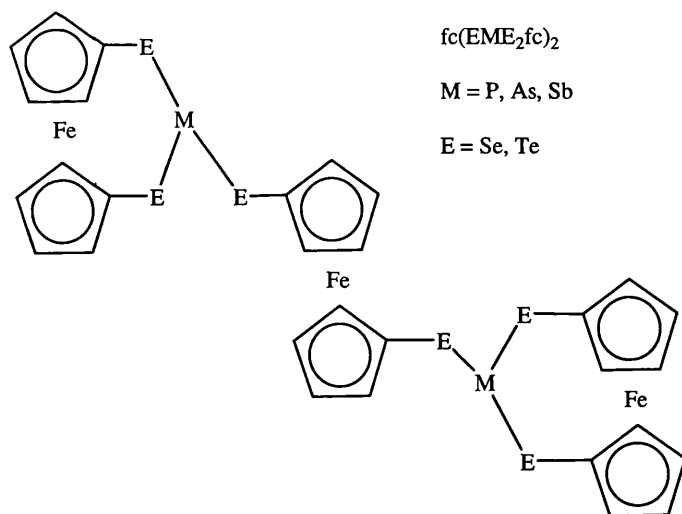


Fig. 2.12 The structure of $fc(EME_2fc)_2$ ($M = P, As, Sb$; $E = Se, Te$)

The reaction between $fc(SeLi)_2$ and the trimeric phosphazene dichloride, hexachlorocyclotriphosphazene ($N_3P_3Cl_6$), under stepwise replacement of the three pairs of geminal chloro-substituents gives spiro-cyclotriphosphazenes, $N_3P_3Cl_{6-2n}[Se_2fc]_n$ ($n = 1, 2, 3$).²⁷

1,3-Trichalcogena[3]ferrocenophanes containing a transition metal complex fragment as E' will be discussed in Chapter Three.

2.12 Compounds with ferrocenyl chalcogenide or 1,1'-ferrocenylene dichalcogenide groups

2.1.2.1 Compounds with ferrocenyl chalcogenide groups

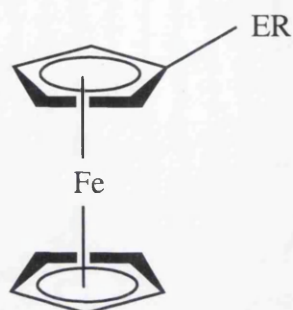


Fig. 2.13 The structure of FcER

There are four routes reported in the literature to synthesize the compounds shown in Fig. 2.13.

(1) From ferrocenyl selenocyanate, differrocenyl selenide and ferrocenyl butyl selenide could be synthesized in high yield (shown in Fig. 2.14),²⁸ but the special starting material made this route unpopular.

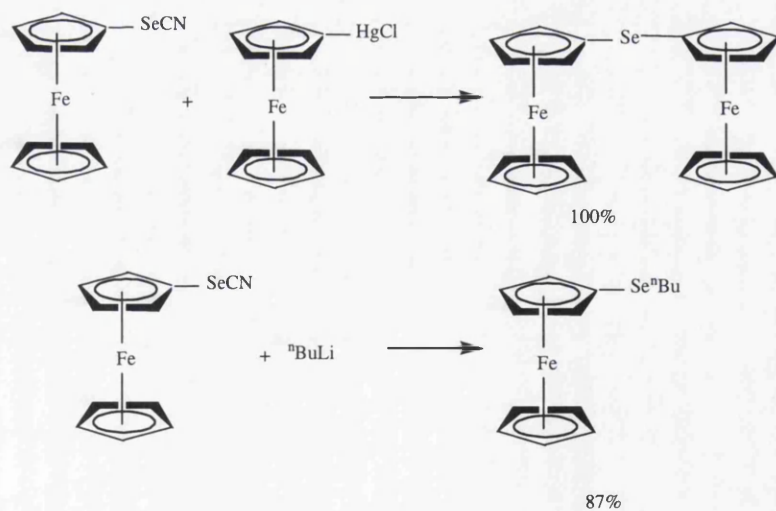


Fig. 2.14 Synthetic methods for differrocenyl selenide and ferrocenyl butyl selenide from ferrocenyl selenocyanate

(2) Honeychuck reported the synthesis of (methylseleno)ferrocene in 1986, by adding Me_2Se_2 to pure ferrocenyllithium.²⁹ The disadvantage of this method is that it requires the availability of an appropriate symmetrical dichalcogenide. A similar method was also used by Singh to synthesise five monosubstituted and five disubstituted ferrocenyl tellurides.³⁰ This method started from ferrocenyllithium, and has the limitation of yielding two products in similar yield. 2-(Phenylseleno)oxazinylferrocene was also synthesized in a similar way.³¹

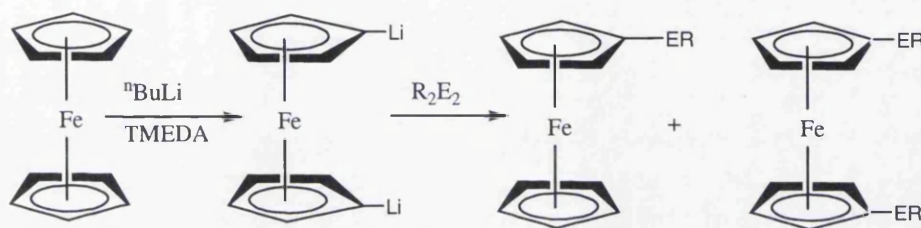


Fig. 2.15 Synthetic scheme from ferrocenyllithium

(3) The third route began with the reaction of LiR and Fc_2Te_2 , followed by oxidation.³²

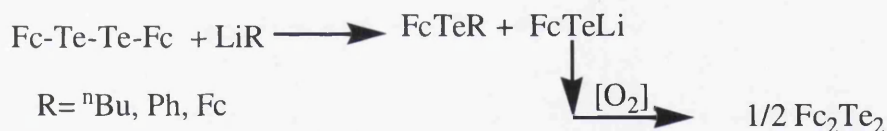


Fig. 2.16 Synthetic scheme from LiR and Fc_2Te_2

(4) By the reduction using NaBH_4 of a diferrocenyl dichalcogenide, followed by addition of the appropriate alkyl or aryl halide, the product was obtained.^{33, 34} The advantage of this route is its high yield (95% or above).

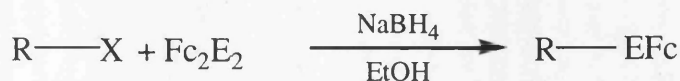
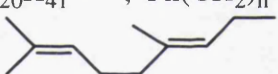
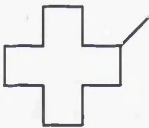
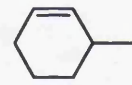



Fig. 2.17 Synthetic scheme from RX and Fc_2E_2

Table 2.2 Literature references to FcER

E	R	Method	Ref.
Se	Me	2	29
	Ph	2	35
	CN	2	28
	SnMe ₃	2	25
	ⁿ Bu, Fc	1	28
	Et, ¹ Pr, ⁿ Pr, ¹ Bu, ¹ Pent, ⁿ Pent, Hex, Oct, CH ₂ Ph	4	36
	Cp*, Cp ¹	3	37
Te	CH ₂ CH=CH ₂	2	38
	Me; ⁿ Bu; C ₆ H ₅ ; <i>p</i> -C ₆ H ₄ OMe; <i>p</i> -C ₆ H ₄ OEt	2	30
	ⁿ Bu, Ph, Fc	3	32
	Et, ¹ Pr, ⁿ Pr, ¹ Bu, ¹ Pent, ⁿ Pent, Hex, Oct	4	36
	SnMe ₃	4	25
	C ₁₂ H ₂₅ CHCH ₃ ; C ₆ H ₁₃ CHCH ₃ ; C ₈ H ₁₇ CHCH ₃ ; C ₁₄ H ₂₉ — C ₁₆ H ₃₃ —; C ₁₈ H ₃₇ —; C ₂₀ H ₄₁ —; Ph(CH ₂) _n — n = 1-6 PhCH = CHCH ₂ — ;   ;  ; 	4	33

An NMR study showed that in the series of ferrocenyl alkyl selenides and tellurides, $\delta(^{125}\text{Te})/\delta(^{77}\text{Se}) = 1.6$, which is in accordance with theoretical calculations.³⁶

2.1.2.2 Compounds with 1, 1'-ferrocenylene dichalcogenide groups

The analogous 1, 1'-ferrocenylene compounds (Fig. 2.18) can be synthesized by the method (2) described in 2.1.2.1.^{29, 30} The existing compounds are summarized in Table 2.3.

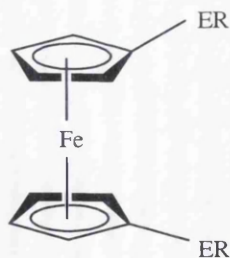


Fig. 2.18 $fc(ER)_2$

Table 2.3 Literature references to $fc(ER)_2$

E	R	Ref.
Se	Me	29
	Ph	29
	CH ₂ Ph	22
	C(R)=CH-COOEt (R= H, Ph)	39
	SnMe ₃	21
	SiMe ₃	40
Te	SnMe ₃	21
	Me, ⁿ Bu, Ph, <i>p</i> -C ₆ H ₄ OMe, <i>p</i> -C ₆ H ₄ OEt	30

The molecular structure of $fc(TEPh)_2$ is pseudo-centrosymmetric and the asymmetric unit consists of the complete molecule (shown in Fig. 2.19). The two cyclopentadienyl rings are nearly parallel and staggered with a *trans* arrangement of TeC_6H_5 substituents. Upon chelation a conformational change to the *cis* arrangement is forced upon the ligand.³⁰

The packing diagram shows that the compound is essentially monomeric, but it is linked to other neighbouring molecules by weak $Te \cdots Te$ intermolecular interactions to give loose dimers. The shortest distances between $Te \cdots Te$ are 3.795(7) Å and 4.392(3) Å, close to the van der Waals distance of 4.40 Å.

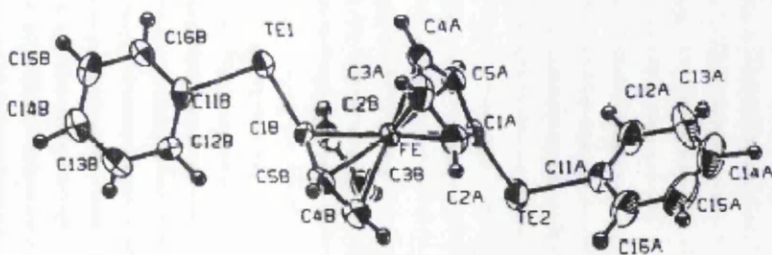


Fig. 2.19 Crystal structure of $\text{Fc}(\text{TePh})_2$

The golden yellow powder $[\text{Fe}(\eta^5\text{-C}_5\text{H}_4\text{SeSiMe}_3)_2]$ was prepared from chlorotrimethylsilane and $[\text{Fe}(\eta^5\text{-C}_5\text{H}_4\text{SeLi})_2(\text{TMEDA})]$ in pentane at 0°C . Its structure shows the selenolate groups are held in a *trans* configuration in the solid state with the two Cp rings adopting a staggered conformation (shown in Fig. 2.20).

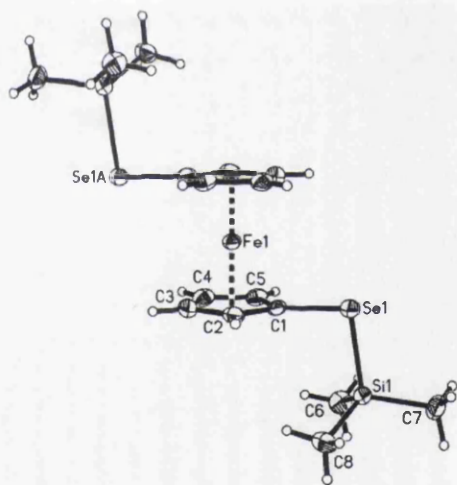


Fig. 2.20 Crystal structure of $\text{Fc}(\text{SeSiMe}_3)_2$

The methyl and phenyl compounds have attracted particular attention as chelating ligands, which will be discussed in Chapter Three.

2.1.2.3 Chalcogeno-esters

The reaction between ferrocenyllithium and elemental chalcogen forms the intermediate FcELi , which was then further reacted with various acyl chlorides to form the chalcogenides.⁴¹

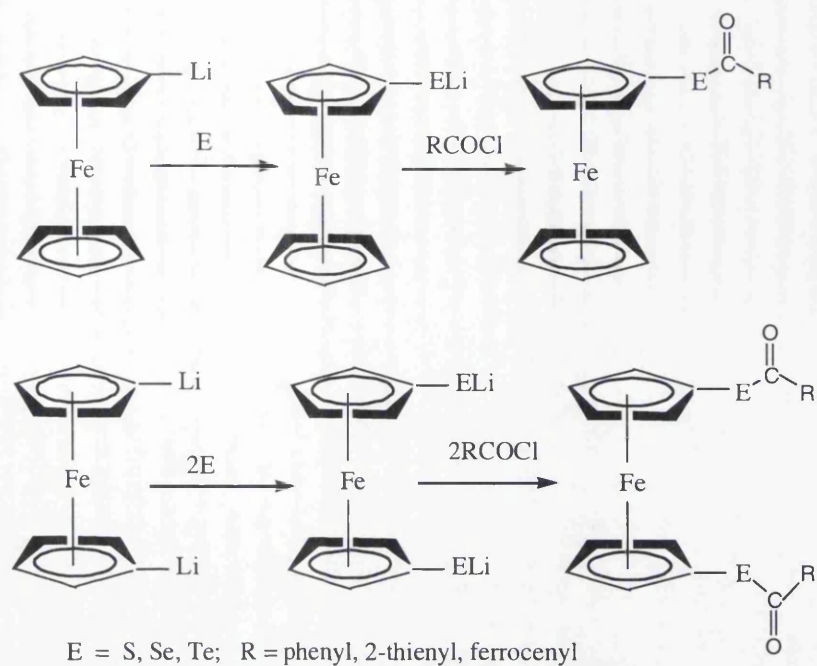
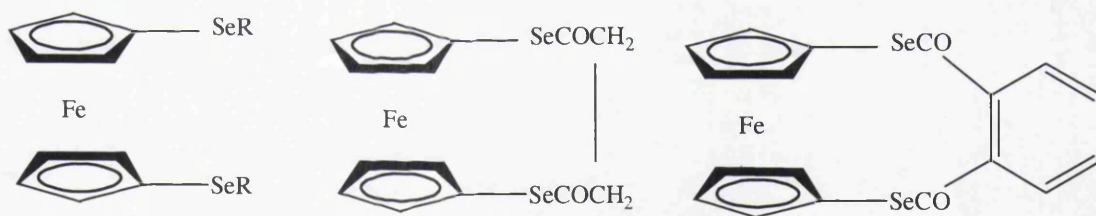


Fig. 2.21 Synthetic scheme for chalcogeno-esters

More compounds of this type (shown in Fig. 2.22) were also obtained.⁴²



R = COCH₂CH₃

Fig. 2.22 Other chalcogeno-esters

2.1.2.4 Ferrocenylamine selenide compounds

The chiral compound [Fe(η^5 -C₅H₅) (η^5 -C₅H₃-1-CH₂NMe₂-2-SeR)] (shown in Fig. 2.23) can be made from the appropriate ferrocene precursor via lithiation and reaction with RSeSeR.²⁹

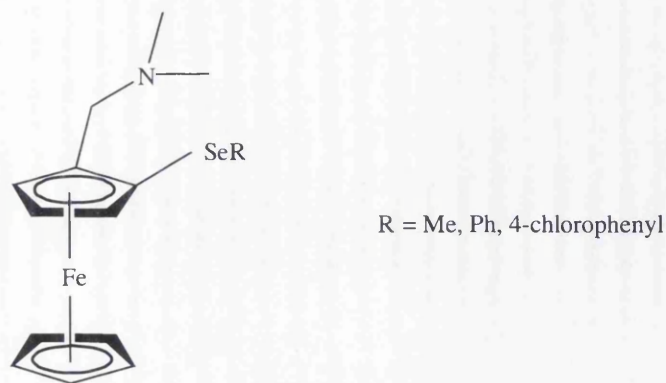


Fig. 2.23 Ferrocenylamine selenide compounds

From the chiral bis[2-{1-(dimethylamino)ethyl}ferrocenyl] dichalcogenides ([R,S;R,S] and [S,R;S,R]), chiral ferrocenyl vinyl, allyl and alkyl selenides can be prepared (example shown in Fig. 2.24).^{43,44}

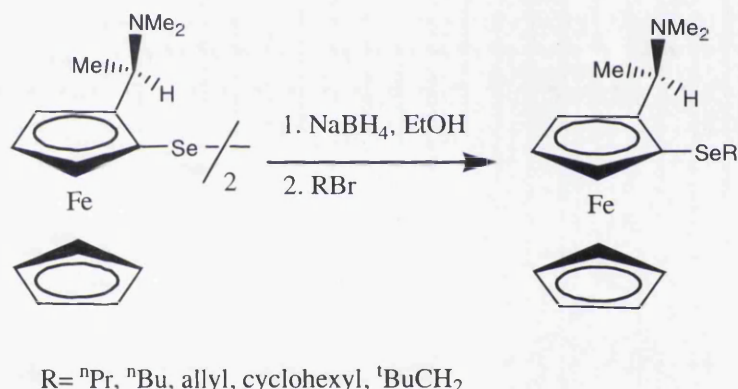


Fig. 2.24 Synthetic scheme for ferrocenylamine selenide compounds

Also this kind of chiral diferrocenyl diselenide can be converted into a chiral ferrocenylselenyl bromide by treatment with bromine in CH₂Cl₂ at -78 °C; the product can react with alkenoic acids, alkenols, olefinic urethanes and alkenes to afford lactones, cyclic ethers, nitrogen-heterocyclic and selenomethoxylated adducts with high facial selectivity.^{45,46}

1,1'-Ferrocenediyl compounds (R,S)-[Fe(η-C₅H₄SeR)(η-C₅H₃-1-CHMeNMe₂-2-SeR)] (R = Me, *p*-C₆H₄Cl) can be synthesized using two equivalents of lithiation reagent.^{47,48}

2.1.3 Diferrocenyl dichalcogenides and their derivatives

2.1.3.1 Diferrocenyl dichalcogenides

(1) The first synthesis of diferrocenyl diselenide was reported by Shu in 1976.²⁸ The scheme is shown below, but it's not practical because it requires the synthesis of chloromercuriferrocene, which is time consuming, and also the diselenide is only the minor product.

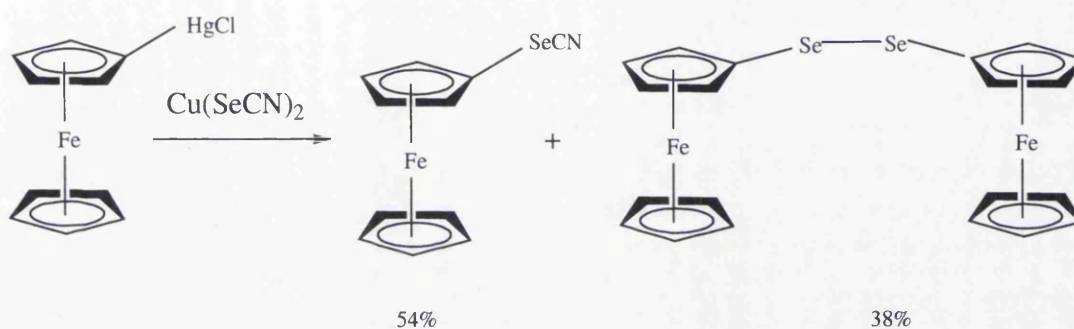


Fig. 2.25 Synthetic scheme for Fc_2E_2 from chloromercuriferrocene

(2) An improved method was reported by Herberhold and Leitner in 1987,³² in which monolithioferrocene, synthesized from the reaction of ferrocenylbromide and butyllithium, was reacted directly with excess selenium or tellurium, forming the intermediate FcELi . Oxidation yields the dichalcogenide.

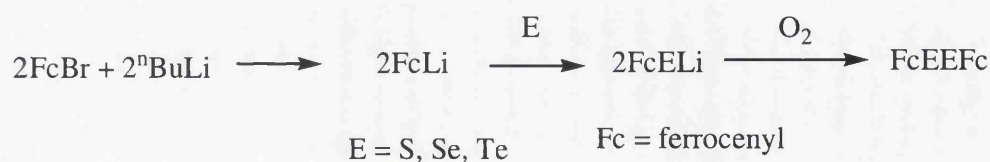


Fig. 2.26 Synthetic scheme for Fc_2Se_2 from ferrocenylbromide and butyllithium

This method used ferrocenyl bromide, which is easier to prepare, instead of chloromercuriferrocene. Also, it gave a good yield of the desired product.

(3) Our group has demonstrated that by direct lithiation of ferrocene, the desired product can be obtained without the need to prepare ferrocenyl bromide.³⁷

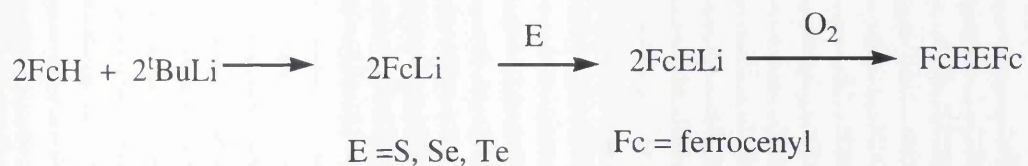


Fig. 2.27 Synthetic scheme for Fc_2E_2 by direct lithiation of ferrocene

Fc_2Se_2 crystallizes in the chiral space group $P2_1$ and the crystal studied contained the right handed helical form with a CSeSeC dihedral angle of $-88.7(4)^\circ$ (shown in Fig. 2.28). The two ferrocenyl subunits connected by the diselenide bridge are also almost coparallel as is evident from the angle between the normals to the substituted cyclopentadienyl rings of 5.0° . The Se-Se bond length is $2.3504(14) \text{ \AA}$.³⁸

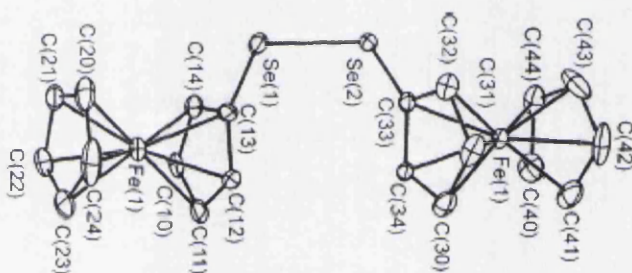


Fig. 2.28 Crystal structure of Fc_2Se_2

The bis(ferrocenylchalcogeno)methanes, FcECH_2EFc ($\text{E} = \text{Se}, \text{Te}$), were obtained from FcELi and CH_2I_2 . The ^{13}C NMR data reveal the shielding of the methylene carbon (CH_2) increased markedly when the chalcogen atoms are changed from sulphur (46.3 ppm) to selenium (24.0 ppm) to tellurium (-35.1 ppm).³²

2.1.3.2 Bis[2-(dimethylaminomethyl)ferrocenyl] dichalcogenides

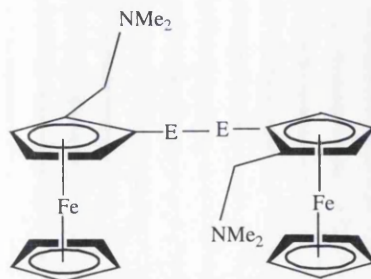


Fig. 2.29 Bis[2-(dimethylaminomethyl)ferrocenyl] dichalcogenides

Similar compounds bis[2-(dimethylaminomethyl)ferrocenyl] dichalcogenides (Fig. 2.29) have also been synthesized by the oxidation of $\text{Li}[\text{CpFe}\{\text{C}_5\text{H}_3(\text{CH}_2\text{NMe}_2)\text{E}\}]$ ($\text{E} = \text{Se}, \text{Te}$) in moderate yields. Bis[2-(dimethylaminomethyl)ferrocenyl] diselenide crystallizes in the space group $P2_12_12_1$ with a CSeSeC dihedral angle of $84.8(1)^\circ$. The Se-Se bond length is $2.362(1) \text{ \AA}$ (shown in Fig. 2.30), a little longer than in Fc_2Se_2 .⁴⁹

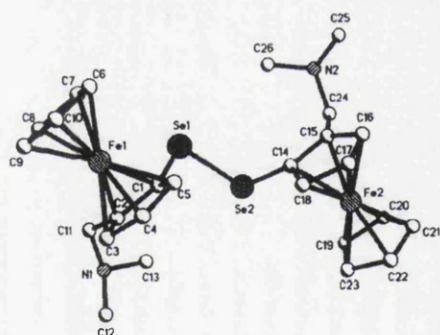


Fig. 2.30 Crystal structure of bis[2-(dimethylaminomethyl)ferrocenyl] diselenide

2.1.3.3 Chiral diferrocenyl dichalcogenides

Four chiral diferrocenyl diselenides were reported by Nishibayashi *et al.* in 1995.^{43, 50} Optically active bis[2-{1-(dimethylamino)ethyl}ferrocenyl] dichalcogenides ($[\text{R},\text{S};\text{R},\text{S}]$ and $[\text{S},\text{R};\text{S},\text{R}]$) were prepared by lithiation of chiral [1-(dimethylamino)ethyl]ferrocenes, followed by reaction with elemental chalcogen and air oxidation, in 60-80% isolated yields (shown in Fig. 2.31). Resembling in some

respects chiral ferrocenyl phosphines, they have applications in asymmetric selenoxide elimination and [2, 3] sigmatropic rearrangements, which lead to chiral allenecarboxylic esters and allylic alcohols. Only one similar ditelluride, (R,R)-bis[2-{1-(dimethylamino)ethyl}ferrocenyl] ditelluride, has been reported.⁵¹ In 1996, this group reported the preparation of dozens of new chiral diferrocenyl diselenides and their derivatives by a similar method.⁴⁴

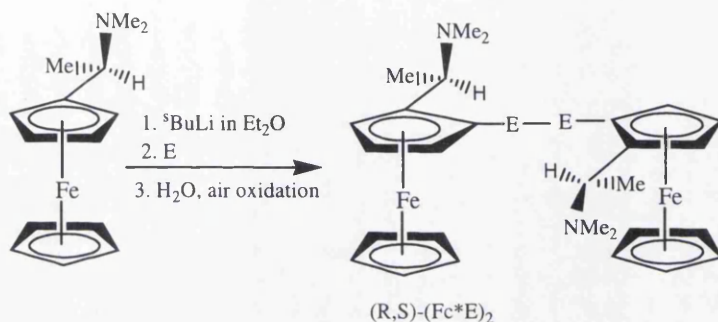


Fig. 2.31 Synthetic scheme for chiral diferrocenyl diselenides

The [S,R;S,R]-diselenide⁴³ was fully characterized by X-ray crystallography (shown in Fig. 2.32), and its absolute configuration was clarified to be *S,R* where the configuration around the ferrocene axis is *R*. The torsional angle C-Se-Se-C is 94.1°, larger than that of 84.8° in bis[2-(dimethylaminomethyl)ferrocenyl] diselenide,⁵² probably due to the greater steric bulkiness resulting from introduction of one additional methyl group. The Se-Se bond length is 2.347(2) Å.

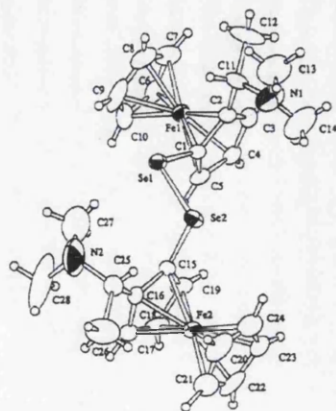


Fig. 2.32 Crystal structure of [S,R;S,R]-diselenide

2.1.4 Chalcogen-bridged ferrocene oligomers and polymers:

2.1.4.1 Trinuclear and tetranuclear chalcogen-bridged ferrocenes

Two kinds of oligonuclear ferrocene derivative, FcE-fc-EFc and FcE-fc-E-E-fc-EFc, can be obtained by the reaction of 1,1'-dilithioferrocene, FcLi_2 , with a diferrocenyl dichalcogenide, Fc_2E_2 (shown in Fig. 2.33).^{52, 53} Interest is concentrated on their study by electrochemistry which will be discussed in Chapter Four.

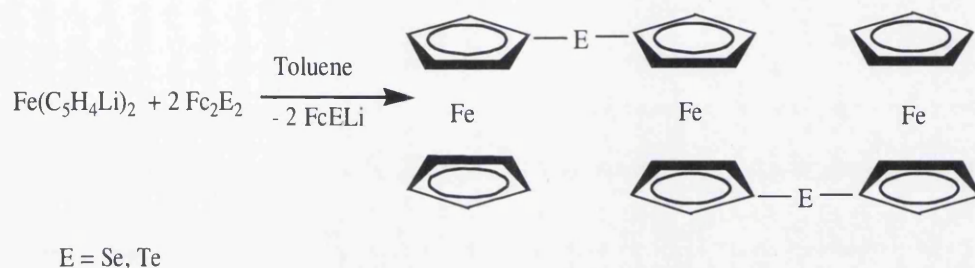


Fig. 2.33 Synthetic scheme for FcE-fc-EFc

2.1.4.2 Poly(ferrocenyl selenide)

Insoluble $[\text{Fe}(\eta\text{-C}_5\text{H}_4)(\eta\text{-C}_5\text{H}_4\text{Se})]_n$ is synthesized by the thermal ring-opening polymerization (ROP) of selenal[1]ferrocenophane (shown in Fig. 2.34).³

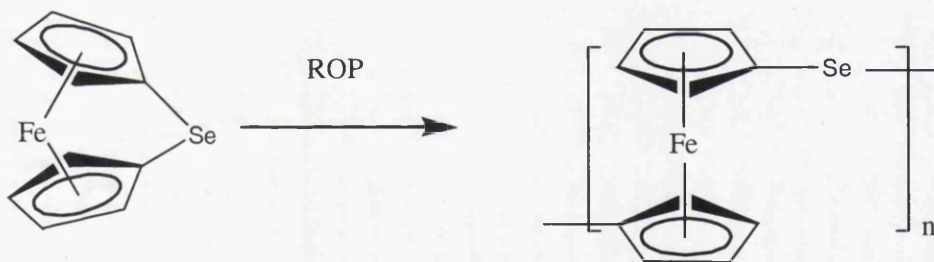


Fig. 2.34 Synthetic scheme for $[\text{Fe}(\eta\text{-C}_5\text{H}_4)(\eta\text{-C}_5\text{H}_4\text{Se})]_n$

2.2 Synthesis and characterization of new ferrocenyl chalcogenide compounds

We have now synthesised a series of new ferrocenylchalcogenide compounds, and studied their relative properties using crystallography, ^1H , ^{13}C , ^{77}Se , ^{125}Te NMR and electronic spectroscopy. Their coordination chemistry will be discussed in Chapter Three and electrochemistry in Chapter Four.

2.2.1 Ferrocenyl chalcogenide compounds with a flexible hydrocarbon chain

2.2.1.1 Synthesis

Bis(ferrocenylchalcogeno)alkanes and 1-ferrocenylchalcogeno-3-halopropanes

Bis(ferrocenylchalcogeno)methanes were originally prepared by Herberhold and Leitner.¹⁸ Bis(ferrocenylchalcogeno)alkanes having a longer hydrocarbon chain can be synthesized by a similar method.

Fc_2Se_2 , Fc_2Te_2 were prepared from $[\text{Fe}(\eta^5\text{-C}_5\text{H}_5)_2]$ (FcH) *via* lithiation in THF with 0.9 equivalents of Li^tBu , treatment with selenium or tellurium, and air oxidation, in a minor modification of a literature procedure.³²

The subsequent synthetic method is shown in Fig. 2.35.

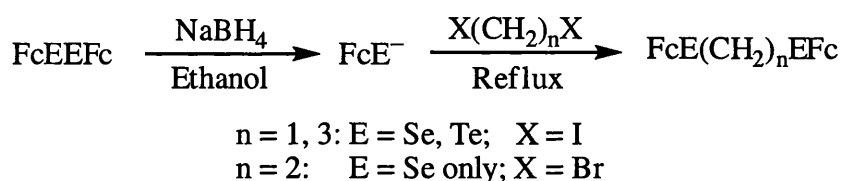


Fig. 2.35 The method to synthesize bis(ferrocenylseleno)alkanes

Reduction of the diferrocenyl dichalcogenide by sodium borohydride in ethanol was followed by addition of a α,ω -dihaloalkane, $\text{X(CH}_2)_n\text{X}$ ($\text{X} = \text{Br, I}$). After column chromatography the product was generally isolated as an orange-yellow ($\text{E} = \text{Se}$) or orange-red ($\text{E} = \text{Te}$) solid in good yield. Care needs to be taken, however, to avoid

the use of a large excess of reducing agent, which results in almost exclusive formation of the monoferrocenyl compounds FcER (R = Me, Et or Pr).

There are some differences between the behaviour of selenium and tellurium in this system, which are presumably a reflection of the greater nucleophilicity of the ferrocenyltelluroate anion (in turn, a consequence of the lower electronegativity of Te (2.1) than Se (2.4)⁵⁴). If the reaction of FcE⁻ (E = Se, Te) with I(CH₂)₃I is carried out under reflux, FcE(CH₂)₃EFc is obtained as the sole product in each case. At room temperature, however, a second compound can be isolated when E = Se, which has been identified as FcSe(CH₂)₃I. The mechanism is shown in Fig. 2.36. In this nucleophilic substitution reaction, the first FcSe⁻ group easily replaces the leaving group I, but the second step is much slower. By contrast, only a little of the 1-iodo byproduct can be obtained during the synthesis of FcTe(CH₂)₃TeFc.

If n = 1, the second iodine is labile, so the target compound can be obtained without byproduct. When n = 2, the diiodoethane needs to be changed to dibromoethane. Iodide ion works as a dehalogenating agent in an 1,2-elimination reaction,⁵⁵ so the intermediate decomposes quickly to ethane. Changing to the dibromide Br(CH₂)₂Br allowed the isolation of the selenide FcSe(CH₂)₂SeFc, but this compound could not be obtained pure and was always contaminated by traces of Fc₂Se₂. FcTe(CH₂)₂TeFc can't be obtained by this method.

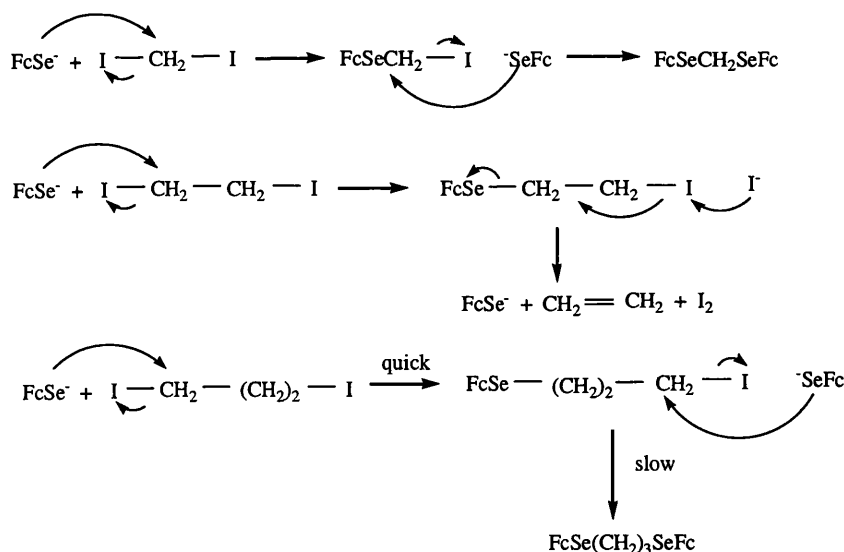


Fig. 2.36 Mechanism of bis(ferrocenylseleno)alkane synthesis

The availability of $\text{FcSe}(\text{CH}_2)_3\text{I}$ allowed the preparation of the mixed Se/Te compound $\text{FcSe}(\text{CH}_2)_3\text{TeFc}$ by a similar method, as shown in Fig. 2.37.

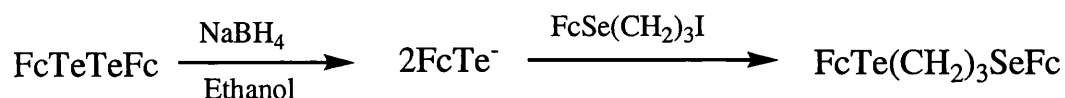


Fig. 2.37 Synthetic scheme for $\text{FcSe}(\text{CH}_2)_3\text{TeFc}$

The mechanism of the synthesis of bis(ferrocenylchalcogeno)alkanes shows that in this nucleophilic substitution reaction, the first FcE^- group easily replaces the leaving group I^- , but the second step is much slower, prompting the idea that by using Br^- instead of I^- , and performing the reaction at 0°C , then $\text{FcE}(\text{CH}_2)_3\text{Br}$ could be obtained as the main product. This was confirmed by experiment. First, four equivalents of sodium borohydride were used to reduce the diferrocenyl dichalcogenide in ethanol. After 1 h, the mixture became a clear orange yellow ($\text{E} = \text{Se}$) or red ($\text{E} = \text{Te}$) solution. Then at 0°C , this solution was slowly transferred to a diluted ethanol solution containing excess 1, 3-dibromopropane. The reaction was allowed to continue for 2 h, with the solution colour changing to yellow. After column chromatography the product $\text{FcE}(\text{CH}_2)_3\text{Br}$ was generally isolated as an orange oil in high yield.

Spectroscopic data for each of the new compounds described in this section are given in Chapter Seven.

$\text{FcSe}(\text{CH}_2)_n\text{SeFc}$ ($n = 4-6$) and $\text{FcTe}(\text{CH}_2)_n\text{TeFc}$ ($n = 4, 6$) were synthesized similarly; their spectroscopic data are given in Chapter Seven.

Linear tridentate ferrocenyl chalcogenide compounds

Several linear tridentate chalcogenide compounds have been synthesized by Levason's group.⁵⁶⁻⁵⁹ The triselenoethers $\text{Se}[(\text{CH}_2)_n\text{SeMe}]_2$ ($n = 2, 3$) were synthesized by the route shown in Fig. 2.37.⁵⁶ $\text{Te}(\text{CH}_2\text{CH}_2\text{CH}_2\text{TeMe})_2$ was also prepared by this method, but it is not generally applicable to tellurium compounds: reaction of $\text{MeTe}(\text{CH}_2)_3\text{OTs}$ with Na_2Te in alcohol or THF resulted in rapid deposition of elemental Te and formation of Me_2Te_2 . An improved scheme was explored to obtain $\text{Te}(\text{CH}_2\text{CH}_2\text{CH}_2\text{TeR})_2$ ($\text{R} = \text{Me}$ or Ph) (shown in Fig. 2.38).⁵⁸ The air sensitive compound $\text{MeS}(\text{CH}_2)_3\text{Te}(\text{CH}_2)_3\text{SMe}$ was synthesized similarly.⁵⁹ The existing route includes three steps and Na_2E was obtained from Na metal in liquid NH_3 , which makes it time consuming and requires critical control of conditions. One aim of our work below was trying to find a more direct and mild route. The target linear tridentate compounds, $\text{FcE}(\text{CH}_2)_3\text{E}'(\text{CH}_2)_3\text{EFc}$, can be obtained by the scheme shown in Fig. 2.39.

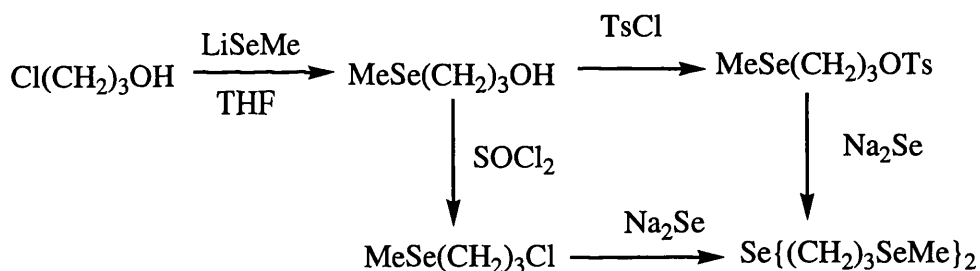


Fig. 2.37 Synthetic route to $\text{Se}[(\text{CH}_2)_n\text{SeMe}]_2$ ($n = 2, 3$)⁵⁶

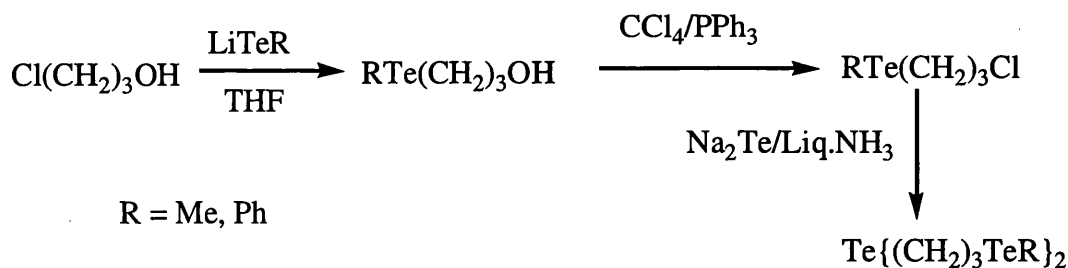
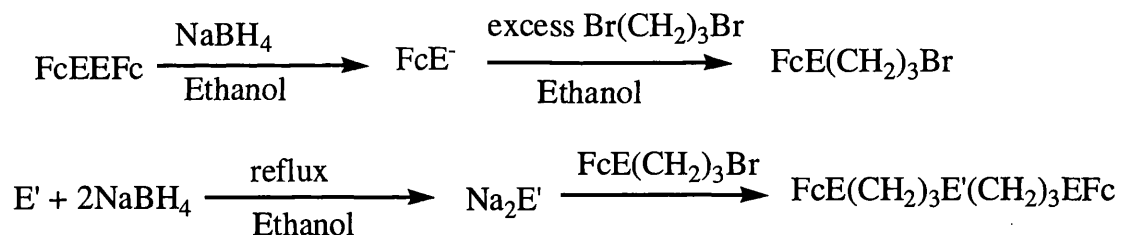


Fig. 2.38 Synthetic route to $\text{Te}(\text{CH}_2\text{CH}_2\text{CH}_2\text{TeR})_2$ ($\text{R} = \text{Me}$ or Ph)⁵⁸



E, E' = Se, Te

Fig. 2.39 Synthetic scheme for $\text{FcE(CH}_2)_3\text{E}'(\text{CH}_2)_3\text{EFc}$

For example, Se powder and two equivalents of NaBH_4 were refluxed in degassed ethanol under N_2 for 1 h to produce a clear pale yellow solution. A THF solution of two equivalents of $\text{FcSe(CH}_2)_3\text{Br}$ was then added slowly, and the solution was left to stir at room temperature for 12 h. After removing the solvent by evaporation under reduced pressure, the residue was treated with water and then extracted with CH_2Cl_2 . The extract was dried over MgSO_4 and evaporated to dryness, then subjected to column chromatography on SiO_2 to produce $\text{FcSe(CH}_2)_3\text{Se(CH}_2)_3\text{SeFc}$, a yellow powder with a yield of 55.7%. The other three compounds $\text{FcE(CH}_2)_3\text{E}'(\text{CH}_2)_3\text{EFc}$ (E = Se, E' = Te; E = Te, E' = Se; E = Te, E' = Te) can be synthesized similarly. Spectroscopic data for each of the new compounds described in this section are given in Chapter Seven.

Tripodal ferrocenyl chalcogenide compounds

The compounds $\text{CH}_3\text{C}(\text{CH}_2\text{SeR})_3$ ($\text{R} = \text{Me}$ or Ph) were synthesized straightforwardly from RSeLi and the relevant organohalide.⁵⁶ The tellurium analogues $\text{CH}_3\text{C}(\text{CH}_2\text{TeR})_3$ ($\text{R} = \text{Me}$ or Ph) were obtained similarly.⁶⁰ This reaction needs to be carried out at quite low temperature, -196°C .

As pure FcELi can't be isolated, it was prepared *in situ* by reduction of FcEEFc . The tripodal ferrocenyl chalcogenide compounds were synthesized by the method shown below (Fig. 2.40), with good yield when excess $(\text{FcE})_2$ was used. For example, excess $(\text{FcSe})_2$ was dissolved in EtOH ; NaBH_4 was then added at 0°C . The mixture became homogeneous after stirring for 1 h at room temperature. $\text{MeC}(\text{CH}_2\text{Br})_3$ was added to the resulting solution. The solution was left to stir overnight at refluxing temperature, and then the solvent was removed by evaporation under reduced pressure. The residue was treated with water and extracted with CH_2Cl_2 . The extract was dried over MgSO_4 and evaporated to dryness, then subjected to column chromatography on SiO_2 . Elution with hexane/dichloromethane (2:1) produced $\text{MeC}(\text{CH}_2\text{SeFc})_3$ as a yellow powder after evaporation.

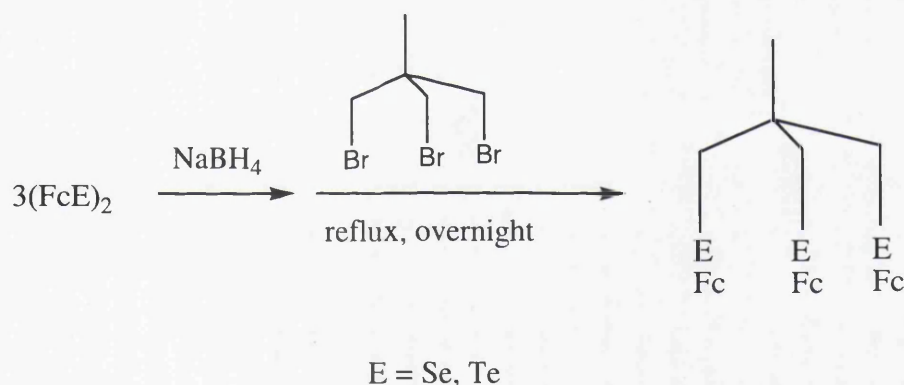


Fig. 2.40 Synthetic scheme for tripodal compounds

The MALDI mass spectra of these two compounds contained molecular ion peaks with a good match to the predicted isotope pattern.

Spectroscopic data for each of the new compounds described in this section are given in Chapter Seven.

Linear tetradentate ferrocenyl chalcogenide compounds

Only one quadridentate selenoether, $\text{MeSe}(\text{CH}_2)_2\text{Se}(\text{CH}_2)_3\text{Se}(\text{CH}_2)_2\text{SeMe}$, has been synthesized.⁶¹ The route (shown in Fig. 2.41) is quite sophisticated and $\text{HSe}(\text{CH}_2)_3\text{SeH}$ is unstable. A new scheme from $\text{FcE}(\text{CH}_2)_3\text{Br}$ and $\text{NCSe}(\text{CH}_2)_3\text{SeCN}$ has been designed, and using it, target products $\text{FcE}(\text{CH}_2)_3\text{Se}(\text{CH}_2)_3\text{Se}(\text{CH}_2)_3\text{EFc}$ ($\text{E} = \text{Se}$ or Te) can be obtained in high yield (near 100%).

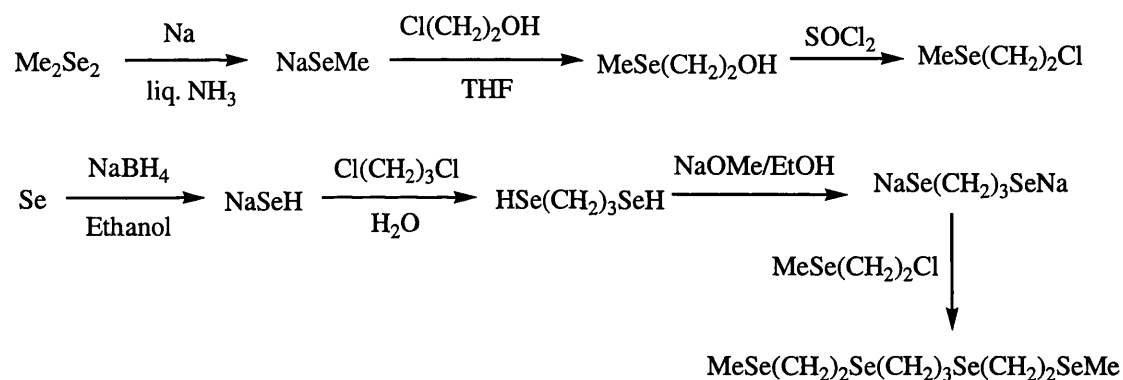
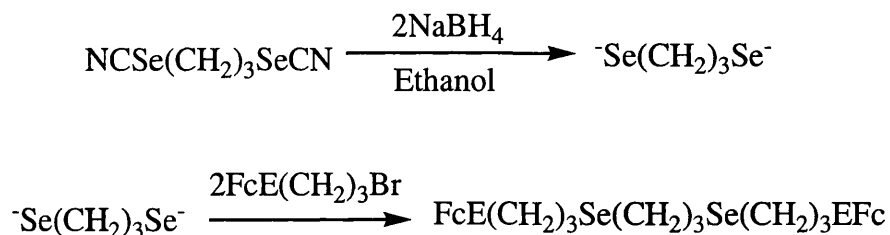


Fig. 2.41 Synthetic route to $\text{MeSe}(\text{CH}_2)_2\text{Se}(\text{CH}_2)_3\text{Se}(\text{CH}_2)_2\text{SeMe}$ ⁶¹

The new route is shown in Fig. 2.42. Two equivalents of NaBH_4 were added to an ethanol solution of $\text{NCSe}(\text{CH}_2)_3\text{SeCN}$ at 0 °C; the solution turned red in 5 minutes. Slowly warming to room temperature, the colour disappeared quickly, and there was intense gas evolution. Two equivalents of $\text{FcE}(\text{CH}_2)_3\text{Br}$ in a small amount of THF were then added. Following reaction at room temperature overnight, the target compounds were obtained via chromatography.



E = Se, Te

Fig. 2.42 Synthetic scheme for linear tetradentate ferrocenyl chalcogenide ligands

Spectroscopic data for each of the new compounds described in this section are given in Chapter Seven.

2.2.1.2 Crystal structures

Structure of FcSe(CH₂)₃SeFc

Crystals of FcSe(CH₂)₃SeFc were obtained as orange plates from CH₂Cl₂/hexanes. Fig. 2.43 depicts a view of a molecule along with the atomic numbering. Pertinent bond parameters are collected in Table 2.4 while crystal data and refinement details are provided in Table 2.5. The compound crystallizes in the space group P-1, triclinic. The two cyclopentadienyl rings attached to the same iron are basically coplanar. There is no tendency toward shorter Fe-C bond distances for the substituted carbon atoms as compared to the other Fe-C bonds within the same ring (as observed in Fc₂Se₂); the Fe-C distances range from 2.002(8) to 2.046(6) Å. The C-C distances in the cyclopentadienyl rings range from 1.390(9) to 1.422(8) Å and the C-C-C bond angles within the ring range from 105.8(6) to 109.8(6) °. The ferrocene-C-Se bond distances (Se(1)-C(4), 1.872(6) Å; Se(2)-C(14), 1.878(6) Å) are shorter than those in Fc₂Se₂ (Se(1)-C(13), 1.898(10) Å; Se(2)-C(33), 1.904(9) Å). The sp³-C-Se bond distances are longer (Se(1)-C(1), 1.995(6) Å; Se(2)-C(3), 1.979(6) Å).

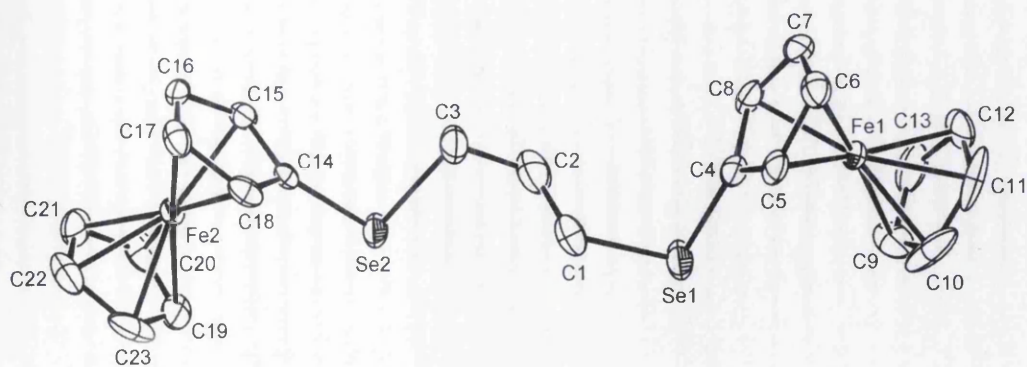


Fig. 2.43 Plot of a molecule of $\text{FcSe}(\text{CH}_2)_3\text{SeFc}$ with atomic numbering scheme

The packing diagram is shown in Fig. 2.44. The title compound is essentially monomeric, but it is linked to other neighbouring molecules by weak $\text{Se}\cdots\text{Se}$ (3.636 Å) and $\text{H}\cdots\text{Se}$ (3.043 Å) intermolecular interactions to give loose dimers.

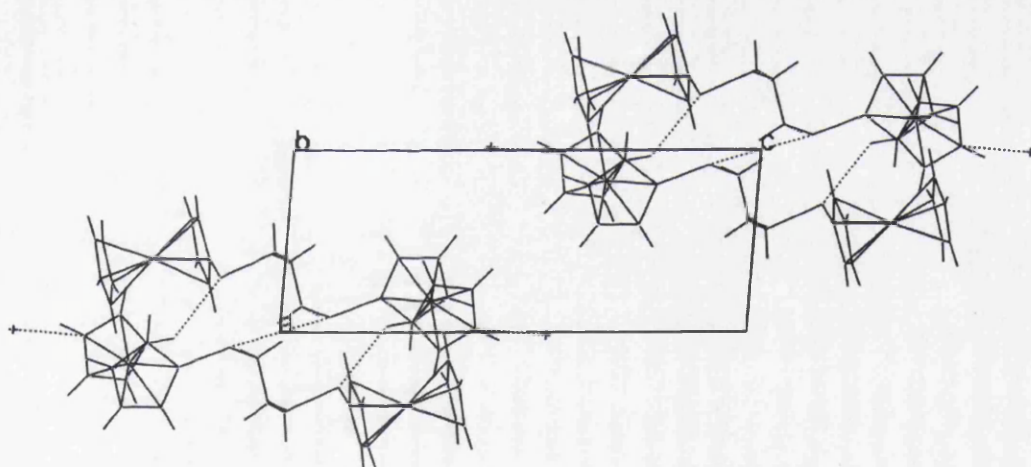


Fig. 2.44 Packing diagram for $\text{FcSe}(\text{CH}_2)_3\text{SeFc}$

Table 2.4 Selected bond lengths (Å) and bond angles (°) for FcSe(CH₂)₃SeFc

<i>Bond lengths</i>					
Se(1)-C(4)	1.872(6)	C(4)-Fe(1)	2.035(6)	Se(1)-C(1)	1.995(6)
C(1)-C(2)	1.509(8)	C(2)-C(3)	1.537(8)	C(3)-Se(2)	1.979(6)
Se(2)-C(14)	1.878(6)	C(14)-Fe(2)	2.056(6)		
<i>Bond angles</i>					
Se(1)-C(4)-Fe(1)	122.6(3)	C(4)-Se(1)-C(1)		97.3(3)	
C(3)-Se(2)-C(14)	97.7(3)	Se(2)-C(14)-Fe(2)		124.5(3)	
<i>Torsion angles</i>					
C(4)-Se(1)-C(1)-C(2)	78.5(6)	Se(1)-C(1)-C(2)-C(3)		-172.2(5)	
C(1)-C(2)-C(3)-Se(2)	-71.6(8)	C(14)-Se(2)-C(3)-C(2)		-177.2 (6)	
C(1)-Se(1)-C(4)-Fe(1)	175.4(4)	C(3)-Se(2)-C(14)-Fe(2)		164.9 (4)	

* The number in bracket means the standard uncertainty, s.u..

Table 2.5 Crystal data and structure refinement for $\text{FcSe}(\text{CH}_2)_3\text{SeFc}$

Empirical formula	$\text{C}_{23}\text{H}_{24}\text{Fe}_2\text{Se}_2$
Formula weight	570.04
T (K)	296(2)
Wavelength (\AA)	0.71069
Crystal system	Triclinic
Space group	P-1
a (\AA)	5.875(1)
b (\AA)	12.077(2)
c (\AA)	15.905(2)
α ($^\circ$)	108.13(1)
β ($^\circ$)	94.07(1)
γ ($^\circ$)	92.25(1)
Volume (\AA^3)	1067.5(3)
Z	2
D_c (Mg m^{-3})	1.773
Absorption coefficient (mm^{-1})	4.774
$F(000)$	564
Crystal size (mm)	$0.60 \times 0.40 \times 0.14$
θ range for data collection ($^\circ$)	4.33 to 26.37
Index ranges	$-7 \leq h \leq 7, -15 \leq k \leq 15, -19 \leq l \leq 19$
Reflections collected	10574
Independent reflections [Rint]	4281 [0.0745]
Data / restraints / parameters	4281 / 24 / 248
Goodness-of-fit on F^2	0.870
Final R indices [$I > 2\sigma(I)$]	$R_1 = 0.0541, wR_2 = 0.1231$
R indices (all data)	$R_1 = 0.0877, wR_2 = 0.1371$
Largest diff. peak and hole ($e \text{\AA}^{-3}$)	1.555, -1.416

* The number in bracket means the standard uncertainty, s.u..

Structure of $\text{FcSe}(\text{CH}_2)_3\text{Se}(\text{CH}_2)_3\text{SeFc}$

Crystals of $\text{FcSe}(\text{CH}_2)_3\text{Se}(\text{CH}_2)_3\text{SeFc}$ were obtained as orange yellow plates from $\text{CH}_2\text{Cl}_2/\text{hexanes}$. Pertinent bond parameters are collected in Table 2.6 while crystal data and refinement details are provided in Table 2.7. Fig. 2.45 depicts a view of a molecule along with the atomic numbering. It crystallizes in the unusual space group, orthorhombic $F2dd$. The symmetry-independent unit consists of only one half of the molecule, since this possesses a twofold axis passing through the central Se atom with a dihedral angle of $-58.1(3)^\circ$. The ferrocene $\text{sp}^2\text{-C-Se}$ bond distance ($\text{Se}(2)\text{-C}(4)$, $1.899(4) \text{ \AA}$) is similar to those in Fc_2Se_2 ($\text{Se}(1)\text{-C}(13)$, $1.898(10) \text{ \AA}$; $\text{Se}(2)\text{-C}(33)$, $1.904(9) \text{ \AA}$) and longer than that in $\text{FcSe}(\text{CH}_2)_3\text{SeFc}$ ($\text{Se}(1)\text{-C}(4)$, $1.872(6) \text{ \AA}$; $\text{Se}(2)\text{-C}(14)$, $1.878(6) \text{ \AA}$). The $\text{sp}^3\text{-C-Se}$ bond distance ($\text{Se}(2)\text{-C}(3)$, $1.956(4) \text{ \AA}$) is shorter than those in $\text{FcSe}(\text{CH}_2)_3\text{SeFc}$ ($\text{Se}(1)\text{-C}(1)$, $1.995(6) \text{ \AA}$; $\text{Se}(2)\text{-C}(3)$, $1.979(6) \text{ \AA}$). The middle Se-C bond distance is shorter still ($\text{Se}(1)\text{-C}(4)$, $1.946(4) \text{ \AA}$).

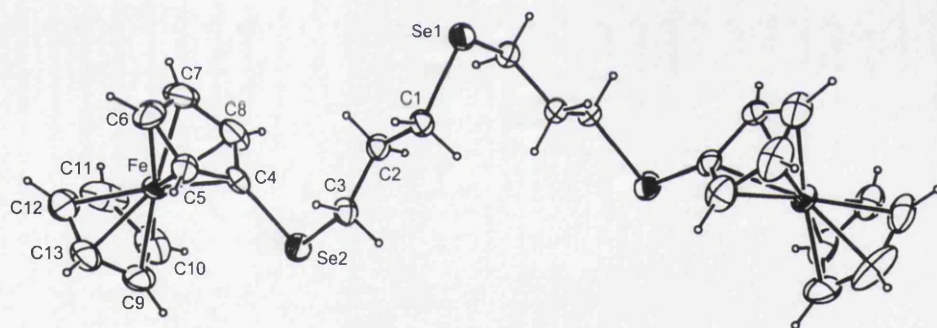


Fig.2.45 Structure of $\text{FcSe}(\text{CH}_2)_3\text{Se}(\text{CH}_2)_3\text{SeFc}$ with atom numbering scheme

The packing diagram is shown in Fig. 2.46 and 2.47. There are one-dimensional infinite chains that run parallel to each other. The adjacent ferrocenyl rings are perpendicular to each other and engage in $\text{H}\cdots\text{H}$ interactions over a distance of 2.309 \AA (Fig. 2.48).

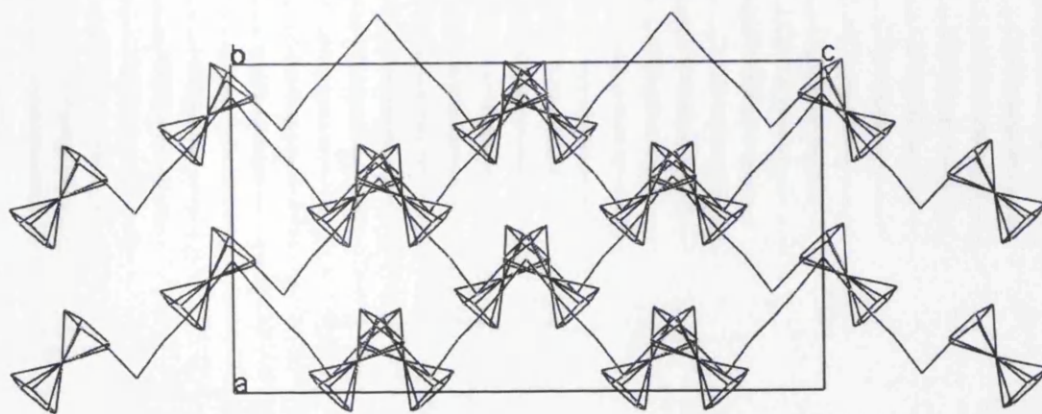


Fig. 2.46 Packing diagram of $\text{FcSe}(\text{CH}_2)_3\text{Se}(\text{CH}_2)_3\text{SeFc}$ in bc plane

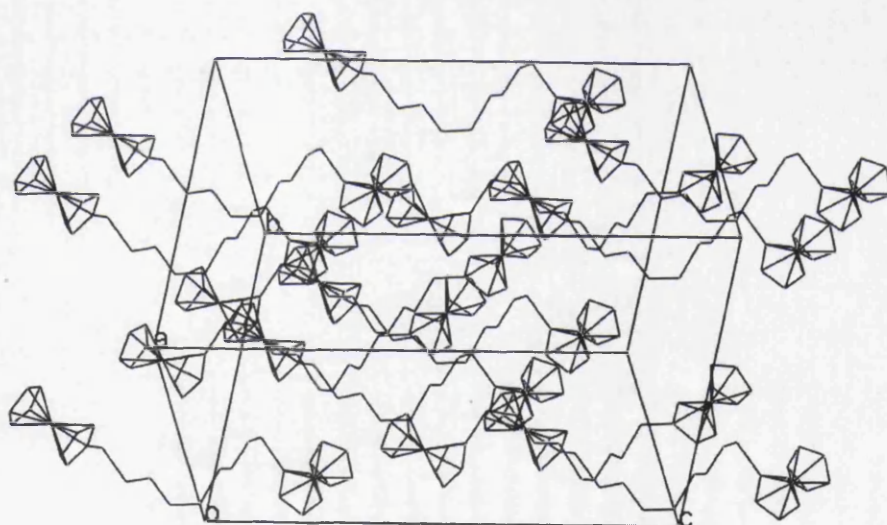


Fig. 2.47 Packing diagram of $\text{FcSe}(\text{CH}_2)_3\text{Se}(\text{CH}_2)_3\text{SeFc}$

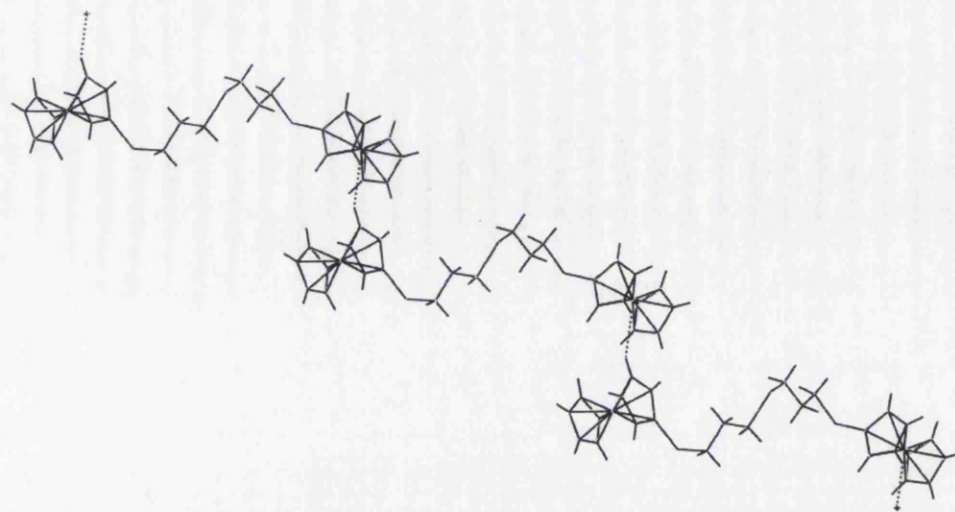


Fig. 2.48 Packing diagram of $\text{FcSe}(\text{CH}_2)_3\text{Se}(\text{CH}_2)_3\text{SeFc}$ with $\text{H}\cdots\text{H}$ interactions

Table 2.6 Selected bond lengths (\AA) and bond angles ($^\circ$) for
 $\text{FcSe}(\text{CH}_2)_3\text{Se}(\text{CH}_2)_3\text{SeFc}$

<i>Bond lengths</i>					
Se(1)-C(1)	1.946(4)	C(1)-C(2)	1.532(6)	C(2)-C(3)	1.516(6)
C(3)-Se(2)	1.956(4)	Se(2)-C(4)	1.899(4)	C(4)-Fe	2.042(4)
<i>Bond angles</i>					
Se(2)-C(4)-Fe	124.6(2)	C(1)-Se(1)-C(1)	100.0(2)		
C(4)-Se(2)-C(3)	96.92(17)				
<i>Torsion angles</i>					
C(3)-Se(2)-C(4)-Fe	-161.9(2)	C(4)-Se(2)-C(3)-C(2)	-63.7(3)		
C(1)-Se(1)-C(1)-C(2)	-58.1(3)				

* The number in bracket means the standard uncertainty, s.u..

Table 2.7 Crystal data and structure refinement for FcSe(CH₂)₃Se(CH₂)₃SeFc

Empirical formula	C ₂₆ H ₃₀ Fe ₂ Se ₃
Formula weight	691.1
T (K)	296(2)
Wavelength (Å)	0.71069
Crystal system	Orthorhombic
Space group	F2dd
<i>a</i> (Å)	12.562(1)
<i>b</i> (Å)	17.311(1)
<i>c</i> (Å)	23.029(1)
α (°)	90
β (°)	90
γ (°)	90
Volume (Å ³)	5007.9(5)
<i>Z</i>	16
<i>D</i> _c (Mg m ⁻³)	1.883
Absorption coefficient (mm ⁻¹)	5.532
<i>F</i> (000)	2720
Crystal size (mm)	0.40 × 0.30 × 0.20
θ range for data collection (°)	4.38 to 35.20
Index ranges	-18 ≤ <i>h</i> ≤ 17, -27 ≤ <i>k</i> ≤ 21, -36 ≤ <i>l</i> ≤ 28
Reflections collected	13036
Independent reflections [Rint]	4120 [0.0823]
Data / restraints / parameters	4120 / 0 / 156
Goodness-of-fit on F ²	0.898
Final <i>R</i> indices [<i>I</i> > 2σ(<i>I</i>)]	<i>R</i> ₁ = 0.0351, <i>wR</i> ₂ = 0.0755
<i>R</i> indices (all data)	<i>R</i> ₁ = 0.0832, <i>wR</i> ₂ = 0.0862
Largest diff. peak and hole (e Å ⁻³)	0.543, -0.571

* The number in bracket means the standard uncertainty, s.u..

2.2.1.3 ^1H and ^{13}C NMR spectroscopy

The ^1H and ^{13}C NMR data have been listed above. All these spectra were recorded in CDCl_3 , with concentrations of around 100 mg/0.5 ml. The scheme used for assignment is shown in Fig. 2.49.

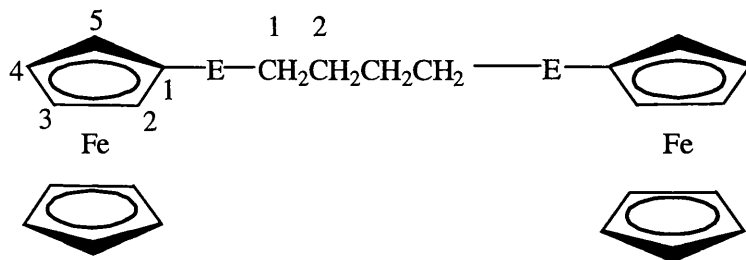


Fig. 2.49 Scheme for assignment of NMR spectra of ferrocenyl chalcogenide compounds

Some characteristics are summarised below.

^1H NMR spectra

(1) Cyclopentadienyl rings

In the series $\text{FcSe}(\text{CH}_2)_n\text{SeFc}$, C_5H_5 appears as a singlet at 4.10 or 4.11 ppm. The $\frac{1}{2}\text{A}_2\text{B}_2$ pattern of C_5H_4 (H-3,4) is at a similar field to the resonance of the unsubstituted cyclopentadienyl ring. C_5H_4 (H-2,5) are shifted a little downfield, but less so than in $\text{FcSe}(\text{CH}_2)_n\text{CH}_3$.

In $\text{FcTeCH}_2\text{TeFc}$ and $\text{FcTe}(\text{CH}_2)_3\text{TeFc}$, $\delta(\text{C}_5\text{H}_5)$ is 4.07 ppm, and $\delta(\text{C}_5\text{H}_4, \text{H-3,4})$ is shifted to 4.17 ppm ($n = 1$) or 4.13 ppm ($n = 3$); $\delta(\text{C}_5\text{H}_4, \text{H-2,5})$ is further downfield at 4.31 ppm ($n = 1$) or 4.24 ppm ($n = 3$).

No obvious ^1H - ^{77}Se or ^1H - ^{125}Te coupling was observed in these series. From the literature, the ^1H - ^{77}Se coupling constant would be expected to be about half of the value of the corresponding ^1H - ^{125}Te coupling constant.⁵⁸

(2) Alkyl chain

$\delta(\text{SeCH}_2)$ is 3.61 ($n = 1$), 2.71 ($n = 2$) and 2.54 ($n = 3$), a little upfield compared to its value in $\text{RSe}(\text{CH}_2)_n\text{SeR}$.⁵⁶ The only $^2J_{\text{Se-H}}$ value obtained for SeCH_2 is 7.8 Hz in $\text{FcSeCH}_2\text{SeFc}$, about half of that in $\text{MeSeCH}_2\text{SeMe}$. In $\text{RSe}(\text{CH}_2)_n\text{SeR}$ ($\text{R} = \text{Me}$, $n = 1, 2, 3, 6, 12$; $\text{R} = \text{Ph}$, $n = 1, 2, 3$),⁵⁶ for SeCH_2 $^2J_{\text{Se-H}}$ is *ca.* 8-10 Hz, except for RSeCH_2SeR where it is *ca.* 12-15 Hz which may be due to a wider Se-C-Se angle

leading to greater s-character in the C-Se bonds.

$\delta(\text{TeCH}_2)$ is 3.40 ppm ($n = 1$) and 2.53 ppm ($n = 3$). ${}^2J_{\text{Te-H}}$ for TeCH_2 is 12.5 Hz in $\text{FcTeCH}_2\text{TeFc}$, half of its value in $\text{MeTeCH}_2\text{TeMe}$. Although in the compounds FcECH_2EFc ${}^2J_{\text{Te-H}}$ is larger than ${}^2J_{\text{Se-H}}$, the difference is not as much as in $\text{RE}(\text{CH}_2)_n\text{ER}$ ($\text{R} = \text{Me}$ or Ph). In $\text{RTe}(\text{CH}_2)_n\text{TeR}$ ($\text{R} = \text{Me}$, $n = 1, 3, 6, 10$; $\text{R} = \text{Ph}$, $n = 1, 3, 6$),⁶⁰ $\delta(\text{TeCH}_2)$ is 2.6-2.8 ppm, except for RTeCH_2TeR , which have $\delta(\text{CH}_2)$ of 3.4-3.8 ppm. Generally, ${}^2J_{\text{Te-H}}$ is 20-30 Hz, approximately 2-3 times greater than ${}^2J_{\text{Se-H}}$ in $\text{RSe}(\text{CH}_2)_n\text{SeR}$.

For the other compounds, the shifts and coupling constants are similar.

${}^{13}\text{C}$ NMR spectra

(1) Cyclopentadienyl rings

The peak due to C-1 is easily recognized, because it behaves as a quaternary carbon, which disappears in the DEPT spectrum. A study of trichalcogena[3]ferrocenophanes found that the chemical shift of this *ipso*-carbon correlates with their electrochemical behaviour.⁵ In $\text{FcSe}(\text{CH}_2)_n\text{SeFc}$, the ${}^{13}\text{C}$ NMR resonance of the *ipso*-carbon atoms bound to selenium is at *ca.* 70 ppm, close to those of the others in the cyclopentadienyl rings. The ${}^{13}\text{C}$ shifts of the *ipso*-carbon atoms bound to tellurium are shifted about 25 ppm upfield compared to those in the selenium analogues. This is the 'heavy-atom effect', meaning that the ${}^{13}\text{C}$ shifts of the carbon atoms bound to tellurium are shifted upfield compared to that in analogous selenides.^{32, 55}

In $\text{FcTe}(\text{CH}_2)_3\text{TeFc}$, ${}^1J_{\text{Te-C}}$ for C-1 is 304 Hz, larger than that for the α -carbon of the alkyl chain (156 Hz). A similar result was found in FcTe^nPr , which has coupling constants of 307 Hz for C-1 and 152 Hz for the α -carbon. The larger coupling constants are associated with bonding that has a higher degree of s character: *i.e.* ${}^1J(\text{sp}^3) < {}^1J(\text{sp}^2) < {}^1J(\text{sp})$.⁶²⁻⁶⁷ This phenomenon can be seen most clearly in the linear tellurium compounds, such as $\text{FcTe}(\text{CH}_2)_3\text{Te}(\text{CH}_2)_3\text{TeFc}$: ${}^1J_{\text{C-Te}}$ for C-1 is 306 Hz and ${}^1J_{\text{C-Te}}$ for the α -carbons are 158 and 156 Hz. The ${}^1J_{\text{Se-C}}$ value for C-1 could not be obtained except in $\text{FcSeCH}_2\text{SeFc}$ in which it is 111 Hz, one third of the equivalent ${}^1J_{\text{Te-C}}$.

In the spectra of $\text{FcTeCH}_2\text{TeFc}$ and $\text{FcTe}(\text{CH}_2)_3\text{TeFc}$, the resonance for C-3,4 in the substituted cyclopentadienyl ring is shifted downfield by 2 ppm and that for C-2,5 by 4 ppm compared to the selenium analogues, as was observed in the $\text{FcTe}(\text{CH}_2)_n\text{CH}_3$

series.³⁶

(2) Alkyl chain

In $\text{FcSeCH}_2\text{SeFc}$, the chemical shift of SeCH_2 is 24.4 ppm, a little downfield of that in $\text{MeSeCH}_2\text{SeMe}$ (17.3 ppm with $^1J_{\text{Se-C}} = 83.9 \text{ Hz}^{56}$). The $^1J_{\text{Se-C}}$ value is 86 Hz smaller than for the *ipso*-carbon of the cyclopentadienyl rings (111 Hz). In $\text{FcSe}(\text{CH}_2)_2\text{SeFc}$, the $^1J_{\text{Se-C}}$ value for the α -carbon is 64 Hz, similar to those in $\text{RSe}(\text{CH}_2)_n\text{SeR}$ ($n > 1$) which have been observed to be almost constant at *ca.* 60 Hz. This consistency is also found in the linear polydentate ferrocenyl selenides, such as $\text{FcSe}(\text{CH}_2)_3\text{Se}(\text{CH}_2)_3\text{Se}(\text{CH}_2)_3\text{SeFc}$ ($^1J_{\text{Se-C}} = 62 \text{ Hz}$ for all the α -carbons). The observation that the CH_2 resonances lie in the order $\text{C}(1) < \text{C}(3) < \text{C}(2)$ in $\text{RSe}(\text{CH}_2)_n\text{SeR}$ ($\text{R} = \text{Me}$, $n = 1, 2, 3, 6, 12$; $\text{R} = \text{Ph}$, $n = 1, 2, 3$),⁵⁶ hasn't been replicated in $\text{FcSe}(\text{CH}_2)_3\text{SeFc}$, and no values of $^2J_{\text{Se-C}}$ and $^3J_{\text{Se-C}}$ were obtained.

Although the 'heavy atom effect' also operated in $\text{RTe}(\text{CH}_2)_n\text{TeR}$, where the CH_2Te resonances are found in the range *ca.* -6 to +6 ppm, except in $\text{MeTeCH}_2\text{TeMe}$, it is surprising to find it absent in $\text{FcE}(\text{CH}_2)_3\text{EFc}$, with $\text{E} = \text{Se}$, $\delta = 29.9 \text{ ppm}$ and $\text{E} = \text{Te}$, $\delta = 34.1 \text{ ppm}$.

In $\text{FcTe}(\text{CH}_2)_3\text{TeFc}$, $^1J_{\text{Te-C}}$ for TeCH_2 is 152 Hz, consistent with the values of 150-180 Hz in $\text{MeTe}(\text{CH}_2)_n\text{TeMe}$ ($n > 1$). Values of 156 or 158 Hz were also found in the linear polydentate compounds.

2.2.1.4 ^{77}Se and ^{125}Te NMR spectroscopy

Compared to the two lighter elements, O and S, which possess only quadrupolar nuclei and of which the dominant isotopes have zero spin, Se and Te possess spin $\frac{1}{2}$ nuclei with adequate natural abundance (^{77}Se , 7.58% and ^{125}Te 6.99%). Thus selenium and tellurium NMR spectroscopy is possible. Since the advent of modern multinuclear FT instrumentation direct observation is straightforward, and their chemical shift ranges are very large, 3000 ppm for ^{77}Se and 7000 ppm for ^{125}Te .⁵⁵ The standards generally used are neat (or nearly neat) Me_2Se and Me_2Te .

For any magnetically active nucleus in the presence of an external field, H_0 , the effective field, H_0' , is given by⁵⁵

$$H_0' = H_0(1 - \sigma) \quad (\text{Equation 1})$$

σ : the magnetic shielding constant for the nucleus under observation.

$$\sigma = \sigma^{\text{dia}} + \sigma^{\text{para}} + \sigma^{\text{N}} \quad (\text{Equation 2})$$

σ^{dia} : the diamagnetic term;

σ^{para} : the paramagnetic term;

σ^{N} : neighbouring-group anisotropy effects.

The value of σ^{para} is zero for nuclei with spherical distributions of electrons, but for Se and Te, which have a valence-shell electron configuration of ns^2np^4 , a non-spherical distribution of electrons exists and variations in paramagnetic terms are expected to be the dominant contributor. The magnitude of σ^{para} is related to several factors:

$$\sigma^{\text{para}} \propto - [r^{-3}]_{\text{np}} \sum Q/\Delta E \quad (\text{Equation 3})$$

r : the radius of the np orbital;

Q : the imbalance of charge in the valence shells;

ΔE : the effective excitation energy.

So the deshielding will increase when (a) the paramagnetic circulation gets closer to the nucleus; (b) the asymmetry of the valence electron cloud increases; (c) ΔE becomes smaller and excitation become easier.

The ^{77}Se NMR and ^{125}Te NMR spectroscopy data for diferrocenyl chalcogenides, diferrocenyl dichalcogenides and bis(ferrocenylchalcogeno)alkanes are summarized in Table 2.8.

Table 2.8 ^{77}Se and ^{125}Te NMR data for diferrocenyl chalcogenides, diferrocenyl dichalcogenides and bis(ferrocenylchalcogeno)alkanes

Compound	$\delta(^{77}\text{Se})/\text{ppm}$		$\delta(^{125}\text{Te})/\text{ppm}$		$\delta(^{125}\text{Te})/\delta(^{77}\text{Se})$
	Cal.	Obv.	Cal.	Obv.	
Fc_2E	-	210	-	347	1.65
Fc_2E_2	-	484	-	381	0.79
FcECH_2EFc	222	252	386	413	1.64
$\text{FcE}(\text{CH}_2)_2\text{EFc}$	225	232	-	-	-
$\text{FcE}(\text{CH}_2)_3\text{EFc}$	179	185	278	295	1.59
$\text{FcSe}(\text{CH}_2)_3\text{TeFc}$	179	188	278	299	1.59
$\text{FcE}(\text{CH}_2)_4\text{EFc}$	184	193	280	302	1.56

As discussed above, σ^{para} is expected to be the dominant contributor for Se and Te. In the dichalcogenides, the asymmetry of the molecules gives rise to deviations from spherical symmetry of the electron cloud, which results in an increase in ΔE^{-1} and ΣQ . Thus a dichalcogenide always has a more deshielded chalcogen nucleus than the corresponding chalcogenide.⁶⁸ So Fc_2E_2 has a downfield shift compared to Fc_2E .

It has been shown that in the unsymmetrical selenides $\text{RR}'\text{Se}$, the ^{77}Se chemical shifts can be predicted with reasonable accuracy since the shift changes with R and R' are additive.^{56, 60, 69}

The calculation starts with $\Delta\delta(\text{Me}) = 0$ from the Me_2Se reference and $\Delta\delta(\text{Fc}) = ca. 105$ ppm from Fc_2Se . From $\text{MeSe}(\text{CH}_2)_3\text{SeMe}$, $\Delta\delta((\text{CH}_2)_n)$ is *ca.* 117 (n = 1), 120 ppm (n = 2) and 74 ppm (n = 3).⁵⁶ The insensitivity of the chemical shift to longer chains is consistent with data for R_2Se ; changes more remote than the γ -carbon atom have negligible effect on $\delta(\text{Se})$.⁵⁵ The calculated chemical shifts showed a good match to the observed ones, except for the observed value being a little larger for $\text{FcSeCH}_2\text{SeFc}$. A contribution of *ca.* 24 ppm has been assigned to the $\text{CH}_2\text{C}(\text{CH}_2)_3$ group,⁵⁶ which leads to a predicted value for $\text{MeC}(\text{CH}_2\text{SeFc})_3$ of 129 ppm (observed 138 ppm). In the compounds $\text{FcE}(\text{CH}_2)_3\text{Se}(\text{CH}_2)_3\text{EFc}$, the FcE groups are too far away to affect the middle Se, which means its chemical shift should be similar to that in Bu_2Se (167 ppm); the observed values were 154 (E = Se) and 151 (E = Te).

A similar method can be used to predict ^{125}Te chemical shifts. From $\text{MeTe}(\text{CH}_2)_3\text{TeMe}$ ⁶⁰ (104 ppm), one can assign a contribution of *ca.* 104 ppm to a $(\text{CH}_2)_n$ - ($n \geq 3$) group, starting with $\Delta\delta(\text{Me}) = 0$ from the Me_2Te reference. Using $\Delta\delta(\text{Fc}) = \text{ca. } 174$ ppm leads to a predicted chemical shift for $\text{FcTe}(\text{CH}_2)_3\text{TeFc}$ of *ca.* 278 ppm. The measured value for the latter is 295 ppm (Table 2.8). Similarly one can assign a value of 212 ppm to $-\text{CH}_2\text{Te}$ from the chemical shift of $\text{MeTeCH}_2\text{TeMe}$, leading to a prediction of 386 ppm for $\text{FcTeCH}_2\text{TeFc}$ (experimental value: 413 ppm). A contribution of *ca.* 21 ppm has been assigned to the $\text{CH}_2\text{C}(\text{CH}_2)_3$ group,⁶⁰ which leads to a predicted value for $\text{MeC}(\text{CH}_2\text{TeFc})_3$ of 195 ppm (observed 216 ppm). Bu_2Te has $\delta(\text{Te}) = 228$ ppm, and similar values of 228 ppm ($\text{E} = \text{Se}$) and 223 ppm ($\text{E} = \text{Te}$) were observed for $\text{FcE}(\text{CH}_2)_3\text{Te}(\text{CH}_2)_3\text{ETeFc}$.

From equation 3, we can predict that if the ΣQ terms for Se and Te are the same in analogous compounds, a plot of $\delta(^{125}\text{Te})/\delta(^{77}\text{Se})$ should be a straight line with a slope of 1.5-1.6.⁵⁵ All the values of $\delta(^{125}\text{Te})/\delta(^{77}\text{Se})$, except for Fc_2E_2 , are in accordance with previous theoretical calculations and empirical investigations. Especially for $\text{FcE}(\text{CH}_2)_3\text{E}'\text{Fc}$, the ratio of 1.59 is the same as that for ferrocenyl alkyl chalcogenides.³⁶ In previous studies, a value of 1.71 was found for phenyl alkyl chalcogenides⁶⁹ and one of 1.8 was reported by McFarlane and McFarlane.⁷⁰ The unusual downfield chemical shift of diferrocenyl diselenide has been noted before. This phenomenon is similar to that exhibited by the diphenyl dichalcogenides, having chemical shifts of 420 ppm (Ph_2Te_2) and 464 ppm (Ph_2Se_2).^{55, 71}

During the study of FcSeR , a very interesting correlation was found: the trend in the ^{13}C chemical shift is the reverse of that in ^{77}Se chemical shift with a linear relationship between them.³⁷ From Table 2.9, it is clear that this relationship does not exist for the new series of compounds. There is also no relationship between $\delta(^{13}\text{C}_1)$ and $\delta(^{125}\text{Te})$ (shown in Table 2.10).

Quite a small coupling constant was observed in $\text{FcSe}(\text{CH}_2)_3\text{TeFc}$, $^4J_{\text{Se-Te}} = 11.7$ Hz. The $^4J_{\text{Te-Te}}$ coupling constants are about 43 Hz in $\text{FcTe}(\text{CH}_2)_3\text{Te}(\text{CH}_2)_3\text{TeFc}$.

Table 2.9 ^{77}Se chemical shifts of FcSe and ^{13}C chemical shifts of C_1

Compound	^{77}Se chemical shift	^{13}C chemical shift (C_1)
Fc_2Se	210	69.7
Fc_2Se_2	484	69.8
$\text{FcSeCH}_2\text{SeFc}$	252	72.1
$\text{FcSe}(\text{CH}_2)_2\text{SeFc}$	232	73.6
$\text{FcSe}(\text{CH}_2)_3\text{SeFc}$	185	69.2
$\text{FcSe}(\text{CH}_2)_3\text{TeFc}$	188	69.7
$\text{CH}_3\text{C}(\text{CH}_2\text{SeFc})_3$	138	72.7
$\text{FcSe}(\text{CH}_2)_3\text{Se}(\text{CH}_2)_3\text{SeFc}$	190	70.9
$\text{FcSe}(\text{CH}_2)_3\text{Te}(\text{CH}_2)_3\text{SeFc}$	189	70.6

Table 2.10 ^{125}Te chemical shifts of FcTe and ^{13}C chemical shifts of C_1

Compound	^{125}Te chemical shift	^{13}C chemical shift (C_1)
Fc_2Te	347	49.2
Fc_2Te_2	381	41.4
$\text{FcTeCH}_2\text{TeFc}$	413	48.1
$\text{FcTe}(\text{CH}_2)_3\text{TeFc}$	295	43.7
$\text{FcSe}(\text{CH}_2)_3\text{TeFc}$	299	43.6
$\text{CH}_3\text{C}(\text{CH}_2\text{TeFc})_3$	216	45.0
$\text{FcTe}(\text{CH}_2)_3\text{Te}(\text{CH}_2)_3\text{TeFc}$	299	43.8
$\text{FcTe}(\text{CH}_2)_3\text{Se}(\text{CH}_2)_3\text{TeFc}$	301	42.3
$\text{FcTe}(\text{CH}_2)_3\text{Se}(\text{CH}_2)_3\text{Se}(\text{CH}_2)_3\text{TeFc}$	301	43.8

2.2.1.5 Electronic absorption spectroscopy

The electronic absorption spectra of ferrocene and its derivatives are well understood.^{72, 73} As shown in Fig. 2.50, the ground state of d⁶ ferrocene is ${}^1A_{1g} - (1e_{2g})^4(2a_{1g})^2$. There exist two similar characteristic bands in the UV-vis spectra: one absorption around 440 nm is attributed to the ${}^1E_{1g} \leftarrow {}^1A_{1g}$ transition; another one around 325 nm can be assigned as the ${}^1E_{2g} \leftarrow {}^1A_{1g}$ transition.

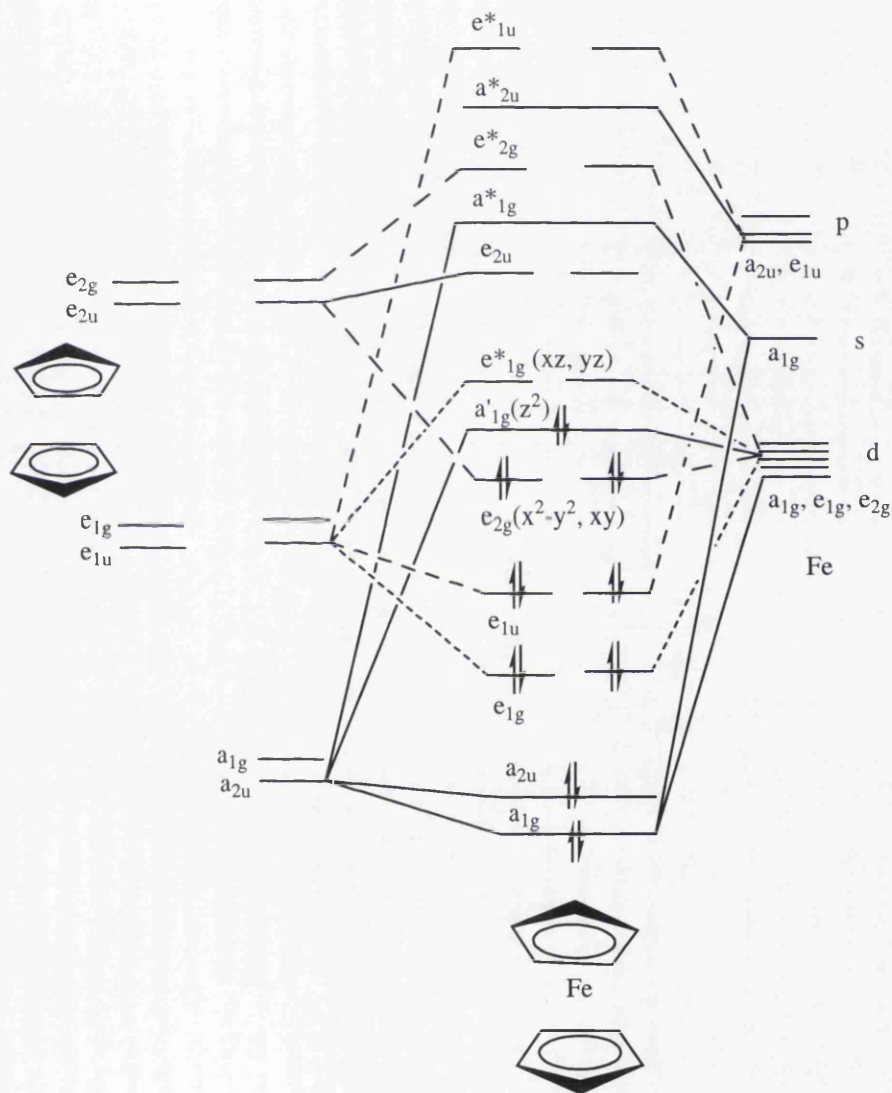


Fig. 2.50 MO diagram of FcH

In Fc_2Se , the band around 325 nm can't be resolved, and only the absorption at 440 nm is apparent. So in Fc_2Se_2 the second band at 370 nm can be attributed to the absorption due to the Se-localized $n \rightarrow \sigma^*(Se-Se)$ transition. It occurs at a slightly

higher wavelength than is typical for organic diselenides.^{74, 75} It has been shown that torsional distortions from 90° of the dihedral angle about the C₂ molecular symmetry axis will result in a bathochromic shift of the lowest UV band of various diselenides, R₂Se₂.^{76, 77} The dihedral angle in FcSeSeFc is -88.7(4)°,³⁸ much closer to 90° than 97.1 (3.0)° in diphenyl diselenide,⁷⁸ which should result in a smaller red shift, so the ferrocenyl group may also affect the HOMO or LUMO energy of the Se-Se bond. Also the unusually large downfield shift of the ⁷⁷Se resonance in Fc₂Se₂ corresponds to greater deshielding of the Se nucleus, which results from a smaller excitation energy ΔE in equation 3, and a larger λ. A similar phenomenon has been observed in the selones,⁷⁹ where ⁷⁷Se chemical shifts correlate linearly with the energy of the n→π* transition. The band due to the Se-Se n→σ* transition disappeared after the Se-Se band was broken, *i.e.* in the spectra of bis(ferrocenylseleno)alkanes.

In FcTeTeFc, the band at 395 nm can be attributed to a Te-localized n→σ*(Te-Te) transition. The wavelength is quite similar to that in organic ditellurides⁸⁰ (406 nm), as is the dihedral angle, which in FcTeTeFc is -86.1(4)°³⁷ and in PhTeTePh is 88.5°.⁸¹ The absorption around 450 nm is attributed to the ¹E_{1g}←¹A_{1g} transition of ferrocene; a small bathochromic shift occurs which may be due to the better donor property of tellurium. In FcTeCH₂TeFc, the band at 330 nm can be assigned as the ¹E_{2g}←¹A_{1g} transition of the ferrocenyl group.

For the other compounds there is just one relatively weak absorption band due to the ¹E_{1g}←¹A_{1g} transition of the ferrocenyl group.



Table 2.11 UV-vis absorption in MeCN at 25 °C

	λ_1 (nm)/ ϵ ($\text{dm}^3 \text{mol}^{-1} \text{cm}^{-1}$)	λ_2 (nm)/ ϵ ($\text{dm}^3 \text{mol}^{-1} \text{cm}^{-1}$)
Fc_2Se	-	440/265
FcSeSeFc	370/ 800	440/555
$\text{FcSeCH}_2\text{SeFc}$	-	440/280
$\text{FcSeCH}_2\text{CH}_2\text{SeFc}$	-	440/280
$\text{FcSe}(\text{CH}_2)_3\text{SeFc}$	-	440/230
Fc_2Te	-	450/190
FcTeTeFc	395/2130	460/1500
$\text{FcTeCH}_2\text{TeFc}$	330/1910	455/320
$\text{FcTe}(\text{CH}_2)_3\text{TeFc}$	-	445/250
$\text{FcSe}(\text{CH}_2)_3\text{TeFc}$	-	445/300

2.2.2 Macrocyclic ferrocenyl selenide ligands

In recent years, the design of macrocyclic systems which are capable of detecting, amplifying or recognizing metal ions has attracted more and more efforts.⁸² As noted in Chapter One, some ferrocene-functionalised crown ethers have been reported to be good sensors for s-block cations.⁸³ Sulphur analogues haven't been extensively studied, with only a few compounds synthesized (examples shown in Fig. 2.52).⁸⁴

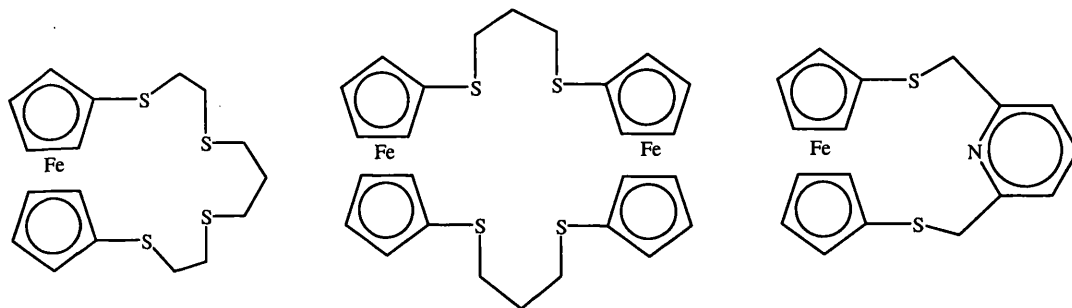


Fig. 2.52 Three examples of macrocyclic ferrocenyl sulphide ligands

It's no surprise then to find only one literature report of a similar selenium ligand, the trichalcogenaferrocenophane shown in Fig. 2.53, obtained from bis(2-bromoethyl) selenium dibromide.⁸⁵

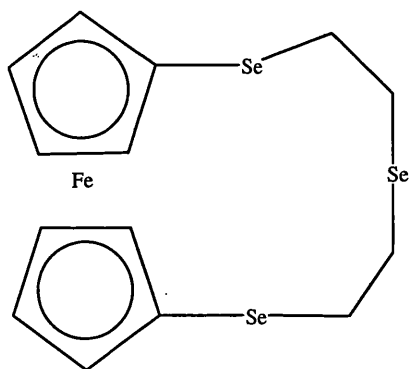


Fig. 2.53 Macroyclic ferrocenyl selenide ligand

As softer donor ligands, macrocyclic ferrocenyl selenides are expected to have a rich chemistry, especially with the second and third row transition metals, and may work as highly sensitive electrochemical sensors for these metals. In this section, the synthesis and characterisation of two new macrocyclic ferrocenyl selenide ligands

are described: 1,5,16,21-tetraselena[5.5]ferrocenophane (shown in Fig. 2.54) and 1,5,9,12-tetraselena[12]ferrocenophane (shown in Fig. 2.55). Discussion of their coordination chemistry and electrochemistry will be deferred until Chapter Three and Chapter Four respectively.

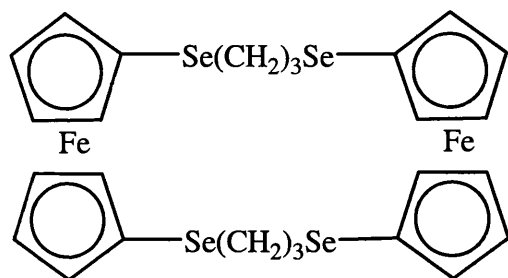


Fig. 2.54 1,5,16,21-Tetraselena[5.5]ferrocenophane (difcSe₄)

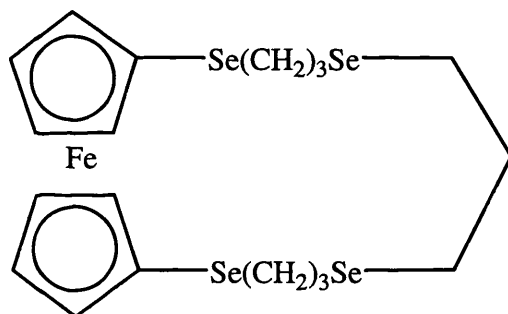


Fig. 2.55 1,5,9,12-Tetraselena[12]ferrocenophane (fcSe₄)

2.2.2.1 Synthesis

fc[Se(CH₂)₃Br] and difcSe₄

Since the first series of cyclic selenoethers [8]aneSe₂, [14]aneSe₄, [16]aneSe₄ and [24]aneSe₆ was reported by Pinto in the late 1980s,^{86, 87} several series of macrocyclic selenoether and telluroether ligands have been obtained.⁸⁸⁻¹⁰⁰ Most synthetic schemes includes a [1+1] cyclisation in high dilution solution (example shown in Fig. 2.56).⁸⁹ Two research groups reported that higher yields can be obtained by utilizing Cs₂CO₃ in DMF solution.^{91, 95}

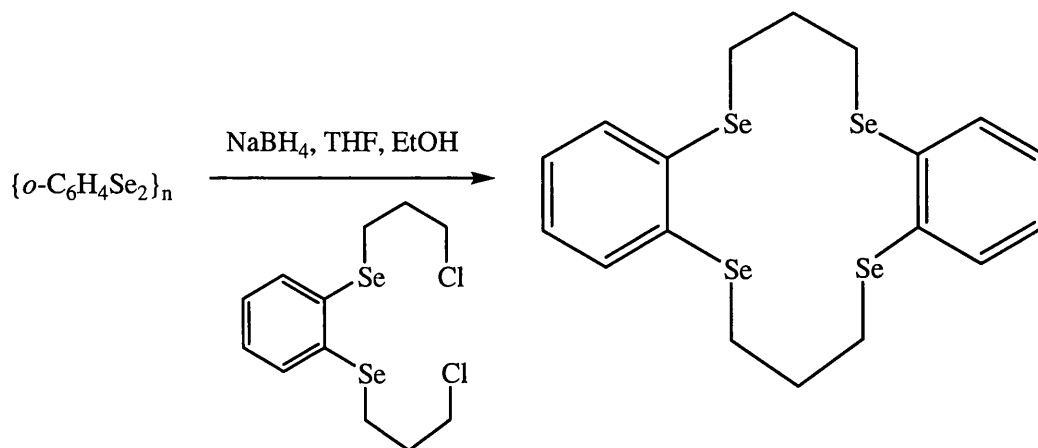


Fig. 2.56 Synthetic scheme for dibenzo[14]aneSe₄

The first scheme designed for the synthesis of difcSe₄ was the *in situ* [2+2] reaction shown in Fig. 2.57. This route resulted in a sticky oily mixture, which could not be separated by column chromatography. There are several possible reasons: (1) The first dilithiation step may not proceed in 100% yield, so some monolithiated compound will be present; (2) the ferrocene unit has a sandwich structure which allows the alternative formation of a linear polymer; (3) the ring closure reaction may include more reagents in, for example, a [3+3] reaction.

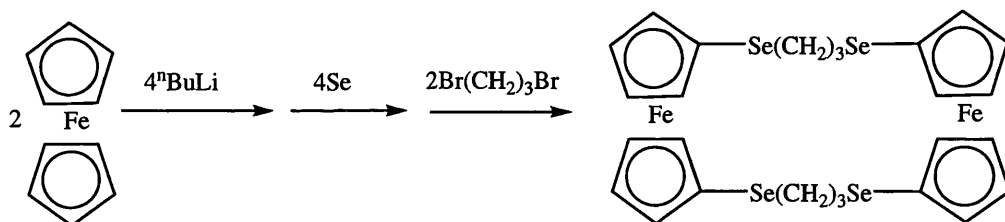


Fig. 2.57 Failed synthetic scheme for difcSe₄

A new synthetic scheme was then designed, using pure triseleno[3]ferrocenophane to obtain 1,1'-bis(3-bromopropylseleno)ferrocene (scheme shown in Fig. 2.58). Adding 1,1'-bis(3-bromopropylseleno)ferrocene to an ethanol solution of fcSe₃ reduced by sodium borohydride can yield the target product 1,5,16,21-tetraselena[5.5]ferrocenophane, difcSe₄, via [1+1] cyclisation (scheme shown in Fig. 2.59). This scheme worked smoothly, fc[Se(CH₂)₃Br]₂ was obtained in about 50% yield and difcSe₄ in about 36% yield.

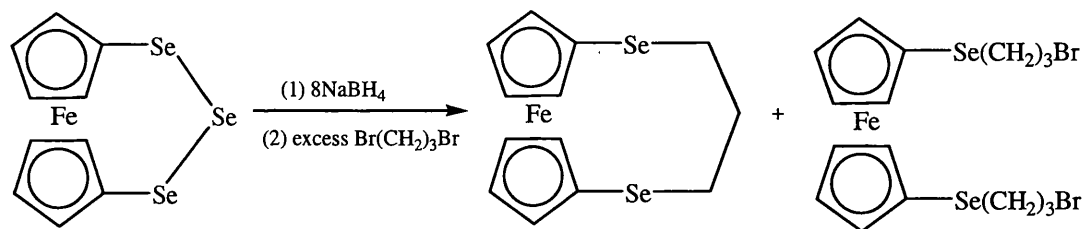


Fig. 2.58 Synthetic scheme for 1,1'-bis(3-bromopropylseleno)ferrocene

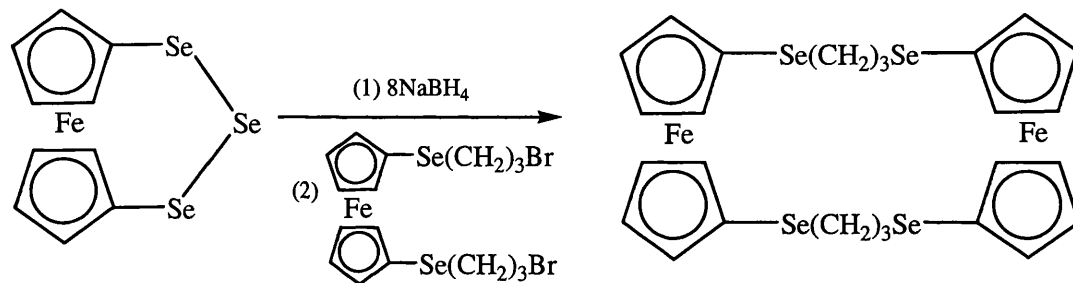


Fig. 2.59 Successful synthetic scheme for difcSe₄

Reduction of fcSe_3 by sodium borohydride in ethanol was followed by addition of excess $\text{Br}(\text{CH}_2)_3\text{Br}$. The mixture was left to stir 2 h. The solvent was then removed by evaporation under reduced pressure. The residue was treated with water and extracted with CH_2Cl_2 . The extract was dried over MgSO_4 and evaporated to dryness, then subjected to column chromatography on SiO_2 . Eluting with hexane/dichloromethane (3:1), an orange-red band and a yellow band were collected sequentially. After evaporation, the orange-red band yielded solid 1,5-diselena[5]ferrocenophane and the yellow band gave the target product 1,1'-bis(3-bromopropylseleno)ferrocene as an orange oil, with the yield about 50%. In order to increase the yield, several variants were performed such as decreasing the reaction temperature to 0°C or transferring the reduced fcSe_3 solution to the $\text{Br}(\text{CH}_2)_3\text{Br}$ solution in high concentration. All these attempts showed no significant improvement. 1,5-Diselena[5]ferrocenophane was always obtained as the main by-product which means that cyclization is quick, possibly because the sodium cation in solution is acting as a good template ion for the process.

Reduction of fcSe_3 by sodium borohydride in ethanol was followed by addition of 1,1'-bis(3-bromopropylseleno)ferrocene in THF. The mixture was left to stir overnight. After column chromatography the product 1,5,16,21-tetraselena[5.5]ferrocenophane was generally isolated as a yellow solid. Efforts to improve the yield by using $\text{K}(\text{I})$ or $\text{Cs}(\text{I})$ as a template ion showed no change, which may be due to the hard nature of these metals, size mismatch or not using DMF as the solvent.

Multinuclear NMR study of difcSe_4 shows that the ^1H and ^{13}C NMR resonances undergo a low field shift compared to those of the open chain compound $\text{FcSe}(\text{CH}_2)_3\text{SeFc}$, especially the *ipso*-carbon atoms bound to selenium which are at 75.5 ppm compared to 70 ppm in $\text{FcSe}(\text{CH}_2)_3\text{SeFc}$. The same chemical shift was observed for the *ipso*-carbon atoms in 1,1'-bis(methylseleno)ferrocene.²⁹ The ^{77}Se resonance is at 170 ppm, shifted 18 ppm to higher field compared to that of $\text{FcSe}(\text{CH}_2)_3\text{SeFc}$, which may be due to the macrocyclic effect.

fcSe_4

Another kind of macrocyclic ligand fcSe_4 (Fig. 2.55) can also be obtained from 1,1'-bis(3-bromopropylseleno)ferrocene, via the synthetic scheme shown in Fig. 2.60. Two equivalents of NaBH_4 were added to an ethanol solution of $\text{NCS}(\text{CH}_2)_3\text{SeCN}$ at 0 °C; the solution turned red in 5 minutes. On slowly warming to room temperature, the colour disappeared quickly, and there was intense gas evolution. One equivalent of $\text{fc}[\text{Se}(\text{CH}_2)_3\text{Br}]_2$ in a small amount of THF was then added. Following reaction at room temperature for 2 h, the target compound was obtained via chromatography.

A ^1H NMR study of fcSe_4 shows that H-2,5 and H-3,4 give rise to only one resonance at room temperature, which is quite unusual for a ferrocenophane. This may result from the compound's structural flexibility. Also the C-1 peak shifts to even lower field in the ^{13}C NMR spectrum, 77.7 ppm. In the ^{77}Se NMR spectrum, there are two resonances at 170 and 161 ppm, which can be assigned to Se attached to the ferrocenyl group and alkyl-attached Se respectively. The alkyl-attached Se has a similar chemical shift in [16]ane Se_4 ($\delta = 157$ ppm).¹⁰¹

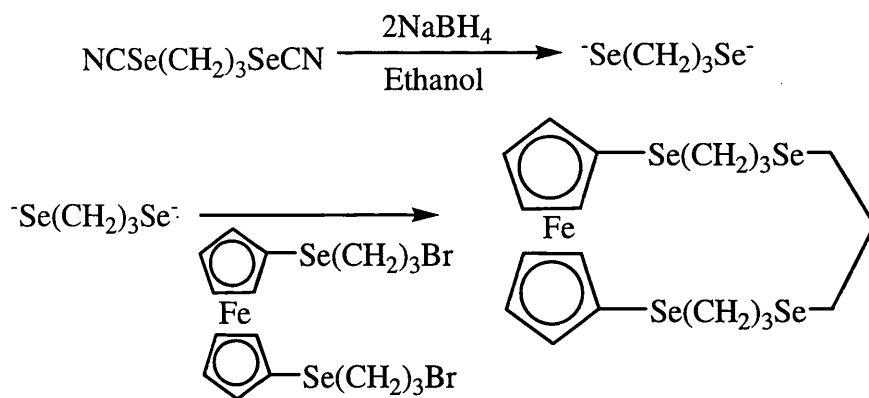


Fig. 2.60 Synthetic scheme for fcSe_4

Spectroscopic data for each of the new compounds described in this section are given in Chapter Seven.

2.2.2.2 Crystal Structure of difcSe_4

Crystals of difcSe_4 were obtained as orange plates from $\text{CH}_2\text{Cl}_2/\text{hexanes}$. Pertinent bond parameters are collected in Table 2.12 while crystal data and refinement details are provided in Table 2.13.

Fig. 2.61 depicts a view of a molecule along with the atomic numbering. Part of the aliphatic chain in the compound is affected by disorder: two carbon atoms of the aliphatic chain are distributed between two positions with almost equal probability. The drawing with atomic labels is of type A: only atoms of the symmetry-independent part are labeled, the A orientation being the (slightly) more populated one. Fig. 2.62 shows the carbon atoms in the type B orientation as grey points.

Similar to its sulfur analogue,^{84(c)} the molecule adopts an *exo* conformation with the Se pointing out of the macrocyclic cavity. The Cp rings adopt a staggered conformation. The intramolecular Se-Se distances are Se(1)-Se(1) 5.134 Å, Se(2)-Se(2) 8.826 Å, Se(1)-Se(2) 5.412 Å.

The ferrocene $\text{sp}^2\text{-C-Se}$ bond distances (Se(1)-C(4), 1.897(5) Å; Se(2)-C(9), 1.884(6) Å) are similar to those in Fc_2Se_2 and $\text{FcSe}(\text{CH}_2)_3\text{Se}(\text{CH}_2)_3\text{SeFc}$, and longer than that in $\text{FcSe}(\text{CH}_2)_3\text{SeFc}$. The $\text{sp}^3\text{-C-Se}$ bond distances are longer than these ferrocene $\text{sp}^2\text{-C-Se}$ bond distances: Se(1)-C(1) 1.922(6) Å; Se(2)-C(3a) 1.993(1) Å; Se(2)-C(3b) 1.925(1) Å. The type A molecule has an angle C(9)-Se(2)-C(3a) of 90.3(4)° while in type B it is 111.6(7)°.

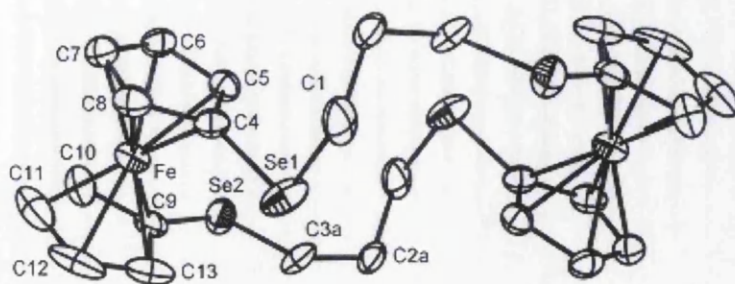


Fig. 2.61 Structure of difcSe₄ molecule of type A

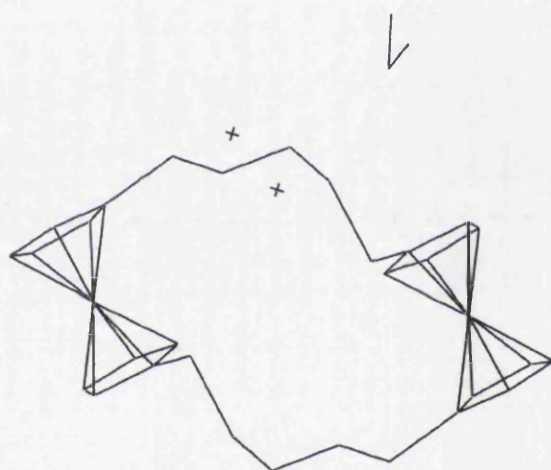


Fig. 2.62 Structure of difcSe₄ in types A and B (grey dots show C atoms in type B)

The packing diagram is shown in Fig. 2.63. The face-centred, monoclinic, unit cell contains four centrosymmetric molecules of the title compound. There are also four solvate dichloromethane molecules in the unit cell, lying on two-fold rotation axes. The asymmetric unit is formed by one half of each of the above molecules.

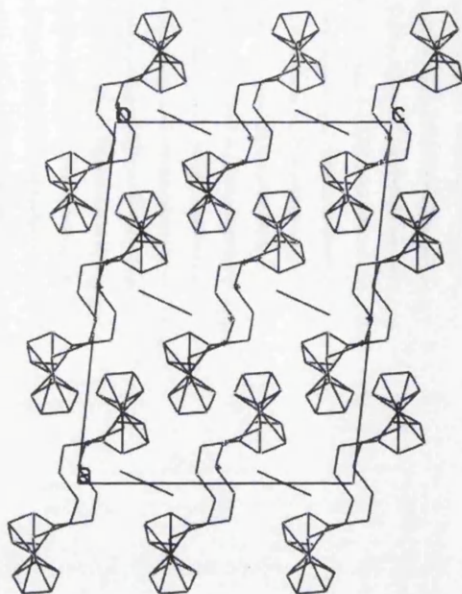


Fig. 2.63 Packing diagram of difcSe₄

Table 2.12 Selected bond lengths (Å) and bond angles (°) for difcSe₄

<i>Bond lengths</i>					
Fe-C(4)	2.019(5)	Fe-C(9)	2.050(6)	Se(1)-C(4)	1.897(5)
Se(2)-C(9)	1.884(6)	Se(1)-C(1)	1.922(6)		
Se(2)-C(3A)	1.993(1)	Se(2)-C(3B)	1.925(1)	C(1)-C(2A)	1.559(1)
C(1)-C(2B)	1.597(1)	C(2A)-C(3A)	1.522(2)	C(2B)-C(3B)	1.522(2)
<i>Bond angles</i>					
C(4)-Se(1)-C(1)	99.5(2)				
C(9)-Se(2)-C(3A)	90.3(4)	C(9)-Se(2)-C(3B)	111.6(7)		
C(2A)-C(1)-Se(1)	126.4(7)	C(2B)-C(1)-Se(1)	99.4(6)		
C(2A)-C(3A)-Se(2)	112.8(1)	C(2B)-C(3B)-Se(2)	108.7(1)		
C(3A)-C(2A)-C(1)	111.3(1)	C(3B)-C(2B)-C(1)	103.1(1)		

* The number in bracket means the standard uncertainty, s.u..

Table 2.13 Crystal data and structure refinement for $\text{difeSe}_4 \cdot \text{CH}_2\text{Cl}_2$

Empirical formula	$\text{C}_{27}\text{H}_{30}\text{Cl}_2\text{Fe}_2\text{Se}_4$
Formula weight	852.94
T (K)	296(2)
Wavelength (Å)	0.71069
Crystal system	monoclinic
Space group	$C 2/c$
a (Å)	17.337(5)
b (Å)	12.526(3)
c (Å)	13.312(3)
α (°)	90
β (°)	96.25(2)
γ (°)	90
Volume (Å ³)	2873.70(13)
Z	4
D_c (Mg m ⁻³)	1.971
Absorption coefficient (mm ⁻¹)	6.278
$F(000)$	1656
Crystal size (mm)	0.60 × 0.30 × 0.25
θ range for data collection (°)	3.78 to 23.81
Index ranges	$-19 \leq h \leq 19, -14 \leq k \leq 14, -15 \leq l \leq 15$
Reflections collected	10412
Independent reflections [Rint]	2201 [0.0836]
Data / restraints / parameters	2201 / 72 / 180
Goodness-of-fit on F^2	0.820
Final R indices [$I > 2\sigma(I)$]	$R_1 = 0.0369, wR_2 = 0.0547$
R indices (all data)	$R_1 = 0.1153, wR_2 = 0.0639$
Largest diff. peak and hole (e Å ⁻³)	0.075, -0.520

* The number in bracket means the standard uncertainty, s.u..

2.2.3 Ferrocenyl chalcogenide compounds with a rigid chain

All the compounds synthesized above have flexible hydrocarbon chains with a preference to yield mononuclear metal complexes. In recent years, enormous research efforts have been seen in the synthesis of rigid bridging ligands, since they allow for a certain control of the steric sequences in the construction of coordination polymers.¹⁰² Incorporation of redox-active ferrocene groups into the polymers has led to materials with useful properties.¹⁰³ No work has been reported regarding ferrocenyl selenide or telluride compounds with a rigid chain. The *p*-xylene group was chosen first due to its structure and the reactivity of dibromo- α,α' -*p*-xylene.

Two kinds of compound were obtained: bis(ferrocenylchalcogeno)- α,α' -*p*-xylene (FcECH₂C₆H₄CH₂EFc, E = Se or Te) and 1,10,22,31-tetraselena[2]-*p*-cyclo[2](1,1')ferroceno-[2]paracyclo[2](1,1')ferrocenophane (difcSe₄-*p*-Xylene, shown in Fig. 2.64).

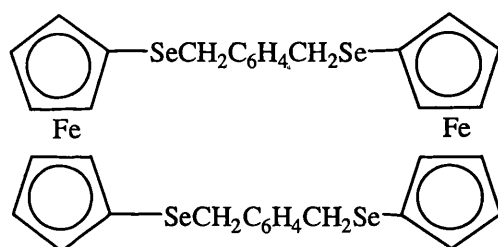


Fig. 2.64 difcSe₄-*p*-Xylene

Synthesis

A scheme similar to that used for FcE(CH₂)₃EFc was adopted here to synthesize FcECH₂C₆H₄CH₂EFc. Reduction of the diferrocenyl dichalcogenide by sodium borohydride in ethanol was followed by addition of one equivalent of dibromo- α,α' -*p*-xylene, BrCH₂C₆H₄CH₂Br. The mixture was left to stir overnight. The solvent was removed by evaporation under reduced pressure. The residue was treated with water and extracted with CH₂Cl₂. The extract was dried over MgSO₄ and evaporated to dryness, then subjected to column chromatography on SiO₂. The product was generally isolated as a yellow solid in good yield.

difcSe₄-*p*-Xylene was synthesized by [2+2] cyclisation (shown in Fig. 2.65) because the lability of dibromo- α,α' -*p*-xylene prevents the isolation of the 1-bromo product

$\text{fc}[\text{SeCH}_2\text{C}_6\text{H}_4\text{CH}_2\text{Br}]_2$. Reduction of fcSe_3 by sodium borohydride in ethanol was followed by addition of a THF solution of dibromo- α,α' -*p*-xylene, $\text{BrCH}_2\text{C}_6\text{H}_4\text{CH}_2\text{Br}$. The mixture was left to stir overnight. The solvent was removed by evaporation under reduced pressure. The residue was treated with water and extracted with CH_2Cl_2 . The extract was dried over MgSO_4 and evaporated to dryness, then subjected to column chromatography on SiO_2 , eluting with hexane/dichloromethane (1:1). After evaporation, the target compound was obtained as yellow solid. The yield is quite low (about 15%); no significant improvement has been found.

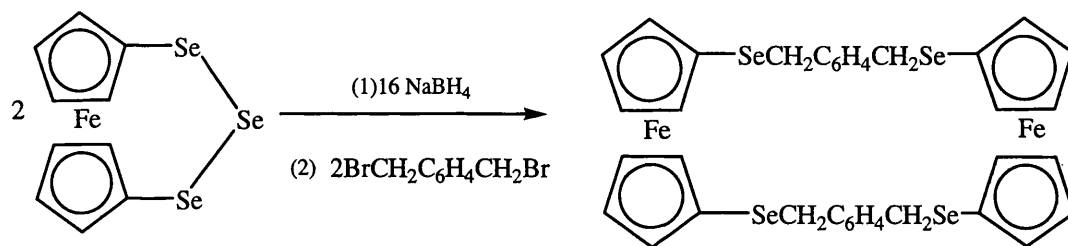


Fig. 2.65 Synthetic scheme for difcSe₄-p-Xylene

The ^1H and ^{13}C NMR spectra showed many of the same features as those of the flexible hydrocarbon analogues. The ^{77}Se chemical shifts of $\text{FcSeCH}_2\text{C}_6\text{H}_4\text{CH}_2\text{SeFc}$ and $\text{fc}(\text{SeCH}_2\text{C}_6\text{H}_4\text{CH}_2\text{Se})_2\text{fc}$ are at quite low field, 286 ppm. The benzyl group at the β -position results in a more deshielded selenium nucleus compared to that in $\text{FcSe}(\text{CH}_2)_3\text{SeFc}$ ($\delta = 185$ ppm). A similar result was obtained for $\text{FcSeCH}_2\text{C}_6\text{H}_5$ ($\delta = 287$ ppm).³⁶

The ^{125}Te chemical shift in $\text{FcTeCH}_2\text{C}_6\text{H}_4\text{CH}_2\text{TeFc}$ is 496 ppm. The ratio of $\delta(^{125}\text{Te})/\delta(^{77}\text{Se})$ is 1.73, a little larger than theoretical calculation predicts (1.5-1.6),⁵⁵ but in accordance with previous studies: a value of 1.71 was found for phenyl alkyl chalcogenides⁶⁹ and one of 1.8 was reported by McFarlane and McFarlane.⁷⁰

Spectroscopic data for each of the new compounds described in this section are given in Chapter Seven.

Structure of $\text{FcSeCH}_2\text{C}_6\text{H}_4\text{CH}_2\text{SeFc}$

Crystals of $\text{FcSeCH}_2\text{C}_6\text{H}_4\text{CH}_2\text{SeFc}$ were obtained as elongated orange plates from CH_2Cl_2 /hexanes. Fig. 2.66 depicts a view of a molecule along with the atomic

numbering. Pertinent bond parameters are collected in Table 2.14 while crystal data and refinement details are provided in Table 2.15. The compound crystallizes in the space group P21/a, monoclinic. There are two centrosymmetric molecules in the monoclinic unit cell. The symmetry-independent unit consists of only one half of a molecule, since this possesses a twofold axis passing through the benzyl ring. The Fe-C distances range from 2.029(2) to 2.054(2) Å. The C-C distances in the cyclopentadienyl rings range from 1.405(3) to 1.425(3) Å and the C-C-C bond angles within the ring range from 107.3(2) to 108.5(2)°. The two cyclopentadienyl rings attached to the same iron are basically coplanar. The Fe-C bond distance is shorter for the substituted carbon atoms as compared to the other Fe-C bonds within the same ring, a feature which is not observed in Fc_2Se_2 and $\text{FcSe}(\text{CH}_2)_3\text{SeFc}$. The ferrocene-C-Se bond distance (Se(1)-C(5), 1.895(2) Å) is similar to those in Fc_2Se_2 (Se(1)-C(13), 1.898(10) Å; Se(2)-C(33), 1.904(9) Å), and longer than those in $\text{FcSe}(\text{CH}_2)_3\text{SeFc}$ (Se(1)-C(4), 1.872(6) Å; Se(2)-C(14), 1.878(6) Å). As usual, the sp^3 -C-Se bond distance is longer (Se(1)-C(4), 1.977(2) Å) than the ferrocene-C-Se bond distance.

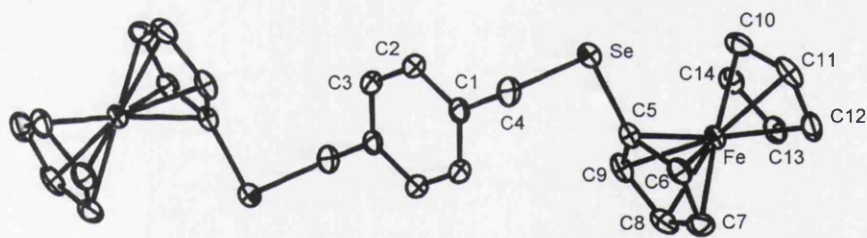


Fig. 2.66 Crystal structure of $\text{FcSeCH}_2\text{C}_6\text{H}_4\text{CH}_2\text{SeFc}$

The packing diagram is shown in Fig.'s 2.67, 2.68. The title compound is essentially monomeric. From some points of view it would seem that there is stacking of the benzene rings, but that is not so because there are also shifts and, looking along the normal to a ring one can see that the closest ring projects out of the periphery of the former. In any case, there is a rather close approach between molecules, due to the short b axis and the distance is 5.767 Å between centroids.

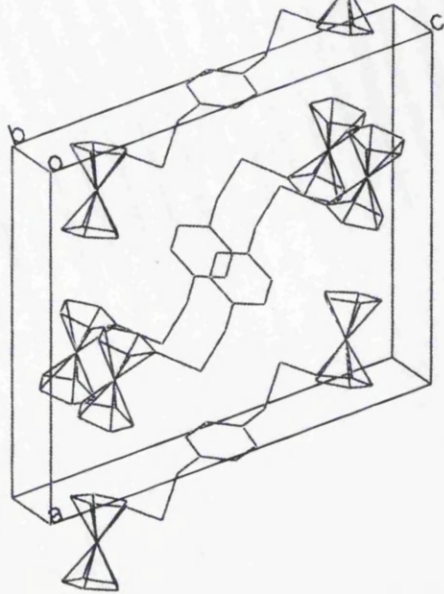


Fig. 2.67 Packing diagram of $\text{FcSeCH}_2\text{C}_6\text{H}_4\text{CH}_2\text{SeFc}$

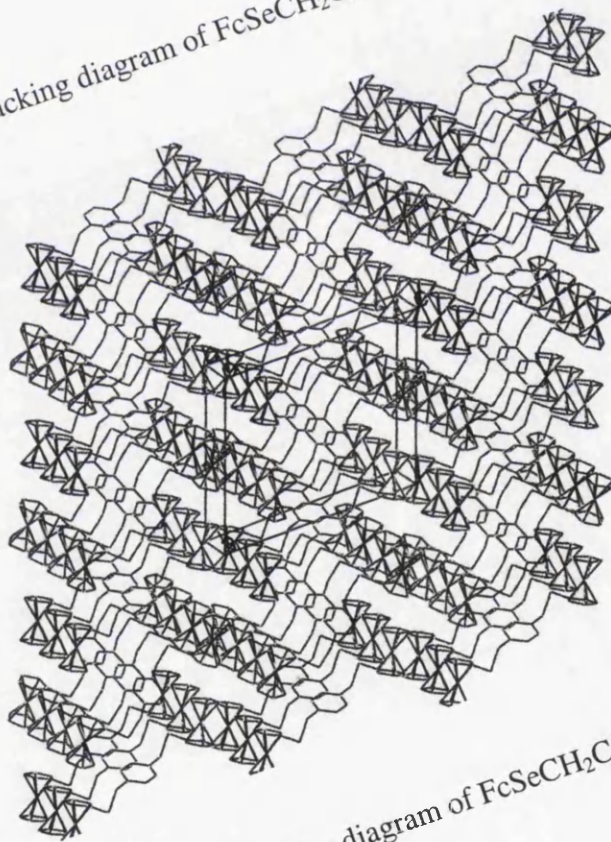


Fig. 2.68 Packing diagram of $\text{FcSeCH}_2\text{C}_6\text{H}_4\text{CH}_2\text{SeFc}$

Table 2.14 Selected bond lengths (Å) and bond angles (°) for FcSeCH₂C₆H₄CH₂SeFc

<i>Bond lengths</i>					
Se-C(5)	1.895(2)	Se-C(4)	1.977(2)	Fe-C(5)	2.029(2)
C(1)-C(3)	1.380(3)	C(1)-C(2)	1.383(3)	C(1)-C(4)	1.494(3)
C(2)-C(3)	1.380(3)				
<i>Bond angles</i>					
C(5)-Se-C(4)	98.9(1)	C(3)-C(1)-C(2)	118.1(2)		
C(3)-C(1)-C(4)	121.5(2)	C(2)-C(1)-C(4)	120.3(2)		
C(3)-C(2)-C(1)	120.7(2)	C(1)-C(4)-Se	112.88(16)		
Se-C(5)-Fe	121.87(11)				
<i>Torsion angles</i>					
C(3)-C(1)-C(4)-Se	87.1(2)	C(2)-C(1)-C(4)-Se	-91.0(2)		
C(5)-Se-C(4)-C(1)	-79.86(19)	C(4)-Se-C(5)-C(6)	-93.96(19)		
C(4)-Se-C(5)-C(9)	91.8(2)	C(4)-Se-C(5)-Fe	179.65(13)		

* The number in bracket means the standard uncertainty, s.u..

Table 2.15 Crystal data and structure refinement for FcSeCH₂C₆H₄CH₂SeFc

Empirical formula	C ₂₈ H ₂₆ Fe ₂ Se ₂
Formula weight	632.10
T (K)	296(2)
Wavelength (Å)	0.71069
Crystal system	monoclinic
Space group	P 21/a
<i>a</i> (Å)	13.722(2)
<i>b</i> (Å)	5.767(1)
<i>c</i> (Å)	15.939(2)
α (°)	90
β (°)	107.96(1)
γ (°)	90
Volume (Å ³)	1199.9(3)
<i>Z</i>	4
<i>D_c</i> (Mg m ⁻³)	1.750
Absorption coefficient (mm ⁻¹)	4.257
<i>F</i> (000)	628
Crystal size (mm)	0.60 × 0.35 × 0.15
θ range for data collection (°)	3.86 to 26.37
Index ranges	-17 ≤ <i>h</i> ≤ 17, -7 ≤ <i>k</i> ≤ 7, -19 ≤ <i>l</i> ≤ 19
Reflections collected	10620
Independent reflections [Rint]	2411 [0.0249]
Data / restraints / parameters	2411 / 0 / 145
Goodness-of-fit on F ²	1.064
Final <i>R</i> indices [<i>I</i> > 2σ(<i>I</i>)]	<i>R</i> ₁ = 0.0239, <i>wR</i> ₂ = 0.0547
<i>R</i> indices (all data)	<i>R</i> ₁ = 0.0334, <i>wR</i> ₂ = 0.0565
Largest diff. peak and hole (e Å ⁻³)	0.575, -0.329

* The number in bracket means the standard uncertainty, s.u..

2.3 References for Chapter Two

1. A. G. Osborne, R. H. Whiteley, *J. Organomet. Chem.*, 1975, **101**, C27
2. M. Herberhold, *Angew. Chem., Int. Ed. Engl.*, 1995, **34**, 1837
3. R. Rulkens, D. P. Gates, D. Balaishis, J. K. Pudelski, D. F. McIntosh, A. J. Lough, I. Manners, *J. Am. Chem. Soc.*, 1997, **119**, 10976
4. H. C. E. McFarlane, W. McFarlane, in P. Laslo (Ed.), *NMR of Newly Accessible Nuclei*, Academic Press, London, 1983, Vol. 2, 275
5. H. Ushijima, T. Akiyama, M. Kajitani, K. Shimizu, M. Aoyama, S. Masuda, Y. Harada, A. Sugimori, *Bull. Chem. Soc. Jpn.*, 1990, **63**, 1015
6. G. Thaler, B. Klotz, K. Wurst, F. Sladky, *J. Organomet. Chem.*, 2001, **637**, 745
7. A. Davison, J. C. Smart, *J. Organomet. Chem.*, 1969, **19**, P7
8. R. E. Hollands, A. G. Osborne, I. Townsend, *Inorg. Chim. Acta*, 1979, **37**, L541
9. M. Herberhold, P. Leitner, U. Thewalt, *Z. Naturforsch., B: Chem. Sci.*, 1990, **45**, 1503
10. J. J. Bishop, A. Davison, M. L. Katcher, D.W. Lichtenberg, R. E. Merrill, J. C. Smart, *J. Organomet. Chem.*, 1971, **27**, 241
11. B. R. Davis, I. Bernal, *J. Cryst. Mol. Struct.*, 1972, **2**, 143
12. E. W. Abel, M. Booth, K. G. Orrell, *J. Organomet. Chem.*, 1980, **186**, c37
13. A. G. Osborne, R. E. Hollands, A. G. Nagy, *J. Organomet. Chem.*, 1989, **373**, 229
14. E. W. Abel, M. Booth, C. A. Brown, K. G. Orrell, R. L. Woodford, *J. Organomet. Chem.*, 1981, **214**, 93
15. A. Davison, J. C. Smart, *J. Organomet. Chem.*, 1979, **174**, 321
16. A. G. Osborne, R. E. Hollands, J. A. K. Howard, R. F. Bryan, *J. Organomet. Chem.*, 1981, **205**, 395
17. R. Broussier, A. Abdulla, B. Gautheron, *J. Organomet. Chem.*, 1987, **332**, 165
18. M. Herberhold, P. Leitner, *J. Organomet. Chem.*, 1991, **411**, 233
19. E. W. Abel, M. Booth, K. G. Orrell, *J. Organomet. Chem.*, 1981, **208**, 213
20. E. W. Abel, K. G. Orrell, A. G. Osborne, V. Sik, W. Guoxiong, *J. Organomet. Chem.*, 1991, **411**, 239
21. M. Herberhold, C. Dörnhöfer, A. Scholz, G. X. Jin, *Phosphorus, Sulfur and Silicon*, 1992, **64**, 161

22. R. Broussier, A. Abdulla, B. Gautheron, *J. Organomet. Chem.*, 1987, **332**, 165
23. A. G. Osborne, R. E. Hollands, R. F. Bryan, S. Lockhart, *J. Organomet. Chem.*, 1982, **226**, 129
24. A. G. Osborne, A. J. Blake, R. E. Hollands, R. F. Bryan, S. Lockhart, *J. Organomet. Chem.*, 1985, **287**, 39
25. M. Herberhold, M. Hubner, B. Wrackmeyer, *Z. Naturforsch. , B: Chem. Sci.*, 1993, **48**, 940
26. A. G. Osborne, R. E. Hollands, R. F. Bryan, S. Lockhart, *J. Organomet. Chem.*, 1985, **288**, 207
27. M. Herberhold, C. Dornhofer, U. Thewalt, *Z. Naturforsch. , B: Chem. Sci.*, 1990, **45**, 741
28. P. Shu, K. Bechgaard, D. Cowan, *J. Org. Chem.*, 1976, **41**, 1849
29. R. V. Honeychuck, M. O. Okoroafor, L. H. Shen, C. H. Brubaker, *Organometallics*, 1986, **5**, 482
30. H. B. Singh, A. V. Regini, J. P. Jasinski, E. S. Paight, R. J. Butcher, *J. Organomet. Chem.*, 1994, **464**, 87
31. Y. Nishibayashi, S. Uemura, *Syn. Lett.*, 1995, 79
32. M. Herberhold, P. Leitner, *J. Organomet. Chem.*, 1987, **336**, 153
33. Y. Nishibayashi, T. Chiba, J. Singh, S. Uemura, *J. Organomet. Chem.*, 1994, **473**, 205
34. Y. Nishibayashi, J. D. Singh, S. Fukuzawa, S. Uemura, *J. Chem. Soc., Perkin Trans. 1*, 1995, 2871
35. R. Broussier, A. Da Rold, B. Gautheron, *J. Organomet. Chem.*, 1992, **427**, 231
36. M. R. Burgess, C. P. Morley, *J. Organomet. Chem.*, 2001, **623**, 101
37. M. R. Burgess, Ph.D. Thesis, University of Wales Swansea, 1999
38. S. Hartmann, R. F. Winter, T. Scheiring, M. Wanner, *J. Organomet. Chem.*, 2001, **637**, 240
39. R. Broussier, M. E. L. Mjidi, B. Gautheron, *J. Organomet. Chem.*, 1991, **408**, 381
40. A. I. Wallbank, J. F. Corrigan, *Chem. Commun.*, 2001, 377
41. M. Herberhold, P. Leitner, C. Dörnhöfer, J. Ott-lastic, *J. Organomet. Chem.*, 1989, **377**, 281-289
42. R. Broussier, A. Abdulla, B. Gautheron, *J. Organomet. Chem.*, 1987, **332**, 165

43. Y. Nishibayashi, J. D. Singh, S. Fukuzawa, S. Uemura, *J. Org. Chem.*, 1995, **60**, 4114
44. Y. Nishibayashi, K. Segawa, J. D. Singh, S. Fukuzawa, K. Ohe, S. Uemura, *Organometallics*, 1996, **15**, 370
45. Y. Nishibayashi, S. K. Srivastava, H. Takada, S. I. Fukuzawa, S. Uemura, *J. Chem. Soc., Chem. Commun.*, 1995, 2321
46. S. I. Fukuzawa, K. Takahashi, H. Kato, H. Yamazaki, *J. Org. Chem.*, 1997, **62**, 7711
47. C. K. Lai, A. A. Naiini, C. H. J. Brubaker, *Inorg. Chim. Acta*, 1989, **164**, 205
48. A. A. Naiini, C. K. Lai, C. H. J. Brubaker, *Inorg. Chim. Acta*, 1989, **160**, 241
49. H. Gornitzka, S. Besser, R. Herbst-Irmer, U. Kilimann, F. T. Edelmann, *J. Organomet. Chem.*, 1992, **437**, 299
50. Y. Nishibayashi, J. D. Singh, S. Fukuzawa, S. Uemura, *J. Chem. Soc., Perkin Trans. 1*, 1995, 2871
51. Y. Nishibayashi, J. D. Singh, S. Kyohei, S. Fukuzawa, S. Uemura, *J. Chem. Soc., Chem. Commun.*, 1994, 1375
52. M. Herberhold, H. D. Brendel, *J. Organomet. Chem.*, 1991, **413**, 65
53. P. Zanello, G. Opromolla, M. Herberhold, H. Brendel, *J. Organomet. Chem.*, 1994, **484**, 67
54. F. A. Carroll, *Perspectives on Structure and Mechanism in Organic Chemistry*, Brooks/Cole Publishing Company, USA, 1998
55. N. Luthra, J. Odom, in S. Patai, Z. Rappaport (Eds.), *The Chemistry of Organic Selenium and Tellurium Compounds*, vol. 1, Wiley, New York, 1986
56. D. J. Gulliver, E. G. Hope, W. Levason, S. G. Murray, D. M. Potter, G. L. Marshall, *J. Chem. Soc., Perkin Trans.*, 1984, **2**, 429
57. E. W. Abel, K. Kite, P. S. Perkins, *Polyhedron*, 1986, **5**, 1459
58. A. J. Barton, W. Levason, G. Reid, A. J. Ward, *Organometallics*, 2001, **20**, 3644
59. M. Hesford, W. Levason, S. D. Orchard, G. Reid, *J. Organomet. Chem.*, 2002, **649**, 214
60. E. G. Hope, T. Kemmitt, W. Levason, *Organometallics*, 1988, **7**, 78
61. W. Levason, C. A. McAuliffe, S. G. Murray, *J. Chem. Soc., Dalton Trans.*, 1976, 269

62. E. Cullen, F. Guziec Jr., C. Murphy, T. Wong, K. Andersen, *J. Chem. Soc., Perkin Trans.*, 1982, 473
63. W. McFarlane, D. Rycroft, C. Turner, *Bull. Soc. Chim. Belg.*, 1977, **86**, 457
64. R. Harris and B. Mann (Eds.), *NMR and the Periodic Table*, Academic Press, New York, 1978
65. M. Garreau, G. Martin, M. Martin, J. Morel, C. Paulmier, *Org. Magn. Reson.*, 1974, **6**, 648
66. T. Wong, E. Engler, *J. Mol. Struct.*, 1980, **67**, 279
67. J. Bartels-Keith, M. Burgess, J. Stevenson, *J. Org. Chem.*, 1977, **42**, 3725
68. W. McFarlane, R. J. Wood, *J. Chem. Soc., Dalton Trans.*, 1972, 1397
69. D. H. O'Brien, N. Dereu, C. K. Huang, K. J. Irgolic, F. F. Knapp, *Organometallics*, 1983, **2**, 305
70. H. McFarlane, W. McFarlane, *J. Chem. Soc., Dalton Trans.*, 1973, 2416
71. P. Granger, S. Chapelle, W. McWhinnie, A. Al-Rubaic, *J. Organomet. Chem.*, 1981, **220**, 149
72. Y.S. Sohn, D. N. Hendrickson, H. B. Gray, *J. Am. Chem. Soc.*, 1971, **93**, 3603
73. A. T. Armstrong, A. T. Smith, E. Elder and S. P. McGlynn, *J. Chem. Phys.*, 1967, **46**, 4321
74. D. H. Brown, R. J. Cross and D. Millington, *J. Chem. Soc., Dalton Trans.*, 1977, 159
75. R. I. Vinokurova, L. A. Sorokina, I. V. Olifirenko, L.M. Kataeva and E. G. Kataev, *J. Gen. Chem. USSR (Engl. Transl.)*, 1983, **53**, 519
76. (a) G. Bergson, *Ark. Kemi*, 1955, **9**, 121; (b) G. Bergson, *Ark. Kemi*, 1958, **13**, 11; (c) G. Bergson, *Ark. Kemi*, 1962, **19**, 215; (d) G. Bergson, G. Claeson, L. Schotte, *Acta Chem. Scand.*, 1962, **16**, 1159.
77. H. Kunkely, A. Vogler, J. K. Nagle, *Inorg. Chem.*, 1995, **34**, 4511
78. R. E. Marsh, *Acta Cryst.*, 1952, **5**, 458.
79. E. R. Cullen, F. S. Guziec, C. J. Murphy, T. C. Wong, K. K. Andersen, *J. Am. Chem. Soc.*, 1981, **103**, 7055
80. A. Ogawa, K. Yokoyama, R. Obayashi, L. B. Han, N. Kambe, N. Sonoda, *Tetrahedron*, 1993, **49**, 1177.
81. G. Llabres, O. Dideberg, L. Dupont, *Acta Cryst.*, 1972, **28**, 2438
82. E. C. Constable, *Coordination Chemistry of Macrocyclic Compounds*, Oxford University Press Inc., New York, 1999

83. T. Saji, *Chem. Lett.*, 1986, **3**, 275
84. For examples see: (a) M. Sato, H. Watanabe, S. Ebine, S. Akabori, *Chem. Lett.*, 1982, 1753; (b) M. Sato, S. Tanaka, S. Ebine, S. Akabori, *Bull. Chem. Soc. Jpn.*, 1984, **57**, 1929; (c) M. Sato, H. Anano, *J. Organomet. Chem.*, 1998, **555**, 167; (d) M. Sato, S. Tanaka, S. Ebine, K. Morinaga, S. Akabori, *J. Organomet. Chem.*, 1985, **282**, 247
85. S. Akabori, Y. Takunohoshi, S. Takagi, *Synth. Commun.*, 1990, **20**, 3187
86. B. M. Pinto, B. D. Johnston, R. J. Batchelor, F. W. B. Einstein, I. D. Gay, *Can. J. Chem.*, 1988, **66**, 2956
87. R. J. Batchelor, F. W. B. Einstein, I. D. Gay, J. H. Gu, B. D. Johnston, B. M. Pinto, *J. Am. Chem. Soc.*, 1989, **111**, 6582
88. I. Cordova-Reyes, H. Hu, J.-H. Gu, E. VandenHoven, A. Mohammed, S. Holdcroft, B. M. Pinto, *Can. J. Chem.*, 1996, **74**, 533
89. I. Cordova-Reyes, E. VandenHoven, A. Mohammed, B. M. Pinto, *Can. J. Chem.*, 1995, **73**, 113
90. R. J. Batchelor, F. W. B. Einstein, I. D. Gay, J.-H. Gu, S. Mehta, B. M. Pinto, X.-M. Zhou, *Inorg. Chem.*, 2000, **39**, 2558
91. L. A. Ochrymowycz, C. P. Mak, J. D. Mitchna, *J. Org. Chem.*, 1974, **39**, 2079
92. R. D. Adams, K. T. McBride, R. D. Rogers, *Organometallics*, 1997, **16**, 3895
93. H. Fujihara, M. Yabe, M. Ikemori, N. Furukawa, *J. Chem. Soc., Perkin Trans. 1*, 1993, 2145
94. H. Fujihara, M. Yabe, N. Furukawa, *J. Chem. Soc. Perkin Trans. I*, 1996, 1783
95. A. Mazouz, P. Meunier, M. M. Kubicki, B. Hanquet, R. Amardeil, C. Bornet, A. Zahidi, *J. Chem. Soc., Dalton Trans.*, 1997, 1043
96. A. Mazouz, J. Bodiguel, P. Meunier, B. Gautheron, *Phosphorus, Sulfur and Silicon*, 1991, **61**, 247.
97. V.W.-W. Yam, Y.-L. Pui, W.-P. Li, K. K.-W. Lo, K.-K. Cheung, *J. Chem. Soc., Dalton Trans.*, 1998, 3615
98. Y. Takaguchi, E. Horn, N. Furukawa, *Organometallics*, 1996, **15**, 5112
99. W. Levason, S. D. Orchard, G. Reid, *Chem. Commun.*, 2001, 427
100. S. C. Menon, H. B. Singh, R. P. Patel, S. K. Kulshreshtha, *J. Chem. Soc., Dalton Trans.*, 1996, 1203
101. N. R. Champness, P. F. Kelly, W. Levason, G. Reid, A. M. Z. Slawin, D. Williams, *Inorg. Chem.*, 1995, **34**, 651

102. C. Janiak, *Dalton Trans.*, 2003, 2781

103. I. Manners, *Science*, 2001, **294**, 1664

CHAPTER THREE

Coordination Chemistry of Ferrocenyl Chalcogenides

BACKGROUND, RESULTS AND DISCUSSION

3.1 Background to coordination chemistry of ferrocenyl chalcogenides

As has been noted in Chapter One, several types of systems containing a metal-chalcogen bond have been studied. However, the coordination chemistry of ferrocene-functionalised chalcogenide ligands has attracted far less attention and is not so systematic. The relevant literature up to now is summarized below in the sequence of monodentate, bidentate and tetradentate ligands.

3.1.1 Monodentate ferrocenyl chalcogenide complexes

Although FcER have been synthesized, no relevant coordination study has been published which may be due to the low reactivity of monodentate ligands or steric crowding.

3.1.2 Complexes of bidentate ferrocenyl chalcogenide ligands

As chelating ligands, 1,1'-bis(methylseleno)ferrocene (**3·1**), 1,1'-bis(phenylseleno)ferrocene (**3·2**), 1,1'-bis(trimethylsilylseleno)ferrocene (**3·3**) have been studied more extensively (shown in Fig. 3.1). Interests are most concentrated on the intramolecular motions of chalcogen-containing molecules coordinated to a transition metal.

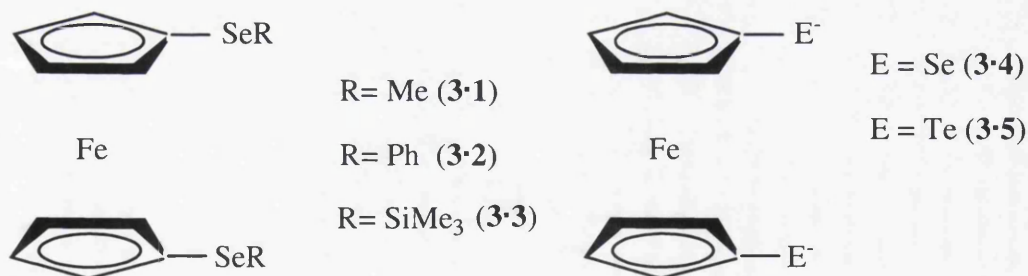


Fig. 3.1 Some bidentate ferrocenyl chalcogenide ligands

Displacement of norbornadiene from $[\text{M}(\text{CO})_4(\text{kbd})]$ ($\text{M} = \text{Cr}, \text{Mo}, \text{W}$) gives *cis*- $[\text{M}(\text{CO})_4(\mathbf{3}\cdot\mathbf{1})]$.¹ These chelate complexes are fluxional molecules in solution, as proved by variable-temperature NMR spectroscopy. The non-rigidity can be ascribed to two possible processes: pyramidal inversion at the chalcogen atom at higher temperature, and bridge reversal involving the central metal M. In this case, only the

rate of pyramidal chalcogen inversion was within the NMR detection timescale, and the inversion barriers fall in the order $W > Cr > Mo$. The crystal structure of {1,1'-bis(methylseleno)ferrocene}tetracarbonyltungsten (Fig. 3.2) shows that the W-Se distances are 2.558(2) to 2.736(2) Å, and the C-O distances are 1.138(12) and 1.135(12) Å for *cis*-CO, 1.187(12) and 1.188(13) Å for *trans*-CO.

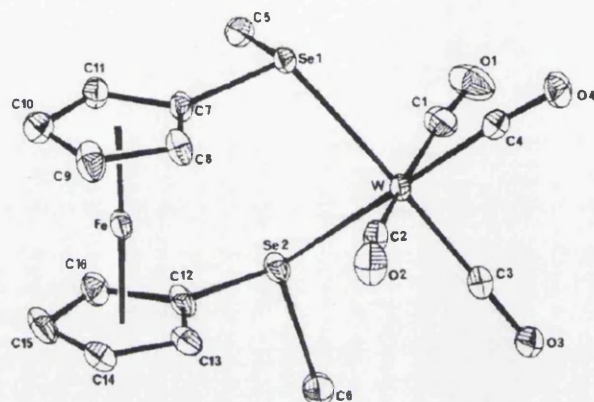


Fig. 3.2 Crystal structure of {1,1'-bis(methylseleno)ferrocene}tetracarbonyltungsten

NMR spectroscopy confirms the complexes $fac-[ReX(CO)_3(\mathbf{3}\cdot\mathbf{1})]^2$ and $fac-[PtXMe_3(\mathbf{3}\cdot\mathbf{1})]^3$ ($X = Cl, Br, I$) exist as *meso*- and *DL*-invertomers in solution. Variable-temperature NMR studies indicate that the barriers to selenium inversion are considerably lower than in five- and six-membered chelate ring diselena-alkane analogues as a result of the high flexibility of the ferrocenyl selenide ring.

The platinum(II) complex $[PtCl_2(\mathbf{3}\cdot\mathbf{1})]$ was synthesized from $[PtCl_2(PhCN)_2]$ and $\mathbf{3}\cdot\mathbf{1}$.⁴ 1H NMR study showed the complex existed as a mixture of *meso*- and *DL*-species in approximately equal proportions.

The palladium(II) and platinum(II) complexes $[PdCl_2(\mathbf{3}\cdot\mathbf{2})]$,⁵ $[Pd(PPh_3)(\mathbf{3}\cdot\mathbf{1})][BF_4]_2$ and $[Pd(PPh_3)(\mathbf{3}\cdot\mathbf{2})][BF_4]_2$ ⁶ have also been prepared. The spectral data indicate that the latter two complexes appear to have some Fe...Pd interaction.

When reacted with various gold or silver species, $\mathbf{3}\cdot\mathbf{2}$ can afford complexes where the ligand acts in either a bridging or a chelating mode (shown in Fig. 3.3).⁷ Single crystal structures show that $[Ag(OTf)(PPh_3)\{fc(SePh)_2\}]$ (Fig. 3.3b) has a monomeric structure (shown in Fig. 3.4), and $[Ag(OTf)\{fc(SePh)_2\}]$ (Fig. 3.3e) consists of dimers being bridged by two oxygen atoms of the triflate ligands and chelated by an

fc(SePh)₂ ligand (shown in Fig. 3.5). Ag–Se bond distances in [Ag(OTf)(PPh₃){fc(SePh)₂}] are also somewhat dissimilar, 2.645(2) and 2.7347(18) Å, and slightly longer than those found in [Ag(OTf){fc(SePh)₂}], 2.5888(4) and 2.6339(3) Å.

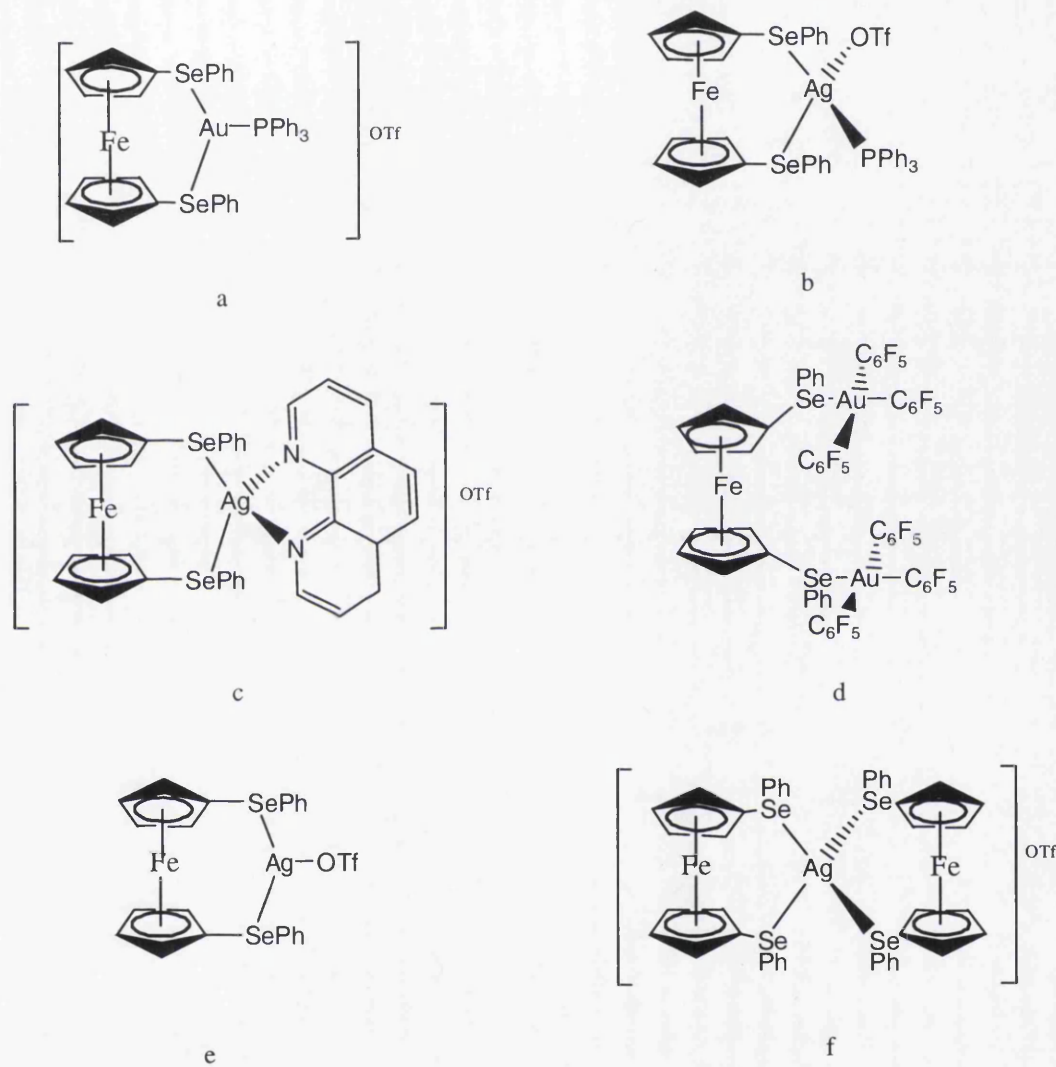


Fig. 3.3 Different Au or Ag complexes of **3·2**

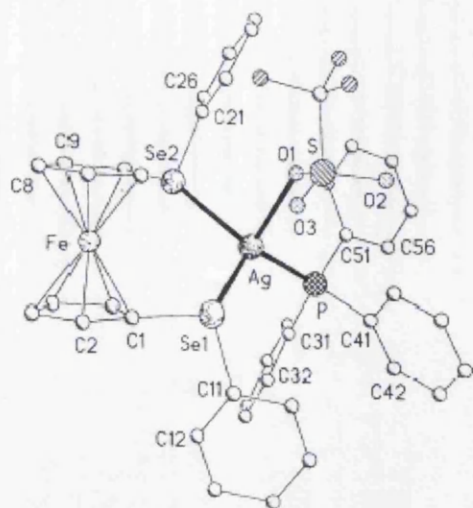


Fig. 3.4 Crystal structure of $[\text{Ag}(\text{OTf})\{\text{fc}(\text{SePh})_2\}]$

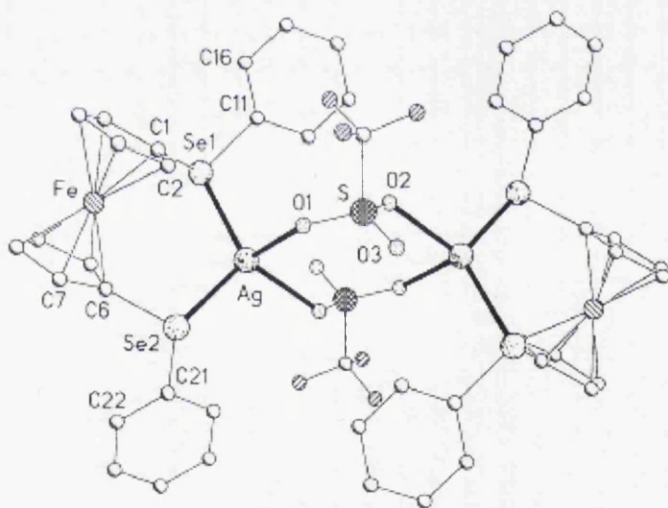


Fig. 3.5 Crystal structure of $[\text{Ag}(\text{OTf})(\text{PPh}_3)\{\text{fc}(\text{SePh})_2\}]$

Starting from **3·3**, the dimeric complexes $[\text{M}_2\{\mu\text{-}\eta^1\text{-Fe}(\eta^5\text{-C}_5\text{H}_4\text{Se})_2\}_2(\text{P}^n\text{Bu}_3)_2]$ ($\text{M} = \text{Pd}, \text{Pt}$), and the monomeric complex $[\text{Pt}\{\eta^2\text{-Fe}(\text{C}_5\text{H}_4\text{Se})_2\}(\text{P}^n\text{Bu}_3)_2]$, have been prepared from *trans*- $[\text{MCl}_2(\text{P}^n\text{Bu}_3)_2]$ and *cis*- $[\text{PtCl}_2(\text{P}^n\text{Bu}_3)_2]$, respectively. Complexes $[\text{M}_2\{\mu\text{-}\eta^1\text{-Fe}(\eta^5\text{-C}_5\text{H}_4\text{Se})_2\}_2(\text{P}^n\text{Bu}_3)_2]$ ($\text{M} = \text{Pd}, \text{Pt}$) contain two edge-sharing, square planar metal centres forming a planar M_2Se_2 four-membered ring (see Fig. 3.6). The Pd - Se bond lengths in $[\text{Pd}_2\{\mu\text{-}\eta^1\text{-Fe}(\eta^5\text{-C}_5\text{H}_4\text{Se})_2\}_2(\text{P}^n\text{Bu}_3)_2]$ range between 2.450(1) and 2.457(1) Å for the terminal bonds and range between

2.459(1) and 2.492(1) Å for the bridging selenium centres. The Pt - Se bond lengths in $[\text{Pt}_2\{\mu\text{-}\eta^1\text{-Fe}(\eta^5\text{-C}_5\text{H}_4\text{Se})_2\}_2(\text{P}^n\text{Bu}_3)_2]$ range between 2.4491(6) Å and 2.4537(7) Å for the terminally bonded ligands and between 2.4499(6) and 2.4889(6) Å for the bridging groups. The crystal structure of the monomeric complex $[\text{Pt}\{\eta^2\text{-Fe}(\text{C}_5\text{H}_4\text{Se})_2\}(\text{P}^n\text{Bu}_3)_2]$ (shown in Fig. 3.7) shows the two Pt - Se bond lengths are equivalent, 2.4855(8) and 2.4855(9) Å, and these lengths are very close to those of the equivalent bonds in the dimeric complexes.⁸

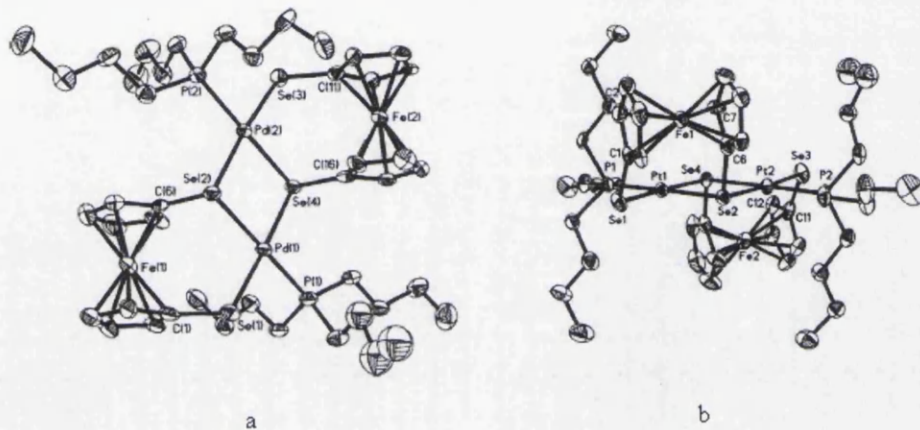


Fig. 3.6 Crystal structure of $[\text{M}_2\{\mu\text{-}\eta^1\text{-Fe}(\eta^5\text{-C}_5\text{H}_4\text{Se})_2\}_2(\text{P}^n\text{Bu}_3)_2]$ (a : M = Pd; b: M = Pt)

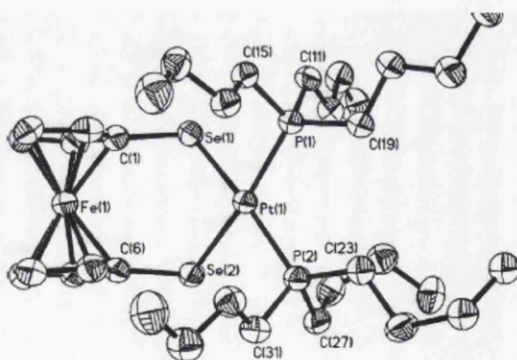


Fig 3.7 Crystal structure of $[\text{Pt}\{\eta^2\text{-Fe}(\text{C}_5\text{H}_4\text{Se})_2\}(\text{P}^n\text{Bu}_3)_2]$

From the related dianionic 1,1'- ferrocene diselenolate **3·4**, $[\text{M}(\mathbf{3}\cdot\mathbf{4})(\text{PPh}_3)]$ (M = Pd, Pt) can't be obtained because of the length of the C-Se and M-Se bonds. Only

[Pt(**3·4**)(PPh₃)₂] can be isolated from a solution of 1,2,3-triseleno[3]ferrocenophane and [Pt(PPh₃)₄], in this compound there is no Fe···Pt interaction.⁹

Ligand **3·4** can also react with the half-sandwich compounds [V(O)CpC1₂] and [V(O)Cp*Cl₂] to prepare bimetallic complexes [V(O)Cp(**3·4**)] and [V(O)Cp*(**3·4**)].¹⁰ The Fe-V distance in [V(O)Cp*(**3·4**)] is 4.014(2) Å which means no interaction between them (Fig. 3.8). The Fe-Fe distance is 3.87 Å in [FeCl₂(**3·4**)], which also rules out a direct bonding interaction between the two transition metals.¹¹

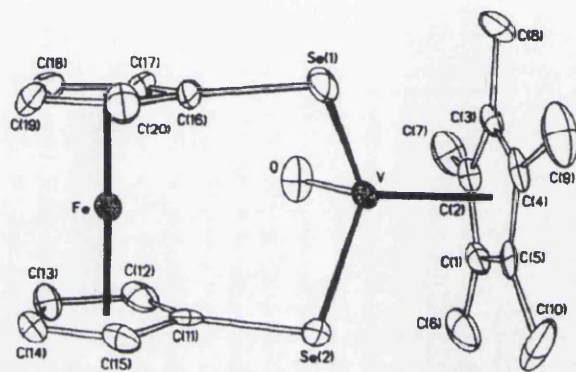


Fig. 3.8 Crystal structure of [V(O)Cp*(**3·4**)]

The complexes [Re(O)Tp(**3·4**)], [Re(O)Cp*(**3·4**)] and [Re(N^tBu)Cp*(**3·4**)] were synthesized by the method shown below (Fig. 3.9).¹²

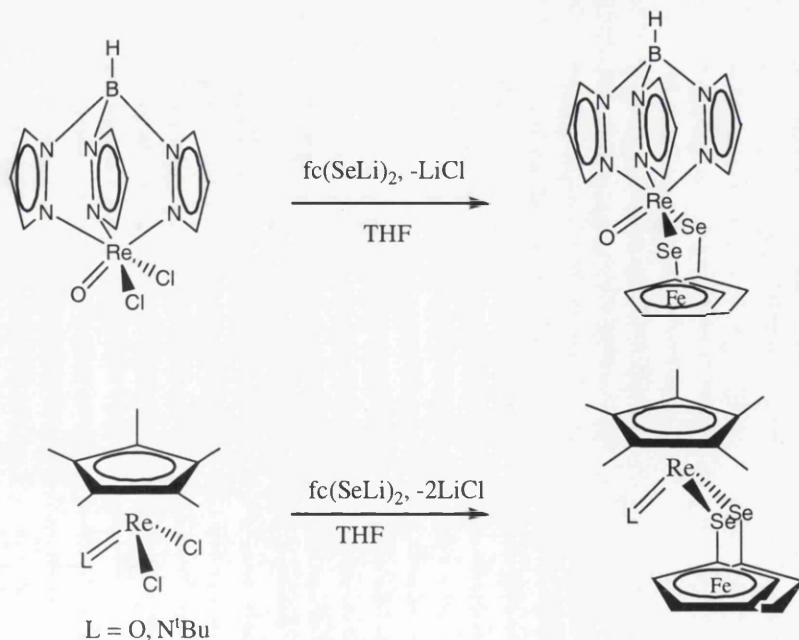


Fig 3.9 Synthetic scheme for $[\text{Re}(\text{O})\text{Tp}(\mathbf{3}\cdot\mathbf{4})]$, $[\text{Re}(\text{O})\text{Cp}^*(\mathbf{3}\cdot\mathbf{4})]$, $[\text{Re}(\text{N}^t\text{Bu})\text{Cp}^*(\mathbf{3}\cdot\mathbf{4})]$

Starting from $[\text{IrCp}^*(\mathbf{3}\cdot\mathbf{4})(\text{PPh}_3)]$, the loss of PPh_3 leads to dimerization via formation of a bridge between the two iridium centres (Fig. 3.10).¹³

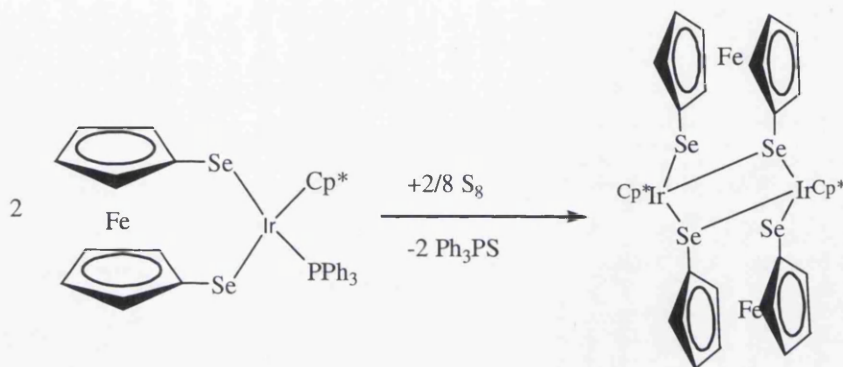


Fig. 3.10 Synthetic scheme for $[\text{IrCp}^*(\mathbf{3}\cdot\mathbf{4})]_2$

Up until now, only one complex having diametric $[3.3]$ ferrocenophane geometry, $[\text{Zr}(\text{C}_5\text{H}_4^t\text{Bu})_2(\mathbf{3}\cdot\mathbf{4})]_2$,¹⁴ has been found, which may be due to steric reasons (Fig. 3.11).

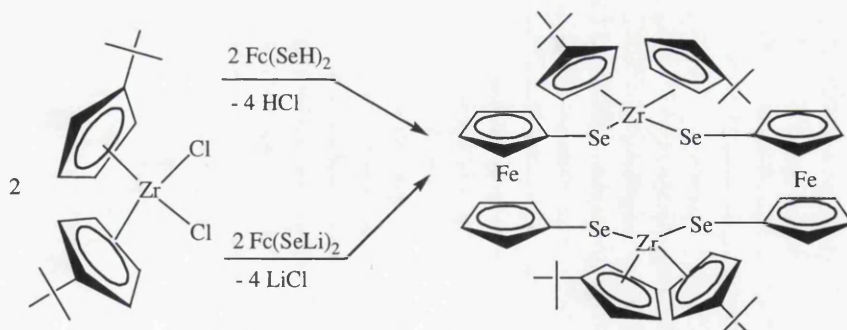


Fig. 3.11 Synthesis of $[\text{Zr}(\text{C}_5\text{H}_4^t\text{Bu})_2(\mathbf{3}\cdot\mathbf{4})]_2$

From $\mathbf{3}\cdot\mathbf{4}$ and the analogous dianion $[\text{Fe}(\text{C}_5\text{H}_4\text{Te})_2]^{2-}$ ($\mathbf{3}\cdot\mathbf{5}$), complexes $[\text{VCp}(\mathbf{3}\cdot\mathbf{4})(\text{CO})_2]_2$, $[\text{VCp}^*(\mathbf{3}\cdot\mathbf{4})(\text{CO})_2]_2$, $[\text{TaCp}^*(\mathbf{3}\cdot\mathbf{4})(\text{CO})_2]_2$,¹⁵ $[\text{VCp}(\mathbf{3}\cdot\mathbf{5})(\text{CO})_2]_2$, $[\text{VCp}^*(\mathbf{3}\cdot\mathbf{5})(\text{CO})_2]_2$, $[\text{TaCp}^*(\mathbf{3}\cdot\mathbf{5})(\text{CO})_2]_2$, $[\text{Rh}_2\text{Cp}^*_2(\mathbf{3}\cdot\mathbf{4})]$, $[\text{Rh}_2\text{Cp}^*_2(\mathbf{3}\cdot\mathbf{5})]$,

$[MCp^*\{(EC_5H_4)_2Fe\}(L)]$ (M = Rh: E = Se, Te, L = PMe_3 , CN^tBu ; M = Ir: E = Se, Te, L = PMe_3 , PPh_3 , CN^tBu)¹³ were also obtained.

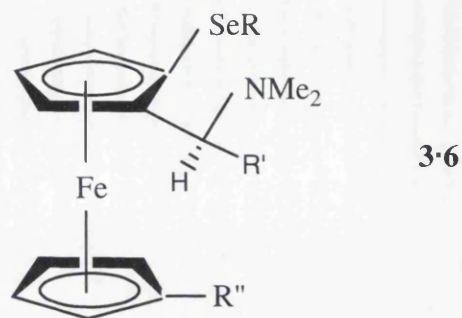


Fig. 3.12 Ferrocenylamine selenide ligands **3·6**

Ferrocenylamine selenide ligands **3·6** also act as SeN bidentate ligands to nickel(II), palladium(II) and platinum(II).¹⁶⁻²⁰ Complexes isolated include *cis*-[PdCl₂(**3·6**)] (R = 4-ClC₆H₄, R' = Me, R'' = SeC₆H₄Cl; R = C₆H₅CH₂, 4-MeC₆H₄, R' = H, R'' = SeC₆H₅, SeC₆H₄Me; R = Ph, R' = Me, CH(CH₃)₂, R'' = H; R = Me, R' = Me, R'' = H) and *cis*-[PtCl₂(**3·6**)] (R = Ph, R' = Me, H, R'' = SePh; R = Me, R' = Me, R'' = H). *cis*-[PdCl₂(**3·6**)] (R = Ph, R' = CH(CH₃)₂, R'' = H) is an effective Grignard cross-coupling agent for coupling of 1-chloro-1-phenylethane with allylmagnesium bromide and allylmagnesium chloride in high yield.¹⁶ The ferrocenylamine selenide ligands with two selenoether groups act only as SeN bidentate ligands forming six-membered chelate rings on coordination. The nickel(II) complexes [NiCl₂(**3·6**)] (R = 4-ClC₆H₄, R' = Me, R'' = SeC₆H₄Cl) were also prepared.²⁰

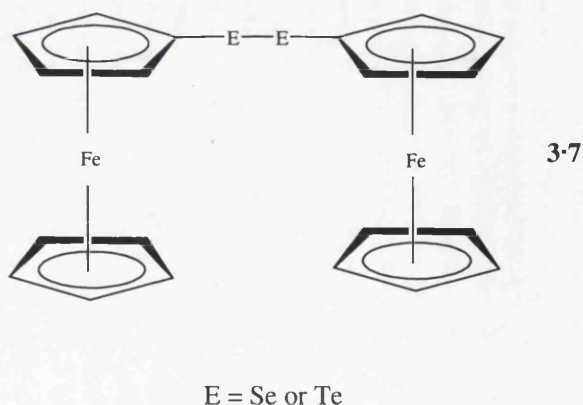


Fig. 3.13 Diferrocenyl dichalcogenides

Diferrocenyl dichalcogenides **3·7** could in principle function as bidentate ligands, but E-E bond cleavage usually occurs instead. Reaction of $[\{\text{Ru}(\eta^5\text{-C}_5\text{Me}_5)(\mu_3\text{-Cl})\}_4]$ with two equivalents of **3·7** gave ferrocenylchalcogenolate-bridged diruthenium complexes.²¹ In our group, the reactions between Fc_2E_2 and $[\text{M}(\text{Cp})(\text{CO})_3]_2$ ($\text{M} = \text{W}, \text{Mo}$) have been studied, which give the products $[\text{M}(\text{FcE})(\text{Cp})(\text{CO})_3]$.²² The reaction between $[\text{W}(\text{CO})_5\text{THF}]$ and Fc_2Se_2 gives the dinuclear complex $[\text{W}_2(\mu\text{-SeFc})_2(\text{CO})_8]$.

3.1.3 Tetradentate ligands

Y. Nishibayashi *et al.* have published a lot of work on the synthesis of chiral ligands, such as **3·8**, and their derivatives for rhodium-, iridium-catalyzed asymmetric reactions.²³⁻³⁰ They succeeded in the isolation of a cationic complex $[\text{Rh}(\mathbf{3}\cdot\mathbf{8})]^+\text{BF}_4^-$. Some analysis shows that the complex may have a structure in which **3·8** coordinates to Rh(I) as a tetradentate ligand.²⁷ Unfortunately there is no crystal structure information to prove it. In another paper,³¹ **3·8** reacted with elemental mercury via E-E bond cleavage to form a complex containing bidentate chalcogenolate ligands.

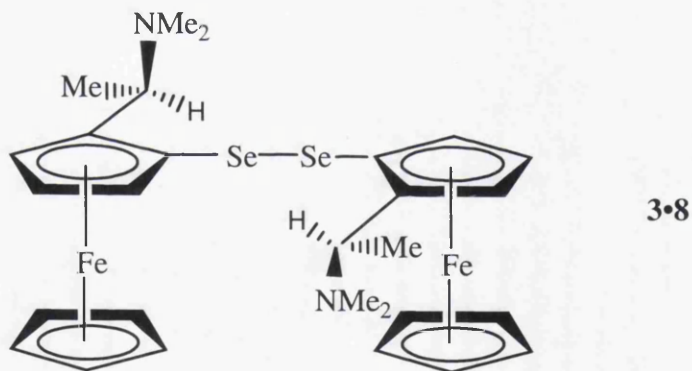


Fig. 3.14 Bis[2-[1-(dimethylamino)ethyl]ferrocenyl] diselenide

As shown in Chapter Two, several series of new ferrocenyl chalcogenide ligands have been synthesized, which gives us the chance to study their ligating properties. Their coordination chemistry was studied systematically and will be discussed in the following sequence: palladium and platinum complexes of ligands with a flexible

saturated hydrocarbon chain; group 6 carbonyl complexes of bis(ferrocenylchalcogeno)propanes; palladium and platinum complexes of macrocyclic ligands; platinum complex of the rigid chain ligand $\text{FcSeCH}_2\text{C}_6\text{H}_4\text{CH}_2\text{SeFc}$. The crystallographic and spectroscopic studies will also be described in the following section. The electrochemistry will be considered in Chapter Four.

3.2 Pd and Pt complexes of ferrocenyl chalcogenide compounds with a flexible hydrocarbon chain

The ligand chemistry of selenium and tellurium has attracted considerable interest over the past twenty years. Since the syntheses of diselenoalkanes $\text{MeSe}(\text{CH}_2)_n\text{SeMe}$ ^{32, 33} and ditelluroalkanes $\text{RTe}(\text{CH}_2)_n\text{TeR}$ ³⁴ were first reported, a lot of papers have been published about the coordination and organometallic chemistry of dichalcogenoethers and transition metals.³⁵⁻³⁷ But although a few papers concerning ferrocenyl selenide and telluride ligands have been published from the 1990s onwards, bis(ferrocenylchalcogeno) derivatives have not previously been investigated systematically. Bis(ferrocenylchalcogeno) derivatives, having two ferrocenyl groups bridged by a saturated hydrocarbon chain, give us the possibility to study the electronic influence of ferrocenyl substituents in soft ligand systems and metal complexes. The synthesis and characterization of a number of compounds of this type have been described in Chapter Two. Now a series of palladium and platinum complexes of the bis(ferrocenylchalcogeno) derivatives have been prepared and studied by a gamut of spectroscopic and structural techniques.

3.2.1 Pd and Pt complexes of $\text{FcE}(\text{CH}_2)_3\text{E}'\text{Fc}$ (E, E' = Se, Te)

3.2.1.1 Synthesis

$\text{FcE}(\text{CH}_2)_3\text{E}'\text{Fc}$ (E & E' = Se or Te) were the ligands of this type chosen first to study complexation to transition metals, as they can form a six-membered ring which is particularly stable.

Direct reaction between $[\text{MCl}_2(\text{NCMe})_2]$ (M = Pd, Pt) and ligands $\text{FcE}(\text{CH}_2)_3\text{E}'\text{Fc}$ (E, E' = Se, Te) gave poorly soluble products, which were difficult to analyse. Replacement of halide with a large anion, such as PF_6^- , has previously proved effective.³⁸ This method was used to synthesize $[\text{M}(\text{FcE}(\text{CH}_2)_3\text{E}'\text{Fc})_2](\text{PF}_6)_2$, which have good solubility in MeCN and acetone. Unfortunately, due to their large molecular weight and pyramidal inversion at room temperature, the NMR spectra show weak and broad features, which means NMR spectroscopy is less useful for these complexes.

The same general procedure was used for the syntheses of all these complexes, which is illustrated below by the example of $[\text{Pd}\{\text{FcSe}(\text{CH}_2)_3\text{SeFc}\}_2](\text{PF}_6)_2$. The experimental details are given in Chapter Seven.

PdCl₂ was refluxed in MeCN (30 ml) for 2 h to give a yellow solution of [PdCl₂(NCMe)₂]. After cooling, two equivalents of TlPF₆ were added and stirring continued for another 15 min. Two equivalents of FcSe(CH₂)₃SeFc in CH₂Cl₂ (5 ml) were then added dropwise, and the mixture stirred at room temperature for 24 h to give a blue liquid and a fine white precipitate of TlCl. The mixture was centrifuged to remove TlCl and reduced to 2 ml *in vacuo*. Diethyl ether (10 ml) was added to precipitate the product as a powder.

3.2.1.2 Structures

Prism crystals suitable for single-crystal X-ray analyses of each of the complexes were obtained by slow diffusion of Et₂O into a solution in MeCN. Data collection and refinement details, selected bond lengths and angles are provided in: Tables 3.1 and 3.2 ([Pd{FcSe(CH₂)₃SeFc}₂](PF₆)₂), Tables 3.3 and 3.4 ([Pt{FcSe(CH₂)₃SeFc}₂](PF₆)₂), Tables 3.5 and 3.6 ([Pd{FcTe(CH₂)₃TeFc}₂](PF₆)₂), Tables 3.7 and 3.8 ([Pt{FcTe(CH₂)₃TeFc}₂](PF₆)₂), Tables 3.9 and 3.10 ([Pd{FcSe(CH₂)₃TeFc}₂](PF₆)₂), Tables 3.11 and 3.12 ([Pt{FcSe(CH₂)₃TeFc}₂](PF₆)₂).

The compounds crystallise as acetonitrile solvates, [M{FcE(CH₂)₃E'Fc}₂](PF₆)₂·2MeCN, which are isostructural. They all crystallize in the space group P-1 in the triclinic crystal system. The structures are all centrosymmetric: there are one cation, two anions and two MeCN molecules in the cell; half of all this forms the symmetry-independent unit. A square planar cation is present with the metal on an inversion centre, coordinated to two ligands. The molecular structures of the cations [Pt{FcSe(CH₂)₃SeFc}₂]²⁺ and [Pd{FcTe(CH₂)₃TeFc}₂]²⁺ are illustrated in Fig. 3.15 and Fig. 3.16 as examples. In each of the complexes the E-M-E angles are all very close to 90°, showing the good match of the six-membered chelate rings formed by the dichalcogenoether and the *cis*-angles required for the square planar geometry.³⁹ The six-membered chelate ring exists in a puckered conformation with the carbon atoms C(1), C(3) and C(2) lying on opposite sides of the metal coordination plane. The Fe-C(Cp) distances are usually used as measures for the valence states of ferrocenes; the average distances are 2.03 Å ([Pd{FcSe(CH₂)₃SeFc}₂](PF₆)₂), 2.02 Å ([Pt{FcSe(CH₂)₃SeFc}₂](PF₆)₂), 2.03 Å ([Pd{FcTe(CH₂)₃TeFc}₂](PF₆)₂), 2.03 Å ([Pt{FcTe(CH₂)₃TeFc}₂](PF₆)₂),

2.04 Å ([Pd{FcSe(CH₂)₃TeFc}₂](PF₆)₂), 2.03 Å ([Pt{FcSe(CH₂)₃TeFc}₂](PF₆)₂), which are typical values for neutral ferrocenes (2.03 Å). The only significant difference between the structures is in the value of the crystallographic β angle, *ca.* 82° for the two complexes [Pd{FcTe(CH₂)₃TeFc}₂](PF₆)₂ and [Pt{FcTe(CH₂)₃TeFc}₂](PF₆)₂ compared to *ca.* 73° for the others (see Fig. 3.17).

The Pd-Se distances in [Pd{FcSe(CH₂)₃SeFc}₂](PF₆)₂ (2.4391(5), 2.4569(5) Å) are slightly longer than those in [Pd([16]aneSe₄)](PF₆)₂·2MeCN (2.435(2), 2.428(1) Å), and the Pt-Se distances in [Pt{FcSe(CH₂)₃SeFc}₂](PF₆)₂ (2.4274(5), 2.4386(7) Å) are similarly longer than those in [Pt{MeSe(CH₂)₃SeMe}₂](PF₆)₂·2MeCN (2.414(2), 2.421(2) Å)⁴⁰ and [Pt([16]aneSe₄)](PF₆)₂·2MeCN (2.420(3), 2.417(3) Å)³⁹. These changes are presumably mainly a result of the presence of the bulky ferrocenyl groups. The ferrocenyl (sp²) C-Se bond distances are 1.9090(42) and 1.9012(37) Å in [Pd{FcSe(CH₂)₃SeFc}₂](PF₆)₂, 1.9101(56) and 1.8944(52) Å in [Pt{FcSe(CH₂)₃SeFc}₂](PF₆)₂, longer than those in the free ligand (1.872(6) and 1.878(6) Å). This could be due to changes in the interaction of the selenium with the π-system of the cyclopentadienyl ring, as there is no equivalent change to the sp³ C-Se bond distance. Electron withdrawal by the metal centre after complexation may cause this phenomenon.

The structure of [Pd{FcTe(CH₂)₃TeFc}₂](PF₆)₂ shows that the Pd-Te distances (2.5938(11)-2.6037(11) Å) are also elongated compared to those in [Pd{*o*-C₆H₄(TeMe)₂]₂](PF₆)₂·MeCN (2.5716(4)-2.5789(5) Å)³⁸. The crystal structures of [Pd{FcSe(CH₂)₃TeFc}₂](PF₆)₂ and [Pt{FcSe(CH₂)₃TeFc}₂](PF₆)₂ show some disorder in the positions of the Te and Se atoms: not only is there Te *trans* to Te, but also Te *trans* to Se. The atoms Se1 and Te1 are therefore composites, and the metal-chalcogen bond lengths for these compounds are an average.

Comparison of the metal-chalcogen bond lengths in the four complexes of the homodonor ligands reveals the expected trends: for a given metal, the bonds to tellurium are *ca.* 0.15 Å longer, due to the larger covalent radius of Te (1.36 Å) than Se (1.16 Å); for a given chalcogen, the bonds to palladium are *ca.* 0.015 Å longer, as Pt(II) (0.80 Å) is slightly smaller than Pd(II) (0.86 Å).

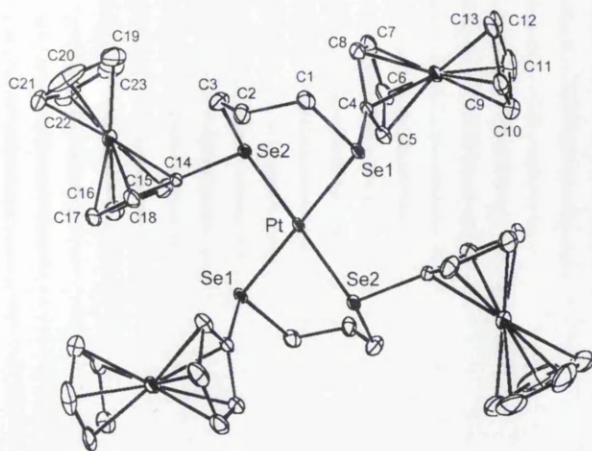


Fig. 3.15 View of the structure of $[\text{Pt}\{\text{FcSe}(\text{CH}_2)_3\text{SeFc}\}_2]^{2+}$ with atomic numbering scheme

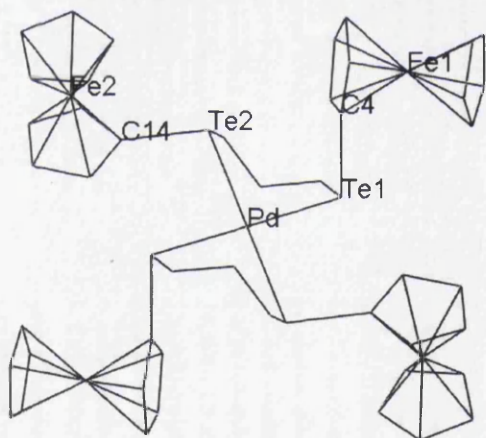
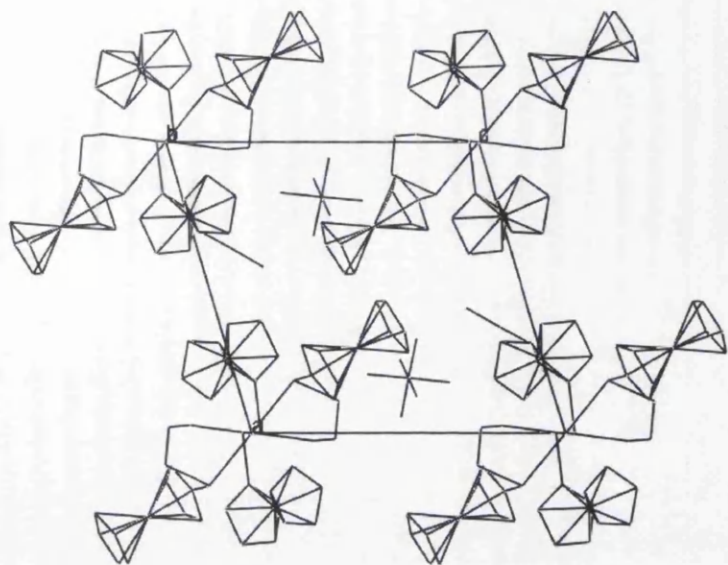
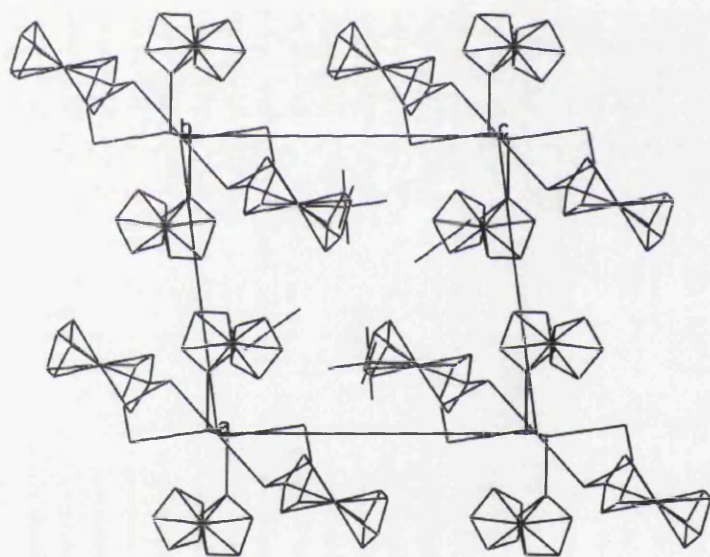


Fig.3.16 View of the structure of $[\text{Pd}\{\text{FcTe}(\text{CH}_2)_3\text{TeFc}\}_2]^{2+}$ with atomic numbering scheme



(a)



(b)

Fig. 3.17 Packing diagrams near ac face of unit cell (a horizontal, c vertical) for diacetonitrile solvates of complexes:

- (a) $[\text{Pd}\{\text{FcSe}(\text{CH}_2)_3\text{SeFc}\}_2](\text{PF}_6)_2$, $[\text{Pt}\{\text{FcSe}(\text{CH}_2)_3\text{SeFc}\}_2](\text{PF}_6)_2$,
 $[\text{Pd}\{\text{FcSe}(\text{CH}_2)_3\text{TeFc}\}_2](\text{PF}_6)_2$, $[\text{Pt}\{\text{FcSe}(\text{CH}_2)_3\text{TeFc}\}_2](\text{PF}_6)_2$;
 (b) $[\text{Pd}\{\text{FcTe}(\text{CH}_2)_3\text{TeFc}\}_2](\text{PF}_6)_2$, $[\text{Pt}\{\text{FcTe}(\text{CH}_2)_3\text{TeFc}\}_2](\text{PF}_6)_2$.

Table 3.1 Crystallographic data collection and refinement parameters of
 $[\text{Pd}\{\text{FcSe}(\text{CH}_2)_3\text{SeFc}\}_2](\text{PF}_6)_2 \cdot 2\text{MeCN}$

Empirical formula	$\text{C}_{50}\text{H}_{54}\text{F}_{12}\text{Fe}_4\text{N}_2\text{P}_2\text{PdSe}_4$
Formula weight	1618.53
T (K)	293(2)
Wavelength (Å)	0.71069
Crystal system	triclinic
Space group	P-1
a (Å)	10.897(1)
b (Å)	11.541(1)
c (Å)	11.751(1)
α (°)	78.95(1)
β (°)	72.88(1)
γ (°)	86.51(1)
Volume (Å ³)	1386.2(2)
Z	1
D_c (Mg m ⁻³)	1.939
Absorption coefficient (mm ⁻¹)	4.10
$F(000)$	792
Crystal size (mm)	0.33 × 0.18 × 0.14
θ range for data collection (°)	4.79 to 26.6
Index ranges	$-13 \leq h \leq 13, -14 \leq k \leq 14, -9 \leq l \leq 14$
Reflections collected	7422
Independent reflections [Rint]	4758 [0.0164]
Data / restraints / parameters	4758 / 0 / 341
Goodness-of-fit on F^2	0.887
Final R indices [$I > 2\sigma(I)$]	$R_1 = 0.0311, wR_2 = 0.0705$
R indices (all data)	$R_1 = 0.0424, wR_2 = 0.0732$
Largest diff. peak and hole (e Å ⁻³)	0.920, -0.449

* The number in bracket means the standard uncertainty, s.u..

Table 3.2 Selected bond lengths (Å) and angles (°) for
 $[\text{Pd}\{\text{FcSe}(\text{CH}_2)_3\text{SeFc}\}_2](\text{PF}_6)_2 \cdot 2\text{MeCN}$

<i>Bond lengths</i>					
Pd-Se(1)	2.4391(4)	Pd-Se(2)	2.4569(5)	Se(1)-C(4)	1.909(4)
Se(1)-C(1)	1.978(4)	Se(2)-C(14)	1.901(4)	Se(2)-C(3)	1.983(4)
Fe(1)-C(4)	2.023(4)	Fe(2)-C(14)	2.019(4)	C(1)-C(2)	1.511(5)
C(2)-C(3)	1.503(6)				
<i>Bond angles</i>					
Se(1)-Pd-Se(2)	87.92(2)	Se(1)-Pd-Se(2)'	92.08(2)		
C(4)-Se(1)-C(1)	102.25(18)	C(4)-Se(1)-Pd	98.58(12)		
C(1)-Se(1)-Pd	104.11(12)	C(14)-Se(2)-C(3)	99.22(18)		
C(14)-Se(2)-Pd	109.21(12)	C(3)-Se(2)-Pd	103.08(14)		

* The number in bracket means the standard uncertainty, s.u..

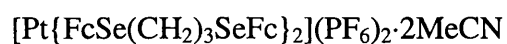
Table 3.3 Crystallographic data collection and refinement parameters of



Empirical formula	$\text{C}_{50}\text{H}_{54}\text{F}_{12}\text{Fe}_4\text{N}_2\text{P}_2\text{PtSe}_4$
Formula weight	1707.22
T (K)	293(2)
Wavelength (Å)	0.71069
Crystal system	triclinic
Space group	P-1
a (Å)	10.883(1)
b (Å)	11.538(1)
c (Å)	11.752(1)
α (°)	78.69(1)
β (°)	72.75(1)
γ (°)	86.44(1)
Volume (Å ³)	1381.9(2)
Z	1
D_c (Mg m ⁻³)	2.051
Absorption coefficient (mm ⁻¹)	6.32
$F(000)$	824
Crystal size (mm)	0.80 × 0.35 × 0.35
θ range for data collection (°)	4.54 to 32.33
Index ranges	$-16 \leq h \leq 14, -17 \leq k \leq 16, -17 \leq l \leq 8$
Reflections collected	13465
Independent reflections [Rint]	8483 [0.0487]
Data / restraints / parameters	8483 / 0 / 341
Goodness-of-fit on F^2	0.778
Final R indices [$I > 2\sigma(I)$]	$R_1 = 0.0501, wR_2 = 0.0922$
R indices (all data)	$R_1 = 0.0739, wR_2 = 0.0969$
Largest diff. peak and hole (e Å ⁻³)	2.892, -2.389

* The number in bracket means the standard uncertainty, s.u..

Table 3.4 Selected bond lengths (Å) and angles (°) for



<i>Bond lengths</i>					
Pt-Se(1)	2.4274(5)	Pt-Se(2)	2.4386(7)	Se(1)-C(4)	1.910(6)
Se(1)-C(1)	1.980(5)	Se(2)-C(14)	1.894(5)	Se(2)-C(3)	1.981(6)
Fe(1)-C(4)	2.017(5)	Fe(2)-C(14)	2.019(5)	C(1)-C(2)	1.493(8)
C(2)-C(3)	1.498(8)				
<i>Bond angles</i>					
Se(1)-Pt-Se(2)	92.13(2)	Se(1)-Pt-Se(2)'	87.87(2)		
C(4)-Se(1)-C(1)	102.37(25)	C(4)-Se(1)-Pt	98.89(16)		
C(1)-Se(1)-Pt	104.36(16)	C(14)-Se(2)-C(3)	98.6(3)		
C(14)-Se(2)-Pt	108.67(16)	C(3)-Se(2)-Pt	103.3(2)		

* The number in bracket means the standard uncertainty, s.u..

Table 3.5 Crystallographic data collection and refinement parameters of



Empirical formula	$\text{C}_{50}\text{H}_{54}\text{F}_{12}\text{Fe}_4\text{N}_2\text{P}_2\text{PdTe}_4$
Formula weight	1813.09
T (K)	293(2)
Wavelength (Å)	0.71069
Crystal system	triclinic
Space group	P-1
a (Å)	10.834(4)
b (Å)	11.472(4)
c (Å)	11.907(4)
α (°)	79.70(3)
β (°)	82.04(3)
γ (°)	84.55(3)
Volume (Å ³)	1438.27(9)
Z	1
D_c (Mg m ⁻³)	2.093
Absorption coefficient (mm ⁻¹)	3.41
$F(000)$	864
Crystal size (mm)	0.44 × 0.27 × 0.13
θ range for data collection (°)	3.97 to 32.33
Index ranges	-15 ≤ h ≤ 15, -15 ≤ k ≤ 17, -11 ≤ l ≤ 17
Reflections collected	12099
Independent reflections [Rint]	8528 [0.0531]
Data / restraints / parameters	8528 / 0 / 341
Goodness-of-fit on F^2	0.716
Final R indices [$I > 2\sigma(I)$]	$R_1 = 0.0661$, $wR_2 = 0.1523$
R indices (all data)	$R_1 = 0.1198$, $wR_2 = 0.1687$
Largest diff. peak and hole (e Å ⁻³)	2.718, -1.975

* The number in bracket means the standard uncertainty, s.u..

Table 3.6 Selected bond lengths (Å) and angles (°) for
 $[\text{Pd}\{\text{FcTe}(\text{CH}_2)_3\text{TeFc}\}_2](\text{PF}_6)_2 \cdot 2\text{MeCN}$

<i>Bond lengths</i>					
Pd-Te(1)	2.5938(11)	Pd-Te(2)	2.6037(11)	Te(1)-C(4)	2.101(9)
Te(1)-C(1)	2.150(9)	Te(2)-C(14)	2.073(9)	Te(2)-C(3)	2.150(10)
Fe(1)-C(4)	2.01(1)	Fe(2)-C(14)	2.046(8)	C(1)-C(2)	1.51(1)
C(2)-C(3)	1.53(1)				
<i>Bond angles</i>					
Te(1)-Pd-Te(2)	87.89(3)	Te(1)-Pd-Te(2)'	92.11(3)		
C(4)-Te(1)-C(1)	98.5(4)	C(4)-Te(1)-Pd	96.9(3)		
C(1)-Te(1)-Pd	102.3(3)	C(14)-Te(2)-C(3)	94.6(4)		
C(14)-Te(2)-Pd	106.3(2)	C(3)-Te(2)-Pd	100.4(3)		

* The number in bracket means the standard uncertainty, s.u..

Table 3.7 Crystallographic data collection and refinement parameters of
 $[\text{Pt}\{\text{FcTe}(\text{CH}_2)_3\text{TeFc}\}_2](\text{PF}_6)_2 \cdot 2\text{MeCN}$

Empirical formula	$\text{C}_{50}\text{H}_{54}\text{F}_{12}\text{Fe}_4\text{N}_2\text{P}_2\text{PtTe}_4$
Formula weight	1901.78
T (K)	293(2)
Wavelength (Å)	0.71069
Crystal system	triclinic
Space group	P-1
a (Å)	10.792(1)
b (Å)	11.490(1)
c (Å)	11.865(1)
α (°)	79.74(1)
β (°)	82.18(1)
γ (°)	84.50(1)
Volume (Å ³)	1430.4(2)
Z	1
D_c (Mg m ⁻³)	2.208
Absorption coefficient (mm ⁻¹)	5.56
$F(000)$	896
Crystal size (mm)	0.40 × 0.40 × 0.20
θ range for data collection (°)	4.60 to 32.34
Index ranges	$-15 \leq h \leq 15, -9 \leq k \leq 17, -17 \leq l \leq 16$
Reflections collected	13808
Independent reflections [Rint]	8744 [0.0274]
Data / restraints / parameters	8744 / 0 / 341
Goodness-of-fit on F^2	0.910
Final R indices [$I > 2\sigma(I)$]	$R_1 = 0.0423, wR_2 = 0.0942$
R indices (all data)	$R_1 = 0.0607, wR_2 = 0.1004$
Largest diff. peak and hole (e Å ⁻³)	5.455, -1.569

* The number in bracket means the standard uncertainty, s.u..

Table 3.8 Selected bond lengths (Å) and angles (°) for
 $[\text{Pt}\{\text{FcTe}(\text{CH}_2)_3\text{TeFc}\}_2](\text{PF}_6)_2 \cdot 2\text{MeCN}$

<i>Bond lengths</i>					
Pt-Te(1)	2.5816(4)	Pt-Te(2)	2.5842(4)	Te(1)-C(4)	2.088(6)
Te(1)-C(1)	2.146(6)	Te(2)-(14)	2.087(5)	Te(2)-C(3)	2.164(6)
Fe(1)-C(4)	2.026(5)	Fe(2)-C(14)	2.014(5)	C(1)-C(2)	1.509(8)
C(2)-C(3)	1.494(9)				
<i>Bond angles</i>					
Te(1)-Pt-Te(2)	91.80(1)	Te(1)-Pt-Te(2)'	88.20(1)		
C(4)-Te(1)-C(1)	97.8(2)	C(4)-Te(1)-Pt	96.52(15)		
C(1)-Te(1)-Pt	102.19(15)	C(14)-Te(2)-C(3)	95.1(2)		
C(14)-Te(2)-Pt	106.95(14)	C(3)-Te(2)-Pt	100.29(18)		

* The number in bracket means the standard uncertainty, s.u..

Table 3.9 Crystallographic data collection and refinement parameters of



Empirical formula	$\text{C}_{50}\text{H}_{54}\text{F}_{12}\text{Fe}_4\text{N}_2\text{P}_2\text{PdSe}_2\text{Te}_2$
Formula weight	1715.81
T (K)	293(2)
Wavelength (Å)	0.71069
Crystal system	triclinic
Space group	P-1
a (Å)	10.923(3)
b (Å)	11.701(4)
c (Å)	11.860(4)
α (°)	79.33(3)
β (°)	73.42(3)
γ (°)	86.88(3)
Volume (Å ³)	1427.7(8)
Z	1
D_c (Mg m ⁻³)	1.996
Absorption coefficient (mm ⁻¹)	3.71
$F(000)$	828
Crystal size (mm)	0.80 × 0.20 × 0.15
θ range for data collection (°)	4.28 to 32.36
Index ranges	$-15 \leq h \leq 16, -17 \leq k \leq 16, -10 \leq l \leq 17$
Reflections collected	13893
Independent reflections [Rint]	8781 [0.0436]
Data / restraints / parameters	8781 / 0 / 342
Goodness-of-fit on F^2	0.736
Final R indices [$I > 2\sigma(I)$]	$R_1 = 0.0558, wR_2 = 0.1323$
R indices (all data)	$R_1 = 0.0934, wR_2 = 0.1385$
Largest diff. peak and hole (e Å ⁻³)	1.995, -1.469

* The number in bracket means the standard uncertainty, s.u..

Table 3.10 Selected bond lengths (Å) and angles (°) for
 $[\text{Pd}\{\text{FcSe}(\text{CH}_2)_3\text{TeFc}\}_2](\text{PF}_6)_2 \cdot 2\text{MeCN}$

<i>Bond lengths</i>					
Pd-Se(1)	2.5176(9)	Pd-Te(1)	2.5540(1)	Te(1)-C(4)	2.019(6)
Te(1)-C(1)	2.098(7)	Se(1)-C(14)	1.999(6)	Se(1)-C(3)	2.061(6)
Fe(1)-C(4)	2.025(6)	Fe(2)-C(14)	2.048(6)	C(1)-C(2)	1.51(1)
C(2)-C(3)	1.512(9)				
<i>Bond angles</i>					
Se(1)-Pd-Te(1)	87.81(4)	Se(1)-Pd-Se(2)	92.19(4)		
C(4)-Te(1)-C(1)	96.8(3)	C(4)-Te(1)-Pd	106.91(17)		
C(1)-Te(1)-Pd	101.5(2)	C(14)-Se(1)-C(3)	99.9(3)		
C(14)-Se(1)-Pd	96.51(16)	C(3)-Se(1)-Pd	103.70(19)		

* The Se1 site has 0.525(2) Se (complementary Te) occupancy; the Te1 site has 0.525(2) Te (complementary Se) occupancy.

* The number in bracket means the standard uncertainty, s.u..

Table 3.11 Crystallographic data collection and refinement parameters of



Empirical formula	$\text{C}_{50}\text{H}_{54}\text{F}_{12}\text{Fe}_4\text{N}_2\text{P}_2\text{PtSe}_2\text{Te}_2$
Formula weight	1804.5
T (K)	293(2)
Wavelength (Å)	0.71069
Crystal system	triclinic
Space group	P-1
a (Å)	10.933(1)
b (Å)	11.698(1)
c (Å)	11.791(1)
α (°)	79.26(1)
β (°)	73.24(1)
γ (°)	86.67(1)
Volume (Å ³)	1417.2(2)
Z	1
D_c (Mg m ⁻³)	2.114
Absorption coefficient (mm ⁻¹)	5.88
$F(000)$	860
Crystal size (mm)	0.60 × 0.20 × 0.15
θ range for data collection (°)	4.05 to 36.79
Index ranges	$-18 \leq h \leq 18, -18 \leq k \leq 19, -19 \leq l \leq 15$
Reflections collected	26853
Independent reflections [Rint]	10508 [0.0326]
Data / restraints / parameters	10508 / 0 / 341
Goodness-of-fit on F^2	0.863
Final R indices [$I > 2\sigma(I)$]	$R_1 = 0.0500, wR_2 = 0.1227$
R indices (all data)	$R_1 = 0.0763, wR_2 = 0.1350$
Largest diff. peak and hole (e Å ⁻³)	4.142, -2.093

* The number in bracket means the standard uncertainty, s.u..

Table 3.12 Selected bond lengths (Å) and angles (°) for
 $[\text{Pt}\{\text{FcSe}(\text{CH}_2)_3\text{TeFc}\}_2](\text{PF}_6)_2 \cdot 2\text{MeCN}$

<i>Bond lengths</i>					
Pt- Se (1)	2.5072(4)	Pt- Te (1)	2.5390(5)	Te (1)-C(4)	2.006(5)
Te (1)-C(1)	2.095(7)	Se (1)-C(14)	2.005(5)	Se (1)-C(3)	2.054(6)
Fe (1)-C(4)	2.006(5)	Fe (2)-C(14)	2.025(4)	C(1)-C(2)	1.510(9)
C(2)-C(3)	1.478(8)				
<i>Bond angles</i>					
Se (1)-Pt- Te (1)	88.17(2)	Se (1)-Pt- Se (2)	91.83(2)		
C(4)- Te (1)-C(1)	96.5(3)	C(4)- Te (1)-Pt	106.88(14)		
C(1)- Te (1)-Pt	100.90(19)	C(14)- Se (1)-C(3)	100.9(2)		
C(14)- Se (1)-Pt	96.84(14)	C(3)- Se (1)-Pt	103.28(15)		

* The **Se**1 site has 0.429(2) **Se** (complementary **Te**) occupancy; the **Te**1 site has 0.429(2) **Te** (complementary **Se**) occupancy.

* * The number in bracket means the standard uncertainty, s.u..

3.2.1.3 Electronic spectra of $[M(\text{FcECH}_2\text{CH}_2\text{CH}_2\text{EFc})_2](\text{PF}_6)_2$ (E, E' = Se, Te)

Table 3.13 lists the UV-Vis data for these six complexes. These complexes give quite different spectra as compared to the free ligands (example shown in Fig. 3.18). There are new absorptions in the near ultra-violet region with high intensity. In ferrocenyl derivatives the lowest energy spin-allowed d-d band of the ferrocene unit occurs in the wavelength range 400-500 nm. Previous studies have shown that this transition undergoes a bathochromic shift on complexation.⁴¹ The compounds $\text{FcE}(\text{CH}_2)_3\text{E}'\text{Fc}$ absorb at 440 nm (E = E' = Se) or 445 nm (E = Te; E' = Se or Te), but in the spectra of the complexes the corresponding band is obscured by a more intense absorption at higher (M = Pd) or lower (M = Pt) wavelength. The dramatically (and consistently) different colours of the palladium (blue) and platinum (red) complexes are similar to those exhibited by the chalcogenolates $[\text{MCl}(\text{ECH}_2\text{CH}_2\text{NMe}_2)(\text{PR}_3)]$, which suggests that the lowest energy transitions are ligand-to-metal charge transfer in character.^{42, 43}

Table 3.13 UV-Vis data^a for complexes in 10^{-4} mol dm⁻³ CH₃CN solution

	λ_1	λ_2	λ_3
$[\text{Pd}\{\text{FcSe}(\text{CH}_2)_3\text{SeFc}\}_2](\text{PF}_6)_2$	310 (11000)	380 (16000)	625 (6700)
$[\text{Pt}\{\text{FcSe}(\text{CH}_2)_3\text{SeFc}\}_2](\text{PF}_6)_2$	Not resolved	310 (18800)	480 (5600)
$[\text{Pd}\{\text{FcSe}(\text{CH}_2)_3\text{TeFc}\}_2](\text{PF}_6)_2$	Not resolved	375 (17200)	565 (6500)
$[\text{Pt}\{\text{FcSe}(\text{CH}_2)_3\text{TeFc}\}_2](\text{PF}_6)_2$	270 (45000)	310 (35500)	460 (9250)
$[\text{Pd}\{\text{FcTe}(\text{CH}_2)_3\text{TeFc}\}_2](\text{PF}_6)_2$	Not resolved	375 (38900)	575 (8200)
$[\text{Pt}\{\text{FcTe}(\text{CH}_2)_3\text{TeFc}\}_2](\text{PF}_6)_2$	265 (16200)	305 (10000)	475 (2600)

^a $\lambda_{\text{max}} / \text{nm}$ ($\epsilon / \text{dm}^3 \text{mol}^{-1} \text{cm}^{-1}$)

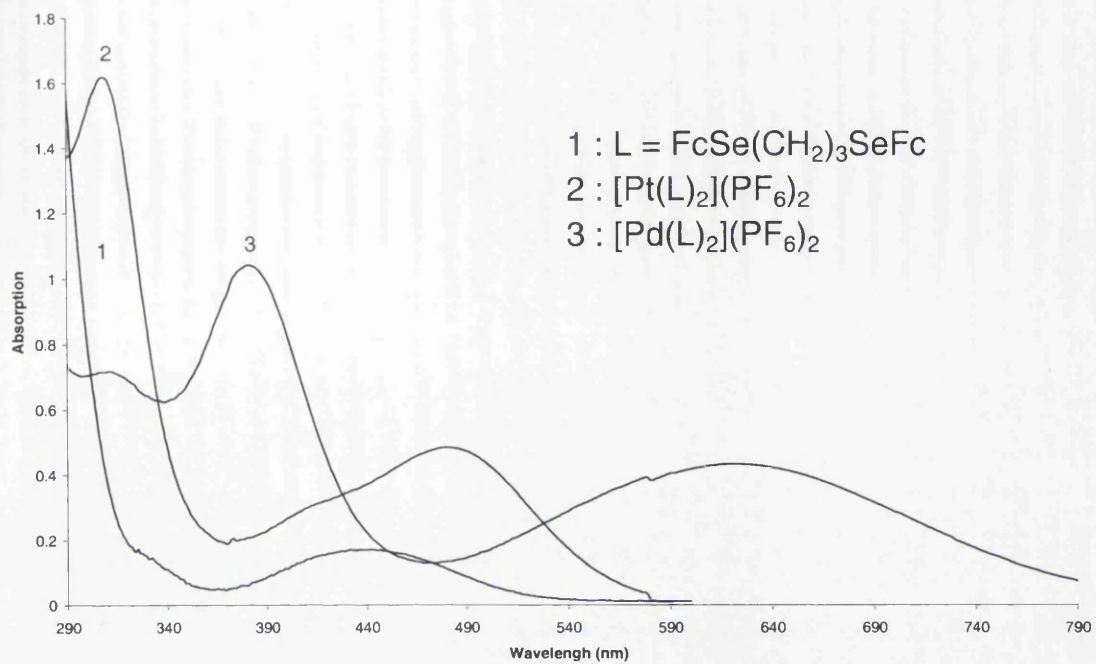


Fig. 3.18 UV-vis spectra for $\text{FcSe}(\text{CH}_2)_3\text{SeFc}$ and complexes in $10^{-4} \text{ mol dm}^{-3}$ CH_3CN solution

3.2.2 Pd and Pt complexes of FcE(CH₂)_nEFc (n = 1, E = Se or

Te; n = 2, E = Se)

3.2.2.1 Synthesis

Single-crystal X-ray diffraction is a very powerful technique for structural characterisation and provides a picture of the molecule. The normal procedure to obtain crystals is performing the reaction first to get the target product, then selecting a suitable method to grow crystals. As insoluble products can't be treated in this way, to obtain this kind of crystalline product, liquid-liquid interface reaction will be a good choice. Direct reaction between [MCl₂(NCPH)₂] and FcE(CH₂)_nEFc immediately gave products which could only be dissolved in the coordinating solvent DMSO and decomposed quickly. As the ligands FcE(CH₂)_nEFc have good solubility in dichloromethane, so do [MCl₂(NCPH)₂] in acetonitrile. Also the density of these two solvents is quite different: 1.325 g cm⁻³ for dichloromethane, 0.786 g cm⁻³ for acetonitrile. A new scheme was designed: in a test tube (d = 5 mm), the dichloromethane solution of ligand was placed in the bottom first; the acetonitrile solution of [MCl₂(NCPH)₂] was then carefully layered onto the dichloromethane solution surface. The reaction starts from the liquid-liquid interface and continues via liquid-liquid diffusion. Due to its insolubility, the product can form a crystal nucleus under suitable conditions. Crystals will then be obtained after standing for several days at room temperature.

3.2.2.2 Structures

[MCl₂(FcSeCH₂SeFc)₂] (M = Pd or Pt)

With a 2:1 stoichiometry of FcSeCH₂SeFc and [MCl₂(NCPH)₂] (M = Pd or Pt), dark brown rhombohedral crystals [PdCl₂(FcSeCH₂SeFc)₂] and orange red prism crystals [PtCl₂(FcSeCH₂SeFc)₂] suitable for single-crystal X-ray analysis were grown. Data collection and refinement details are provided in Tables 3.14 (Pd) and 3.15 (Pt); selected bond lengths and angles are listed in Tables 3.16 (Pd) and 3.17 (Pt).

Because of the high strain of a four-membered ring, the potentially bidentate FcSeCH₂SeFc behaves as a monodentate ligand, to form the *trans* complexes with the metal on a centre of symmetry; a similar structure has been observed before in [PdCl₂(PhSCH₂SPh)₂].⁴⁴

The molecular structure of $[\text{PdCl}_2(\text{FcSeCH}_2\text{SeFc})_2]$ is illustrated in Fig. 3.19 and the packing diagram is shown in Fig. 3.20. The molecular structure of $[\text{PtCl}_2(\text{FcSeCH}_2\text{SeFc})_2]$ is illustrated in Fig. 3.21 and the packing diagram is shown in Fig. 3.22. These two complexes all crystallize in the space group P21/a in the monoclinic crystal system. There is no close contact between the free selenium and neighboring molecules. A weak $\text{Cl}\cdots\text{H}$ (2.866 Å) intermolecular interaction exists in $[\text{PdCl}_2(\text{FcSeCH}_2\text{SeFc})_2]$.

In $[\text{PdCl}_2(\text{FcSeCH}_2\text{SeFc})_2]$, the coordinated Se-C ferrocenyl distance (sp^2) (1.907(3) Å) is close to those in $[\text{Pd}\{\text{FcSe}(\text{CH}_2)_3\text{SeFc}\}_2](\text{PF}_6)_2$ (1.9090(42) and 1.9012(37) Å), and is longer than the uncoordinated one (1.898(3) Å), a direct result of electron withdrawal by Pd after coordination. The sp^3 C-Se bond distances are quite different, 0.019 Å longer to the coordinated Se than to the uncoordinated one. Similarly in $[\text{PtCl}_2(\text{FcSeCH}_2\text{SeFc})_2]$, the coordinated Se-C ferrocenyl distance (sp^2) (1.914(3) Å) is longer than the uncoordinated one (1.903(4) Å). The sp^3 C-Se bond distance is 0.027 Å longer to the coordinated Se than to the uncoordinated one. The Pd-Se bond length (2.4351(4) Å) is shorter than those in $[\text{Pd}\{\text{FcSe}(\text{CH}_2)_3\text{SeFc}\}_2](\text{PF}_6)_2 \cdot 2\text{MeCN}$ (2.4391(5), 2.4569(5) Å), but similar to those in $[\text{Pd}([\text{16}] \text{aneSe}_4)](\text{PF}_6)_2 \cdot 2\text{MeCN}$ (2.435(2), 2.428(1) Å). The Se-Pd bond is *ca.* 0.013 Å longer than Se-Pt bond due to the radius difference between Pd(II) and Pt(II). A similar trend has been observed in $[\text{M}\{\text{FcE}(\text{CH}_2)_3\text{E}'\text{Fc}\}_2](\text{PF}_6)_2$ (M = Pd or Pt; E & E' = Se or Te). The Pd-Cl bond length (2.2965(8) Å) is a little greater than that in $[\text{PdCl}_2(\text{PhSCH}_2\text{SPh})_2]$ (2.292(1) Å), which can be attributed to the better donor property of Se.

Around the square planar coordinated Pd, the Cl-Pd-Se angle is 94.07(3)°, smaller than that in $[\text{PdCl}_2(\text{PhSCH}_2\text{SPh})_2]$ (95.3(1)°). The Cl-Pt-Se angle is even smaller at 86.08(3)°.

Changing the ratio of $\text{FcSeCH}_2\text{SeFc}$ and $[\text{MCl}_2(\text{PhCN})_2]$ to 1:1 produced the same compound. It seems that the equilibrium in the system is driven by the insolubility of the 1:2 complexes.

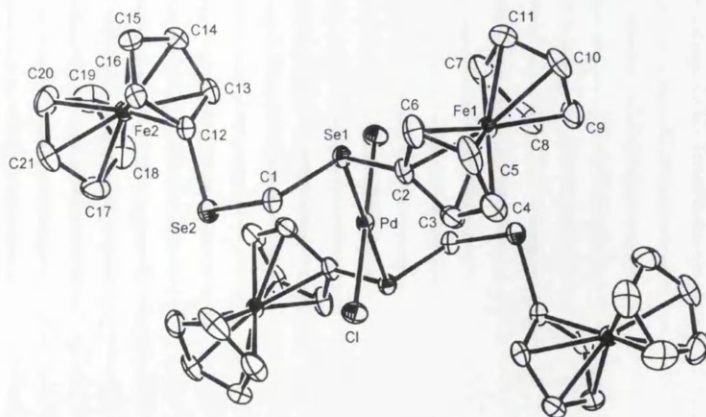


Fig. 3.19 Plot of a molecule of $[\text{PdCl}_2(\text{FcSeCH}_2\text{SeFc})_2]$ with atomic numbering scheme

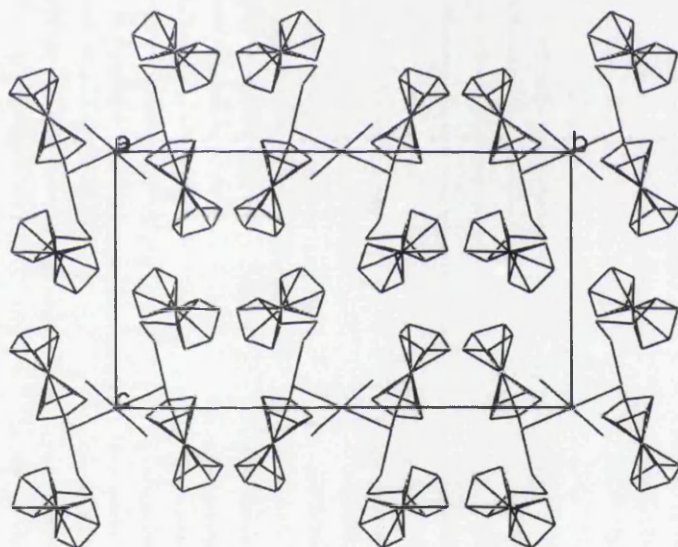


Fig. 3.20 Packing diagram for $[\text{PdCl}_2(\text{FcSeCH}_2\text{SeFc})_2]$

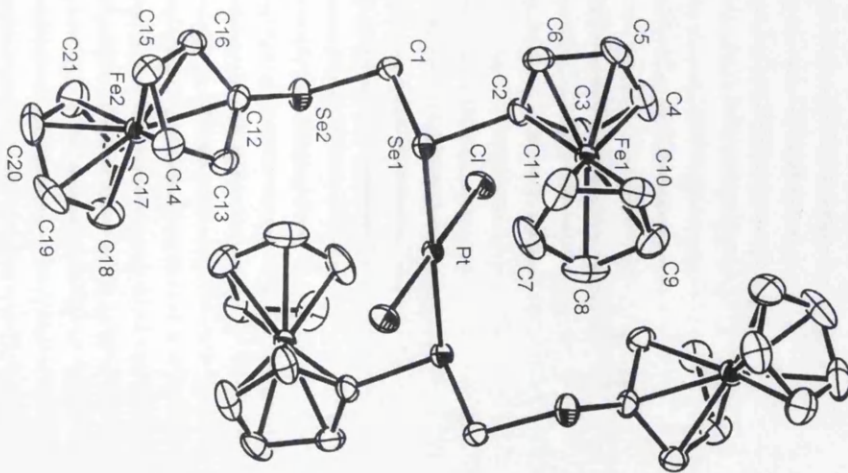


Fig. 3.21 Plot of a molecule of $[\text{PtCl}_2(\text{FcSeCH}_2\text{SeFc})_2]$ with atomic numbering scheme

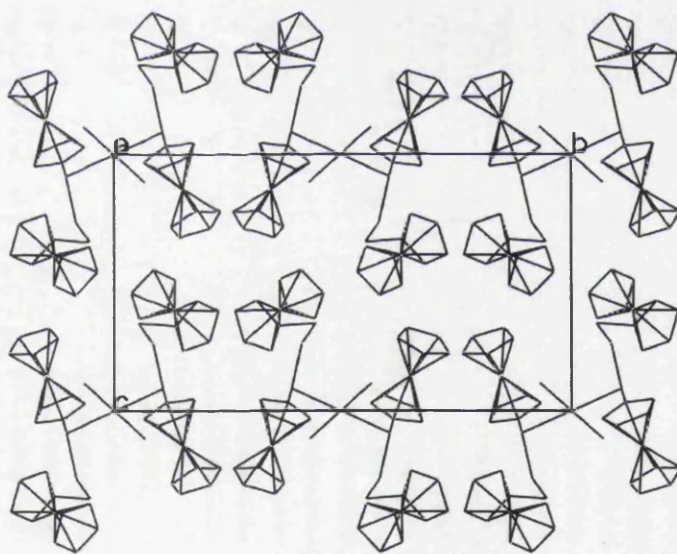


Fig. 3.22 Packing diagram for $[\text{PtCl}_2(\text{FcSeCH}_2\text{SeFc})_2]$

Table 3.14 Crystal data and structure refinement for [PdCl₂(FcSeCH₂SeFc)₂]

Empirical formula	C ₄₂ H ₄₀ Cl ₂ Fe ₂ PdSe ₄
Formula weight	1261.28
T (K)	293(2)
Wavelength (Å)	0.71069
Crystal system	Monoclinic
Space group	P21/a
<i>a</i> (Å)	9.851(1)
<i>b</i> (Å)	19.226(2)
<i>c</i> (Å)	10.791(1)
α (°)	90.00
β (°)	99.24(1)
γ (°)	90.00
Volume (Å ³)	2017.3(2)
<i>Z</i>	2
<i>D_c</i> (Mg m ⁻³)	2.077
Absorption coefficient (mm ⁻¹)	5.614
<i>F</i> (000)	1224
Crystal size (mm)	0.40 × 0.40 × 0.25
θ range for data collection (°)	4.32 to 26.36
Index ranges	-12 ≤ <i>h</i> ≤ 12, -24 ≤ <i>k</i> ≤ 23, -13 ≤ <i>l</i> ≤ 13
Reflections collected	20154
Independent reflections [Rint]	4095 [0.0361]
Data / restraints / parameters	4095 / 0 / 241
Goodness-of-fit on F ²	0.981
Final <i>R</i> indices [<i>I</i> > 2σ(<i>I</i>)]	<i>R</i> ₁ = 0.0277, <i>wR</i> ₂ = 0.0638
<i>R</i> indices (all data)	<i>R</i> ₁ = 0.0387, <i>wR</i> ₂ = 0.0600
Largest diff. peak and hole (e Å ⁻³)	0.558, -0.441

* The number in bracket means the standard uncertainty, s.u..

Table 3.15 Crystal data and structure refinement for [PtCl₂(FcSeCH₂SeFc)₂]

Empirical formula	C ₄₂ H ₄₀ Cl ₂ Fe ₂ PtSe ₄
Formula weight	1349.96
T (K)	293(2)
Wavelength (Å)	0.71069
Crystal system	Monoclinic
Space group	P21/a
<i>a</i> (Å)	9.861(1)
<i>b</i> (Å)	19.238(1)
<i>c</i> (Å)	10.865(1)
α (°)	90.00
β (°)	99.132(5)
γ (°)	90.00
Volume (Å ³)	2035.0(3)
Z	2
<i>D_c</i> (Mg m ⁻³)	2.203
Absorption coefficient (mm ⁻¹)	8.557
<i>F</i> (000)	1288
Crystal size (mm)	0.30 × 0.20 × 0.15
θ range for data collection (°)	3.70 to 26.37
Index ranges	-12 ≤ <i>h</i> ≤ 12, -24 ≤ <i>k</i> ≤ 24, -13 ≤ <i>l</i> ≤ 13
Reflections collected	20174
Independent reflections [Rint]	4122 [0.0314]
Data / restraints / parameters	4122 / 0 / 241
Goodness-of-fit on F ²	0.983
Final <i>R</i> indices [<i>I</i> > 2σ(<i>I</i>)]	<i>R</i> ₁ = 0.0240, <i>wR</i> ₂ = 0.0498
<i>R</i> indices (all data)	<i>R</i> ₁ = 0.0400, <i>wR</i> ₂ = 0.0519
Largest diff. peak and hole (e Å ⁻³)	1.155, -0.496

* The number in bracket means the standard uncertainty, s.u..

Table 3.16 Selected bond lengths (Å) and bond angles (°) for [PdCl₂(FcSeCH₂SeFc)₂]

<i>Bond lengths</i>					
Pd-Cl	2.2965(8)	Pd-Se(1)	2.4351(4)	Se(1)-C(2)	1.907(3)
Se(1)-C(1)	1.950(3)	Se(2)-C(12)	1.898(3)	Se(2)-C(1)	1.931(3)
Fe(1)-C(2)	2.008(3)	Fe(2)-C(12)	2.016(3)		
<i>Bond angles</i>					
Cl-Pd-Cl	180.00(6)	Cl-Pd-Se(1)		94.07(3)	
C(2)-Se(1)-C(1)	99.36(13)	C(2)-Se(1)-Pd		106.85(11)	
C(1)-Se(1)-Pd	102.54(10)	Se(2)-C(1)-Se(1)		111.02(16)	
Se(1)-C(2)-Fe(1)	121.51(17)				

Table 3.17 Selected bond lengths (Å) and bond angles (°) for [PtCl₂(FcSeCH₂SeFc)₂]

<i>Bond lengths</i>					
Pt-Cl	2.3085(9)	Pt-Se(1)	2.4225(4)	Se(1)-C(2)	1.914(3)
Se(1)-C(1)	1.962(3)	Se(2)-C(12)	1.903(4)	Se(2)-C(1)	1.935(3)
Fe(1)-C(2)	2.006(4)	Fe(2)-C(12)	2.024(3)		
<i>Bond angles</i>					
Cl-Pt-Cl	180.00(6)	Cl-Pt-Se(1)		86.08(3)	
C(2)-Se(1)-C(1)	99.10(15)	C(2)-Se(1)-Pt		106.70(12)	
C(1)-Se(1)-Pt	103.81(11)	Se(2)-C(1)-Se(1)		111.39(17)	
Se(1)-C(2)-Fe(1)	121.93(18)				

* The number in bracket means the standard uncertainty, s.u..

[MCl₂(FcTeCH₂TeFc)] (M = Pd or Pt)

With a 1:1 stoichiometry of FcTeCH₂TeFc and [MCl₂(PhCN)₂] (M = Pd or Pt), dark black rod-like crystals of [PdCl₂(FcTeCH₂TeFc)] and elongated prism orange crystals of [PtCl₂(FcTeCH₂TeFc)] suitable for single-crystal X-ray analysis were grown. Data collection and refinement details are provided in Tables 3.18 (Pd) and 3.19 (Pt); selected bond lengths and angles are listed in Tables 3.20 (Pd) and 3.21 (Pt).

The Pd complex crystallizes in the space group P-1 in the triclinic crystal system, but the Pt complex crystallizes in the space group C 2/c in the monoclinic crystal system. The molecular structures all contain a four-membered ring with FcTeCH₂TeFc behaving as a bidentate ligand. A similar complex, [PdCl₂{(4-CH₃OC₆H₄Te)₂CH₂}],⁴⁴ has been characterized by X-ray crystallography.

In the structure of [PdCl₂(FcTeCH₂TeFc)] (fig. 3.21), the geometry around palladium is distorted square planar: the angle of Te(1)-Pd(1)-Te(2) is 82.32(4)° and that of Te(2)-C(1)-Te(1) is 100.5(4)°; Te(1), Te(2) and Pd(1) are almost coplanar with C(1) out of the plane. The Pd-Te bond distances are 2.5207(11) and 2.5439(13) Å, longer than those in [PdCl₂{(4-CH₃OC₆H₄Te)₂CH₂}] (2.530(2) Å) and [PdBr₂{*meso*-PhTe(CH₂)₃TePh}] (2.528(1), 2.525(1) Å).⁴⁵ They are quite a lot shorter than those in [Pd{FcTe(CH₂)₃Te}](PF₆)₂ (2.5938(11) and 2.6037(11) Å), which is due to the smaller *trans* influence of the Cl⁻ anion compared to that of TeR₂. The Pd-Cl bond distances (2.366(3) and 2.378(3) Å) are similar to that reported in [PdCl₂{(4-CH₃OC₆H₄Te)₂CH₂}] (2.367(7) Å).

The Te-C ferrocenyl (sp²) distances (2.098(11) and 2.097(10) Å) are close to those in [Pd{FcTe(CH₂)₃Te}](PF₆)₂ (2.101(9) and 2.073(9) Å). The sp³ C-Te bond distances, 2.176(11) and 2.160(11), are longer than the sp² C-Te ones.

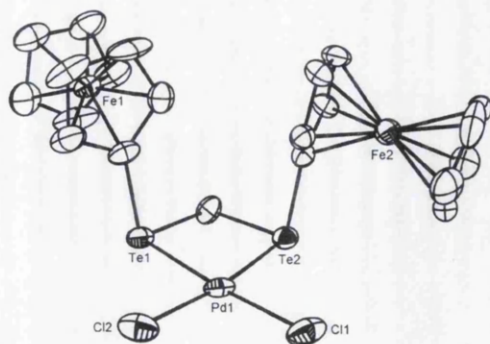


Fig. 3.21 Plot of a molecule of $[\text{PdCl}_2(\text{FcTeCH}_2\text{TeFc})]$

The packing diagram of $[\text{PdCl}_2(\text{FcTeCH}_2\text{TeFc})]$ is shown in Fig.3.22. There are three molecules in the asymmetric unit (six in the triclinic unit cell, with two CH_2Cl_2 solvates), differing from each other in conformational details. The molecules are packed in pairs, with the coordination planes of members of each pair facing each other. Molecule 1 (containing Pd(1)) forms such a pair with a symmetry-related molecule (molecule 1') which, therefore, does not belong to the same asymmetric unit as its mate. The coordination planes of these two molecules are parallel, by symmetry. The arrangement is shown in Fig. 3.23 (a). Molecules 2 and 3, form another pair. Their coordination planes are almost parallel (shown in Fig. 3.23 (b)).

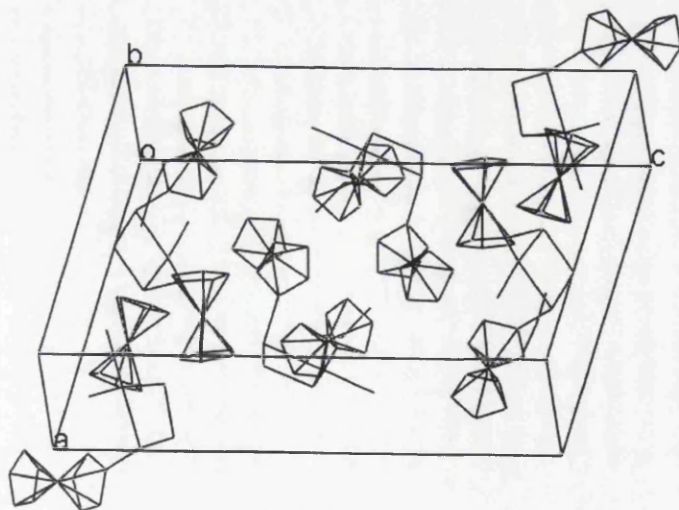


Fig. 3.22 Packing diagram for $[\text{PdCl}_2(\text{FcTeCH}_2\text{TeFc})]$

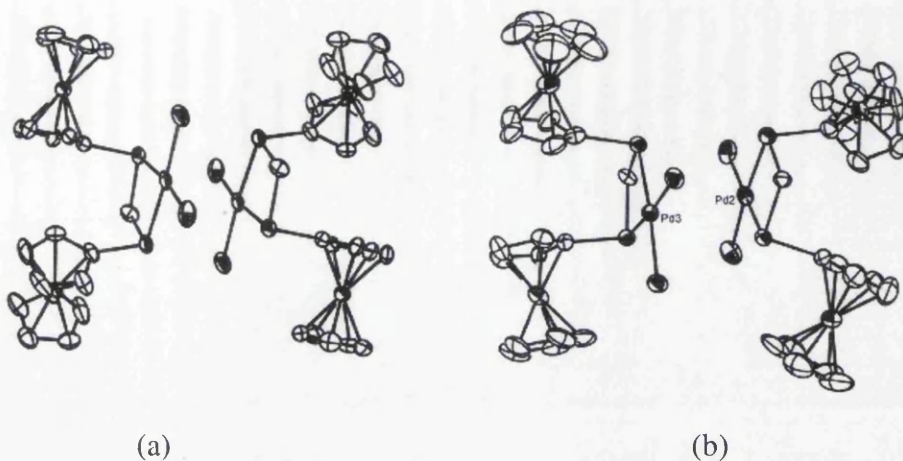


Fig. 3.23 (a) A pair of molecules 1 and 1'; (b) A pair of molecules 2 and 3

The geometry around platinum in the structure of $[\text{PtCl}_2(\text{FcTeCH}_2\text{TeFc})]$ (shown in Fig. 3.24) is distorted square planar: the angle of $\text{Te}(1)\text{-Pt}(1)\text{-Te}(2)$ is $82.31(2)^\circ$. The angle of $\text{Te}(2)\text{-C}(1)\text{-Te}(1)$ is $98.6(4)^\circ$ which is smaller than that in $[\text{PdCl}_2(\text{FcTeCH}_2\text{TeFc})]$ ($100.5(4)^\circ$). $\text{Te}(1)$, $\text{Te}(2)$ and $\text{Pt}(1)$ are almost coplanar with $\text{C}(1)$ out of the plane. The Pt-Te bond distances are $2.5203(7)$ and $2.5319(8)$ Å, which are quite a lot shorter than those in $[\text{Pt}\{\text{FcTe}(\text{CH}_2)_3\text{Te}\}_2](\text{PF}_6)_2$ ($2.5816(4)$ and $2.5842(4)$ Å) due to the smaller *trans* influence of the Cl^- anion compared to that of TeR_2 .

The Te-C ferrocenyl (sp^2) distances are $2.093(9)$ and $2.101(9)$ Å; the sp^3 C-Te bond distances, $2.197(9)$ and $2.188(9)$ Å, are longer.

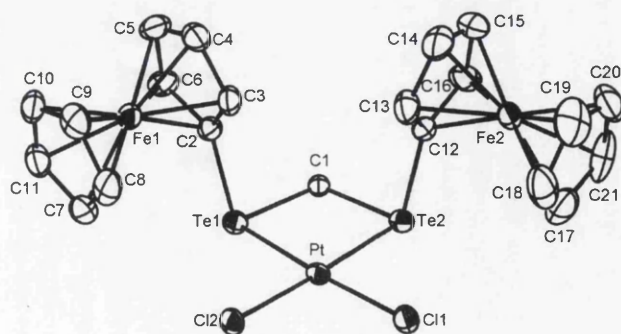


Fig. 3.24 Crystal structure of $[\text{PtCl}_2(\text{FcTeCH}_2\text{TeFc})]$ with atomic numbering scheme

The packing diagram of $[\text{PtCl}_2(\text{FcTeCH}_2\text{TeFc})]$ is shown in Fig. 3.25. In the structure there are molecules of the compound and solvate acetonitrile molecules in a 1:1 ratio. Eight of these complex/solvate molecule pairs are in the unit cell, one such pair forming the asymmetric unit.

A group of four complex and solvate molecules are related by the symmetry elements of the space group and the other four pairs in the unit cell are related to the former by the fractional lattice translation of the face centring operation. The acetonitrile molecule is disorderly distributed over two contiguous sites.

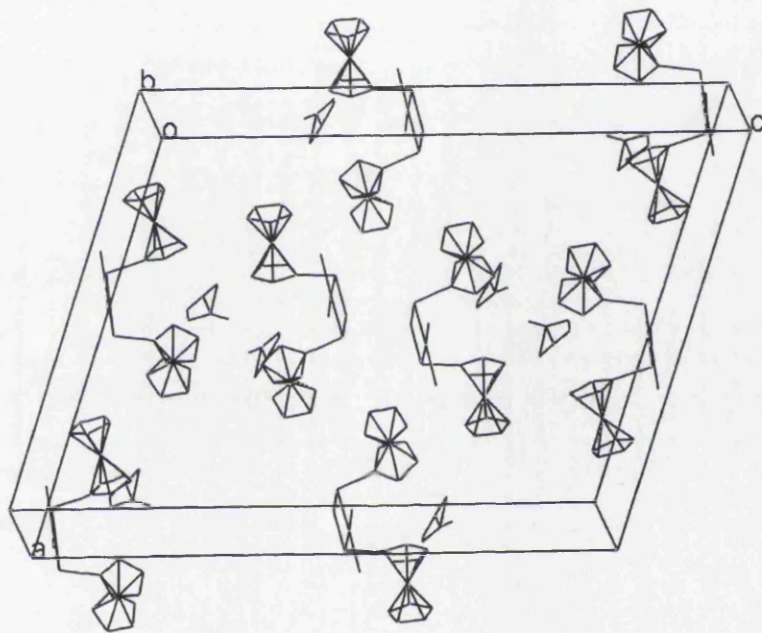
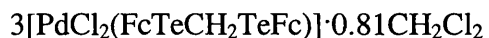


Fig. 3.25 Packing diagram for $[\text{PtCl}_2(\text{FcTeCH}_2\text{TeFc})]$

Table 3.18 Crystal data and structure refinement for



Empirical formula	$\text{C}_{63.81}\text{H}_{61.63}\text{Cl}_{7.63}\text{Fe}_6\text{Pd}_3\text{Te}_6$
Formula weight	2518.74
T (K)	293(2)
Wavelength (Å)	0.71069
Crystal system	triclinic
Space group	P-1
a (Å)	12.112(2)
b (Å)	16.481(2)
c (Å)	20.762(3)
α (°)	97.56(1)
β (°)	106.40(1)
γ (°)	103.66(1)
Volume (Å ³)	3775.0(9)
Z	2
D_c (Mg m ⁻³)	2.216
Absorption coefficient (mm ⁻¹)	4.393
$F(000)$	2360
Crystal size (mm)	0.40 × 0.30 × 0.10
θ range for data collection (°)	3.84 to 26.37
Index ranges	$-15 \leq h \leq 15, -20 \leq k \leq 20, -25 \leq l \leq 25$
Reflections collected	37257
Independent reflections [Rint]	14981 [0.0623]
Data / restraints / parameters	14981 / 244 / 805
Goodness-of-fit on F^2	1.010
Final R indices [$I > 2\sigma(I)$]	$R_1 = 0.0548, wR_2 = 0.1412$
R indices (all data)	$R_1 = 0.1102, wR_2 = 0.1482$
Largest diff. peak and hole (e Å ⁻³)	1.422, -1.173

* The number in bracket means the standard uncertainty, s.u..

Table 3.19 Crystal data and structure refinement for [PtCl₂(FcTeCH₂TeFc)]·MeCN

Empirical formula	C ₂₃ H ₂₃ Cl ₂ Fe ₂ NPtTe ₂
Formula weight	946.31
T (K)	293(2)
Wavelength (Å)	0.71069
Crystal system	monoclinic
Space group	C 2/c
<i>a</i> (Å)	22.913(1)
<i>b</i> (Å)	7.838(1)
<i>c</i> (Å)	30.034(2)
α (°)	90
β (°)	105.37(1)
γ (°)	90
Volume (Å ³)	5201.0(8)
<i>Z</i>	8
<i>D</i> _c (Mg m ⁻³)	2.417
Absorption coefficient (mm ⁻¹)	8.884
<i>F</i> (000)	3488
Crystal size (mm)	0.80 × 0.12 × 0.08
θ range for data collection (°)	3.97 to 26.37
Index ranges	-28 ≤ <i>h</i> ≤ 28, -9 ≤ <i>k</i> ≤ 9, -37 ≤ <i>l</i> ≤ 36
Reflections collected	23238
Independent reflections [Rint]	5251 [0.0252]
Data / restraints / parameters	5251 / 29 / 312
Goodness-of-fit on F ²	1.303
Final <i>R</i> indices [<i>I</i> > 2σ(<i>I</i>)]	<i>R</i> ₁ = 0.0441, <i>wR</i> ₂ = 0.0786
<i>R</i> indices (all data)	<i>R</i> ₁ = 0.0589, <i>wR</i> ₂ = 0.0810
Largest diff. peak and hole (e Å ⁻³)	1.902, -1.001

Table 3.20 Selected bond lengths (Å) and bond angles (°) for
 $3[\text{PdCl}_2(\text{FcTeCH}_2\text{TeFc})] \cdot 0.81\text{CH}_2\text{Cl}_2$

Bond lengths

Pd(1)-Cl(1)	2.366(3)	Pd(1)-Cl(2)	2.378(3)	Pd(2)-Cl(3)	2.361(3)
Pd(2)-Cl(4)	2.376(3)	Pd(3)-Cl(5)	2.394(3)	Pd(3)-Cl(6)	2.386(3)
Pd(1)-Te(1)	2.5207 (11)	Pd(1)-Te(2)	2.5439(13)	Pd(2)-Te(3)	2.5394(11)
Pd(2)-Te(4)	2.5325(12)	Pd(3)-Te(5)	2.5311(12)	Pd(3)-Te(6)	2.5360(11)
Te(1)-C(2)	2.098(11)	Te(1)-C(1)	2.176(11)	Te(2)-C(12)	2.097(10)
Te(2)-C(1)	2.160(11)	Te(3)-C(23)	2.091(13)	Te(3)-C(22)	2.172(9)
Te(4)-C(33)	2.082(12)	Te(4)-C(22)	2.189(9)	Te(5)-C(44)	2.082(11)
Te(5)-C(43)	2.169(10)	Te(6)-C(54)	2.132(12)	Te(6)-C(43)	2.163(10)
Fe(1)-C(2)	2.005(10)	Fe(2)-C(12)	2.042(10)	Fe(3)-C(23)	2.045(11)
Fe(4)-C(33)	2.053(11)	Fe(5)-C(44)	2.045(10)	Fe(6)-C(54)	2.016(11)

Bond angles

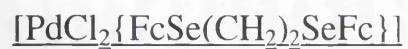
Cl(1)-Pd(1)-Cl(2)	95.36(14)	Cl(1)-Pd(1)-Te(1)	174.99(11)
Cl(2)-Pd(1)-Te(1)	89.18(9)	Cl(1)-Pd(1)-Te(2)	93.04(11)
Cl(2)-Pd(1)-Te(2)	171.12(9)	Cl(3)-Pd(2)-Cl(4)	92.78(13)
Cl(3)-Pd(2)-Te(4)	91.63(9)	Cl(4)-Pd(2)-Te(4)	174.43(10)
Cl(3)-Pd(2)-Te(3)	171.19(10)	Cl(4)-Pd(2)-Te(3)	95.19(9)
Cl(6)-Pd(3)-Cl(5)	96.45(11)	Cl(6)-Pd(3)-Te(5)	91.15(8)
Cl(5)-Pd(3)-Te(5)	172.38(8)	Cl(6)-Pd(3)-Te(6)	172.82(8)
Cl(5)-Pd(3)-Te(6)	90.55(8)	Te(2)-C(1)-Te(1)	100.5(4)
Te(1)-Pd(1)-Te(2)	82.32(4)	C(1)-Te(1)-Pd(1)	88.6(3)
C(1)-Te(2)-Pd(1)	88.3(3)	Te(3)-C(22)-Te(4)	97.6(4)
Te(4)-Pd(2)-Te(3)	80.65(3)	C(22)-Te(3)-Pd(2)	90.9(2)
C(22)-Te(4)-Pd(2)	90.7(2)	Te(3)-C(22)-Te(4)	97.6(4)
Te(6)-C(43)-Te(5)	100.1(4)	Te(5)-Pd(3)-Te(6)	81.88(3)
C(43)-Te(5)-Pd(3)	88.5(3)	C(43)-Te(6)-Pd(3)	88.5(3)

* The number in bracket means the standard uncertainty, s.u..

Table 3.21 Selected bond lengths (Å) and bond angles (°) for
 $[\text{PtCl}_2(\text{FcTeCH}_2\text{TeFc})] \cdot \text{MeCN}$

<i>Bond lengths</i>					
Pt-Cl(2)	2.357(2)	Pt-Cl(1)	2.357(2)	Pt-Te(2)	2.5203(7)
Pt-Te(1)	2.5319(8)	Te(1)-C(2)	2.101(9)	Te(1)-C(1)	2.197(9)
Te(2)-C(12)	2.093(9)	Te(2)-C(1)	2.188(9)	Fe(1)-C(2)	2.020(9)
Fe(2)-C(12)	2.023(10)				
<i>Bond angles</i>					
Cl(2)-Pt-Cl(1)	91.90(8)	Cl(2)-Pt-Te(2)		175.88(6)	
Cl(1)-Pt-Te(2)	92.20(6)	Cl(2)-Pt-Te(1)		93.59(6)	
Cl(1)-Pt-Te(1)	174.48(6)	Te(2)-Pt-Te(1)		82.31(2)	
C(2)-Te(1)-C(1)	97.3(3)	C(2)-Te(1)-Pt		102.9(3)	
C(1)-Te(1)-Pt	89.3(2)	C(12)-Te(2)-C(1)		98.4(3)	
C(12)-Te(2)-Pt	101.4(3)	C(1)-Te(2)-Pt		89.8(2)	
Te(2)-C(1)-Te(1)	98.6(4)	C(3)-C(2)-Te(1)		129.2(7)	
C(6)-C(2)-Te(1)	123.0(7)	Fe(1)-C(2)-Te(1)		122.8(5)	

* The number in bracket means the standard uncertainty, s.u..



With a 1:1 stoichiometry of $\text{FcSe}(\text{CH}_2)_2\text{SeFc}$ and $[\text{PdCl}_2(\text{PhCN})_2]$, dark blue plate crystals were obtained. The crystal quality was not good enough, but a partly solved structure shows that the ligand acts as a bidentate ligand to form a five-membered ring. The molecular structure is illustrated in Fig. 3.26.

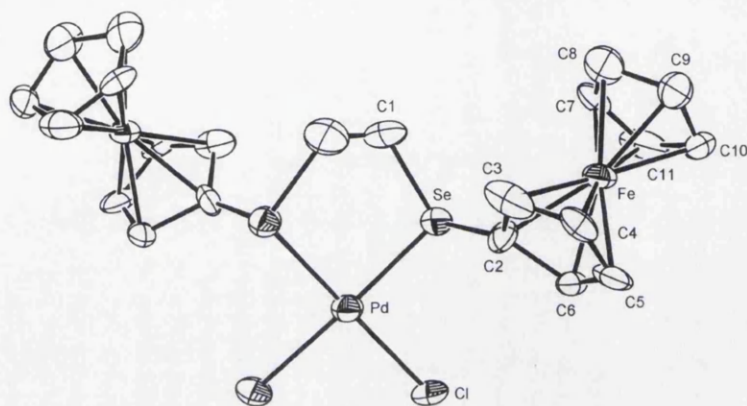


Fig. 3.26 Plot of a molecule of $[\text{PdCl}_2\{\text{FcSe}(\text{CH}_2)_2\text{SeFc}\}]$

3.2.3 Pd and Pt complexes of $\text{FcE}(\text{CH}_2)_3\text{E}'(\text{CH}_2)_3\text{EFc}$ (E, E' = Se or Te)

3.2.3.1 Synthesis

The reaction of a linear tridentate ligand with $[\text{MCl}_2(\text{NCMe})_2]$ (M = Pd or Pt) and TIPF_6 in a 1:1:1 ratio can afford planar $[\text{MCIL}]^+$.^{46, 47} A similar method was adopted for the synthesis of Pd and Pt complexes of $\text{FcE}(\text{CH}_2)_3\text{E}'(\text{CH}_2)_3\text{EFc}$ (E, E' = Se, Te). An example procedure is listed below; the experimental details will be given in Chapter Seven.

PtCl_2 was refluxed in MeCN for 2 h to give a yellow solution of $[\text{PtCl}_2(\text{NCMe})_2]$. One equivalent of TIPF_6 was added and the mixture stirred for another 15 min. One equivalent of the ligand $\text{FcSe}(\text{CH}_2)_3\text{Se}(\text{CH}_2)_3\text{SeFc}$ in CH_2Cl_2 was then added dropwise; the mixture was stirred at room temperature for 20 h to give a peach red liquid and a fine white precipitate of TlCl . The solution was centrifuged to remove TlCl and reduced to 2 ml *in vacuo*; diethyl ether (10 ml) was added to precipitate an orange red powder.

The eight complexes obtained are described below with relevant information. All complexes show multiplet peaks with the correct isotope structure in the mass spectra consistent with $[\text{MCIL}]^+$. Compared to the complexes of the bidentate ligands, their molecular weights are smaller and allow NMR spectroscopic study.

The NMR spectra obtained from these complexes are very complex: at 300K they show doubling of some or all of the expected resonances, and generally broad signals for the CH_2 groups, consistent with the presence of both *meso* and *DL* invertomers. Compared to free ligand, there is a high frequency coordination shift of the chalcogen resonance, but solvent effect may partly be responsible for this.

The ^{77}Se NMR resonances of $[\text{PdCl}\{\text{FcSe}(\text{CH}_2)_3\text{Se}(\text{CH}_2)_3\text{SeFc}\}]\text{PF}_6$ ($\delta = 202, 227$ ppm) and $[\text{PtCl}\{\text{FcSe}(\text{CH}_2)_3\text{Se}(\text{CH}_2)_3\text{SeFc}\}]\text{PF}_6$ ($\delta = 200, 220$ ppm) in CD_3COCD_3 shift about 50 ppm to low field compared to the free ligand $\text{FcSe}(\text{CH}_2)_3\text{Se}(\text{CH}_2)_3\text{SeFc}$ in CDCl_3 ($\delta = 154, 190$ ppm). The chemical shift of the terminal selenium is larger than that of the middle one, but the difference between them ($\Delta\delta$) becomes smaller on coordination: 20 ppm, compared to 36 ppm in the free ligand. The coupling constant between platinum and the terminal seleniums was 388 Hz in $[\text{PtCl}\{\text{FcSe}(\text{CH}_2)_3\text{Se}(\text{CH}_2)_3\text{SeFc}\}]\text{PF}_6$. The observation of only one pair of peaks means that the *meso* invertomer is the only or main form in solution, which is

in accordance with the crystal structure: *meso*-[PtCl{FcSe(CH₂)₃Se(CH₂)₃SeFc}]PF₆. The ⁷⁷Se NMR spectrum of [PtCl{FcSe(CH₂)₃Te(CH₂)₃SeFc}]PF₆ (δ = 217 ppm) is consistent with that of [PtCl{FcSe(CH₂)₃Se(CH₂)₃SeFc}]PF₆ (δ = 200, 220 ppm), the coupling constant between platinum and the terminal seleniums being 399 Hz. Similarly, δ = 195 ppm was observed for [PdCl{FcSe(CH₂)₃Te(CH₂)₃SeFc}]PF₆. Two peaks were observed for the complexes [Pd(FcTe(CH₂)₃Se(CH₂)₃TeFc)Cl]PF₆ (δ = 226, 232 ppm) and [PtCl{FcTe(CH₂)₃Se(CH₂)₃TeFc}]PF₆ (δ = 204.0, 204.4 ppm), implying the presence of both *DL* and *meso* invertomers and that the inversion energies are higher than in [MCl{FcSe(CH₂)₃Se(CH₂)₃SeFc}]PF₆ (M = Pd or Pt) at room temperature. The chemical shift difference between these two invertomers is larger in the Pd complex. The coupling constant between platinum and the middle selenium was 187 Hz in [PtCl{FcTe(CH₂)₃Se(CH₂)₃TeFc}]PF₆, nearly half the typical value of ¹J_{Pt-Se} for terminal seleniums, which reflects the lack of a ferrocenyl group attached to the Se atom.

In the case of [PtCl{FcTe(CH₂)₃Se(CH₂)₃TeFc}]PF₆, the ¹²⁵Te NMR spectrum at 300K also showed two sharp resonances at 357.0 ppm (¹J_{Pt-Te} = 480 Hz), 356.7 ppm due to the two kinds of invertomers. In the ¹²⁵Te NMR spectrum of [PtCl{FcTe(CH₂)₃Te(CH₂)₃TeFc}]PF₆ three peaks were observed: 355 ppm (¹J_{Pt-Te} = 515 Hz), 354 ppm, 369 ppm. The resonance at 355 ppm can be assigned to the terminal-Te-Fc of the *meso* form by comparison with the data for [PtCl{FcTe(CH₂)₃Se(CH₂)₃TeFc}]PF₆; the resonance at 354 ppm is then attributed to the terminal-Te of the *DL* form. The third resonance, at 369 ppm, is due to the middle Te of the *meso* form; Δδ between the terminal and middle telluriums is 14 ppm, much smaller compared to 76 ppm in the free ligand FcTe(CH₂)₃Te(CH₂)₃TeFc. Only a broad peak was observed in the ¹²⁵Te NMR spectrum of [PdCl{FcSe(CH₂)₃Te(CH₂)₃SeFc}]PF₆, at around 385 ppm; no peaks were resolved for [PdCl{FcTe(CH₂)₃Se(CH₂)₃TeFc}]PF₆ and [PdCl{FcTe(CH₂)₃Te(CH₂)₃TeFc}]PF₆, suggesting these complexes are fluxional on the timescale of the ¹²⁵Te NMR spectrum.

Spectroscopic data for each of the new compounds described in this section are provided in Chapter Seven.

3.2.3.2 Structure of [PtCl{FcSe(CH₂)₃Se(CH₂)₃SeFc}](PF₆)

Crystals suitable for single-crystal X-ray analyses of each of the complexes were obtained by slow diffusion of Et₂O into a solution in acetone. [PtCl{FcSe(CH₂)₃Se(CH₂)₃SeFc}](PF₆) crystallized as orange plates in the monoclinic space group P21/c. Pertinent bond parameters are collected in Table 3.22 while crystal data and refinement details are provided in Table 3.23. The molecular structure of the cation [PtCl{FcSe(CH₂)₃Se(CH₂)₃SeFc}]⁺ is illustrated in Fig. 3.27. The packing diagram is shown in Fig. 3.28. H···H interactions between the adjacent ferrocenyl rings in the free ligand do not exist in the complex. Instead, there are weak Cl···H (2.726 Å) and H···F (2.523 Å) intermolecular interactions.

The molecular structure shows that it contains one cation with the *meso* form of the ligand and one PF₆⁻ anion. The Cl-Pt-Se(2) angle is 172.96°, and the Se(1)-Pt-Se(3) angle is 167.77°, which means the Pt(II) coordination is not strictly planar. The Se(1)-Pt-Se(2) (94.17(3)°) and Se(2)-Pt-Se(3) (97.40(3)°) angles deviate from 90°, not showing such a good match of the six-membered chelate rings to the square planar geometry as in the diselenoether complexes. The two six-membered chelate rings exist in a puckered conformation with the alkyl carbon atoms lying on the same side of the metal coordination plane, and the two ferrocenyl groups on the opposite side.

The two cyclopentadienyl rings attached to the same iron are basically coplanar. The eclipse angle is different for the two ferrocenyl moieties, being much larger for Fe(2). The average of the Fe(1)-C(Cp) distances is 2.04 Å and that of the Fe(2)-C(Cp) distances is 2.03 Å.

The ferrocene sp²-C-Se bond distances (Se(1)-C(7), 1.901(8)Å; Se(3)-C(17) 1.903(9)) are a little longer than that in the free ligand (Se(2)-C(4), 1.899(4) Å), as are the sp³-C-Se bond distances (1.960(9) and 1.965(10) Å in the complex; 1.956(4) Å in the free ligand). The Pt-Cl_{transSe} bond length is 2.316(2) Å, shorter than those in [PtCl{MeS(CH₂)₃Te(CH₂)₃SMe}]PF₆ (Pt-Cl_{transTe} = 2.354 Å)⁴⁸ and *cis*-[PtCl₂(EtOC₆H₄TeCH₂CH₂SMe)] (Pt-Cl_{transTe} = 2.336(3) and 2.541(1) Å)⁴⁹; this can be attributed to the weaker donor property of Se compared to Te.

By contrast, the Pt-Se(2) (2.3699(9) Å) bond is obviously shorter than the other two Pt-Se bonds, 2.4126(9) and 2.4158(9) Å), and is also out of the range of normal Pt-Se bond lengths, for example: 2.4275(5) and 2.4386(7) Å in

$[\text{Pt}\{\text{FcSe}(\text{CH}_2)_3\text{SeFc}\}_2](\text{PF}_6)_2 \cdot 2\text{MeCN}$; 2.414(2), 2.421(2) Å in
 $[\text{Pt}\{\text{MeSe}(\text{CH}_2)_3\text{SeMe}\}_2](\text{PF}_6)_2 \cdot 2\text{MeCN}$; 2.420(3), 2.417(3) Å in $[\text{Pt}(\{16\}\text{aneSe}_4)]$
 $(\text{PF}_6)_2 \cdot 2\text{MeCN}$. This is good evidence that the *trans* influence of the Cl^- anion is
smaller than that of SeR_2 .

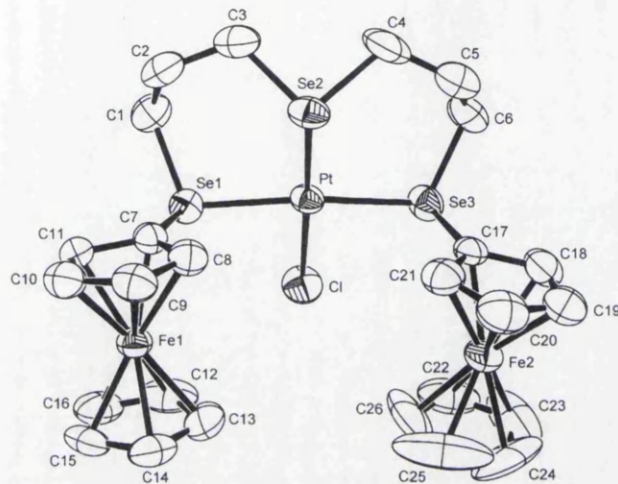


Fig. 3.27 A view of cation $[\text{PtCl}\{\text{FcSe}(\text{CH}_2)_3\text{Se}(\text{CH}_2)_3\text{SeFc}\}]^+$

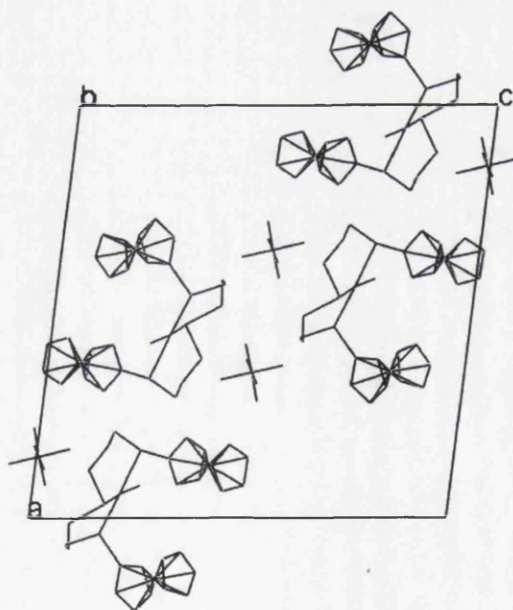


Fig. 3.28 Packing diagram of $[\text{PtCl}\{\text{FcSe}(\text{CH}_2)_3\text{Se}(\text{CH}_2)_3\text{SeFc}\}]\text{PF}_6$

Table 3.19 Crystal data and structure refinement for



Empirical formula	$\text{C}_{26}\text{H}_{30}\text{ClFe}_2\text{PtSe}_3\text{PF}_6$
Formula weight	1066.59
T (K)	293(2)
Wavelength (Å)	0.71069
Crystal system	monoclinic
Space group	P21/c
a (Å)	20.049(2)
b (Å)	7.631(1)
c (Å)	20.181(2)
α (°)	90
β (°)	97.54(1)
γ (°)	90
Volume (Å ³)	3060.9(6)
Z	4
D_c (Mg m ⁻³)	2.315
Absorption coefficient (mm ⁻¹)	9.255
$F(000)$	2016
Crystal size (mm)	0.04 × 0.34 × 0.48
θ range for data collection (°)	4.06 to 26.37
Index ranges	$-24 \leq h \leq 25, -9 \leq k \leq 9, -25 \leq l \leq 25$
Reflections collected	42961
Independent reflections [Rint]	6203 [0.0464]
Data / restraints / parameters	6203 / 18 / 362
Goodness-of-fit on F^2	1.124
Final R indices [$I > 2\sigma(I)$]	$R_1 = 0.0480, wR_2 = 0.1045$
R indices (all data)	$R_1 = 0.0603, wR_2 = 0.1142$
Largest diff. peak and hole (e Å ⁻³)	1.606, -1.467

* The number in bracket means the standard uncertainty, s.u..

Table 3.20 Selected bond lengths (Å) and bond angles (°) for
 $[\text{PtCl}\{\text{FcSe}(\text{CH}_2)_3\text{Se}(\text{CH}_2)_3\text{SeFc}\}]\text{PF}_6$

<i>Bond lengths</i>					
Pt-Cl	2.316(2)	Pt-Se(2)	2.3699(9)	Pt-Se(1)	2.4126(9)
Pt-Se(3)	2.4158(9)	Se(1)-C(7)	1.901(8)	Se(1)-C(1)	1.960(9)
Se(2)-C(3)	1.959(10)	Se(2)-C(4)	1.971(9)	Se(3)-C(17)	1.903(9)
Se(3)-C(6)	1.965(10)	Fe(1)-C(7)	2.011(8)	Fe(2)-C(17)	2.019(8)
C(1)-C(2)	1.49(1)	C(2)-C(3)	1.52(1)	C(4)-C(5)	1.49(2)
C(5)-C(6)	1.50(2)				
<i>Bond angles</i>					
Cl-Pt-Se(2)	172.96(7)	Cl-Pt-Se(1)	83.90(7)		
Se(2)-Pt-Se(1)	94.17(3)	Cl-Pt-Se(3)	85.08(7)		
Se(2)-Pt-Se(3)	97.40(3)	Se(1)-Pt-Se(3)	167.77(3)		
C(1)-Se(1)-Pt	106.7(3)	C(3)-Se(2)-Pt	108.1(3)		
C(4)-Se(2)-Pt	110.1(4)	Se(1)-C(7)-Fe(1)	123.6(4)		
<i>Torsion angles</i>					
Cl-Pt-Se(1)-C(7)	112.6(3)	Se(2)-Pt-Se(1)-C(7)	-60.6(2)		
Se(3)-Pt-Se(1)-C7	138.4(3)	Cl-Pt-Se(1)-C(1)	-142.8(3)		
Se(2)-Pt-Se(1)-C(1)	44.0(3)	Se(3)-Pt-Se(1)-C(1)	-116.9(3)		
Cl-Pt-Se(2)-C(3)	-117.7(6)	Se(1)-Pt-Se(2)-C(3)	-44.0(3)		
Se(3)-Pt-Se(2)-C(3)	132.0(3)	Cl-Pt-Se(2)-C(4)	141.9(7)		
Se(1)-Pt-Se(2)-C(4)	-144.4(4)	Se(3)-Pt-Se(2)-C(4)	31.6(4)		
Cl-Pt-Se(3)-C(17)	-100.9(3)	Se(2)-Pt-Se(3)-C(17)	72.5(2)		
Se(1)-Pt-Se(3)-C(17)	-126.6(3)	Cl-Pt-Se(3)-C(6)	156.6(4)		
Se(2)-Pt-Se(3)-C(6)	-30.0(4)	Se(1)-Pt-Se(3)-C(6)	130.8(4)		
C(7)-Se(1)-C(1)-C(2)	48.2(8)	Pt-Se(1)-C(1)-C(2)	-62.6(8)		

* The number in bracket means the standard uncertainty, s.u..

3.2.4 Pd and Pt Complexes of

FcE(CH₂)₃Se(CH₂)₃Se(CH₂)₃EFc (E = Se or Te)

The reaction of a linear tetradentate ligand with [MCl₂(NCMe)₂] (M = Pd or Pt) and TlPF₆ in a 1:1:2 ratio can afford planar [ML]²⁺. An example procedure is listed below; the experimental details will be given in Chapter Seven.

PtCl₂ was refluxed in MeCN for 2 h to give a yellow solution of [PtCl₂(NCMe)₂]. Two equivalents of TlPF₆ were added and the mixture stirred for another 15 min. One equivalent of the ligand FcSe(CH₂)₃Se(CH₂)₃Se(CH₂)₃SeFc in CH₂Cl₂ was then added dropwise; the mixture was stirred at room temperature for 48 h to give a peach red liquid and a fine white precipitate of TlCl. The solution was centrifuged to remove TlCl and reduced to 2 ml *in vacuo*; diethyl ether (10 ml) was added to precipitate an orange red powder.

The four complexes show multiplet peaks with the correct isotope structure in the mass spectra consistent with [M-PF₆]⁺. The NMR spectra only show weak and broad features because of their large molecular weight and pyramidal inversion at room temperature. Effort to grow single crystals failed, suggesting that there are many invertomers in the solution.

3.3 Group 6 carbonyl complexes of $\text{FcE}(\text{CH}_2)_3\text{E}'\text{Fc}$ (E, E' = Se, Te)

3.3.1 Synthesis and NMR spectra

The syntheses of the group 6 carbonyl complexes of the bidentate ligands $\text{FcE}(\text{CH}_2)_3\text{E}'\text{Fc}$ (E & E' = Se or Te) were straightforward, using reactions of the ligand with $[\text{M}(\text{CO})_4(\text{nbd})]$ (M = Cr or Mo) or $[\text{W}(\text{CO})_4(\text{TMPDA})]$ in toluene. An example of the synthetic route is shown below, and experimental details will be given in Chapter Seven.

$[\text{Mo}(\text{CO})_4(\text{nbd})]$ was dissolved in degassed toluene and one equivalent of the ligand $\text{FcSe}(\text{CH}_2)_3\text{SeFc}$ in toluene was added via a syringe. The reaction mixture was stirred at room temperature overnight and then the toluene removed *in vacuo*. The residue was dissolved in CH_2Cl_2 (5 ml), filtered and cold hexane added to yield a brown powder. The powder was collected, washed with hexane and dried under vacuum.

The attempts to synthesize $[\text{Cr}(\text{CO})_4\{\text{FcSe}(\text{CH}_2)_3\text{SeFc}\}]$, $[\text{Cr}(\text{CO})_4\{\text{FcSe}(\text{CH}_2)_3\text{TeFc}\}]$, $[\text{W}(\text{CO})_4\{\text{FcSe}(\text{CH}_2)_3\text{SeFc}\}]$ and $[\text{W}(\text{CO})_4\{\text{FcSe}(\text{CH}_2)_3\text{TeFc}\}]$ failed, IR spectra showed only the presence of starting materials.

The complexes obtained are air-stable in the solid state. They are poorly soluble in hydrocarbons, but well soluble in chlorocarbon solvents with slow decomposition. The FAB mass spectra showed a parent ion, and occasionally the fragments corresponding to sequential carbonyl loss could be observed.

The NMR spectra were recorded in freshly prepared CD_2Cl_2 solution. With the slow decomposition, there will appear resonances attributed to the free ligands.

There are two possible intramolecular processes in these complexes: pyramidal inversion of the coordinated chalcogen atoms, and ring reversal. If either or both processes are slow on the NMR timescale, four configurational isomers can exist: *meso*-1, *meso*-2 and a degenerate *DL* pair (Fig. 3.29). Normally the bridge reversal process is rapid due to the low torsional barriers associated with M-E bonds. Also the *meso*-2 structure is not favoured due to the high steric crowding. Two sets of signals will therefore be observed: an intense set for the degenerate *DL* pair and a weaker set for *meso*-1.¹

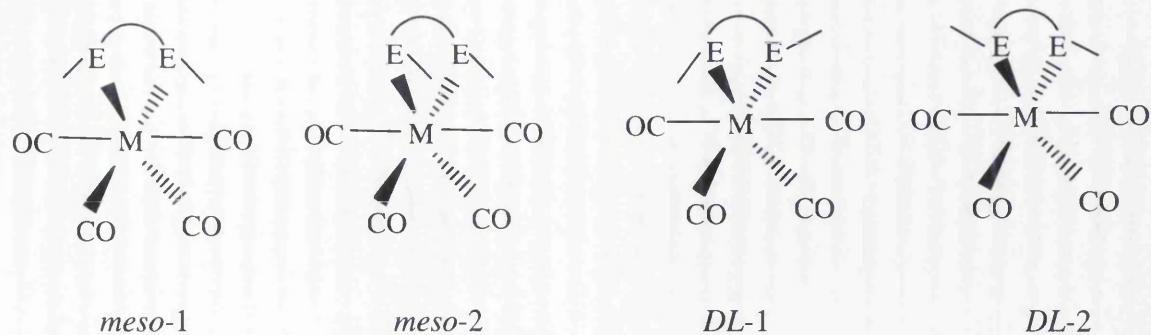


Fig. 3.29 *Meso* and *DL* invertomers of $[M(CO)_4(L-L)]$

Previous studies have proved that for dichalcogenoether complexes, the energy barriers to inversion have the sequence: $Te > Se > S$ and $W > Cr > Mo$.^{50,51} The 1H spectra of $[Mo(CO)_4\{FcTe(CH_2)_3TeFc\}]$ and $[Mo(CO)_4\{FcSe(CH_2)_3SeFc\}]$ show resonances for both invertomers consistent with relatively high inversion barriers. The spectrum of $[Mo(CO)_4\{FcSe(CH_2)_3TeFc\}]$ is very complicated due to the mixed Se/Te ligand. Four isomers exist as shown in Fig. 3.30.

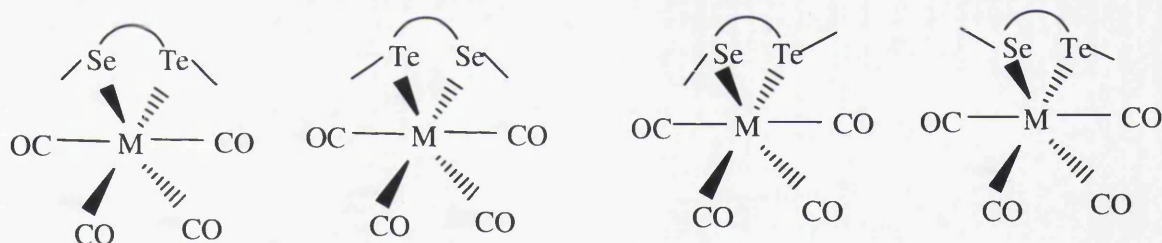


Fig. 3.30 *Meso* and *DL* invertomers of $[Mo(CO)_4\{FcSe(CH_2)_3TeFc\}]$

In the ^{13}C NMR spectra, when inversion is rapid on the ^{13}C NMR timescale, there will appear to be only two CO environments: CO groups *trans* to a CO group and CO groups *trans* to a ligand. Slow inversion will afford five resonances: two for CO groups *trans* to a ligand in the *meso* and *DL* invertomers, one for CO groups *trans* to a CO in the *DL* form, and another two for CO groups *trans* to a CO in the *meso* form. Sometimes only four resonances can be observed due to the coincidence of the chemical shifts of CO groups *trans* to a ligand in the two invertomers.⁵¹ The ^{13}C -NMR spectra of $[Mo(CO)_4\{FcSe(CH_2)_3SeFc\}]$, $[Mo(CO)_4\{FcTe(CH_2)_3TeFc\}]$ and $[W(CO)_4\{FcTe(CH_2)_3TeFc\}]$ only exhibit two CO resonances which means the pyramidal inversion is faster than in $[M(CO)_4\{RTe(CH_2)_3TeR\}]$ ($M = Cr, Mo, W; R$

= Me, Ph).⁵¹ The ¹³C-NMR spectrum of [Mo(CO)₄{FcSe(CH₂)₃TeFc}] shows four CO resonances which is in accordance with ¹H spectrum. That of [Cr(CO)₄{FcTe(CH₂)₃TeFc}] appears to show only one CO resonance, but the signal-to-noise ratio of the spectrum was poor.

The ¹²⁵Te chemical shifts of complexes generally decrease in the sequence Cr > Mo > W for the same ligand.⁴⁹ The ¹²⁵Te chemical shift of the free ligand FcTe(CH₂)₃TeFc is 299 ppm in CD₂Cl₂, similar as that in CDCl₃. After complexation, δ(¹²⁵Te) are 429 ppm for [Cr(CO)₄{FcTe(CH₂)₃TeFc}], 344 ppm for [Mo(CO)₄{FcTe(CH₂)₃TeFc}] and 272, 269 ppm for [W(CO)₄{FcTe(CH₂)₃TeFc}], in good agreement with the results for [M(CO)₄{RTe(CH₂)₃TeR}] (M = Cr, Mo, W; R = Me, Ph).⁵¹ It was possible to measure a W-Te coupling constant for the first time in *DL*- [W(CO)₄{FcTe(CH₂)₃TeFc}] (74 Hz) due to the high intensity of the signal, but the *meso* signal was too weak to reveal its satellites; the same phenomenon has been observed for [W(CO)₄{(CH₃SeC₅H₄)₂Fe}].¹ The two ¹²⁵Te resonances of [W(CO)₄{TcSe(CH₂)₃TeFc}] also prove that the tungsten complex has a larger inversion energy barrier.

The ⁷⁷Se chemical shifts of [Mo(CO)₄{FcSe(CH₂)₃SeFc}] and [Mo(CO)₄{FcSe(CH₂)₃TeFc}] are similar at around 175 ppm, a shift of only 10 ppm to high field compared to the free ligands.

NMR spectroscopic data for each of the new compounds described in this section are provided in Chapter Seven.

3.3.2 Structures of $[M(CO)_4\{FcE(CH_2)_3E'Fc\}]$ ($M = Cr, E = E' = Te; M = Mo, E, E' = Se \text{ or } Te; M = W, E = E' = Te$)

Crystals were grown as orange plates by slow evaporation from CH_2Cl_2 /hexanes. Five structures were solved: $[Cr(CO)_4\{FcTe(CH_2)_3TeFc\}]$, $[Mo(CO)_4\{FcSe(CH_2)_3SeFc\}]$, $[Mo(CO)_4\{FcSe(CH_2)_3TeFc\}]$, $[Mo(CO)_4\{FcTe(CH_2)_3TeFc\}]$ and $[W(CO)_4\{FcTe(CH_2)_3TeFc\}]$. They all crystallize in the monoclinic crystal system and the space group $P21/c$, with one molecule in the asymmetric unit (no solvent). Crystal data and refinement details and pertinent bond parameters are collected in: Tables 3.24 and 3.25 for $[Cr(CO)_4\{FcTe(CH_2)_3TeFc\}]$, Tables 3.26 and 3.27 for $[Mo(CO)_4\{FcSe(CH_2)_3SeFc\}]$, Tables 3.28 and 3.29 for $[Mo(CO)_4\{FcSe(CH_2)_3TeFc\}]$, Tables 3.30 and 3.31 for $[Mo(CO)_4\{FcTe(CH_2)_3TeFc\}]$, Tables 3.32 and 3.33 for $[W(CO)_4\{FcTe(CH_2)_3TeFc\}]$.

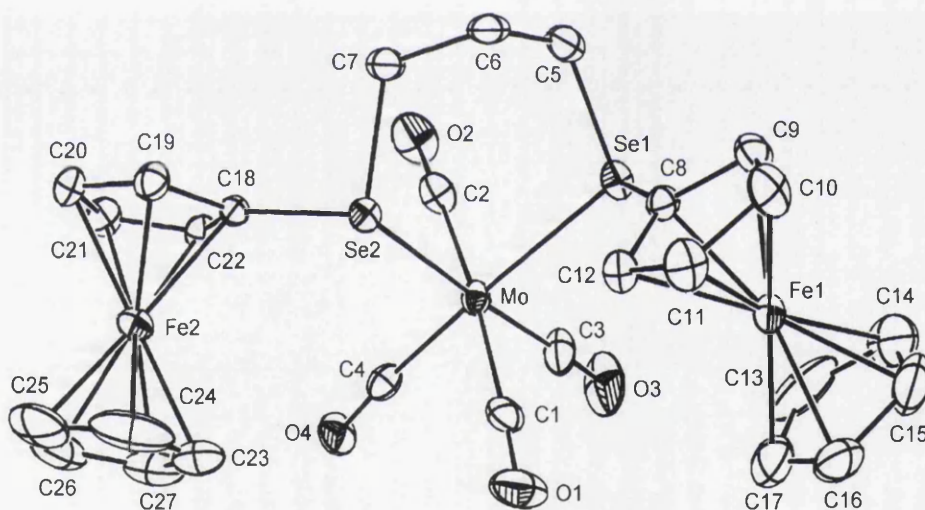


Fig. 3.31 Structure of $[Mo(CO)_4\{FcSe(CH_2)_3SeFc\}]$ with atom numbering scheme

As an example, the molecular structure of $[Mo(CO)_4\{FcSe(CH_2)_3SeFc\}]$ is shown in Fig. 3.31. The structure reveals the expected *cis* substituted octahedron about Mo, with an angle of Se-Mo-Se $86.51(2)^\circ$. The range of the iron to carbon distances in the cyclopentadienyl rings (2.0023 to 2.0452 Å) is within that expected for ferrocenyl compounds.

The ferrocenyl (sp^2) C-Se bond distances are 1.9001(37) and 1.8928(38) Å, shorter than those in $[Pd\{FcSe(CH_2)_3SeFc\}_2](PF_6)_2$ (1.9090(42) and 1.9012(37) Å) and

[Pt{FcSe(CH₂)₃SeFc}₂](PF₆)₂ (1.9101(56) and 1.8944(52) Å), but still longer than in the free ligand FcSe(CH₂)₃SeFc (1.872(6) and 1.878(6) Å). The results are in accordance with the weaker electron-withdrawing strength of the Mo(0) centre compared to that of Pd(II) or Pt(II). The sp³ C-Se bond distances (1.9555(41) and 1.9733(37) Å) are also shorter than in the free ligand FcSe(CH₂)₃SeFc (1.995(6) Å and 1.979(6) Å), which was not observed in the structures of [Pd{FcSe(CH₂)₃SeFc}₂](PF₆)₂ and [Pt{FcSe(CH₂)₃SeFc}₂](PF₆)₂.

The ligand adopts the *DL* conformation with Mo-Se 2.6649(7) Å, 2.6751(7) Å, Mo-C_{cisSe} 1.9988(48), 2.0332(49) Å and Mo-C_{transSe} 1.9411(49), 1.9569(49) Å, so the equatorial M-C bonds *trans* to the Mo-E bonds are significantly shorter than the two axial Mo-C bonds, reflecting the fact that the two Mo-E bonds result in more electron density being available for back-bonding to the two equatorial carbonyls. The same phenomenon has been observed in other three complexes' structures; these will be discussed later in more detail.

The ferrocenyl (sp²) C-Te bond distances in [M(CO)₄{FcTe(CH₂)₃TeFc}] (M = Cr, Mo, W) are quite similar: 2.101(8) and 2.088(4) Å in [Cr(CO)₄{FcTe(CH₂)₃TeFc}], 2.101(4) and 2.089(4) Å in [Mo(CO)₄{FcTe(CH₂)₃TeFc}], 2.098(5) and 2.096(5) Å in [W(CO)₄{FcTe(CH₂)₃TeFc}].

The structure of [Mo(CO)₄{FcSe(CH₂)₃TeFc}] also shows one molecule in the asymmetric unit (no solvent). The refinement was quite sensitive to the assignment of the Se/Te positions. Actually, the ligand is disorderly oriented, with a slight preference of Te for one site ("Te1") and, obviously, of Se for the other coordination site.

The packing diagram of [Mo(CO)₄{FcSe(CH₂)₃SeFc}] is shown in Fig. 3.32. The compound is essentially monomeric, but it is linked to other neighbouring molecules by weak H···H (2.391 Å), C···H (2.774, 2.868, 2.715 Å) and O···H (2.715 Å) intermolecular interactions. There are also short intermolecular contacts in the other structures studied, although the interactions are different in each complex: H···H (2.715 Å) and C···H (2.786 Å) in [Mo(CO)₄{FcTe(CH₂)₃TeFc}]; H···H (2.360 Å), C···H (2.774 Å) and O···H (2.709 Å) in [Mo(CO)₄{FcSe(CH₂)₃TeFc}]; H···H (2.395 Å), C···H (2.753 Å) and O···H (2.692 Å) in [Cr(CO)₄{FcTe(CH₂)₃TeFc}]; H···H (2.361 Å), C···H (2.746 Å) and O···H (2.695 Å) in [W(CO)₄{FcTe(CH₂)₃TeFc}].

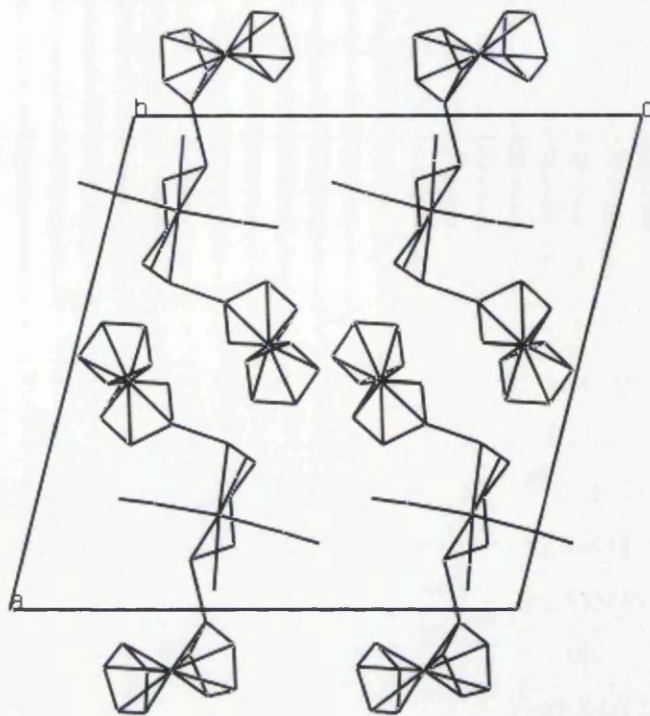


Fig. 3.32 Packing diagram of $[\text{Mo}(\text{CO})_4\{\text{FcSe}(\text{CH}_2)_3\text{SeFc}\}]$

Table 3.24 Crystallographic data collection and refinement parameters of



Empirical formula	$\text{C}_{27}\text{H}_{24}\text{Fe}_2\text{CrO}_4\text{Te}_2$
Formula weight	831.36
T (K)	293(2)
Wavelength (Å)	0.71069
Crystal system	monoclinic
Space group	P21/c
a (Å)	15.186(3)
b (Å)	12.369(1)
c (Å)	15.535(1)
α (°)	90
β (°)	103.55(1)
γ (°)	90
Volume (Å ³)	2800.3(3)
Z	4
D_c (Mg m ⁻³)	1.972
Absorption coefficient (mm ⁻¹)	3.476
$F(000)$	1592
Crystal size (mm)	0.40 × 0.40 × 0.25
θ range for data collection (°)	4.30 to 26.37
Index ranges	$-18 \leq h \leq 18, -15 \leq k \leq 15, -19 \leq l \leq 19$
Reflections collected	27434
Independent reflections [Rint]	5680 [0.0356]
Data / restraints / parameters	5680/0/325
Goodness-of-fit on F^2	1.015
Final R indices [$I > 2\sigma(I)$]	$R_1 = 0.0335, wR_2 = 0.0776$
R indices (all data)	$R_1 = 0.0436, wR_2 = 0.0813$
Largest diff. peak and hole (e Å ⁻³)	1.341, -0.73

* The number in bracket means the standard uncertainty, s.u..

Table 3.25 Selected bond lengths (Å) and angles (°) for [Cr(CO)₄{FcTe(CH₂)₃TeFc}]

<i>Bond lengths</i>					
Te(1)-Cr(1)	2.6557(7)	Te(1)-C(5)	2.165(4)	Te(1)-C(8)	2.101(8)
C(8)-Fe(1)	2.016(4)	Te(2)-Cr(1)	2.6661(7)	Te(2)-C(7)	2.161(4)
Te(2)-C(18)	2.088(4)	C(18)-Fe(2)	2.030(4)	Cr(1)-C(1)	1.870(5)
Cr(1)-C(2)	1.893(5)	Cr(1)-C(3)	1.818(5)	Cr(1)-C(4)	1.836(5)
O(1)-C(1)	1.154(5)	O(2)-C(2)	1.140(6)	O(3)-C(3)	1.160(6)
O(4)-C(4)	1.157(5)				
<i>Bond angles</i>					
Cr(1)-Te(1)-C(8)	111.78(11)	Cr(1)-Te(1)-C(5)	108.20(12)		
C(8)-Te(1)-C(5)	92.76(15)	Cr(1)-Te(2)-C(7)	105.17(12)		
Cr(1)-Te(2)-C(18)	110.03(10)	C(7)-Te(2)-C(18)	92.00(15)		
Te(1)-Cr(1)-Te(2)	88.75(2)	Te(1)-Cr(1)-C(1)	94.00(13)		
Te(1)-Cr(1)-C(2)	88.59(14)	Te(1)-Cr(1)-C(3)	87.17(15)		
Te(1)-Cr(1)-C(4)	173.89(14)	Te(2)-Cr(1)-C(1)	88.39(15)		
Te(2)-Cr(1)-C(2)	89.12(14)	Te(2)-Cr(1)-C(3)	175.20(16)		
Te(2)-Cr(1)-C(4)	97.24(13)	C(1)-Cr(1)-C(2)	176.4(2)		
C(2)-Cr(1)-C(3)	93.3(2)	C(2)-Cr(1)-C(4)	90.3(2)		
C(3)-Cr(1)-C(4)	86.9(2)				

* The number in bracket means the standard uncertainty, s.u..

Table 3.26 Crystallographic data collection and refinement parameters of



Empirical formula	$\text{C}_{27}\text{H}_{24}\text{Fe}_2\text{MoO}_4\text{Se}_2$
Formula weight	778.02
T (K)	293(2)
Wavelength (Å)	0.71069
Crystal system	monoclinic
Space group	P21/c
a (Å)	15.030(3)
b (Å)	12.468(3)
c (Å)	15.066(3)
α (°)	90
β (°)	104.46(2)
γ (°)	90
Volume (Å ³)	2733.8(1)
Z	4
D_c (Mg m ⁻³)	1.890
Absorption coefficient (mm ⁻¹)	4.193
$F(000)$	1520
Crystal size (mm)	0.60 × 0.50 × 0.30
θ range for data collection (°)	4.0 to 22.0
Index ranges	$-18 \leq h \leq 18, -15 \leq k \leq 15, -18 \leq l \leq 14$
Reflections collected	12969
Independent reflections [Rint]	5330 [0.0499]
Data / restraints / parameters	5330/0/326
Goodness-of-fit on F^2	1.015
Final R indices [$I > 2\sigma(I)$]	$R_1 = 0.0320, wR_2 = 0.0600$
R indices (all data)	$R_1 = 0.0522, wR_2 = 0.0634$
Largest diff. peak and hole (e Å ⁻³)	0.606, -0.718

* The number in bracket means the standard uncertainty, s.u..

Table 3.27 Selected bond lengths (Å) and angles (°) for [Mo(CO)₄{FcSe(CH₂)₃SeFc}]

<i>Bond lengths</i>					
Se(1)- Mo(1)	2.6649(7)	Se(1)-C(5)	1.9555(41)	Se(1)-C(8)	1.9001(37)
C(8)-Fe(1)	2.0105(38)	Se(2)-Mo(1)	2.6751(7)	Se(2)-C(7)	1.9733(37)
Se(2)-C(18)	1.8928(38)	C(18)-Fe(2)	2.0265(37)	Mo(1)-C(1)	1.9988(48)
Mo(1)-C(2)	2.0332(49)	Mo(1)-C(3)	1.9411(49)	Mo(1)-C(4)	1.9569(49)
O(1)-C(1)	1.1408(45)	O(2)-C(2)	1.1317(49)	O(3)-C(3)	1.1428(49)
O(4)-C(4)	1.1470(46)				
<i>Bond angles</i>					
Mo(1)-Se(1)-C(8)	113.36(12)	Mo(1)-Se(1)-C(5)		108.93(13)	
C(8)-Se(1)-C(5)	95.63(17)	Mo(1)-Se(2)-C(7)		106.34(13)	
Mo(1)-Se(2)-C(18)	111.04(11)	C(7)-Se(1)-C(18)		92.98(16)	
Se(1)-Mo(1)-Se(2)	86.51(2)	Se(1)-Mo(1)-C(1)		96.21(12)	
Se(1)-Mo(1)-C(2)	89.23(13)	Se(1)-Mo(1)-C(3)		88.96(14)	
Se(1)-Mo(1)-C(4)	174.05(12)	Se(2)-Mo(1)-C(1)		96.21(12)	
Se(2)-Mo(1)-C(2)	89.23(13)	Se(2)-Mo(1)-C(3)		174.66(14)	
Se(2)-Mo(1)-C(4)	99.21(12)	C(1)-Mo(1)-C(2)		174.53(18)	
C(2)-Mo(1)-C(3)	92.1(2)	C(2)-Mo(1)-C(4)		89.07(17)	
C(3)-Mo(1)-C(4)	85.41(18)				

* The number in bracket means the standard uncertainty, s.u..

Table 3.28 Crystallographic data collection and refinement parameters of



Empirical formula	C ₂₇ H ₂₄ Fe ₂ MoO ₄ SeTe
Formula weight	826.66
T (K)	293(2)
Wavelength (Å)	0.71069
Crystal system	monoclinic
Space group	P21/c
<i>a</i> (Å)	15.1636(8)
<i>b</i> (Å)	12.5154(6)
<i>c</i> (Å)	15.2988(8)
α (°)	90.000(5)
β (°)	103.680(5)
γ (°)	90.000(5)
Volume (Å ³)	2821.0(2)
<i>Z</i>	4
<i>D</i> _c (Mg m ⁻³)	1.946
Absorption coefficient (mm ⁻¹)	3.787
<i>F</i> (000)	1592
Crystal size (mm)	0.35 × 0.25 × 0.15
θ range for data collection (°)	4.26 to 34.61
Index ranges	-22 ≤ <i>h</i> ≤ 23, -18 ≤ <i>k</i> ≤ 19, -21 ≤ <i>l</i> ≤ 20
Reflections collected	31435
Independent reflections [Rint]	9413 [0.0298]
Data / restraints / parameters	9413 / 0 / 326
Goodness-of-fit on F ²	0.870
Final <i>R</i> indices [<i>I</i> > 2σ(<i>I</i>)]	<i>R</i> ₁ = 0.0359, <i>wR</i> ₂ = 0.0847
<i>R</i> indices (all data)	<i>R</i> ₁ = 0.0770, <i>wR</i> ₂ = 0.0947
Largest diff. peak and hole (e Å ⁻³)	1.204, -0.663

* The number in bracket means the standard uncertainty, s.u..

Table 3.29 Selected bond lengths (Å) and angles (Å) for
 $[\text{Mo}(\text{CO})_4\{\text{FcSe}(\text{CH}_2)_3\text{TeFc}\}]$

<i>Bond lengths</i>					
Te(1)-Mo(1)	2.7547(4)	Te(1)-C(5)	2.0769(37)	Te(1)-C(8)	2.0282(32)
C(8)-Fe(1)	2.021(3)	Se(1)-Mo(1)	2.7467(4)	Se(1)-C(7)	2.0579(35)
Se(1)-C(18)	1.9789(32)	C(18)-Fe(2)	2.033(3)	Mo(1)-C(1)	2.0072(43)
Mo(1)-C(2)	2.0442(43)	Mo(1)-C(3)	1.9418(40)	Mo(1)-C(4)	1.9640(35)
O(1)-C(1)	1.1459(45)	O(2)-C(2)	1.1413(46)	O(3)-C(3)	1.1559(46)
O(4)-C(4)	1.1518(41)				
<i>Bond angles</i>					
Mo(1)-Te(1)-C(8)	111.50(9)	Mo(1)-Te(1)-C(5)	107.65(10)		
C(8)-Te(1)-C(5)	94.10(13)	Mo(1)-Se(1)-C(7)	105.28(11)		
Mo(1)-Se(1)-C(18)	109.55(9)	C(7)-Se(1)-C(18)	93.73(14)		
Te(1)-Mo(1)-Se(1)	87.24(1)	Te(1)-Mo(1)-C(1)	95.11(10)		
Te(1)-Mo(1)-C(2)	88.59(10)	Te(1)-Mo(1)-C(3)	88.59(11)		
Te(1)-Mo(1)-C(4)	173.78(10)	Se(1)-Mo(1)-C(1)	88.61(13)		
Se(1)-Mo(1)-C(2)	90.22(11)	Se(1)-Mo(1)-C(3)	175.03(12)		
Se(1)-Mo(1)-C(4)	98.73(10)	C(1)-Mo(1)-C(2)	176.06(15)		
C(2)-Mo(1)-C(3)	92.73(18)	C(2)-Mo(1)-C(4)	89.64(15)		
C(3)-Mo(1)-C(4)	85.53(15)				

* The number in bracket means the standard uncertainty, s.u..

Table 3.30 Crystallographic data collection and refinement parameters of



Empirical formula	C ₂₇ H ₂₄ Fe ₂ MoO ₄ Te ₂
Formula weight	875.30
T (K)	293(2)
Wavelength (Å)	0.71069
Crystal system	monoclinic
Space group	P21/c
<i>a</i> (Å)	15.253(5)
<i>b</i> (Å)	12.512(4)
<i>c</i> (Å)	15.411(5)
α (°)	90
β (°)	103.14(3)
γ (°)	90
Volume (Å ³)	2864.1(16)
Z	4
<i>D_c</i> (Mg m ⁻³)	2.030
Absorption coefficient (mm ⁻¹)	3.457
<i>F</i> (000)	1664
Crystal size (mm)	0.40 × 0.35 × 0.30
θ range for data collection (°)	4.24 to 28.28
Index ranges	-20 ≤ <i>h</i> ≤ 19, -16 ≤ <i>k</i> ≤ 16, -20 ≤ <i>l</i> ≤ 20
Reflections collected	30720
Independent reflections [<i>R</i> _{int}]	7049 [0.0421]
Data / restraints / parameters	7049/0/326
Goodness-of-fit on <i>F</i> ²	0.960
Final <i>R</i> indices [<i>I</i> > 2σ(<i>I</i>)]	<i>R</i> ₁ = 0.0342, <i>wR</i> ₂ = 0.0740
<i>R</i> indices (all data)	<i>R</i> ₁ = 0.0513, <i>wR</i> ₂ = 0.0791
Largest diff. peak and hole (e Å ⁻³)	0.963, -0.734

* The number in bracket means the standard uncertainty, s.u..

Table 3.31 Selected bond lengths (Å) and angles (°) for [Mo(CO)₄{FcTe(CH₂)₃TeFc}]

<i>Bond lengths</i>					
Te(1)- Mo(1)	2.7988(8)	Te(1)-C(5)	2.165(4)	Te(1)-C(8)	2.101(4)
C(8)-Fe(1)	2.024(4)	Te(2)-Mo(1)	2.8093(8)	Te(2)-C(7)	2.170(4)
Te(2)-C(18)	2.089(4)	C(18)-Fe(2)	2.030(4)	Mo(1)-C(1)	2.009(5)
Mo(1)-C(2)	2.041(5)	Mo(1)-C(3)	1.943(5)	Mo(1)-C(4)	1.969(4)
O(1)-C(1)	1.146(5)	O(2)-C(2)	1.143(5)	O(3)-C(3)	1.155(5)
O(4)-C(4)	1.156(5)				
<i>Bond angles</i>					
Mo(1)-Te(1)-C(8)	111.03(10)	Mo(1)-Te(1)-C(5)		107.41(11)	
C(8)-Te(1)-C(5)	93.07(14)	Mo(1)-Te(2)-C(7)		104.23(11)	
Mo(1)-Te(2)-C(18)	108.59(10)	C(7)-Te(2)-C(18)		93.05(15)	
Te(1)-Mo(1)-Te(2)	87.46(3)	Te(1)-Mo(1)-C(1)		94.01(12)	
Te(1)-Mo(1)-C(2)	88.47(12)	Te(1)-Mo(1)-C(3)		88.13(13)	
Te(1)-Mo(1)-C(4)	174.47(12)	Te(2)-Mo(1)-C(1)		88.69(15)	
Te(2)-Mo(1)-C(2)	89.00(13)	Te(2)-Mo(1)-C(3)		175.15(14)	
Te(2)-Mo(1)-C(4)	97.88(12)	C(1)-Mo(1)-C(2)		176.53(18)	
C(2)-Mo(1)-C(3)	92.9(2)	C(2)-Mo(1)-C(4)		90.17(18)	
C(3)-Mo(1)-C(4)	85.58(18)				

* The number in bracket means the standard uncertainty, s.u..

Table 3.32 Crystallographic data collection and refinement parameters of



Empirical formula	$\text{C}_{27}\text{H}_{24}\text{Fe}_2\text{WO}_4\text{Te}_2$
Formula weight	963.21
T (K)	293(2)
Wavelength (Å)	0.71069
Crystal system	monoclinic
Space group	P21/c
a (Å)	15.254(1)
b (Å)	12.476(1)
c (Å)	15.396(1)
α (°)	90
β (°)	103.19(1)
γ (°)	90
Volume (Å ³)	2852.7(3)
Z	4
D_c (Mg m ⁻³)	2.243
Absorption coefficient (mm ⁻¹)	7.061
$F(000)$	1792
Crystal size (mm)	0.30 × 0.20 × 0.15
θ range for data collection (°)	4.25 to 26.37
Index ranges	$-19 \leq h \leq 19, -15 \leq k \leq 15, -19 \leq l \leq 19$
Reflections collected	28246
Independent reflections [Rint]	5803 [0.0339]
Data / restraints / parameters	5803/0/325
Goodness-of-fit on F^2	0.977
Final R indices [$I > 2\sigma(I)$]	$R_1 = 0.0305, wR_2 = 0.0656$
R indices (all data)	$R_1 = 0.0428, wR_2 = 0.0688$
Largest diff. peak and hole (e Å ⁻³)	1.181, -0.828

* The number in bracket means the standard uncertainty, s.u..

Table 3.33 Selected bond lengths (Å) and angles (°) for [W(CO)₄{FcTe(CH₂)₃TeFc}]

<i>Bond lengths</i>					
Te(1)-W(1)	2.7903(7)	Te(1)-C(5)	2.162(5)	Te(1)-C(8)	2.098(5)
C(8)-Fe(1)	2.030(5)	Te(2)-W(1)	2.8013(4)	Te(2)-C(7)	2.153(5)
Te(2)-C(18)	2.096(5)	C(18)-Fe(2)	2.028(5)	W(1)-C(1)	2.006(7)
W(1)-C(2)	2.039(6)	W(1)-C(3)	1.943(6)	W(1)-C(4)	1.967(6)
O(1)-C(1)	1.151(7)	O(2)-C(2)	1.137(7)	O(3)-C(3)	1.157(7)
O(4)-C(4)	1.153(6)				
<i>Bond angles</i>					
W(1)-Te(1)-C(8)	111.09(13)	W(1)-Te(1)-C(5)		107.54(14)	
C(8)-Te(1)-C(5)	92.57(18)	W(1)-Te(2)-C(7)		104.47(15)	
W(1)-Te(2)-C(18)	108.41(13)	C(7)-Te(2)-C(18)		92.81(19)	
Te(1)-W(1)-Te(2)	87.477(12)	Te(1)-W(1)-C(1)		93.87(15)	
Te(1)-W(1)-C(2)	88.24(16)	Te(1)-W(1)-C(3)		87.47(17)	
Te(1)-W(1)-C(4)	174.40(15)	Te(2)-W(1)-C(1)		88.28(18)	
Te(2)-W(1)-C(2)	89.02(17)	Te(2)-W(1)-C(3)		174.48(17)	
Te(2)-W(1)-C(4)	97.87(15)	C(1)-W(1)-C(2)		176.5(2)	
C(2)-W(1)-C(3)	93.0(3)	C(2)-W(1)-C(4)		90.2(2)	
C(3)-W(1)-C(4)	87.2(2)				

* The number in bracket means the standard uncertainty, s.u..

3.3.3 Comparison of ligand properties

As mentioned in the discussion of the structure of $[\text{Mo}(\text{CO})_4\{\text{FcSe}(\text{CH}_2)_3\text{SeFc}\}]$ in the previous section, the equatorial M-C bonds *trans* to the Mo-E bonds are significantly shorter than the two axial Mo-C bonds. This results from greater back-bonding to the two equatorial carbonyls, and reflects the strength of the donor atom. Analysis of this and related effects allows comparison of the ferrocenyl chalcogenide ligands' properties. As an introduction to this topic some basic knowledge is presented first.

The CO molecule has 10 valence electrons. The molecular orbital scheme (Fig. 3.33) shows that the HOMO has σ symmetry. The LUMOs of CO are the degenerate π^* orbitals.

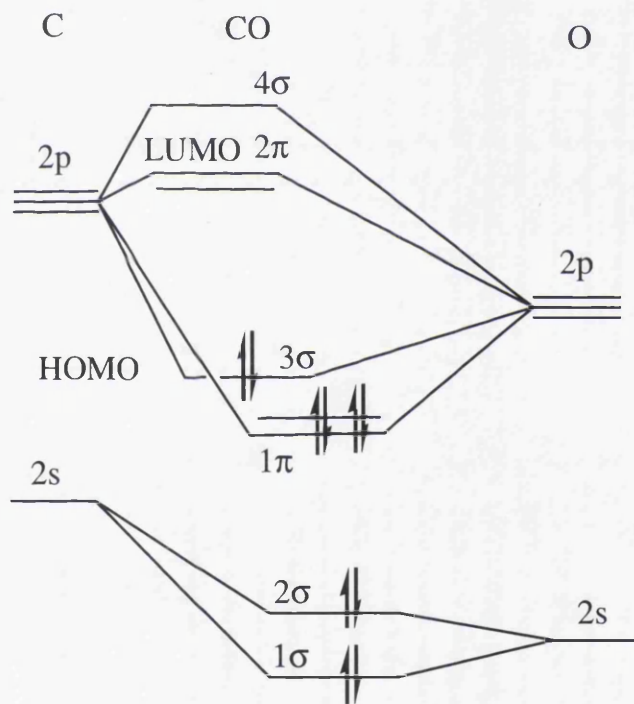


Fig. 3.33 The MO scheme for CO

So carbon monoxide often acts as a two-electron ligand which can be depicted in the diagram below. There are two kinds of interactions. The first is a ligand-to-metal σ bond resulting from transfer of electron density from the carbon lone pair to an empty metal d orbital ($\text{OC} \rightarrow \text{M} \sigma$ bond). The second interaction is between filled metal d orbitals and the empty π^* orbitals of the CO, which leads to a reverse metal-

to-ligand electron transfer resulting in a second bond ($M \rightarrow CO$ π backbonding). So the CO behaves as a σ donor and a π acceptor (Fig. 3.34).

Strong σ donor ligands attached to a mixed ligand metal carbonyl, or a formal negative charge on a metal carbonyl anion, will increase the electron density on the metal atom. Then backbonding induces a filling of the carbonyl π^* level, which causes a weakening of the C-O bond. This weakening can be reflected in two ways: in the IR spectrum, the $\nu(CO)$ will shift from 2143 cm^{-1} in free CO to below 2100 cm^{-1} in a terminal carbonyl, so the IR stretching frequency of coordinated CO is a good measure of the balance of σ -donation and π -back-donation; in the structure, the C-O bond length will increase from 1.1282 \AA in free CO to about 1.15 \AA in a terminal $2e$ carbonyl ligand.^{52, 53}

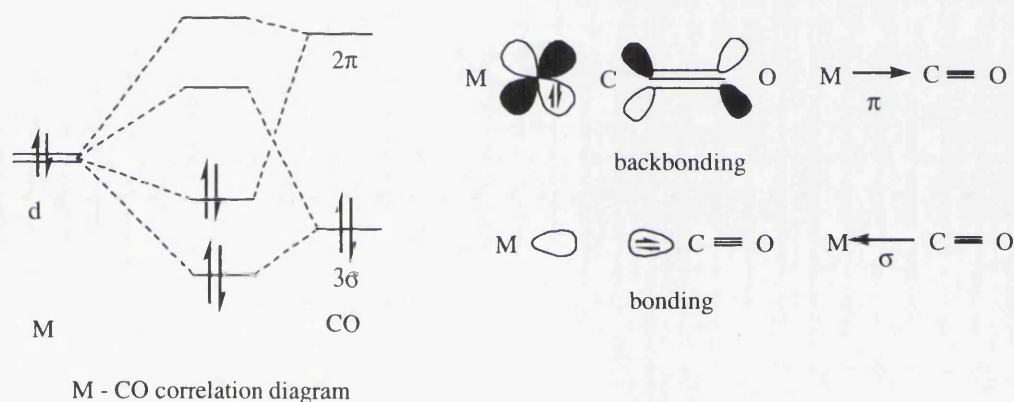


Fig. 3.34 M-CO correlation diagram

The number and intensities of carbonyl stretching bands in the vibrational spectra of carbonyl complexes depend on the local symmetry around the central atom; the expected number of IR-active bands can be derived from group theory. For a disubstituted octahedral complex $[M(CO)_4L_2]$, there should be one IR active mode (E_u) for the *trans* isomer and four ($2A_1 + B_1 + B_2$) for the *cis* one. The IR spectra of the *cis*- $[M(CO)_4\{FcE(CH_2)_3E'Fc\}]$ complexes show four $\nu(CO)$ bands as expected (Table 3.34). For the Mo complexes, the frequency of the A_1 mode falls with a change in donor from Se to Te: 2018 cm^{-1} , $[Mo(CO)_4\{FcSe(CH_2)_3SeFc\}]$; 2015 cm^{-1} , $[Mo(CO)_4\{FcSe(CH_2)_3TeFc\}]$; 2012 cm^{-1} , $[Mo(CO)_4\{FcTe(CH_2)_3TeFc\}]$. This reflects the weakening of the C-O bond: the tellurium ligand places greater electron density on the metal centre resulting in greater π -back-bonding to CO. The C-O

bond lengths confirm this interpretation: those which are *trans* to the donor ligand are significantly longer in [Mo(CO)₄{FcSe(CH₂)₃TeFc}] (1.1559(46) and 1.1518(41) Å) than in [Mo(CO)₄{FcSe(CH₂)₃SeFc}] (1.1428(49) and 1.1470(46) Å).

Comparing the complexes of the same ligand FcTe(CH₂)₃TeFc, the frequency of the A₁ mode falls in the sequence Mo > W > Cr.

Table 3.34 IR spectroscopic data

Complex	$\nu(\text{CO}) \text{ cm}^{-1}$
[Cr(CO) ₄ {FcTe(CH ₂) ₃ TeFc}]	1995, 1908, 1877, 1846
[Mo(CO) ₄ {FcSe(CH ₂) ₃ SeFc}]	2018, 1912(sh), 1879, 1841
[Mo(CO) ₄ {FcSe(CH ₂) ₃ TeFc}]	2015, 1914, 1881, 1843(sh)
[Mo(CO) ₄ {FcTe(CH ₂) ₃ TeFc}]	2012, 1917, 1884, 1849(sh)
[W(CO) ₄ {FcTe(CH ₂) ₃ TeFc}]	2006, 1908, 1874, 1841(sh)

More information can be obtained from the structures. The M-C and C-O bond lengths are listed in Table 3.35 and Table 3.36 respectively. The equatorial M-C bonds *trans* to the M-E bonds (M-C(3) and M-C(4)) are significantly shorter than the two axial M-C bonds (M-C(1) and M-C(2)), as increased backbonding strengthens the M-C bond; it also induces a filling of the carbonyl π^* level, which causes a weakening of the C-O bond. The C(3)-O(3) and C(4)-O(4) bonds are thus longer than the other two. For example, in [Mo(CO)₄{FcTe(CH₂)₃TeFc}], the bond lengths Mo-C(3) and Mo-C(4) are 1.943(5) and 1.969(4) Å respectively, shorter than Mo-C(1) and Mo-C(2) (2.009(5) and 2.041(5) Å), but C(3)-O(3) and C(4)-O(4) (1.155(5) and 1.156(5) Å) are longer than C(1)-O(1) and C(2)-O(2) (1.146(5) and 1.143(5) Å). For the three complexes of the same ligand FcTe(CH₂)₃TeFc, the *trans*-C-O bond lengths decrease in the sequence Cr > W > Mo: [Cr(CO)₄{FcTe(CH₂)₃TeFc}], 1.160(6) and 1.157(5) Å; [W(CO)₄{FcTe(CH₂)₃TeFc}], 1.157(7) and 1.153(6) Å; [Mo(CO)₄{FcTe(CH₂)₃TeFc}], 1.155(5) and 1.156(5) Å. This trend mirrors what is observed in the IR spectra. Both effects result from the change in electron density on the metal, which is also reflected in the stability of the complexes towards air oxidation: [Cr(CO)₄{FcTe(CH₂)₃TeFc}] is the least stable of those which could be isolated.

Table 3.35 M-C bond lengths in the complexes (Å)

	M-C(1)	M-C(2)	M-C(3)	M-C(4)
[Cr(CO) ₄ {FcTe(CH ₂) ₃ TeFc}]	1.870(5)	1.893(5)	1.818(5)	1.836(5)
[Mo(CO) ₄ {FcSe(CH ₂) ₃ SeFc}]	1.9988(48)	2.0332(49)	1.9411(49)	1.9569(49)
[Mo(CO) ₄ {FcSe(CH ₂) ₃ TeFc}]	2.0072(43)	2.0442(43)	1.9418(40)	1.9640(35)
[Mo(CO) ₄ {FcTe(CH ₂) ₃ TeFc}]	2.009(5)	2.041(5)	1.943(5)	1.969(4)
[W(CO) ₄ {FcTe(CH ₂) ₃ TeFc}]	2.006(7)	2.039(6)	1.943(6)	1.967(6)

Table 3.36 C-O bond lengths in the complexes (Å)

	C(1)-O(1)	C(2)-O(2)	C(3)-O(3)	C(4)-O(4)
[Cr(CO) ₄ {FcTe(CH ₂) ₃ TeFc}]	1.154(5)	1.140(6)	1.160(6)	1.157(5)
[Mo(CO) ₄ {FcSe(CH ₂) ₃ SeFc}]	1.1408(45)	1.1317(49)	1.1428(49)	1.1470(46)
[Mo(CO) ₄ {FcSe(CH ₂) ₃ TeFc}]	1.1459(45)	1.1413(46)	1.1559(46)	1.1518(41)
[Mo(CO) ₄ {FcTe(CH ₂) ₃ TeFc}]	1.146(5)	1.143(5)	1.155(5)	1.156(5)
[W(CO) ₄ {FcTe(CH ₂) ₃ TeFc}]	1.151(7)	1.137(7)	1.157(7)	1.153(6)

3.4 Pd and Pt complexes of macrocyclic ferrocenyl

chalcogenide ligands

Two macrocyclic ferrocenyl selenide compounds, fcSe_4 and difcSe_4 , have been synthesized and characterized as described in Chapter Two. From the viewpoints of macrocyclic effect, cavity size and soft donor atom Se, they should coordinate well to late transition metals. They are also expected to be efficient electrochemical sensors to late transition cations. The Pd and Pt complexes were first synthesized and characterized by multinuclear NMR spectroscopy. Consideration of an electrochemistry study will be deferred until Chapter Four.

A similar general procedure was used for the syntheses of all these complexes, which is illustrated below by the example of $[\text{Pd}(\text{fcSe}_4)](\text{PF}_6)_2$. The experimental details are given in Chapter Seven.

PdCl_2 was refluxed in MeCN for 2 h to give a yellow solution of $[\text{PdCl}_2(\text{NCMe})_2]$. After cooling, two equivalents of TlPF_6 were added and stirring continued for another 15 min. One equivalent of fcSe_4 in CH_2Cl_2 (5 ml) was then added dropwise, and the mixture stirred at room temperature for 24 h to give a blue liquid and a fine white precipitate of TlCl . The mixture was centrifuged to remove TlCl and reduced to 2 ml *in vacuo*. Diethyl ether was added to precipitate the product as a powder.

The four complexes show multiplet peaks with the correct isotope structure in the mass spectra consistent with $[\text{M}-\text{PF}_6]^+$.

The ^1H NMR spectra of $[\text{M}(\text{fcSe}_4)](\text{PF}_6)_2$ ($\text{M} = \text{Pd}$ or Pt) show two groups of four single resonances in the range for Cp ring protons, while for the free ligand there is only one. So the Cp rings in the ferrocene unit become rigid after complexation, and the total number of resonances suggests the presence of more than one invertomer in the solution. In the study of $[\text{M}(\text{[16]aneSe}_4)]^{2+}$,⁵⁴ three invertomers (*up, up, up, up*; *up, up, down, down*; *up, down, up, down*) were suggested to be more stable than the fourth one (*up, up, up, down*) due to ring strain. As one trimethylene chain in [16]aneSe_4 has been changed to a ferrocene unit, in $[\text{M}(\text{fcSe}_4)]^{2+}$ there may only exist two invertomers: *up, up, up* or *up, down, up*. ^{13}C and ^1H NMR spectra all show there are two sets of signals for the atoms of the Cp rings.

Free fcSe_4 ligand shows two resonances in the ^{77}Se solution NMR spectrum at 170 and 161 ppm. At 298 K in CD_3COCD_3 solution, the ^{77}Se NMR spectrum of $[\text{Pd}(\text{fcSe}_4)](\text{PF}_6)_2$ shows four resonances: two weak ones at 256 and 219 ppm, two

strong ones at 215 and 186 ppm, which are consistent with the presence of two isomers. The isomer with chemical shifts of 256 and 219 ppm is the preferred one in solution. $[\text{Pt}(\text{fcSe}_4)](\text{PF}_6)_2$ also show two pairs of resonances in the ^{77}Se NMR spectrum: two weak ones at 236 and 194 ppm, two strong ones at 215 and 170 ppm. In the series of complexes $[\text{PtCl}\{\text{FcE}(\text{CH}_2)_3\text{E}'(\text{CH}_2)_3\text{EFc}\}]\text{PF}_6$ (E, E' = Se or Te), Pt-SeFc coupling constant is always larger (*ca.* 390 Hz) than that for the middle Se (*ca.* 270 Hz). So the stronger ^{77}Se NMR resonances at 215 ($^1J_{\text{Pt-Se}} = 388$ Hz) and 170 ($^1J_{\text{Pt-Se}} = 55$ Hz) can be attributed to the SeFc and SeCH₂ atoms respectively of the main invertomer. Weaker ones at 236 ($^1J_{\text{Pt-Se}} = 348$ Hz) and 194 ($^1J_{\text{Pt-Se}} = 116$ Hz) can be attributed to another invertomer with low concentration.

In the complexes $[\text{M}(\text{difcSe}_4)](\text{PF}_6)_2$ (M = Pd or Pt), the dynamic behaviour is more complicated: the inversion at the Se atoms and the flipping motion of the central methylene group in the trimethylene-chain may result in four invertomers (shown in Fig. 3.35): *syn(up, up)*, *anti(up, up)*, *syn(up, down)* and *anti(up, down)*.

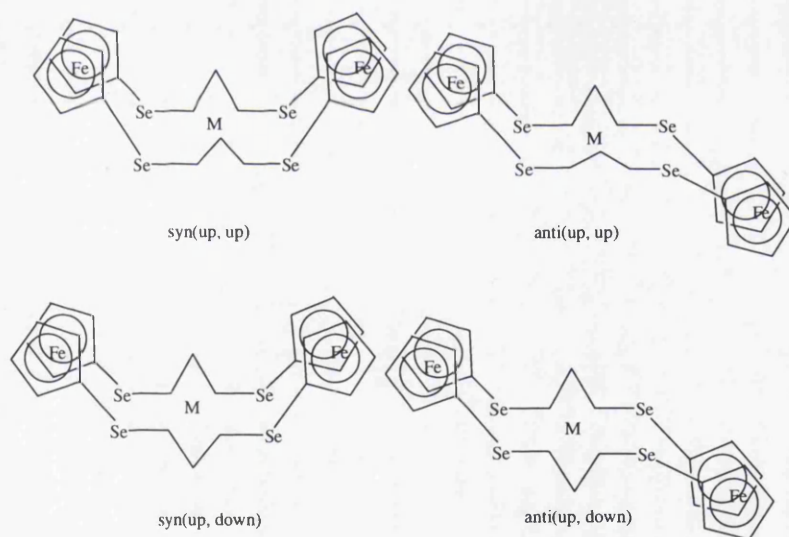


Fig. 3.35 Four possible invertomers of $[\text{M}(\text{difcSe}_4)]^{2+}$ (M = Pd or Pt)

There are only two resonances in the ^{77}Se NMR spectrum of $[\text{Pd}(\text{difcSe}_4)](\text{PF}_6)_2$: a weak one at 292 ppm, and a strong one at 261 ppm, which suggests that at room temperature only two invertomers in solution can be observed. $[\text{Pt}(\text{difcSe}_4)](\text{PF}_6)_2$ also has two resonances: a weak one at 264 ppm, and a strong one at 242 ppm with $^1J_{\text{Pt-Se}} = 300$ Hz. The resonance at 264 ppm was too weak for $^1J_{\text{Pt-Se}}$ to be measured.

The ^1H NMR spectrum of $[\text{Pt}(\text{difcSe}_4)](\text{PF}_6)_2$ shows four pairs (“doublet”) of resonances of Cp ring protons at 5.47, 5.20, 4.92, 4.61 ppm, due to the inequivalence of H(2,5) and H(3,4) and the presence of two invertomers. In the ^1H NMR spectrum of $[\text{Pd}(\text{difcSe}_4)](\text{PF}_6)_2$ there are only three “doublet” resonances for Cp ring protons as the first two resonances have coalesced. The ^1H NMR spectra of the sulphur analogues $[\text{M}(\text{difcS}_4)](\text{PF}_6)_2$ showed broad signals for the Cp ring protons, which split into four pairs of signals at low temperature ($-40\text{ }^\circ\text{C}$).⁵⁵ This is in accordance with the sequence of the inversion energy barriers $\text{Se} > \text{S}$.^{50, 51} In the free ligand difcSe₄, the chemical shifts of the protons of the Cp ring are 4.29 and 4.21 ppm in CDCl_3 . The large downfield shift of these protons in the complexes may result from a strong interaction between Fe and the Pd(Pt) atom. Similar phenomena were observed in the sulphur analogues $[\text{M}(\text{difcS}_4)](\text{PF}_6)_2$.⁵⁵

The UV-vis spectra of these four complexes show a very strong absorption in the ultraviolet region.

NMR spectroscopic data for each of the new compounds described in this section are provided in Chapter Seven.

3.5 Pt complex of FcSeCH₂C₆H₄CH₂SeFc

Since the first introduction of the concept of “supramolecular chemistry” by Lehn in 1988,⁵⁶ it has developed at a rapid rate. The interest in this field is to synthesize materials with specific properties and functions through controlling the form, shape and distribution of building blocks.⁵⁷ As the covalent coordination bonds formed between transition metals and donor atoms have medium strength as compared to weak interactions (such as hydrogen bonding, van der Waals forces *etc*), and the strong covalent carbon-carbon bonds, they have been used extensively in the construction of supramolecular assemblies. Up to now, in the field of superamolecular coordination chemistry, the existing synthetic strategies can be divided into three categories: (1) directional-bonding approach; (2) symmetry interaction approach; (3) weak link approach.⁵⁸ The Pt(II) cations so far incorporated into supramolecular complexes are all coordinated to nitrogen or phosphorus atoms, and have been synthesized through a directional-bonding approach. As the Pt(II) cation prefers square planar coordination geometry, its supramolecular complexes can be divided into three types: dinuclear macrocycles,⁵⁹⁻⁶⁷ molecular triangles⁶⁸⁻⁶⁹ and molecular squares.^{62, 63, 70-89}

As shown in Chapter Two, two rigid chain bidentate compounds FcECH₂C₆H₄CH₂EFc (E = Se or Te) have been successfully synthesized and characterized. They will not behave as chelate ligands in complexation, so can be a good building block to construct supramolecular complexes or coordination polymers. The impetus of the work described below is thus to explore novel supramolecular complexes constructed from Pt and softer donor atoms – Se or Te. Also the supramolecular complexes incorporating a redox-active functional group, the ferrocene unit, may be suitable for sensing applications.

The starting reaction was aimed at synthesizing a dinuclear complex [Pt₂{FcSeCH₂C₆H₄CH₂SeFc}₄](PF₆)₄ with cage-like geometry, by using ligand FcSeCH₂C₆H₄CH₂SeFc, [PtCl₂(NCMe)₂] and TlPF₆ in a 2:1:2 stoichiometry. The procedure was performed as follows: One equivalent of PtCl₂ was refluxed in MeCN for 2 h to give a yellow solution of [PtCl₂(NCMe)₂]. Two equivalents of TlPF₆ were added and the mixture stirred for another 15 min. Two equivalents of the ligand FcSeCH₂C₆H₄CH₂SeFc in CH₂Cl₂ were then added dropwise; the mixture was stirred at room temperature for 20 h to give a red liquid and a fine white precipitate of TlCl.

The solution was centrifuged to remove TiCl_4 and reduced to 2 ml *in vacuo*. Diethyl ether was added to precipitate a red powder. The experimental details will be given in Chapter Seven.

The mass spectrum shows that the target complex $[\text{Pt}_2\{\text{FcSeCH}_2\text{C}_6\text{H}_4\text{CH}_2\text{SeFc}\}_4](\text{PF}_6)_4$ was not obtained. Instead, there are multiplet peaks with the correct isotope structure consistent with $[\text{M-PF}_6]^+$ and $[\text{M-PF}_6]^{2+}$ for dinuclear complex $[\text{Pt}_2\text{Cl}_2\{\text{FcSeCH}_2\text{C}_6\text{H}_4\text{CH}_2\text{SeFc}\}_3](\text{PF}_6)_2$. It was proved by mass spectrometry that changing stoichiometry of $\text{FcSeCH}_2\text{C}_6\text{H}_4\text{CH}_2\text{SeFc}$, $[\text{PtCl}_2(\text{NCMe})_2]$ and TiPF_6 to a 1:1:2 ratio yielded the same product.

Multinuclear NMR spectroscopic study only showed weak and broad features because of the complex's large molecular weight or pyramidal inversion at room temperature.

Red-violet thin plate crystals suitable for single-crystal X-ray analysis of the complex were obtained by slow diffusion of Et_2O into a solution in MeCN . It crystallizes in the monoclinic C-centred space group $C2/c$, with four dimetal $[\text{Pt}_2\text{Cl}_2\text{L}_3]^{2+}$ units and eight, disorderly arranged PF_6^- anions in the unit cell (packing diagram shown in Fig. 3.36). Crystal data and refinement details, and pertinent bond parameters are collected in Tables 3.37 and 3.38 respectively.

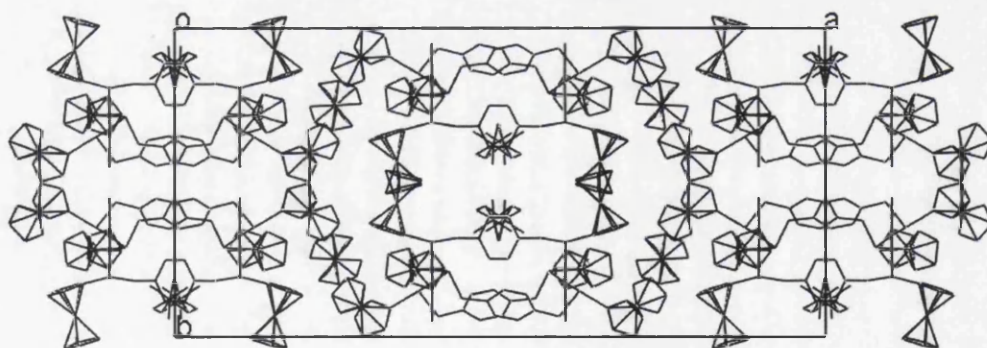


Fig. 3.36 Packing diagram of $[\text{Pt}_2\text{Cl}_2\{\text{FcSeCH}_2\text{C}_6\text{H}_4\text{CH}_2\text{SeFc}\}_3](\text{PF}_6)_2$

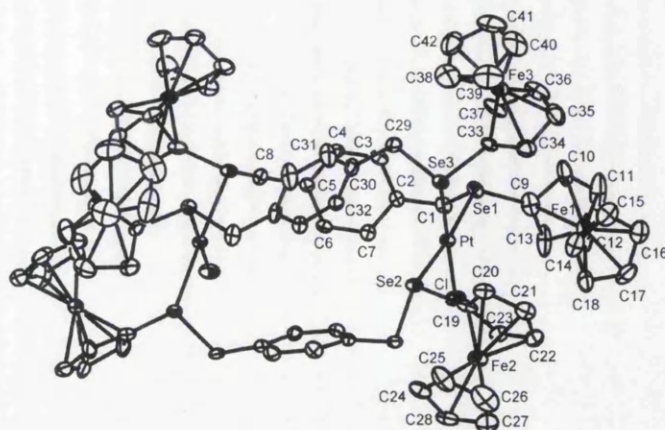


Fig. 3.37 Structure of cation $[\text{Pt}_2\text{Cl}_2\{\text{FcSeCH}_2\text{C}_6\text{H}_4\text{CH}_2\text{SeFc}\}_3]^{2+}$

The whole cation (Fig. 3.37) has an unusual geometry similar to that of a binuclear triple helicate. Normally, binuclear triple helicates can be formed by combining metals which prefer octahedral coordination geometry.⁵⁸ This is the first time this kind of geometry has been observed for Pt, although it can't be described as a real binuclear triple helicate, because there is no identical C_3 axis through the two coordination planes. The two chelate planes are also not parallel to each other; the angle between the planes is $7.01(4)^\circ$. The dinuclear cation possesses a two-fold symmetry axis lying in the plane of one of the benzene rings and bisecting two of its bonds. The $\text{Pt}\cdots\text{Pt}$ intramolecular distance is 7.70 \AA , clearly too far for a metal-metal bond.

The cation, of which only half belongs to the asymmetric unit, is accompanied by two anions, both disorderly arranged. One of the fractions of the anion lies with its P atom on an inversion centre and contributes with P ($pp = 0.5$) and three F atoms ($pp = 1$) to the symmetry-independent part of the model. In order to account for orientational disorder, each of the F atoms is considered to be distributed between two positions, yielding two complementary octahedral of F atoms around the P atom position.

The other anion is in the region of a two-fold axis and it almost overlaps with its symmetry-related image: each one of these fractions is assigned half occupancy; actually, only one of these is considered in the calculations, since only one-half of this anion (as is the case for the other one) belongs to the asymmetric unit.

The ferrocene sp^2 -C-Se bond distances (Se(1)-C(9), 1.902(12) Å; Se(2)-C(19), 1.893(1) Å; Se(3)-C(33) 1.89(19) Å) are similar to that in the free ligand (Se-C(5), 1.895(2) Å), as are the sp^3 -C-Se bond distances (1.965(8), 1.979(7) and 1.964(10) Å in the complex; 1.977(2) Å in the free ligand). The Pt-Cl_{transSe} bond length is 2.313(2) Å, similar to that in [PtCl{FcSe(CH₂)₃Se(CH₂)₃SeFc}]PF₆ (2.316(2) Å).

The Pt-Se(3) (2.4066(8) Å) bond is shorter than the other two Pt-Se bonds, 2.4193(9) and 2.4452(9) Å) due to the weaker *trans* influence of the Cl⁻ anion than that of SeR₂. The Cl-Pt-Se(3) angle is 176.74(7)°, and the Se(1)-Pt-Se(2) angle is 173.40(3)°, which means the Pt(II) coordination is not strictly planar. The Se(1)-Pt-Se(3) (91.01(3)°) and Se(2)-Pt-Se(3) (83.32(3)°) angles deviate from 90°, not showing such a good match of the six-membered chelate rings to the square planar geometry as in the diselenoether complexes.

So why can't the target complex [Pt₂{FcSeCH₂C₆H₄CH₂SeFc}₄](PF₆)₄ be obtained? The space filling diagram of the observed product (Fig. 3.38) shows that because of the square planar geometry of Pt(II), there is no enough space for the fourth ligand which contains the bulky ferrocene unit or even for an acetonitrile molecule. Self-assembly organization chooses the smaller Cl⁻ anion instead.

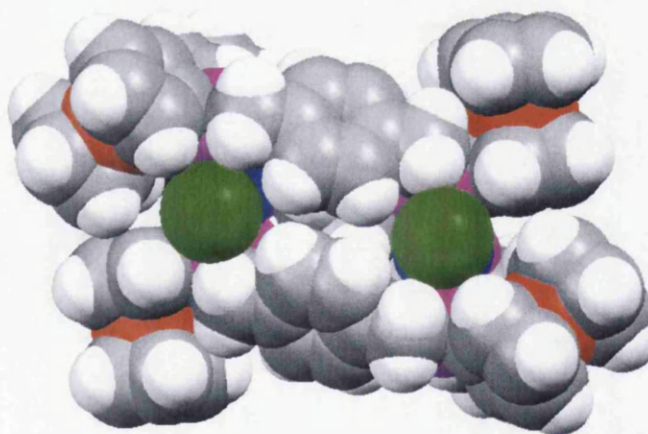


Fig. 3.38 Space filling diagram of cation [Pt₂Cl₂{FcSeCH₂C₆H₄CH₂SeFc}₃]²⁺
(Cl: green; Fe: orange red; Se: violet; Pt: blue)

Table 3.37 Crystallographic data collection and refinement parameters of



Empirical formula	$\text{C}_{42}\text{H}_{39}\text{ClF}_6\text{Fe}_3\text{PPtSe}_3$
Formula weight	1323.67
T (K)	293(2)
Wavelength (Å)	0.71069
Crystal system	monoclinic
Space group	$C2/c$
a (Å)	39.000(2)
b (Å)	17.855(1)
c (Å)	13.070(1)
α (°)	90
β (°)	104.174(5)
γ (°)	90
Volume (Å ³)	8824.2(10)
Z	8
D_c (Mg m ⁻³)	1.993
Absorption coefficient (mm ⁻¹)	6.755
$F(000)$	5080
Crystal size (mm)	0.35 × 0.35 × 0.10
θ range for data collection (°)	3.87 to 26.37
Index ranges	$-47 \leq h \leq 48, -21 \leq k \leq 21, -16 \leq l \leq 16$
Reflections collected	38709
Independent reflections [Rint]	8818 [0.1333]
Data / restraints / parameters	8818/132/578
Goodness-of-fit on F^2	0.905
Final R indices [$I > 2\sigma(I)$]	$R_1 = 0.0576, wR_2 = 0.1195$
R indices (all data)	$R_1 = 0.1134, wR_2 = 0.1321$
Largest diff. peak and hole (e Å ⁻³)	2.592, -1.530

* The number in bracket means the standard uncertainty, s.u..

Table 3.38 Selected bond lengths (Å) and angles (°) for
 $[\text{Pt}_2\text{Cl}_2\{\text{FcSeCH}_2\text{C}_6\text{H}_4\text{CH}_2\text{SeFc}\}_3](\text{PF}_6)_2$

<i>Bond lengths</i>					
Pt-Cl	2.313(2)	Pt-Se(3)	2.4066(8)	Pt-Se(1)	2.4193(9)
Pt-Se(2)	2.4452(9)	Se(1)-C(9)	1.902(12)	Se(1)-C(1)	1.965(8)
Se(2)-C(19)	1.893(11)	Se(2)-C(8)	1.979(7)	Se(3)-C(33)	1.896(9)
Se(3)-C(29)	1.964(10)	Fe(1)-C(9)	2.014(12)	Fe(2)-C(19)	2.001(9)
Fe(3)-C(33)	2.019(8)	P(1)-F(2B)	1.576(13)	P(1)-F(1B)	1.576(12)
P(1)-F(3B)	1.592(13)	P(1)-F(2A)	1.60(4)	P(1)-F(1A)	1.61(4)
P(1)-F(3A)	1.61(4)	P(2)-F(8)	1.541(15)	P(2)-F(4)	1.545(15)
P(2)-F(6)	1.546(14)	P(2)-F(7)	1.547(14)	P(2)-F(5)	1.547(14)
P(2)-F(9)	1.551(15)				
<i>Bond angles</i>					
Cl-Pt-Se(3)	176.74(7)	Cl-Pt-Se(1)		91.71(6)	
Se(3)-Pt-Se(1)	91.01(3)	Cl-Pt-Se(2)		94.07(6)	
Se(3)-Pt-Se(2)	83.32(3)	Se(1)-Pt-Se(2)		173.40(3)	
C(9)-Se(1)-C(1)	96.3(4)	C(9)-Se(1)-Pt		114.2(3)	
C(1)-Se(1)-Pt	103.5(3)	C(19)-Se(2)-C(8)		97.6(3)	
C(19)-Se(2)-Pt	97.4(3)	C(8)-Se(2)-Pt		109.3(3)	
C(33)-Se(3)-C(29)	101.6(4)	C(33)-Se(3)-Pt		108.3(3)	
C(29)-Se(3)-Pt	103.6(3)				

* The number in bracket means the standard uncertainty, s.u..

3.6 References for Chapter Three

1. E. W. Abel, N. J. Long, K. G. Orrell, A. G. Osborne, V. Sik, P. A. Bates, M. B. Hursthouse, *J. Organomet. Chem.*, 1989, **367**, 275
2. E. W. Abel, N. J. Long, K. G. Orrell, A. G. Osborne, V. Sik, P. A. Bates, M. B. Hursthouse, *J. Organomet. Chem.*, 1990, **383**, 253
3. E. W. Abel, N. J. Long, K. G. Orrell, A. G. Osborne, V. Sik, *J. Organomet. Chem.*, 1989, **378**, 473
4. E. W. Abel, N. J. Long, K. G. Orrell, A. G. Osborne, V. Sik, *J. Organomet. Chem.*, 1991, **405**, 375
5. R. V. Honeychuck, M. O. Okoroafor, L. H. Shen, C. H. Brubaker, *Organometallics*, 1986, **5**, 482
6. M. Sato, M. Sekino, M. Katada, S. Akabori, *J. Organomet. Chem.*, 1989, **377**, 327
7. M. Canales, O. Crespo, A. Fortea, M. C. Gimeno, P. G. Jones, A. Laguna, *J. Chem. Soc., Dalton Trans.*, 2002, 2250
8. M. J. Brown, J. F. Corrigan, *J. Organomet. Chem.*, 2004, **689**, 2872
9. S. Akabori, T. Kumagai, T. Shirahige, S. Sato, K. Kawazoe, C. Tamura, M. Sato, *Organometallics*, 1987, **6**, 526
10. M. Herberhold, M. Schrepfermann, A. L. Rheingold, *J. Organomet. Chem.*, 1990, **394**, 113
11. M. Herberhold, C. Dörnhöfer, A. Scholz, G. X. Jin, *Phosphorus, Sulfur and Silicon*, 1992, **64**, 161
12. M. Herberhold, G. X. Jin, W. Milius, *J. Organomet. Chem.*, 1996, **512**, 111
13. M. Herberhold, G. X. Jin, A. L. Rheingold, G. F. Sheats, *Z. Naturforsch., B: Chem. Sci.*, 1992, **47**, 1091
14. (a) R. Broussier, A. Darold, M. Kubicki, B. Gautheron, *Bull. Soc. Chim. Fr.*, 1994, **131**, 951; (b) R. Broussier, Y. Gobet, R. Amardeil, A. Da Rold, M. M. Kubicki, B. Gautheron, *J. Organomet. Chem.*, 1993, **445**, C4
15. M. Herberhold, J. Peukert, M. Krüger, D. Daschner, W. Milius, *Z. Anorg. Allg. Chem.*, 2000, **626**, 1289
16. R. V. Honeychuck, M. O. Okoroafor, L. H. Shen, C. H. Brubaker, *Organometallics*, 1986, **5**, 482

17. M. O. Okoroafor, L. H. Shen, R. V. Honeychuck, C. H. Brubaker, *Organometallics*, 1988, **7**, 1297
18. C. K. Lai, A. A. Naiini, C. H. Brubaker, *Inorg. Chim. Acta*, 1989, **164**, 205
19. A. A. Naiini, C. K. Lai, D. L. Ward, C. H. Brubaker, *J. Organomet. Chem.*, 1990, **390**, 73
20. H. M. Ali, C. H. Brubaker, *J. Mol. Catal.*, 1990, **60**, 331
21. H. Matsuzaka, J.P. Qu, T. Ogino, M. Nishio, Y. Nishibayashi, Y. Shii, S. Uemura, M. Hidai, *J. Chem. Soc., Dalton Trans.*, 1996, 4307
22. M. R. Burgess, Ph.D. Thesis, University of Wales Swansea, 1999
23. Y. Nishibayashi, J. D. Singh, S. Fukuzawa, S. Uemura, *J. Chem. Soc., Perkin Trans 1*, 1995, 2871
24. Y. Nishibayashi, J. D. Singh, S. Fukuzawa, S. Uemura, *J. Org. Chem.*, 1995, **60**, 4114
25. Y. Nishibayashi, S. K. Srivastava, H. Takada, S. I. Fukuzawa, S. Uemura, *J. Chem. Soc., Chem. Commun.*, 1995, 2321
26. Y. Nishibayashi, C. S. Cho, S. Uemura, *J. Organomet. Chem.*, 1996, **507**, 197
27. Y. Nishibayashi, K. Segawa, J. D. Singh, S. Fukuzawa, K. Ohe, S. Uemura, *Organometallics*, 1996, **15**, 370
28. Y. Nishibayashi, J. D. Singh, Y. Arikawa, S. Uemura, M. Hidai, *J. Organomet. Chem.*, 1997, **531**, 13
29. S. I. Fukuzawa, Y. Kasugahara, S. Uemura, *Tetrahedron Lett.*, 1994, **35**, 9403
30. S. I. Fukuzawa, K. Takahashi, H. Kato, H. Yamazaki, *J. Org. Chem.*, 1997, **62**, 7711
31. R. Kaur, H. B. Singh, R. P. Patel, S. K. Kulshreshtha, *J. Chem. Soc., Dalton Trans.*, 1996, 461
32. E. E. Aynsley, N. N. Greenwood, J. B. Leach, *Chem. Ind.*, 1966, 379
33. D. J. Gulliver, E. G. Hope, W. Levason, S. G. Murray, D. M. Potter, G. L. Marshall, *J. Chem. Soc., Perkin Trans.*, 1984, **2**, 429
34. C. H. W. Jones, R. D. Sharma, *Organometallics*, 1986, **5**, 805
35. E. G. Hope, W. Levason, *Coord. Chem. Rev.*, 1993, **12**, 109
36. W. Levason, S. D. Orchard, G. Reid, *Coord. Chem. Rev.*, 2002, **225**, 159
37. A. K. Singh, S. Sharma, *Coord. Chem. Rev.*, 2000, **209**, 49
38. W. Levason, S. D. Orchard, G. Reid, V. A. Tolhurst, *J. Chem. Soc., Dalton Trans.*, 1999, 2071

39. N. R. Champness, J. P. F. Kelly, W. Levason, G. Reid, A. M. Z. Slawin, D. J. Williams, *Inorg. Chem.*, 1995, **34**, 651
40. N. R. Champness, W. Levason, J. J. Quirk, G. Reid, *Polyhedron*, 1995, **14**, 2753
41. J. D. Carr, S. J. Coles, M. B. Hursthouse, J. H. R. Tucker, *J. Organomet. Chem.*, 2001, **637-639**, 304
42. S. Dey, V. K. Jain, A. Knödler, W. Kaim, S. Zálíš, *Eur. J. Inorg. Chem.*, 2001, **11**, 2965
43. S. Dey, V. K. Jain, A. Knödler, A. Klein, W. Kaim, S. Zálíš, *Inorg. Chem.*, 2002, **41**, 2864
44. B. L. Khandelwal, A. Khalid, A. K. Singh, T. P. Singh, S. Karthikeyan, *J. Organomet. Chem.*, 1996, **507**, 65
45. E. W. Abel, D. G. Evans, J. R. Koe, V. Sik, P. A. Bates, M. B. Hursthouse, *J. Chem. Soc. Dalton Trans.*, 1989, 2315
46. T. Kemmitt, W. Levason, M. Webster, *Inorg. Chem.*, 1989, **28**, 692
47. M. Hesford, W. Levason, S. D. Orchard, G. Reid, *J. Organomet. Chem.*, 2002, **649**, 214
48. A. J. Barton, W. Levason, G. Reid, A. J. Ward, *Organometallics*, 2001, **20**, 3644
49. A. K. Singh, V. Srivastava, S. K. Dhingra, J. E. Drake, J. H. E. Bailey, *Acta Crystallogr. Sect. C*, 1992, **48**, 665
50. E. W. Abel, S. K. Bhargava, K. G. Orrell, *Prog. Inorg. Chem.*, 1984, **32**, 1
51. A. J. Barton, W. Levason, G. Reid, *J. Organomet. Chem.*, 1999, **579**, 235
52. F. Mathey, A. Sevin, *Molecular Chemistry of the Transition Elements - an Introductory Course*, Wiley, 1996
53. D. F. Shriver, P.W. Atkins, *Inorganic Chemistry (3rd Ed.)*, Oxford University Press, 1999
54. N. R. Champness, P. F. Kelly, W. Levason, G. Reid, A. M. Z. Slawin, D. Williams, *Inorg. Chem.*, 1995, **34**, 651
55. M. Sato, H. Anano, *J. Organomet. Chem.*, 1998, **555**, 167
56. J.-M. Lehn, *Angew. Chem., Int. Ed. Engl.*, 1988, **112**, 90
57. B. Olenyuk, A. Fechtenkötter, P. J. Stang, *J. Chem. Soc., Dalton Trans.*, 1998, 1707
58. B. J. Holliday, C. A. Mirkin, *Angew. Chem., Int. Ed. Engl.*, 2001, **40**, 2022
59. M. Schmitz, S. Leininger, J. Fan, A. M. Artif, P. J. Stang, *Organometallics*, 1999, **18**, 4817

60. P. J. Stang, K. Chen, *J. Am. Chem. Soc.*, 1995, **117**, 1667
61. P. J. Stang, K. Chen, A. M. Arif, *J. Am. Chem. Soc.*, 1995, **117**, 8793
62. J. Manna, J. A. Whiteford, P. J. Stang, D. C. Muddiman, R. D. Smith, *J. Am. Chem. Soc.*, 1996, **118**, 8731
63. J. Manna, C. J. Kuehl, J. A. Whiteford, P. J. Stang, D. C. Muddiman, S. A. Hofstadler, R. D. Smith, *J. Am. Chem. Soc.*, 1997, **119**, 11611
64. P. J. Stang, B. Olenyuk, J. Fan, A. M. Arif, *Organometallics*, 1996, **15**, 904
65. B. Olenyuk, J. A. Whiteford, P. J. Stang, *J. Am. Chem. Soc.*, 1996, **118**, 8221
66. P. J. Stang, D. H. Cao, K. Chen, G. M. Gray, D. C. Muddiman, R. D. Smith, *J. Am. Chem. Soc.*, 1997, **119**, 5163
67. T. Habicher, J.-F. Nierengarten, V. Gramlich, F. Diederich, *Angew. Chem., Int. Ed. Engl.*, 1998, **37**, 1916
68. S.-W. Lai, M. C.-W. Chan, S.-M. Peng, C.-M. Che, *Angew. Chem., Int. Ed. Engl.*, 1999, **38**, 669
69. R.-D. Schnebeck, L. Randaccio, E. Zangrando, B. Lippert, *Angew. Chem., Int. Ed. Engl.*, 1998, **37**, 119
70. M. Fujita, O. Sasaki, T. Mitsuhashi, T. Fujita, J. Yazaki, K. Yamaguchi, K. Ogura, *Chem. Commun.*, 1996, 1535
71. M. Fujita, J. Yazaki, K. Ogura, *J. Am. Chem. Soc.*, 1990, **112**, 5645
72. M. Fujita, J. Yazaki, K. Ogura, *Tetrahedron Lett.*, 1991, **32**, 5589
73. M. Fujita, J. Yazaki, K. Ogura, *Chem. Lett.*, 1991, 1031
74. P. J. Stang, D. H. Cao, *J. Am. Chem. Soc.*, 1994, **116**, 4981
75. P. J. Stang, D. H. Cao, K. Chen, G. M. Gray, D. C. Muddiman, R. D. Smith, *J. Am. Chem. Soc.*, 1997, **119**, 5163
76. P. J. Stang, J. A. Whiteford, *Organometallics*, 1994, **13**, 3776
77. J. A. Whiteford, C. V. Lu, P. J. Stang, *J. Am. Chem. Soc.*, 1997, **119**, 2524
78. P. J. Stang, D. H. Cao, S. Saito, A. M. Arif, *J. Am. Chem. Soc.*, 1995, **117**, 6273
79. P. J. Stang, B. Olenyuk, *Angew. Chem., Int. Ed. Engl.*, 1996, **35**, 732
80. J. Fan, J. A. Whiteford, B. Olenyuk, M. D. Levin, P. J. Stang, E. B. Fleischer, *J. Am. Chem. Soc.*, 1999, **121**, 2741
81. P. J. Stang, N. E. Persky, *Chem. Commun.*, 1997, 77
82. J. A. Whiteford, P. J. Stang, S. D. Huang, *Inorg. Chem.*, 1998, **37**, 5595
83. C. Müller, J. A. Whiteford, P. J. Stang, *J. Am. Chem. Soc.*, 1998, **120**, 9827

84. H. Rauter, E. C. Hillgeris, B. Lippert, *J. Chem. Soc. Chem. Commun.*, 1992, 1385
85. H. Rauter, E. C. Hillgeris, A. Erxleben, B. Lippert, *J. Am. Chem. Soc.*, 1994, **116**, 616
86. H. Rauter, I. Mutikainen, M. Blomberg, C. J. L. Lock, P. Amo-Ochoa, E. Freisinger, L. Randaccio, E. Zangrando, E. Chiarparin, B. Lippert, *Angew. Chem., Int. Ed. Engl.*, 1997, **36**, 1296
87. J. A. R. Navarro, M. B. L. Janik, E. Freisinger, B. Lippert, *Inorg. Chem.*, 1999, **38**, 426
88. S. M. Al-Qaisi, K. J. Galat, M. Chai, D. G. Ray III, P. L. Rinaldi, C. A. Tessier, W. J. Youngs, *J. Am. Chem. Soc.*, 1998, **120**, 12149
89. F. Wurthner, A. Sautter, *Chem. Commun.*, 2000, 445

CHAPTER FOUR

Electrochemistry Study of Novel Ferrocenyl Chalcogenide Compounds and Their Transition Metal Complexes

BACKGROUND, RESULTS AND DISCUSSION

4.1 Background

As introduced in Chapter One, the electrochemical properties of carbon or silicon-bridged ferrocenes have been extensively studied. Much less progress has been made with the selenium- or tellurium-bridged compounds which may be due to the difficulty of their synthesis. The successful preparation of a series of novel ferrocenyl chalcogenide compounds and their metal complexes has provided an opportunity to study their electrochemical properties. Before presenting the results of this work, the relevant literature is summarised below in sections dealing with chalcogenaferrocenophanes, ferrocenyl alkyl chalcogenides, and polyferrocenes bridged by selenium or tellurium atoms.

The half-wave potentials listed below are referenced to $\text{FcH} / [\text{FcH}]^+$.

4.1.1 Electrochemistry of chalcogenaferrocenophanes

The half-wave oxidation potential of seleno[1]ferrocenophane, $[\text{Fe}\{(\eta\text{-C}_5\text{H}_4)_2\text{Se}\}]$ (Fig. 4.1), was found to be -20 mV in DCM at a scan rate of 250 mV s^{-1} , meaning that it is more easily oxidised than free ferrocene.¹

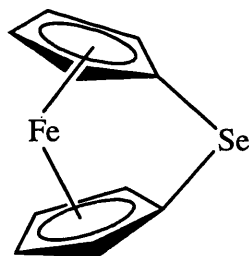


Fig. 4.1 Seleno[1]ferrocenophane $[\text{Fe}\{(\eta\text{-C}_5\text{H}_4)_2\text{Se}\}]$

Electrochemical study of chalcogena[3]ferrocenophanes (Fig. 4.2) showed that all the compounds undergo a chemically reversible one electron oxidation and all but one are less easily oxidised than free ferrocene. The oxidation potentials are progressively lowered in the sequence S, Se, Te, as these atoms are introduced into the intramolecular trichalcogen bridge. Changing the chalcogen atoms at the 1, 3-positions in the bridge causes a larger positive shift of the half-wave potential than changing that at the 2-position.²⁻⁵

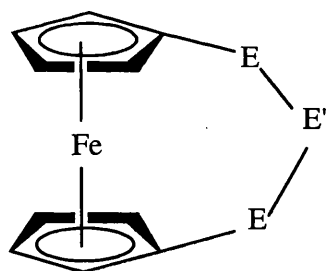


Fig. 4.2 Chalcogena [3]ferrocenophanes

Table 4.1 Half-wave potentials of some chalcogena[3]ferrocenophanes

E	E'	$E_{1/2}/\text{mV}$	Ref.
Se	Se	213	3, 4
Se	CH ₂	181	4
Se	S	252	4
S	Se	268	4
S	Te	200	2
Se	C(Ph) ₂	236	2
Se	PPh	317	2
Se	P(S)Ph	318	2
Te	Te	130	5
Te	CH ₂	-220	5
Te	S	180	5

The spiro compounds $[\text{Fe}(\text{C}_5\text{H}_4\text{Se})_2]\text{X}$ ($\text{X} = \text{Si}, \text{Sn}$) (Fig. 4.3) and the dichalcogenide $[\text{Fe}(\text{C}_5\text{H}_5)(\text{C}_5\text{H}_4\text{Se})_2]$ exhibit two consecutive one-electron oxidation steps, showing that there is an electronic interaction between the ferrocene and ferricenium units in the mono-cation through the side chain.²

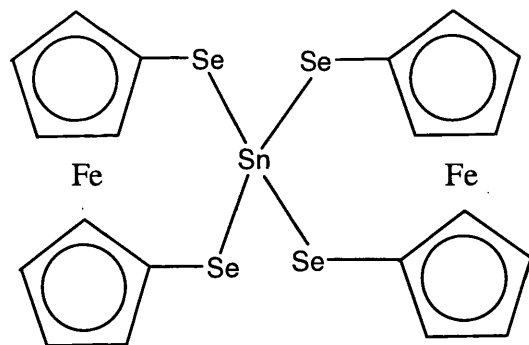


Fig. 4.3 $\text{Sn}(\text{Se}_2\text{fc})_2$

4.1.2 Electrochemistry of ferrocenyl alkyl chalcogenides

Monodentate ferrocenyl alkyl chalcogenides, $[\text{Fe}(\eta\text{-C}_5\text{H}_5)(\eta\text{-C}_5\text{H}_4\text{ER})]$ ($\text{E} = \text{Se}, \text{R} = \text{Me}, \text{Et}, \text{}^n\text{Pr}, \text{}^n\text{Bu}, \text{}^n\text{Pent}, \text{Hex}, \text{Oct}, \text{}^i\text{Pr}, \text{}^i\text{Bu}, \text{}^i\text{Pent}, \text{CH}_2\text{Ph}$; $\text{E} = \text{Te}, \text{R} = \text{Me}, \text{Et}, \text{}^n\text{Pr}, \text{}^n\text{Bu}, \text{}^n\text{Pent}, \text{Hex}, \text{Oct}, \text{}^i\text{Pr}, \text{}^i\text{Bu}, \text{}^i\text{Pent}, p\text{-C}_6\text{H}_4\text{OMe}$) (Fig. 4.4), undergo a one electron reversible oxidation at slightly more positive potentials than free ferrocene (about 25 to 70 mV depending on the substituent). The tellurides exhibit a second quasi-reversible process at higher potentials due to the tellurium acting as a redox centre (about 320 to 435 mV depending on the substituent).^{6,7}

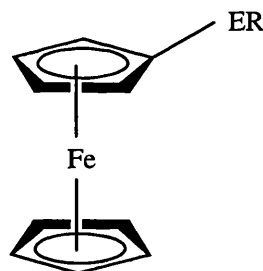


Fig. 4.4 $[\text{Fe}(\eta\text{-C}_5\text{H}_5)(\eta\text{-C}_5\text{H}_4\text{ER})]$ ($\text{E} = \text{Se}$ or Te)

Bidentate 1,1'-disubstituted ferrocene tellurium ligands of the type $[\text{Fe}(\eta\text{-C}_5\text{H}_4\text{TeR})_2]$ ($\text{R} = \text{Me}, \text{}^n\text{Bu}, \text{C}_6\text{H}_5, p\text{-C}_6\text{H}_4\text{OMe}, p\text{-C}_6\text{H}_4\text{OEt}$) (Fig. 4.5) also show a well-defined quasi-reversible single-electron redox wave at a more positive potential compared to the mono-substituted derivatives.⁶ The oxidation potential of 1,1'-bis(methylseleno)ferrocene (24 mV) is more negative than those of chalcogen-bridged ferrocenes, for example, fcSe_3 (213 mV).⁴

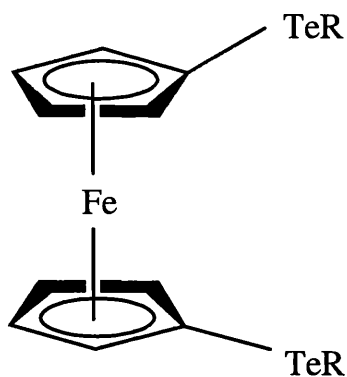


Fig. 4.5 $[\text{Fe}(\eta\text{-C}_5\text{H}_4\text{TeR})_2]$

4.1.3 Electrochemistry of poly-ferrocenes linked by selenium and tellurium bridges

CVs of Fc_2Se and Fc_2Se_2 show two oxidation waves with $\Delta E_{1/2}$ of 220 mV and 140 mV respectively in acetonitrile. So a -Se- bridge allows a greater inductive communication between the two ferrocene moieties than does a -CH₂- bridge ($\Delta E_{1/2} = 170$ mV in Fc_2CH_2),⁸ but less than a -S- bridge ($\Delta E_{1/2} = 290$ mV in Fc_2S). The first half-wave potential of Fc_2Se_2 shifts 70 mV positively compared to that of Fc_2Se , and further still compared to that of diferrocenylmethane.⁹

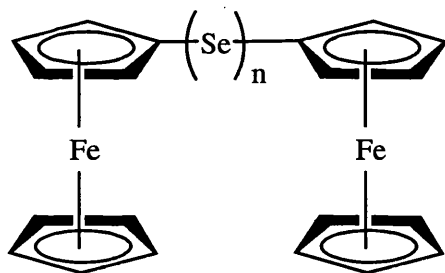


Fig. 4.6 Fc_2Se_n ($n = 1, 2$)

The electrochemical behaviour of the trinuclear and tetranuclear chalcogen-bridged ferrocenes Fc-E-fc-E-Fc (Fig. 4.7) and $\text{Fc-E-fc-EE-fc-E-Fc}$ (Fig. 4.8) has been studied in dichloromethane solution ($\text{E} = \text{Se}$ or Te). The trinuclear selenium complex showed a similar redox pattern to its sulphur analogue with three oxidation steps; the

expected reversible one-electron oxidation of each ferrocene unit takes place through two nearly overlapping one-electron steps followed by a one-electron process at higher potential. The trinuclear tellurium complex showed a different pattern with three well separated oxidation steps, one of which may be associated with Te, which can act as a redox centre. The separation between the potentials of the first two steps decreases in the order $S \geq Se > Te$. The tetranuclear selenium species behaves like its sulphur analogue, with a single two-electron oxidation of the terminal ferrocenyl units, followed by two separate one-electron steps centred on the inner chalcogen-bridged diferrocene unit; the behaviour of the tellurium analogue is more complicated.¹⁰

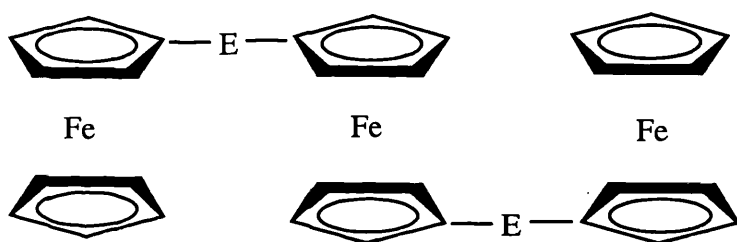


Fig. 4.7 Fc-E-fc-E-Fc

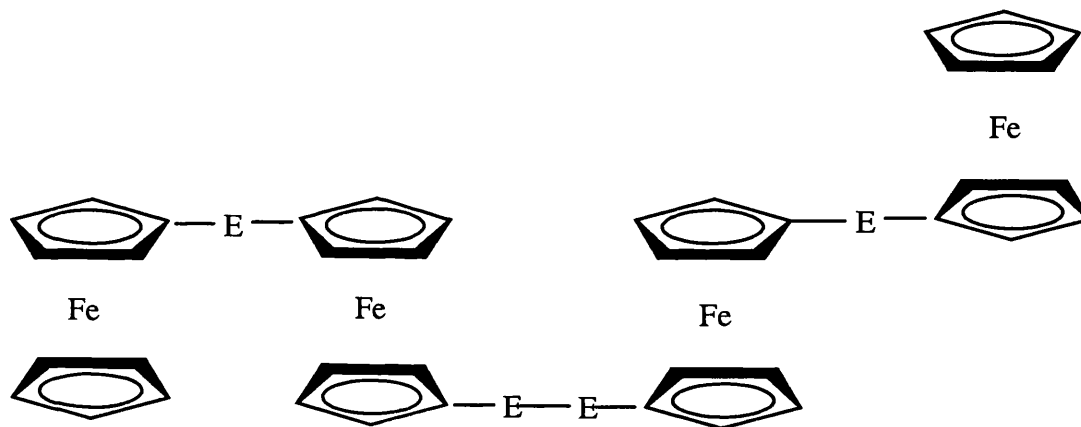


Fig. 4.8 Fc-E-fc-EE-fc-E-Fc

Poly-[Fe(C₅H₃ⁿBuSe)(C₅H₄Se)] exhibits metal-metal interactions ($\Delta E_{1/2} = 285$ mV) similar to those in the S₂-bridged analogues.¹¹

4.1.4 Electrochemistry of transition metal complexes

In an electrochemical study, $[M_2\{\mu-\eta^1\text{-Fe}(\eta^5\text{-C}_5\text{H}_4\text{Se})_2\}_2(\text{P}^n\text{Bu}_3)_2]$ ($M = \text{Pd}, \text{Pt}$) (Fig. 4.9) exhibited two one-electron redox waves indicating electronic communication between the two Fe centres. The difference between the first and second ferrocenyl oxidations, $\Delta E_{1/2}$, was 162 mV for the Pd complex and 135 mV for the Pt one. Although $[\text{Pt}\{\eta^2\text{-Fe}(\eta^5\text{-C}_5\text{H}_4\text{Se})_2\}(\text{P}^n\text{Bu}_3)_2]$ also has two one-electron oxidation waves, the second wave at higher potential was assigned to the one-electron oxidation of one of the Se atoms.¹²

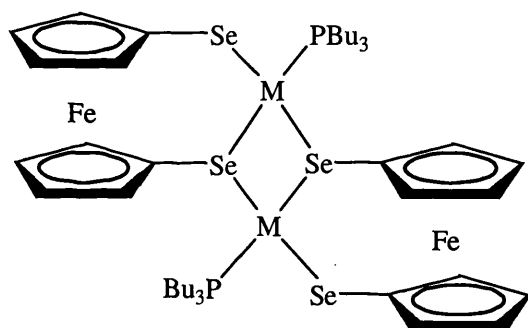


Fig. 4.9 $[M_2\{\mu-\eta^1\text{-Fe}(\eta^5\text{-C}_5\text{H}_4\text{Se})_2\}_2(\text{P}^n\text{Bu}_3)_2]$ ($M = \text{Pd}, \text{Pt}$)

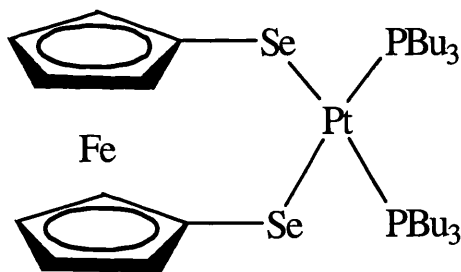


Fig. 4.10 $[\text{Pt}\{\eta^2\text{-Fe}(\eta^5\text{-C}_5\text{H}_4\text{Se})_2\}(\text{P}^n\text{Bu}_3)_2]$

4.2 Electrochemistry of novel ferrocenyl chalcogenide compounds

The new ferrocenyl chalcogenide compounds were studied by cyclic and differential pulse voltammetries to investigate the behaviour of the ferrocenium-ferrocene redox couple.

4.2.1 FcE(CH₂)_nE'Fc (E, E' = Se or Te; n = 0, 1, 2, 3)

In this part of the work, several series of selenium- and tellurium-bridged diferrocenes, comprising diferrocenyl chalcogenides, diferrocenyl dichalcogenides, and bis(ferrocenylchalcogeno)alkanes were studied by cyclic and differential pulse voltammetries, in order to observe the effect of bridge length upon the electrochemistry.

Shu *et al.* reported that Fc₂Se and Fc₂Se₂ showed two waves centred on the ferrocenyl fragment in the cyclic voltammogram with the half wave potential difference $\Delta E_{1/2} = 220$ mV and 140 mV respectively.⁸ In order to make the study more comprehensive, these two compounds were also checked.

The cyclic voltammogram of diferrocenyl selenide showed two clearly reversible one-electron oxidation processes, with $E_{1/2}$ values of 26 mV and 234 mV, $\Delta E_{1/2} = 208$ mV. The cyclic voltammogram of diferrocenyl diselenide was similar, showing two clearly reversible waves with $E_{1/2}$ values of 84 mV and 245 mV, $\Delta E_{1/2} = 161$ mV. The CV and DPV of Fc₂Se₂ are shown in Fig.'s 4.11 and 4.12. These data are in accord with the literature results. The ferrocenyl units are not acting independently in these two compounds; the interaction in FcSeSeFc is weaker than that in FcSeFc.

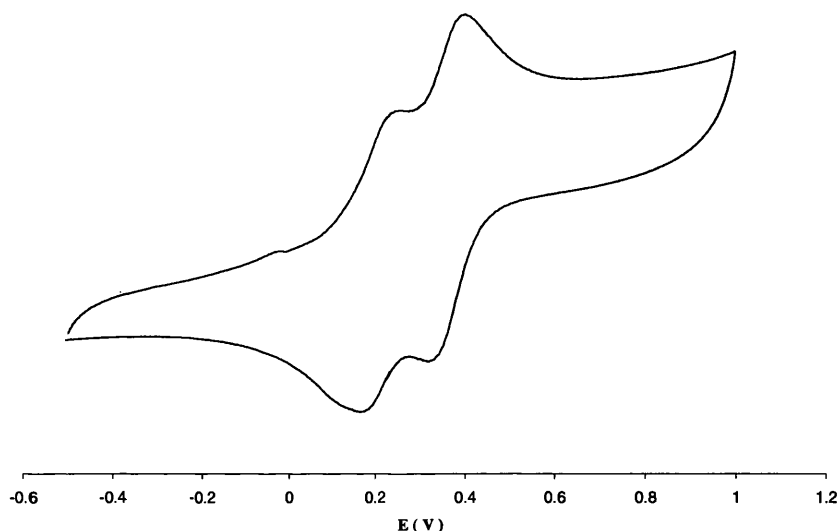


Fig. 4.11 CV of FcSeSeFc in dry acetonitrile, 0.1 M [NBu₄][PF₆] at a scan rate of 100 mV s⁻¹

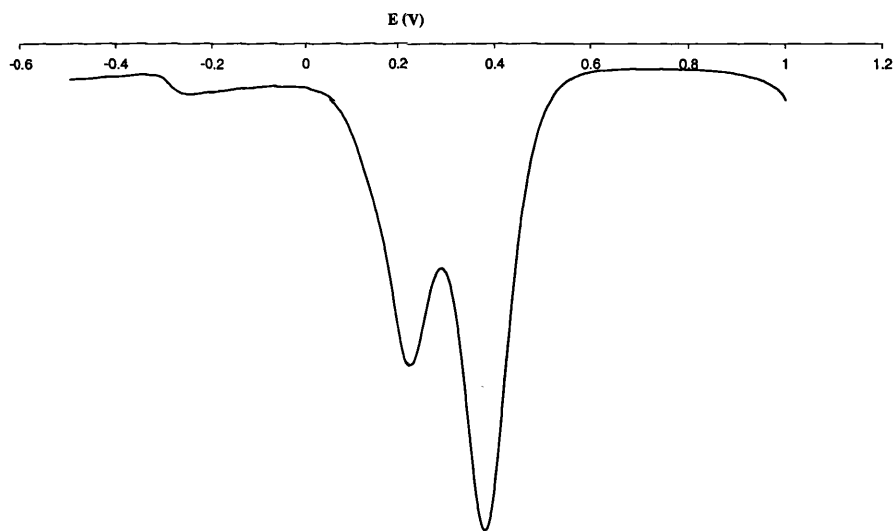


Fig. 4.12 DPV of FcSeSeFc in dry acetonitrile, 0.1 M [NBu₄][PF₆] at a scan rate of 100 mV s⁻¹

The cyclic voltammogram of FcSeCH₂SeFc also showed two waves: $E_{1/2}(1) = 41$ mV ($|E_{pa} - E_{pc}| = 66$ mV) and $E_{1/2}(2) = 145$ mV ($|E_{pa} - E_{pc}| = 77$ mV). The separation of the two half wave potentials has decreased to 111 mV from its value in Fc₂Se₂, showing that the interaction between the two ferrocene units has become weaker. The CV and DPV of FcSeCH₂SeFc are shown in Fig.s' 4.13 and 4.14.

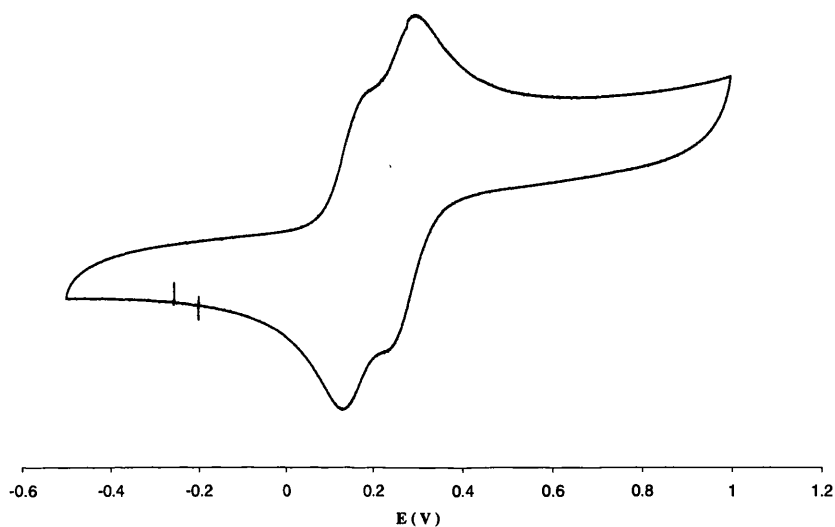


Fig. 4.13 CV of FcSeCH₂SeFc in dry acetonitrile, 0.1 M [NBu₄][PF₆] at a scan rate of 100 mV s⁻¹

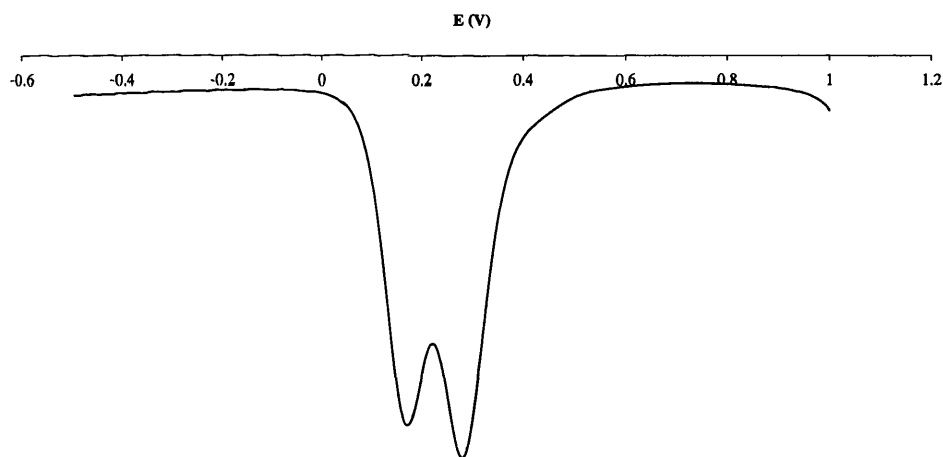


Fig. 4.14 DPV of FcSeCH₂SeFc in dry acetonitrile, 0.1 M [NBu₄][PF₆] at a scan rate of 100 mV s⁻¹

Introducing a longer hydrocarbon chain results in only one well-defined quasi-reversible wave, as observed for FcSe(CH₂)₂SeFc with $E_{1/2} = 72$ mV ($|E_{pa} - E_{pc}| = 130$ mV) (the CV of FcSe(CH₂)₂SeFc is shown in Fig. 4.15). Similarly, FcSe(CH₂)₃SeFc has one well resolved quasi-reversible wave, $E_{1/2} = 48$ mV ($|E_{pa} - E_{pc}| = 102$ mV) (the CV of FcSe(CH₂)₃SeFc is shown in Fig. 4.16).

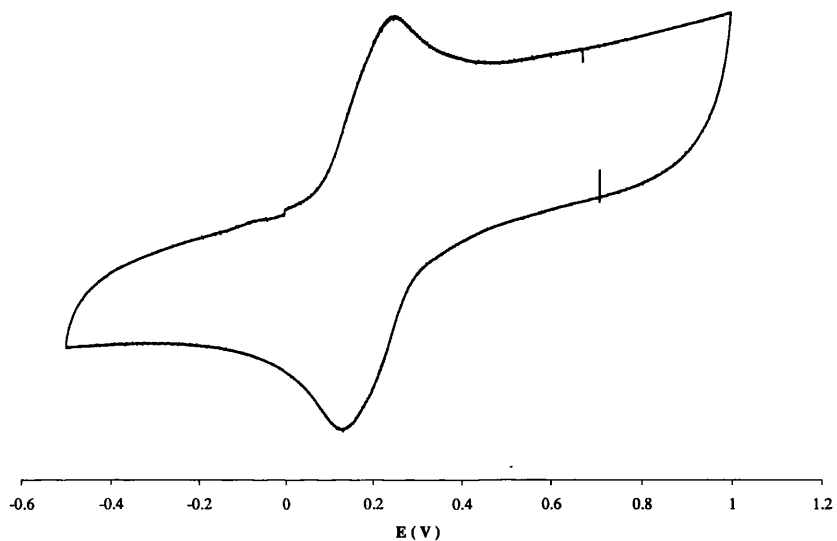


Fig. 4.15 CV of $\text{FcSe}(\text{CH}_2)_2\text{SeFc}$ in dry acetonitrile, 0.1 M $[\text{NBu}_4][\text{PF}_6]$ at a scan rate of 100 mV s^{-1}

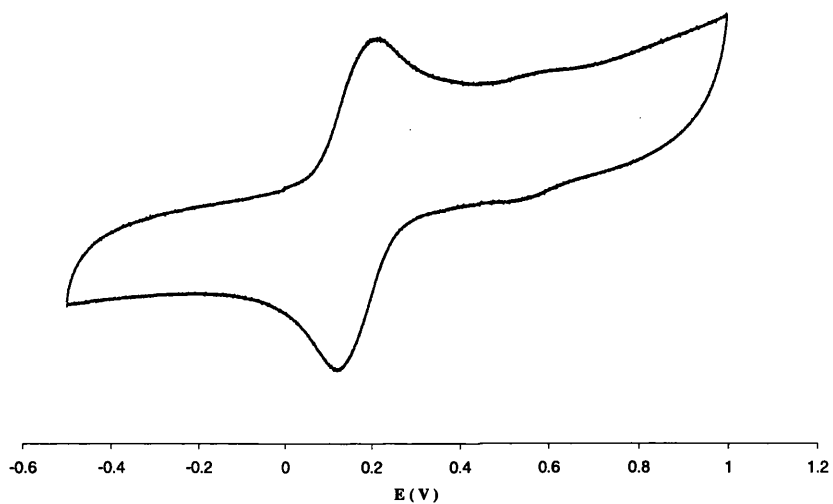


Fig. 4.16 CV of $\text{FcSe}(\text{CH}_2)_3\text{SeFc}$ in dry acetonitrile, 0.1 M $[\text{NBu}_4][\text{PF}_6]$ at a scan rate of 100 mV s^{-1}

The half-wave potentials ($E_{1/2}$) determined by CV, and the peak potentials (E_p) measured by DPV of the above compounds are listed in Table 4.2.

Table 4.2 CV and DPV results for FcSeFc and FcSe(CH₂)_nSeFc (n = 0, 1, 2, 3)

	E_1		E_2	
	<u>CV</u>	<u>DPV</u>	<u>CV</u>	<u>DPV</u>
	$E_{1/2} (E_{pa} - E_{pc})$	E_p	$E_{1/2} (E_{pa} - E_{pc})$	E_p
Fc ₂ Se	26 (65)	35	234 (60)	236
Fc ₂ Se ₂	84 (73)	96	245 (83)	252
FcSeCH ₂ SeFc	41 (66)	40	145 (77)	151
FcSe(CH ₂) ₂ SeFc	72 (130)	96	-	-
FcSe(CH ₂) ₃ SeFc	48 (102)	50	-	-

The $E_{1/2}/E_p$ values of the selenium-containing compounds are all more positive than that of ferrocene itself. This can be attributed to the electronegative selenium atom, which is bonded directly to the Cp ring, causing the oxidation to be more difficult than that of unsubstituted ferrocene.^{7, 13}

There are two possible mechanisms for communication between ferrocenes: "through space" or "through bond". The two waves observed in the cyclic voltammograms of FcSeFc, FcSeSeFc and FcSeCH₂SeFc indicate that the ferrocenyl moieties are not acting independently. With increased distance between the ferrocenyl moieties the interaction between them decreases quickly: $\Delta E_{1/2} = 208, 161$ and 111 mV respectively. Comparison between the behaviour of FcSeSeFc and that of FcCH₂CH₂Fc shows the importance of the nature of the bridging atoms (particularly those bound directly to the cyclopentadienyl rings): the cyclic voltammogram of FcSeSeFc shows two waves, whereas for FcCH₂CH₂Fc there is only one.⁸ It is therefore generally accepted that the through bond mechanism is operating in these systems. Only one wave was observed in FcSe(CH₂)₂SeFc and FcSe(CH₂)₃SeFc, suggesting that the two iron centres are oxidised in one step, undergoing independent one-electron transfer at the same potential. Thus in the series of bis(ferrocenylseleno)alkanes, FcSe(CH₂)_nSeFc, as the length of the hydrocarbon chain increases, the Fe...Fe through bond distance becomes greater, and the difference between the two half-wave potentials decreases, until it is undetectable when $n \geq 2$.

The electrochemical data obtained for the diferrocenyl tellurides are more complicated. The cyclic voltammogram of diferrocenyl telluride showed two

reversible waves, with $E_{1/2}$ values of 6 mV and 221 mV ($\Delta E_{1/2} = 215$ mV), and one quasi-reversible wave with an $E_{1/2}$ value of 376 mV. With the benefit of the information obtained for ferrocenyl alkyl tellurides,⁷ we can easily attribute the third wave to the tellurium acting as a redox centre.

Similarly there exist three waves for diferrocenyl ditelluride, with $E_{1/2}$ values of 35 mV and 172 mV for the ferrocenyl moieties, $\Delta E_{1/2} = 137$ mV. The oxidation process centred on Te can't be clearly resolved by CV (Fig. 4.17), but DPV (Fig. 4.18) gives a better result. The difference between the value of ΔE in FcTeFc and FcTeTeFc is 78 mV, so the effect of adding an extra chalcogen atom is greater than for the Se analogues (the difference is 47 mV between the $\Delta E_{1/2}$ values for FcSeFc and FcSeSeFc). This is in accordance with the difference in Fe...Fe through bond distance (10.21 Å for Fc₂Se₂, 11.01 Å for Fc₂Te₂).^{14,15}

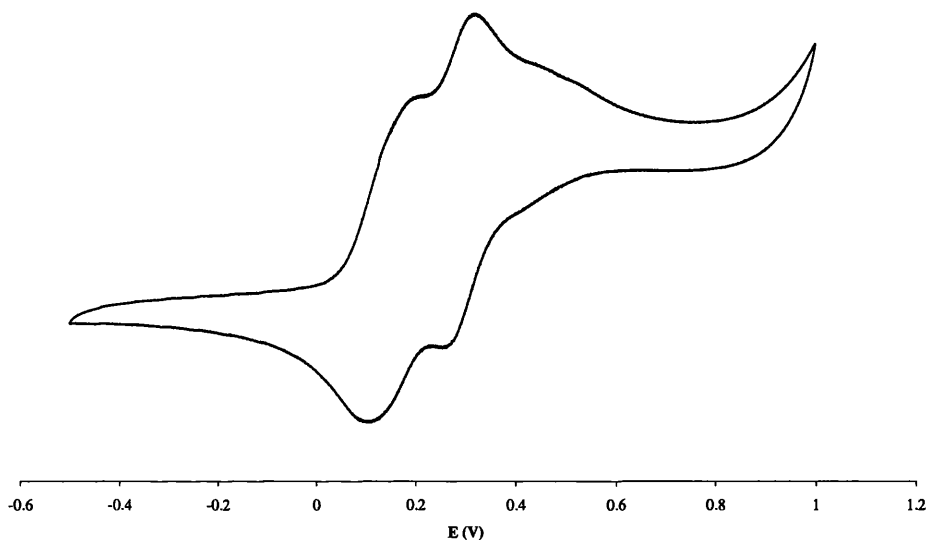


Fig. 4.17 CV of FcTeTeFc in dry acetonitrile, 0.1 M [NBu₄][PF₆] at a scan rate of 100 mV s⁻¹

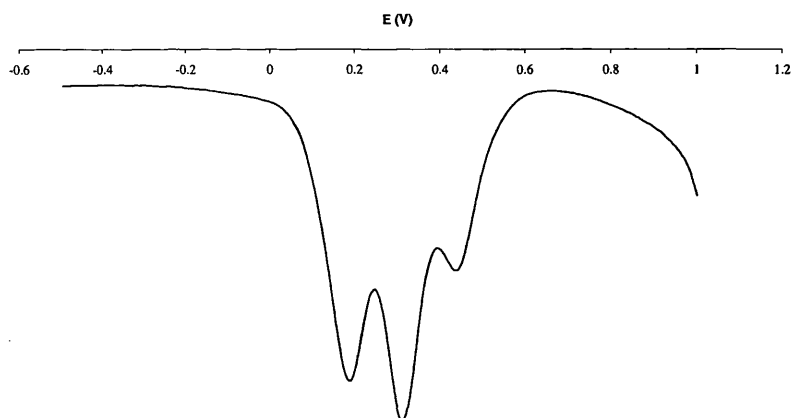


Fig.4.18 DPV of FcTeTeFc in dry acetonitrile, 0.1 M [NBu₄][PF₆] at a scan rate of 100 mV s⁻¹

The communication between the ferrocenyl groups decreases in FcTeCH₂TeFc, with $\Delta E_{1/2} = 99$ mV, 12 mV less than in FcSeCH₂SeFc. Based on the behaviour of its Se analogue, FeTe(CH₂)₃TeFc should exhibit no interaction between the iron centres; as expected the cyclic voltammogram contains only one ferrocene-based wave (the CV and DPV are shown in Fig.'s 4.19 and 4.20). This occurs, however, at unusually low potential ($E_{1/2} = -11$ mV); the tellurium-based wave with $E_{1/2} = 410$ mV also has quite a large separation between cathodic and anodic peaks ($|E_{pa} - E_{pc}| = 268$ mV). There is no explanation for these features at present.

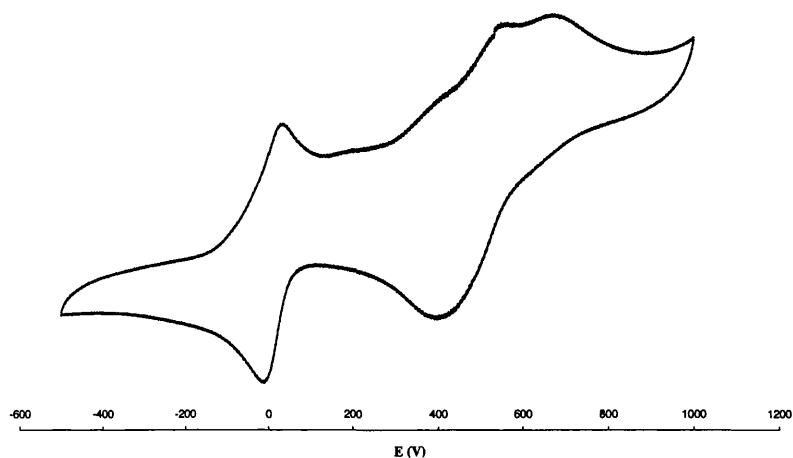


Fig.4.19 CV of FcTe(CH₂)₃TeFc in dry acetonitrile, 0.1 M [NBu₄][PF₆] at a scan rate of 100 mV s⁻¹

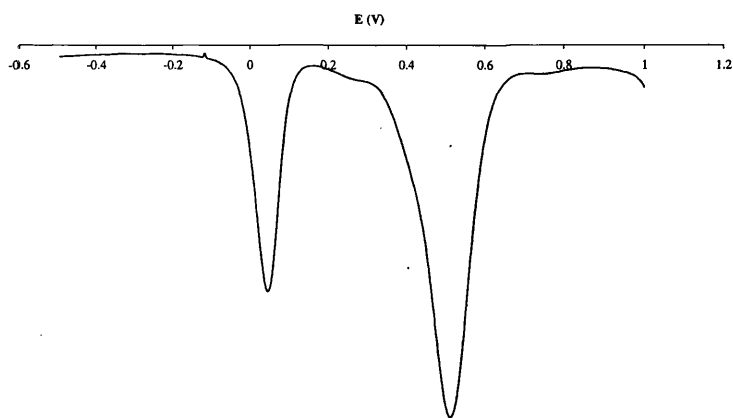


Fig. 4.20 DPV of $\text{FcTe}(\text{CH}_2)_3\text{TeFc}$ in dry acetonitrile, 0.1 M $[\text{NBu}_4][\text{PF}_6]$ at a scan rate of 100 mV s^{-1}

More complicated electrochemical behaviour might have been predicted for $\text{FcSe}(\text{CH}_2)_3\text{TeFc}$, but it appears that the oxidation potentials of the two chemically different ferrocene units are too close for the resolution of separate features in the voltammograms (Fig. 4.21). The relative intensity of the tellurium-based redox process ($E_{1/2} = 352 \text{ mV}$) is of course approximately half that exhibited by the compounds containing two tellurium atoms.

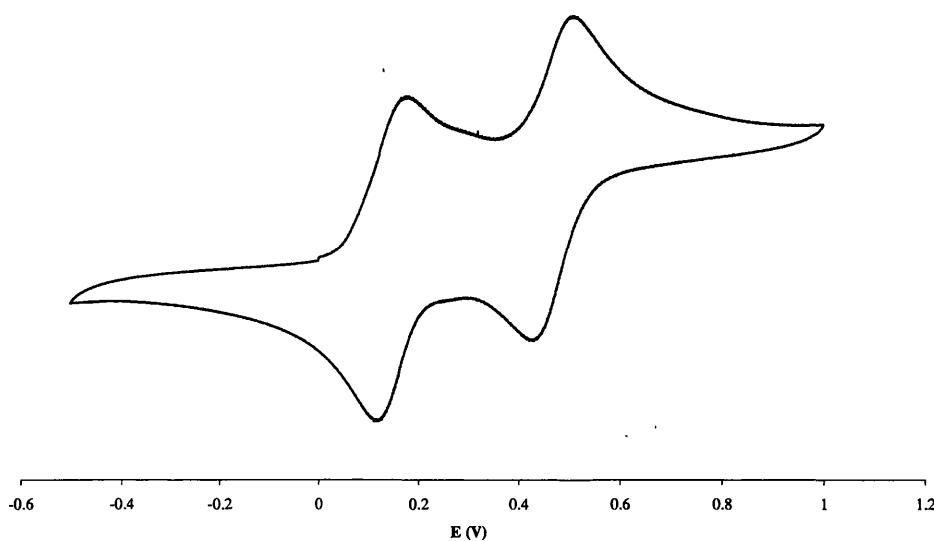


Fig.4.21 CV of $\text{FcSe}(\text{CH}_2)_3\text{TeFc}$ in dry acetonitrile, 0.1 M $[\text{NBu}_4][\text{PF}_6]$ at a scan rate of 100 mV s^{-1}

The half wave potentials ($E_{1/2}$) determined by CV, and the peak potentials (E_p) measured by DPV of the above compounds are listed in Table 4.3.

Table 4.3 CV and DPV results for FcTeFc, FcTe(CH₂)_nTeFc (n = 0, 1, 3) and FcSe(CH₂)₃TeFc in dry acetonitrile, 0.1 M [NBu₄][PF₆] at a scan rate of 100 mV s⁻¹

	E_1		E_2		E_3	
	<u>CV</u> $E_{1/2} (E_{pa} - E_{pc})$	<u>DPV</u> E_p	<u>CV</u> $E_{1/2} (E_{pa} - E_{pc})$	<u>DPV</u> E_p	<u>CV</u> $E_{1/2} (E_{pa} - E_{pc})$	<u>DPV</u> E_p
Fc ₂ Te	6 (65)	5	221 (52)	237	376 (88)	402
Fc ₂ Te ₂	35 (93)	60	172 (69)	186	unresolved	312
FcTeCH ₂ TeFc	27 (56)	35	126 (70)	130	364 (99)	362
FcTe(CH ₂) ₃ TeFc	-11 (92)	-26	-	-	410 (268)	393
FcSe(CH ₂) ₃ TeFc	31 (71)	38	-	-	352 (95)	357

4.2.2 Other ferrocenyl chalcogenide ligands

4.2.2.1 $\text{FcE}(\text{CH}_2)_3\text{E}'(\text{CH}_2)_3\text{EFc}$

The crystal structure data of $\text{FcSe}(\text{CH}_2)_3\text{Se}(\text{CH}_2)_3\text{SeFc}$ show that the through-bond distance between the iron atoms is 21.78 Å, too long for significant interaction. It's not surprising therefore that only one wave is observed in the cyclic voltammogram; $E_{1/2} = 43$ mV, quite similar to that in $\text{FcSe}(\text{CH}_2)_3\text{SeFc}$. In the cyclic voltammogram of $\text{FcSe}(\text{CH}_2)_3\text{Te}(\text{CH}_2)_3\text{SeFc}$ there are two reversible waves: $E_{1/2} = 60$ and 254 mV. From the results for $\text{FcSe}(\text{CH}_2)_3\text{Se}(\text{CH}_2)_3\text{SeFc}$ and $\text{FcTe}(\text{CH}_2)_n\text{TeFc}$, it can be concluded that only the first one is based on the ferrocenes, and the second one is based on tellurium. The other tellurium-containing compounds, $\text{FcTe}(\text{CH}_2)_3\text{E}'(\text{CH}_2)_3\text{TeFc}$ ($\text{E}' = \text{Se}$ or Te), behave similarly, the only significant difference being that the relative intensity of the tellurium-based redox process depends on the number of tellurium atoms in the compound.

The half wave potentials ($E_{1/2}$) determined by cyclic voltammetry, and the peak potentials (E_p) measured by CV and DPV of these four compounds are listed in Table 4.4.

Table 4.4 CV and DPV results for $\text{FcE}(\text{CH}_2)_3\text{E}'(\text{CH}_2)_3\text{EFc}$ ($\text{E}, \text{E}' = \text{Se}$ or Te) (mV) in dry acetonitrile, 0.1 M $[\text{NBu}_4][\text{PF}_6]$ at a scan rate of 100 mV s^{-1}

E	Se	Se	Te	Te
E'	Se	Te	Se	Te
<u>CV</u>	43(75)	60 (100)	43 (106)	66 (90)
$E_{1/2} (E_{pa} - E_{pc})$		254 (77)	332 (72)	281 (63)
<u>DPV</u>	46	51	80	73
E_p		253	362	308

From the above results, it can be assumed that a longer hydrocarbon chain will not affect the electrochemistry, so the two $\text{FcE}(\text{CH}_2)_3\text{Se}(\text{CH}_2)_3\text{Se}(\text{CH}_2)_3\text{EFc}$ ($\text{E} = \text{Se}$ or Te) compounds were not checked.

4.2.2.2 FcECH₂C₆H₄CH₂EFc (E = Se or Te)

The cyclic voltammogram of FcSeCH₂C₆H₄CH₂SeFc only showed one well-defined wave, $E_{1/2} = 55$ mV ($|E_{pa} - E_{pc}| = 88$ mV), which is in the same region as those for FcSe(CH₂)₃SeFc and FcSeCH₂Ph.⁷

Like FcTe(CH₂)₃EFc (E = Se or Te), the cyclic voltammogram of FcTeCH₂C₆H₄CH₂TeFc, contains only one well-defined reversible ferrocene-based wave (Fig. 4.22) at $E_{1/2} = 70$ mV ($|E_{pa} - E_{pc}| = 70$ mV) and a tellurium-based quasi-reversible wave with $E_{1/2} = 370$ mV ($|E_{pa} - E_{pc}| = 184$ mV).

The *p*-xylene group is therefore no more effective at facilitating interaction between the ferrocenes than a saturated hydrocarbon bridge.

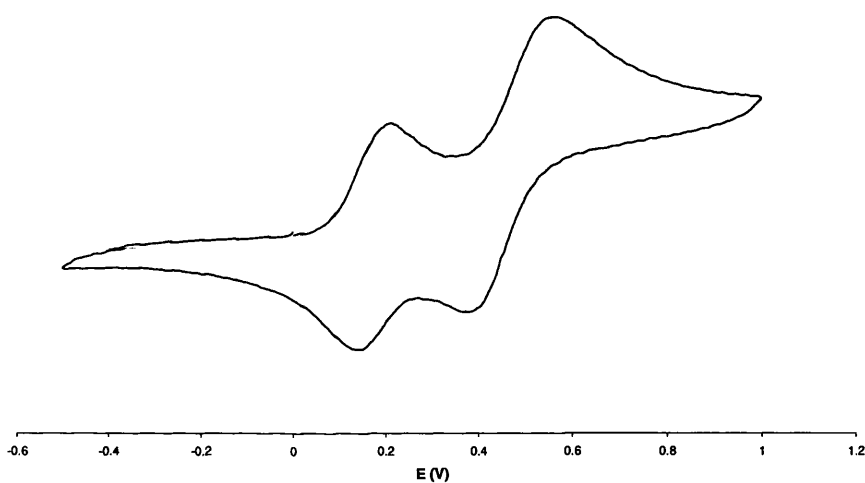


Fig. 4.22 CV of FcTeCH₂C₆H₄CH₂TeFc in dry acetonitrile, 0.1 M [NBu₄][PF₆] at a scan rate of 100 mV s⁻¹

4.2.2.3 fcSe₄ and difcSe₄

The half-wave potential of fcSe₄ is 32 mV, with $|E_{pa} - E_{pc}| = 97$ mV, similar to that of 1,1'-bis(methylseleno)ferrocene (24 mV).⁴ Compared to mono-substituted compounds, the 1,1'-ferrocenediyl unit is generally a little easier to oxidise. This is however, not the case for difcSe₄, which has $E_{1/2} = 76$ mV ($|E_{pa} - E_{pc}| = 124$ mV). In these two macrocyclic compounds, no redox process centered on the selenium atoms was observed up to potentials as high as 2 V, in contrast to the behavior of the open chain compounds.

4.3 Electrochemistry of transition metal complexes

4.3.1 $[M\{FcE(CH_2)_3E'Fc\}_2](PF_6)_2$ ($M = Pd$ or Pt , $E, E' = Se$ or Te)

Cyclic voltammetry (supplemented by differential pulse voltammetry where appropriate) was used to investigate the electrochemistry of the complexes in acetonitrile solution. From the studies of the ligands and related systems, communication between the ferrocenyl groups is believed to occur by a “through bond”, rather than a “through space” mechanism. The through-bond distance between the iron atoms for each complex was obtained from the crystal structure data. In $FcSe(CH_2)_3SeFc$ this distance is 14.79 Å, too long for significant interaction, and only one wave is observed in the cyclic voltammogram (CV). On complexation, however, the through bond $Fe\cdots Fe$ distance becomes shorter, 12.75 Å ($[Pd\{FcSe(CH_2)_3SeFc\}_2](PF_6)_2$) and 12.71 Å ($[Pt\{FcSe(CH_2)_3SeFc\}_2](PF_6)_2$), and communication between the ferrocenyl moieties is established. Two quasi-reversible waves are observed in the CV of $[Pd\{FcSe(CH_2)_3SeFc\}_2](PF_6)_2$ at $E_{1/2}(1) = 96$ mV and $E_{1/2}(2) = 297$ mV (with respect to $FcH/[FcH]^+$), the difference between the first and second ferrocenyl oxidations, $\Delta E_{1/2}$, being 201 mV (CV in Fig. 4.23 and DPV in Fig. 4.24).

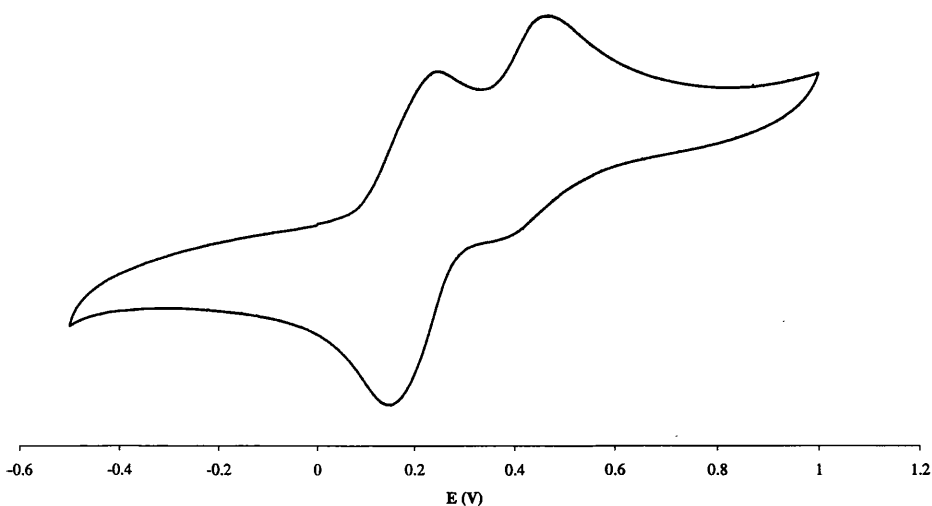


Fig. 4.23 CV of $[Pd\{FcSe(CH_2)_3SeFc\}_2](PF_6)_2$ in dry acetonitrile, 0.1 M $[NBu_4][PF_6]$ at a scan rate of 100 mV s^{-1}

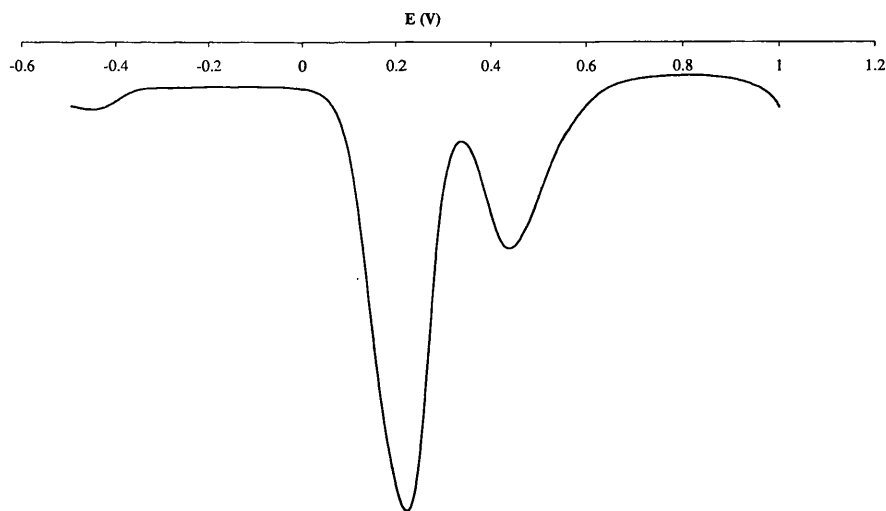


Fig. 4.24 DPV of $[\text{Pd}\{\text{FcSe}(\text{CH}_2)_3\text{SeFc}\}_2](\text{PF}_6)_2$ in dry acetonitrile, 0.1 M $[\text{NBu}_4][\text{PF}_6]$ at a scan rate of 100 mV s^{-1}

For $[\text{Pt}\{\text{FcSe}(\text{CH}_2)_3\text{SeFc}\}_2](\text{PF}_6)_2$, there are one quasi-reversible wave at $E_{1/2}(1) = 59 \text{ mV}$ and another at $E_{1/2}(2) = 305 \text{ mV}$, $\Delta E_{1/2} = 246 \text{ mV}$ (CV in Fig. 4.25 and DPV in Fig. 4.26). The change from palladium to platinum slightly increases the extent of electronic interaction between the two iron centres, which is in accord with their through bond $\text{Fe}\cdots\text{Fe}$ distances. Related ferrocenylthiolates and ferrocenylselenolates showed the opposite trend, which may imply a difference in behaviour between anionic and neutral ligands.^{16, 17} For both $[\text{Pd}\{\text{FcSe}(\text{CH}_2)_3\text{SeFc}\}_2](\text{PF}_6)_2$ and $[\text{Pt}\{\text{FcSe}(\text{CH}_2)_3\text{SeFc}\}_2](\text{PF}_6)_2$ (and the other four complexes discussed below) the lowest oxidation potential of the complex is more positive than that of the “free” ligand, $\text{FcSe}(\text{CH}_2)_3\text{SeFc}$: this effect has previously been assigned to the electron-withdrawing nature of the $\text{M}(\text{II})$ ($\text{M} = \text{Pd}, \text{Pt}$) centre.¹⁸

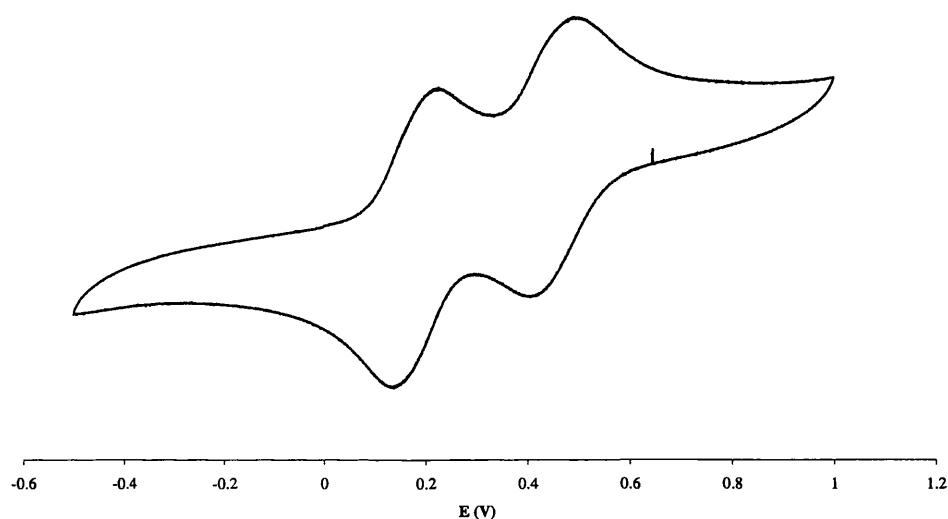


Fig. 4.25 CV of $[\text{Pt}\{\text{FcSe}(\text{CH}_2)_3\text{SeFc}\}_2](\text{PF}_6)_2$ in dry acetonitrile, 0.1 M $[\text{NBu}_4][\text{PF}_6]$ at a scan rate of 100 mV s^{-1}

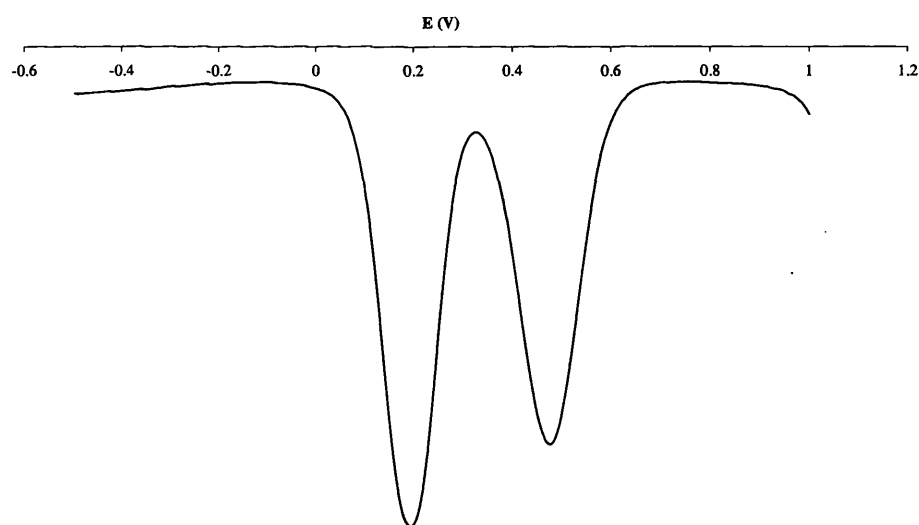


Fig. 4.26 DPV of $[\text{Pt}\{\text{FcSe}(\text{CH}_2)_3\text{SeFc}\}_2](\text{PF}_6)_2$ in dry acetonitrile, 0.1 M $[\text{NBu}_4][\text{PF}_6]$ at a scan rate of 100 mV s^{-1}

In the cyclic voltammograms of $\text{FcTe}(\text{CH}_2)_3\text{EFc}$ ($\text{E} = \text{Se}, \text{Te}$) there are two waves, but only one corresponds to ferrocene oxidation; the other is associated with the tellurium. Although precise bond length data are not available for these compounds, as their crystal structures have not been determined, it can be safely assumed that the

through-bond Fe...Fe distances are greater than in the analogous selenide (probably by *ca.* 0.18 Å and 0.36 Å for E = Se and Te respectively). The lack of interaction between the ferrocenes is therefore as expected.

On complexation, FcTe(CH₂)₃SeFc behaves like its all-selenium analogue, in that communication between the ferrocenes is established as a result of the decreased through-bond distance (13.16 Å in [Pd{FcSe(CH₂)₃TeFc}₂](PF₆)₂ and 13.09 Å in [Pt{FcSe(CH₂)₃TeFc}₂](PF₆)₂), and two ferrocene-based waves are observed in the cyclic voltammograms.

By contrast, the complexes of FcTe(CH₂)₃TeFc ([Pd{FcTe(CH₂)₃TeFc}₂](PF₆)₂ and [Pt{FcTe(CH₂)₃TeFc}₂](PF₆)₂) show only one wave (the CV and DPV of [Pd{FcTe(CH₂)₃TeFc}₂](PF₆)₂ are shown in Fig.'s 4.27, 4.28). The longer through-bond Fe...Fe distance presumably exceeds the threshold for interaction between the ferrocene moieties, which must therefore be in the range 13.17 – 13.37 Å. For both series of complexes, oxidation at tellurium occurs outside the potential range employed; the change from the behaviour of the free ligand may be explained at a simple level on the basis of the use of a lone pair in bonding to the metal.

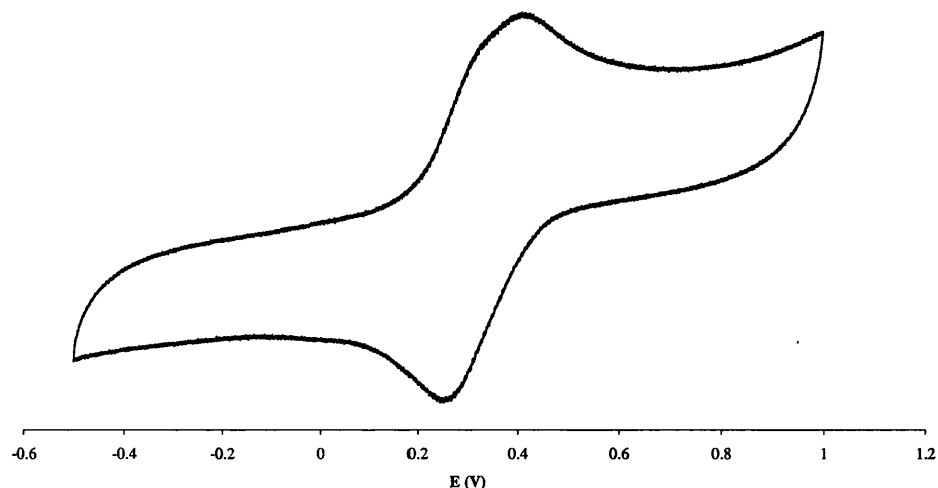


Fig. 4.27 CV of [Pd{FcTe(CH₂)₃TeFc}₂](PF₆)₂ in dry acetonitrile, 0.1 M [NBu₄][PF₆] at a scan rate of 100 mV s⁻¹

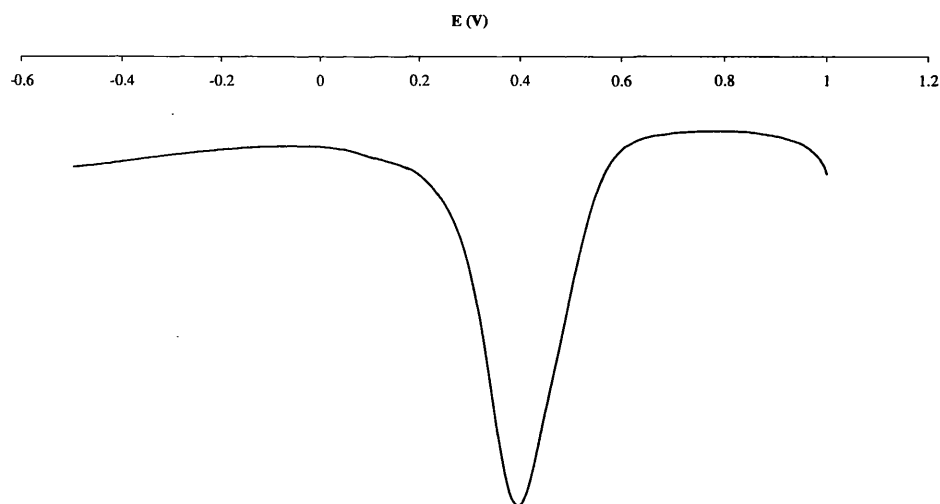


Fig. 4.28 DPV of $[\text{Pd}\{\text{FcTe}(\text{CH}_2)_3\text{TeFc}\}_2](\text{PF}_6)_2$ in dry acetonitrile, 0.1 M $[\text{NBu}_4][\text{PF}_6]$ at a scan rate of 100 mV s^{-1}

The half wave potentials ($E_{1/2}$) determined by cyclic voltammetry, and the peak potentials (E_p) measured by DPV of $\text{FcE}(\text{CH}_2)_3\text{E}'\text{Fc}$ complexes are listed in Table 4.5.

Table 4.5 Cyclic and differential pulse voltammetric data for $\text{FcE}(\text{CH}_2)_3\text{E}'\text{Fc}$ complexes (mV) in dry acetonitrile, 0.1 M $[\text{NBu}_4][\text{PF}_6]$ at a scan rate of 100 mV s^{-1}

	E_1		E_2		$\Delta E_{1/2}$
	<u>CV</u>	<u>DPV</u>	<u>CV</u>	<u>DPV</u>	
	$E_{1/2} (E_{pa} - E_{pc})$	E_p	$E_{1/2} (E_{pa} - E_{pc})$	E_p	
$[\text{Pd}\{\text{FcSe}(\text{CH}_2)_3\text{SeFc}\}_2](\text{PF}_6)_2$	96 (57)	97	297 (72)	293	201
$[\text{Pt}\{\text{FcSe}(\text{CH}_2)_3\text{SeFc}\}_2](\text{PF}_6)_2$	59 (111)	66	305 (74)	328	246
$[\text{Pd}\{\text{FcTe}(\text{CH}_2)_3\text{TeFc}\}_2](\text{PF}_6)_2$	247 (75)	277	-	-	0
$[\text{Pt}\{\text{FcTe}(\text{CH}_2)_3\text{TeFc}\}_2](\text{PF}_6)_2$	205 (164)	267	-	-	0
$[\text{Pd}\{\text{FcSe}(\text{CH}_2)_3\text{TeFc}\}_2](\text{PF}_6)_2$	137 (140)	124	256 (104)	262	119
$[\text{Pt}\{\text{FcSe}(\text{CH}_2)_3\text{TeFc}\}_2](\text{PF}_6)_2$	160 (108)	170	285 (101)	308	125

4.3.2 $[\text{MCl}\{\text{FcE}(\text{CH}_2)_3\text{E}'(\text{CH}_2)_3\text{EFc}\}]\text{PF}_6$ ($\text{M} = \text{Pd}$ or Pt , $\text{E}, \text{E}' = \text{Se}$ or Te)

Calculated from the crystal structure data for $[\text{PtCl}\{\text{FcSe}(\text{CH}_2)_3\text{Se}(\text{CH}_2)_3\text{SeFc}\}]\text{PF}_6$, the through-bond distance between the iron atoms is 12.66 Å. This distance is even smaller than that in $[\text{Pt}\{\text{FcSe}(\text{CH}_2)_3\text{SeFc}\}_2](\text{PF}_6)_2$ (12.71 Å), so on this basis stronger communication between the ferrocenyl moieties would be predicted. However, only one quasi-reversible wave is observed in the CV at $E_{1/2} = 335$ mV (Fig. 4.29), and the DPV also doesn't show the expected two peaks (Fig. 4.30).

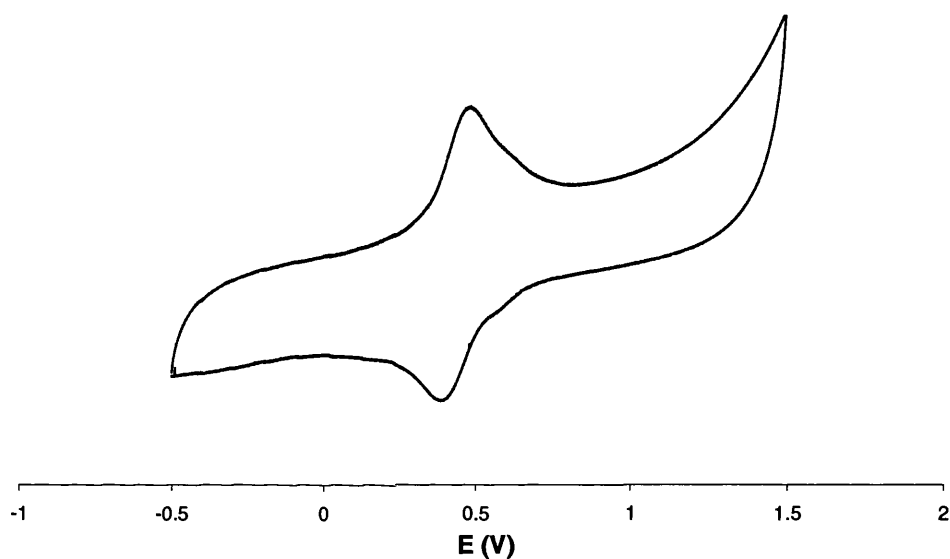


Fig. 4.29 CV of $[\text{PtCl}\{\text{FcSe}(\text{CH}_2)_3\text{Se}(\text{CH}_2)_3\text{SeFc}\}](\text{PF}_6)$ in dry acetonitrile, 0.1 M $[\text{NBu}_4][\text{PF}_6]$ at a scan rate of 100 mV s^{-1}

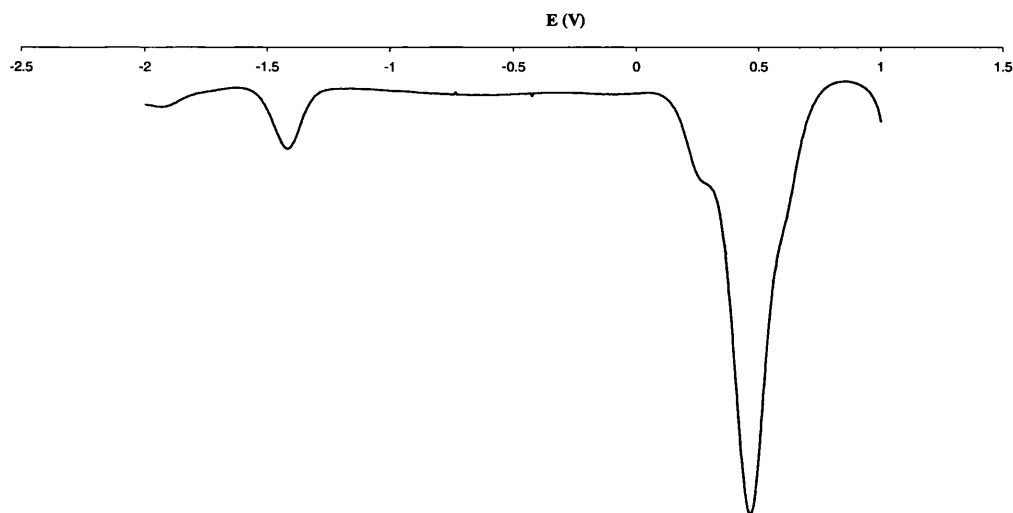


Fig. 4.30 DPV of $[\text{PtCl}\{\text{FcSe}(\text{CH}_2)_3\text{Se}(\text{CH}_2)_3\text{SeFc}\}]\text{PF}_6$ in dry acetonitrile, 0.1 M $[\text{NBu}_4][\text{PF}_6]$ at a scan rate of 100 mV s^{-1}

This surprising result makes it necessary to consider the structural difference between $[\text{PtCl}\{\text{FcSe}(\text{CH}_2)_3\text{Se}(\text{CH}_2)_3\text{SeFc}\}]\text{PF}_6$ and $[\text{Pt}\{\text{FcSe}(\text{CH}_2)_3\text{SeFc}\}_2](\text{PF}_6)_2$ (the space filling diagrams of these two complexes are shown in Fig. 4.31). In $[\text{Pt}\{\text{FcSe}(\text{CH}_2)_3\text{SeFc}\}_2](\text{PF}_6)_2$, there are four ferrocenyl moieties: from its crystal structure, the Pt is on an inversion centre, which means the *trans* ferrocenes are structurally equivalent, so they will be oxidized at the same potential; due to steric crowding, the *cis* ones are inequivalent and after oxidation of one of them, they will be able to interact with each other. In $[\text{PtCl}\{\text{FcSe}(\text{CH}_2)_3\text{Se}(\text{CH}_2)_3\text{SeFc}\}]\text{PF}_6$, there are two ferrocenyl moieties in *trans* positions, which are symmetry-related, so they are equivalent and will be oxidized at the same potential. The crystal structure and ^{77}Se NMR spectrum (Chapter Three) of $[\text{PtCl}\{\text{FcSe}(\text{CH}_2)_3\text{Se}(\text{CH}_2)_3\text{SeFc}\}]\text{PF}_6$ show that the *meso* invertomer is the only or main form in solution. In the *meso* form, the two ferrocenyl units are structurally equivalent. The only reasonable explanation is that communication can only happen between inequivalent units. The small shoulder beside the main peak in the DPV of $[\text{PtCl}\{\text{FcSe}(\text{CH}_2)_3\text{Se}(\text{CH}_2)_3\text{SeFc}\}]\text{PF}_6$, may mean that there is a small amount of the *DL* invertomer present in the solution.

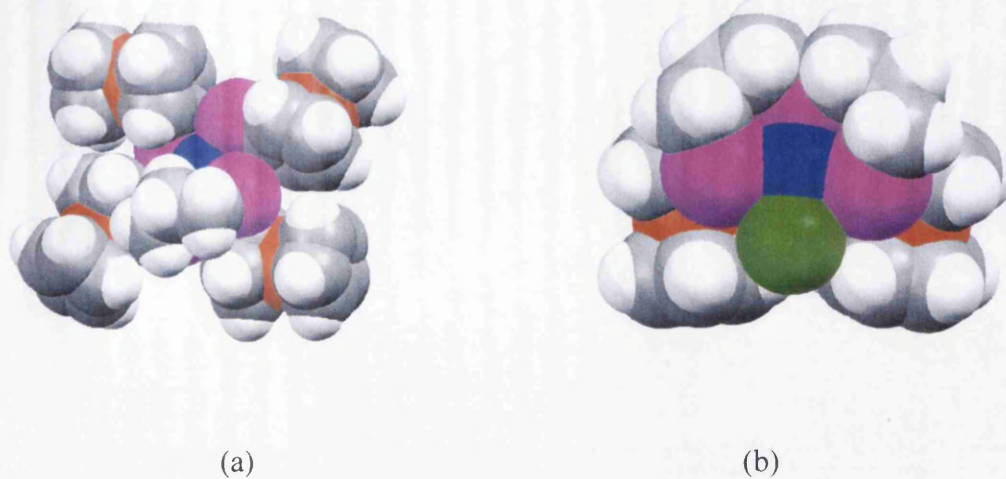


Fig. 4.31 Space filling diagrams of
 (a) $[\text{Pt}\{\text{FcSe}(\text{CH}_2)_3\text{SeFc}\}_2]^{2+}$; (b) $[\text{PtCl}\{\text{FcSe}(\text{CH}_2)_3\text{Se}(\text{CH}_2)_3\text{SeFc}\}]^+$
 (Cl: green; Fe: orange red; Se: violet; Pt: blue)

Similarly, $[\text{PdCl}\{\text{FcSe}(\text{CH}_2)_3\text{Se}(\text{CH}_2)_3\text{SeFc}\}]\text{PF}_6$ only exhibits one quasi-reversible wave at $E_{1/2} = 399 \text{ mV}$ with $|E_{\text{pa}} - E_{\text{pc}}| = 113 \text{ mV}$ (CV in Fig. 4.32 and DPV in Fig. 4.33).

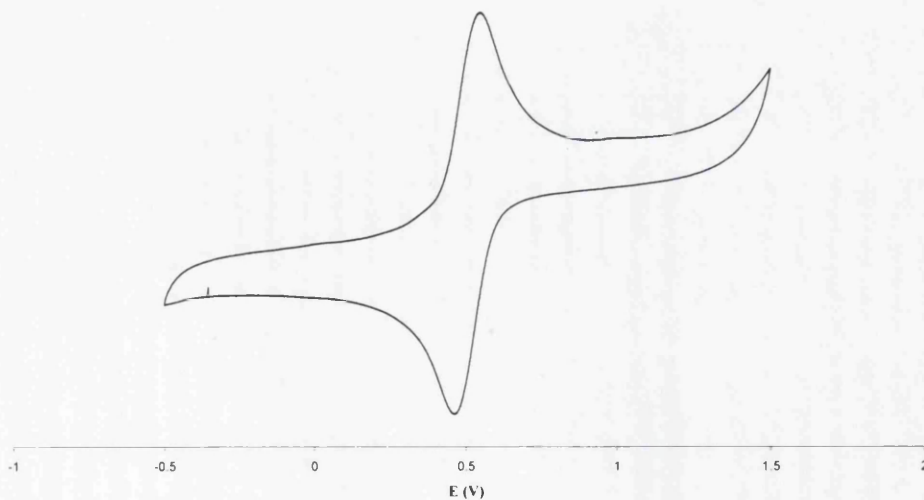


Fig. 4.32 CV of $[\text{PdCl}\{\text{FcSe}(\text{CH}_2)_3\text{Se}(\text{CH}_2)_3\text{SeFc}\}]\text{PF}_6$ in dry acetonitrile, 0.1 M $[\text{NBu}_4][\text{PF}_6]$ at a scan rate of 100 mV s^{-1}

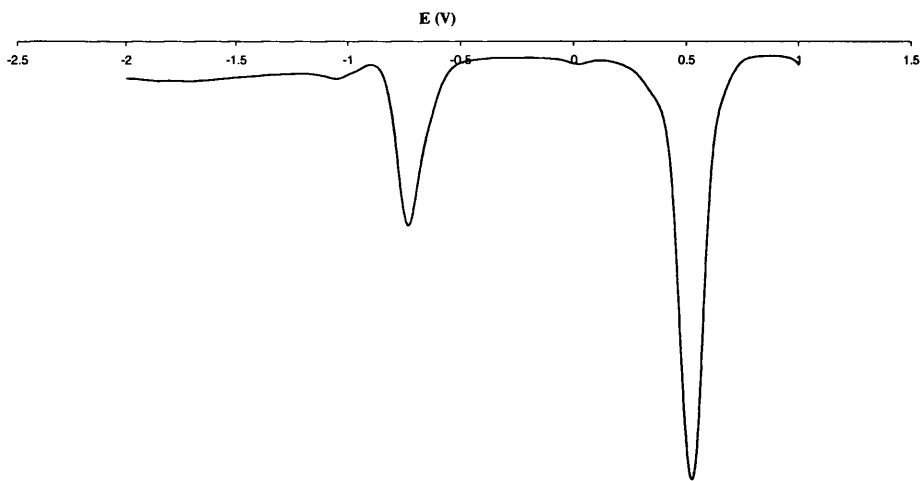


Fig. 4.33 DPV of $[\text{PdCl}\{\text{FcSe}(\text{CH}_2)_3\text{Se}(\text{CH}_2)_3\text{SeFc}\}]\text{PF}_6$ in dry acetonitrile, 0.1 M $[\text{NBu}_4][\text{PF}_6]$ at a scan rate of 100 mV s^{-1}

$[\text{PdCl}\{\text{FcSe}(\text{CH}_2)_3\text{Te}(\text{CH}_2)_3\text{SeFc}\}]\text{PF}_6$ shows one well-defined quasi-reversible wave at $E_{1/2} = 291 \text{ mV}$ with $|E_{\text{pa}} - E_{\text{pc}}| = 114 \text{ mV}$. Close examination of the CV (Fig.4.34) reveals the presence of a weak second redox wave, which gives rise to a peak in the DPV at $E_p = 115 \text{ mV}$ (Fig. 4.35).

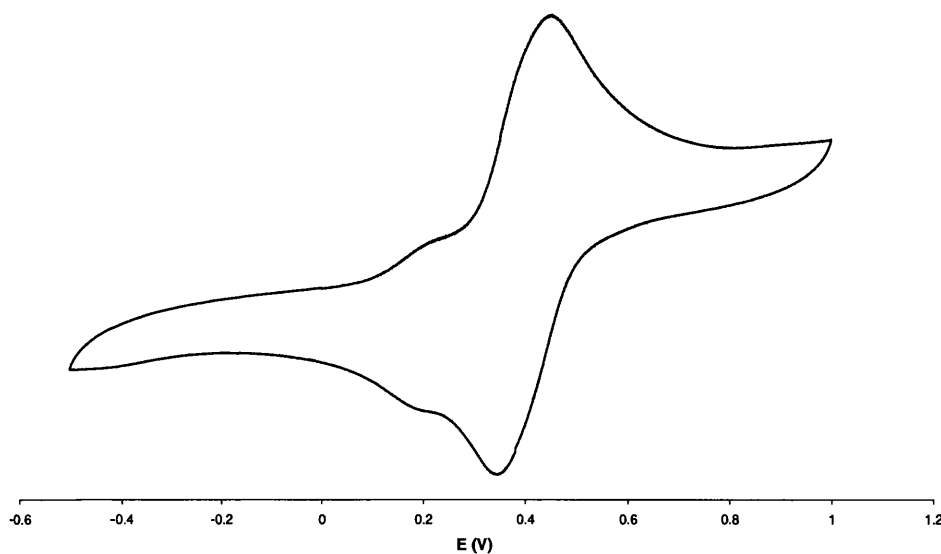


Fig. 4.34 CV of $[\text{PdCl}\{\text{FcSe}(\text{CH}_2)_3\text{Te}(\text{CH}_2)_3\text{SeFc}\}]\text{PF}_6$ in dry acetonitrile, 0.1 M $[\text{NBu}_4][\text{PF}_6]$ at a scan rate of 100 mV s^{-1}

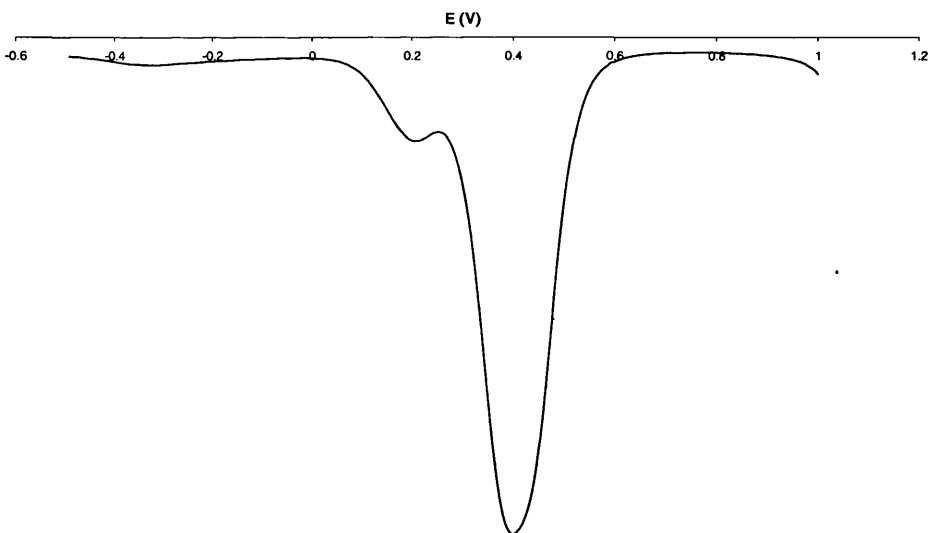


Fig. 4.35 DPV of $[\text{PdCl}\{\text{FcSe}(\text{CH}_2)_3\text{Te}(\text{CH}_2)_3\text{SeFc}\}]\text{PF}_6$ in dry acetonitrile, 0.1 M $[\text{NBu}_4][\text{PF}_6]$ at a scan rate of 100 mV s^{-1}

$[\text{PtCl}\{\text{FcSe}(\text{CH}_2)_3\text{Te}(\text{CH}_2)_3\text{SeFc}\}]\text{PF}_6$ also shows one well-defined quasi-reversible wave at $E_{1/2} = 305 \text{ mV}$ with $|E_{\text{pa}} - E_{\text{pc}}| = 112 \text{ mV}$, and a weak second redox wave ($E_p = 45 \text{ mV}$) (CV in Fig. 4.36).

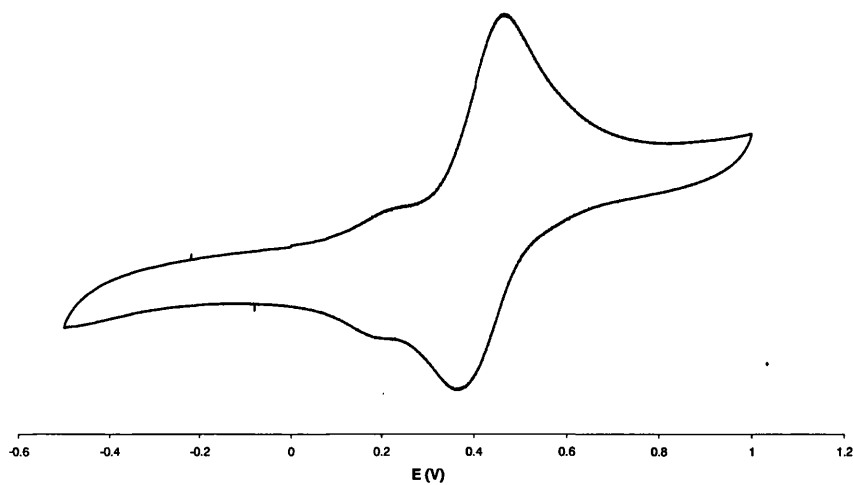


Fig. 4.36 CV of $[\text{PtCl}\{\text{FcSe}(\text{CH}_2)_3\text{Te}(\text{CH}_2)_3\text{SeFc}\}]\text{PF}_6$ in dry acetonitrile, 0.1 M $[\text{NBu}_4][\text{PF}_6]$ at a scan rate of 100 mV s^{-1}

Other complexes of this type only show one well-defined quasi-reversible wave (see Table 4.6). Although no crystal structures were obtained for these four complexes, by extrapolation of information relating to the bidentate ligand $\text{FcTe}(\text{CH}_2)_3\text{TeFc}$, we can predict that the through bond distance between the $\text{Fe}\cdots\text{Fe}$ centres is too long for communication. So regardless of the molecular symmetry, the ferrocene units can have no interaction.

All the complexes display an irreversible reduction process in the range -0.85 to -1.45 V (examples in Fig. 4.30 and 4.33), which is attributed to the $\text{M}(\text{II})/\text{M}(\text{0})$ couple.¹⁹

Table 4.6 CV and DPV data for complexes of $\text{FcE}(\text{CH}_2)_3\text{E}'(\text{CH}_2)_3\text{EFc}$ (mV) in dry acetonitrile, 0.1 M $[\text{NBu}_4][\text{PF}_6]$ at a scan rate of 100 mV s^{-1}

	$[\text{PdClL}]\text{PF}_6$		$[\text{PtClL}]\text{PF}_6$	
	<u>CV</u>	<u>DPV</u>	<u>CV</u>	<u>DPV</u>
	$E_{1/2} (E_{\text{pa}} - E_{\text{pc}})$	E_{p}	$E_{1/2} (E_{\text{pa}} - E_{\text{pc}})$ (mV)	E_{p}
$\text{E} = \text{E}' = \text{Se}$	399 (113)	337	335 (114)	398
$\text{E} = \text{Se}, \text{E}' = \text{Te}$	291 (114)	307	305 (112)	277
$\text{E} = \text{Te}, \text{E}' = \text{Se}$	275 (107)	261	246 (116)	282
$\text{E} = \text{E}' = \text{Te}$	252 (98)	252	256 (123)	247

4.3.3 $[M\{FcE(CH_2)_3Se(CH_2)_3Se(CH_2)_3EFc\}](PF_6)_2$ ($M = Pd$ or Pt , $E = Se$ or Te)

$[Pd\{FcSe(CH_2)_3Se(CH_2)_3Se(CH_2)_3SeFc\}](PF_6)_2$ only shows one well-defined quasi-reversible wave at $E_{1/2} = 310$ mV with $|E_{pa} - E_{pc}| = 142$ mV (CV in Fig. 4.37). Although no crystal structure was obtained, it can be predicted that the ferrocene units occupy *cis*-positions, and that the $Fe \cdots Fe$ through bond distance may be similar to that in $[PdCl\{FcSe(CH_2)_3Se(CH_2)_3SeFc\}]PF_6$. The observation of only one wave with a positive potential shift compared to free ligand implies that the two ferrocene units are structurally equivalent.

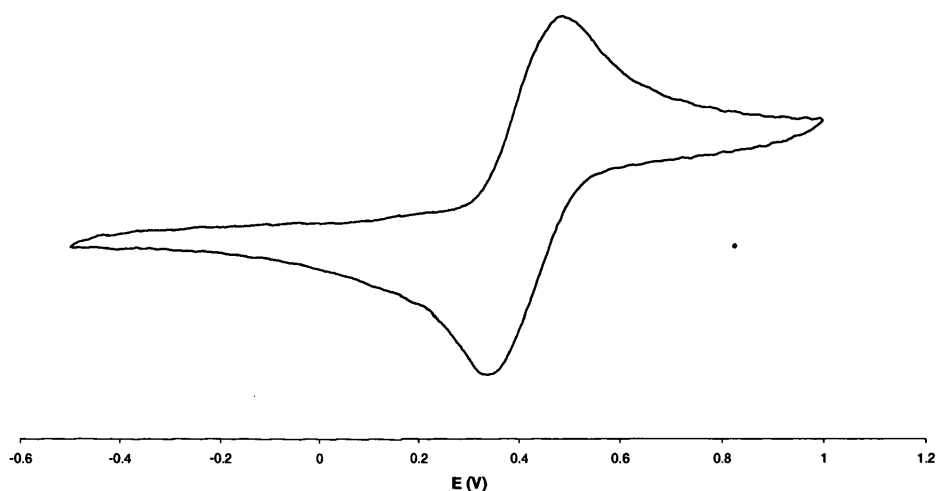


Fig. 4.37 CV of $[Pd\{FcSe(CH_2)_3Se(CH_2)_3Se(CH_2)_3SeFc\}](PF_6)_2$ in dry acetonitrile, 0.1 M $[NBu_4][PF_6]$ at a scan rate of 100 mV s^{-1}

Other complexes of this type also only show only one well-defined quasi-reversible wave (see Table 4.7).

Table 4.7 CV data for complexes of $\text{FcE}(\text{CH}_2)_3\text{Se}(\text{CH}_2)_3\text{Se}(\text{CH}_2)_3\text{EFc}$ in dry acetonitrile, 0.1 M $[\text{NBu}_4][\text{PF}_6]$ at a scan rate of 100 mV s^{-1}

$E_{1/2} (|E_{\text{pa}} - E_{\text{pc}}|) \text{ (mV)}$

	$[\text{PdL}](\text{PF}_6)_2$	$[\text{PtL}](\text{PF}_6)_2$
E = Se	310 (142)	312 (169)
E = Te	295 (88)	300 (115)

4.3.4 $[M(\text{fcSe}_4)](\text{PF}_6)_2$ and $[M(\text{difcSe}_4)](\text{PF}_6)_2$ (M = Pd or Pt)

The cyclic voltammograms of $[M(\text{fcSe}_4)](\text{PF}_6)_2$ show one quasi-reversible redox wave at 639 mV (M = Pd) and 642 mV (M = Pt). It's a large positive potential shift compared to the free ligand of about 600 mV (the CV of $[\text{Pt}(\text{fcSe}_4)](\text{PF}_6)_2$ shown in Fig. 4.38). The complexes of open chain ligands, such as $[M\{\text{FcSe}(\text{CH}_2)_3\text{Se}(\text{CH}_2)_3\text{Se}(\text{CH}_2)_3\text{SeFc}\}](\text{PF}_6)_2$ (M = Pd or Pt), only show a shift of about 200 mV. This may be due to the macrocyclic effect or direct interaction between Fe-M (Pd or Pt). Changing the metal from Pd to Pt didn't bring about a significant change in electrochemical behaviour; this may be because Pd(II) and Pt(II) have quite similar ionic radii. Investigating the effect of metal ions of different radius could be the aim of future work.

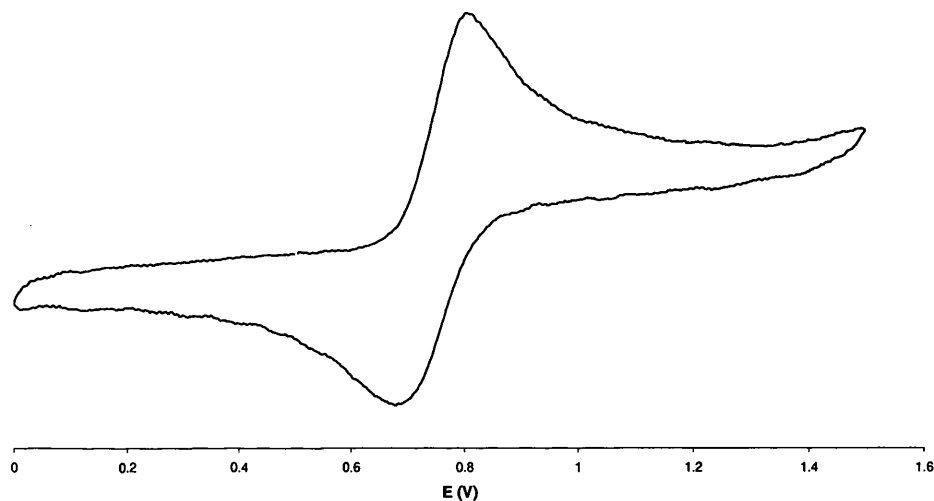


Fig. 4.38 CV of $[\text{Pt}(\text{fcSe}_4)](\text{PF}_6)_2$ in dry acetonitrile, 0.1 M $[\text{NBu}_4][\text{PF}_6]$ at a scan rate of 100 mV s^{-1}

The bis-ferrocenophane macrocyclic complexes $[M(\text{difcSe}_4)](\text{PF}_6)_2$ also showed one wave at 661 mV for M = Pd complex and 675 mV for M = Pt, indicating the ferrocene units act independently. This is reasonable because they are structurally equivalent. Compared to $[M(\text{fcSe}_4)](\text{PF}_6)_2$, the more positive half-wave potential shows that the ferrocene units are more difficult to oxidise.

The half-wave potentials ($E_{1/2}$) determined by cyclic voltammetry of the complexes of fcSe_4 and difcSe_4 are listed in Table 4.8.

Table 4.8 CV data for complexes of fcSe_4 and difcSe_4 in dry acetonitrile, 0.1 M $[\text{NBu}_4][\text{PF}_6]$ at a scan rate of 100 mV s^{-1}

$E_{1/2} (|E_{\text{pa}} - E_{\text{pc}}|) \text{ (mV)}$

	$[\text{PdL}](\text{PF}_6)_2$	$[\text{PtL}](\text{PF}_6)_2$
fcSe_4	639 (133)	642 (130)
difcSe_4	661 (159)	675 (160)

4.3.5 $[\text{Pt}_2\text{Cl}_2\{\text{FcSeCH}_2\text{C}_6\text{H}_4\text{CH}_2\text{SeFc}\}_3](\text{PF}_6)_2$

For $\text{FcSeCH}_2\text{C}_6\text{H}_4\text{CH}_2\text{SeFc}$, only one wave is observed in the cyclic voltammogram, $E_{1/2} = 55 \text{ mV}$ ($|E_{\text{pa}} - E_{\text{pc}}| = 88 \text{ mV}$). The CV of the dinuclear complex $[\text{Pt}_2\text{Cl}_2\{\text{FcSeCH}_2\text{C}_6\text{H}_4\text{CH}_2\text{SeFc}\}_3](\text{PF}_6)_2$ shows one quasi-reversible wave at $E_{1/2}(1) = 48 \text{ mV}$ ($|E_{\text{pa}} - E_{\text{pc}}| = 88 \text{ mV}$) and another at $E_{1/2}(2) = 300 \text{ mV}$ ($|E_{\text{pa}} - E_{\text{pc}}| = 136 \text{ mV}$), $\Delta E_{1/2} = 252 \text{ mV}$ (CV shown in Fig. 4.39), and resemble that obtained for $[\text{Pt}\{\text{FcSe}(\text{CH}_2)_3\text{SeFc}\}_2](\text{PF}_6)_2$. Calculated from the crystal structure of $[\text{Pt}_2\text{Cl}_2\{\text{FcSeCH}_2\text{C}_6\text{H}_4\text{CH}_2\text{SeFc}\}_3](\text{PF}_6)_2$, the through bond $\text{Fe}\cdots\text{Fe}$ distance is *ca.* 12.67 \AA , which is similar to that in $[\text{Pt}\{\text{FcSe}(\text{CH}_2)_3\text{SeFc}\}_2](\text{PF}_6)_2$ (12.71 \AA), and the ferrocenyl groups are structurally inequivalent as shown in Fig. 3.37. This results in strong communication between the ferrocenyl moieties.

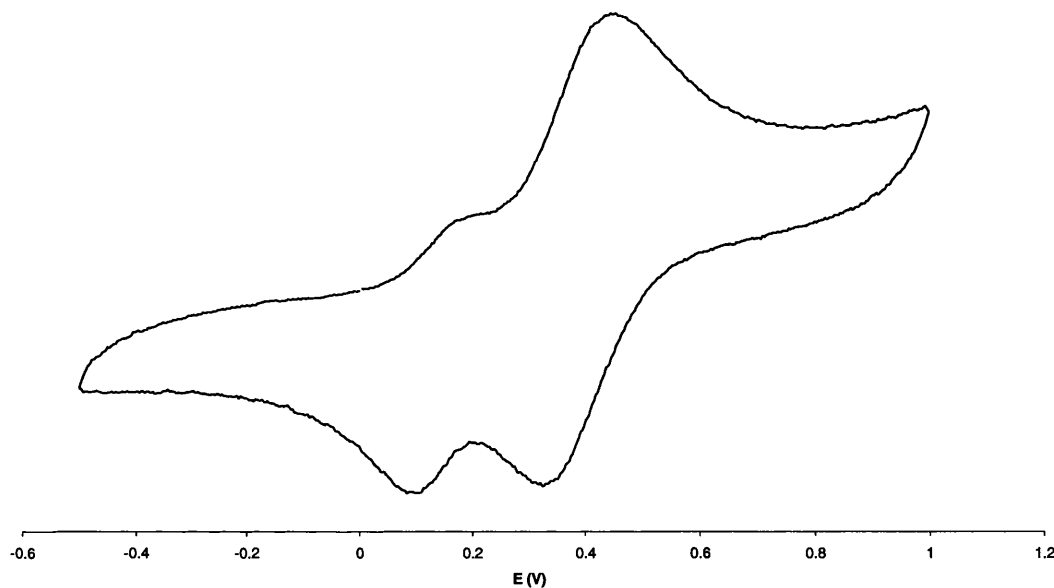


Fig. 4.39 CV of $[\text{Pt}_2\text{Cl}_2\{\text{FcSeCH}_2\text{C}_6\text{H}_4\text{CH}_2\text{SeFc}\}_3](\text{PF}_6)_2$ in dry acetonitrile, 0.1 M $[\text{NBu}_4][\text{PF}_6]$ at a scan rate of 100 mV s^{-1}

4.3.6 $[M(CO)_4\{FcE(CH_2)_3E'Fc\}]$ ($M = Cr, E = E' = Te; M = Mo, E, E' = Se \text{ or } Te; M = W, E = E' = Te$)

The electrochemistry study in MeCN solution of $[Mo(CO)_4\{FcE(CH_2)_3E'Fc\}]$ was unsuccessful as the carbonyl complexes are unstable and decomposed to free ligand and $[M(CO)_4(NCMe)_2]$. The carbonyl complexes were therefore studied in dichloromethane solution.

The CV of $[Cr(CO)_4\{FcTe(CH_2)_3TeFc\}]$ shows two redox processes at 181 and 322 mV. From the crystal data, the through bond Fe...Fe distance is 13.56 Å, far beyond the communication threshold. Only the first process is due to the ferrocene units and the second one is attributed to the Cr(0)/Cr(I) couple

The CV of $[Mo(CO)_4\{FcSe(CH_2)_3SeFc\}]$ (Fig. 4.40) shows two quasi-reversible waves at 30 and 242 mV and one irreversible wave at 517 mV. The first two waves can be easily assigned to the redox processes at the iron centres of the ferrocenes; the third irreversible one corresponds to the redox couple Mo(0)/Mo(I). The through bond Fe...Fe distance is 13.17 Å, which is short enough for communication. The difference between the two half wave potentials is 212 mV. Complex $[Pd\{FcSe(CH_2)_3TeFc\}_2](PF_6)_2$ has a similar through bond Fe...Fe distance (13.16 Å), but a $\Delta E_{1/2}$ of only 119 mV. This difference emphasises the importance of the nature of the intervening atoms in determining the magnitude of the interaction between ferrocene groups. It is not only dependent on the distance between them. It may also be relevant that the dielectric constant of dichloromethane is 9, which is much lower than that of acetonitrile (38), and results in higher cell resistance.²⁰

The CV of $[Mo(CO)_4\{FcSe(CH_2)_3TeFc\}]$ only exhibits one quasi-reversible wave centred on ferrocene units with $E_{1/2} (|E_{pa} - E_{pc}|) = 214$ (225) mV. The through bond Fe...Fe distance is 13.56 Å, which is too long for communication. The irreversible wave assigned to Mo(0)/Mo(I) is at 487 mV.

A similar result was obtained for $[Mo(CO)_4\{FcTe(CH_2)_3TeFc\}]$ which has a through bond Fe...Fe distance of 13.85 Å, with $E_{1/2} = 172$ mV ($|E_{pa} - E_{pc}| = 184$ mV). The irreversible wave due to Mo(0)/Mo(I) is at 436 mV.

In these three complexes, the oxidation potential of Mo(0) shifts negatively as the donor atoms change from Se to Te, meaning that the Mo becomes easier to oxidise. As has been discussed in Chapter Three, Te is a better σ donor atom than Se, so it will increase the electron density on the Mo, resulting in an easier oxidation process.

Because the through bond Fe...Fe distance is 13.84 Å in $[\text{W}(\text{CO})_4\{\text{FcTe}(\text{CH}_2)_3\text{TeFc}\}]$, its CV only has one quasi-reversible wave due to the ferrocene units with $E_{1/2} = 264 \text{ mV}$ ($|E_{\text{pa}} - E_{\text{pc}}| = 208 \text{ mV}$). The irreversible wave centred on W is not resolved.

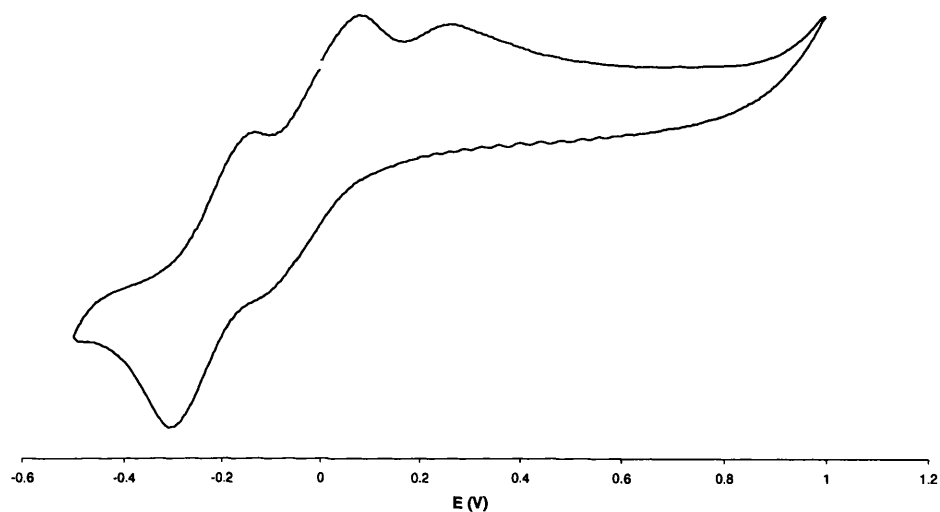


Fig. 4.40 CV of $[\text{Mo}(\text{CO})_4\{\text{FcSe}(\text{CH}_2)_3\text{SeFc}\}]$ in dry dichloromethane, 0.1 M $[\text{NBu}_4][\text{PF}_6]$ at a scan rate of 100 mV s^{-1}

The half wave potentials ($E_{1/2}$) determined by cyclic voltammetry of the complexes $[\text{M}(\text{CO})_4\{\text{FcE}(\text{CH}_2)_3\text{E}'\text{Fc}\}]$ are listed in Table 4.9.

Table 4.9 CV data for complexes $[\text{M}(\text{CO})_4\{\text{FcE}(\text{CH}_2)_3\text{E}'\text{Fc}\}]$ in dry dichloromethane, 0.1 M $[\text{NBu}_4][\text{PF}_6]$ at a scan rate of 100 mV s^{-1}
 $E_{1/2} (|E_{\text{pa}} - E_{\text{pc}}|) \text{ (mV)}$

	E = E' = Se	E = Se; E' = Te	E = E' = Te
Cr	-	-	181 (218)
Mo	30 (151), 242 (184)	214 (225)	172 (184)
W	-	-	264 (208)

4.4 References for Chapter Four

1. R. Rulkens, D. P. Gates, D. Balaishis, J. K. Pudelski, D. F. McIntosh, A. J. Lough, I. Manners, *J. Am. Chem. Soc.*, 1997, **119**, 10976
2. A. G. Osborne, R. E. Hollands, A. G. Nagy, *J. Organomet. Chem.*, 1989, **373**, 229
3. H. Ushijima, T. Akiyama, M. Kajitani, K. Shimizu, M. Aoyama, S. Masuda, Y. Harada, A. Sugimori, *Chem. Lett.*, 1987, 2197
4. H. Ushijima, T. Akiyama, M. Kajitani, K. Shimizu, M. Aoyama, S. Masuda, Y. Harada, A. Sugimori, *Bull. Chem. Soc. Jpn.*, 1990, **63**, 1015
5. P. Zanello, G. Opromolla, M. Casarin, M. Herberhold, P. Leitner, *J. Organomet. Chem.*, 1993, **443**, 199
6. H. B. Singh, A. V. Regini, J. P. Jasinski, E. S. Paight, R. J. Butcher, *J. Organomet. Chem.*, 1994, **464**, 87
7. M. R. Burgess, C. P. Morley, *J. Organomet. Chem.*, 2001, **623**, 101
8. P. Shu, K. Bechgaard, D. Cowan, *J. Org. Chem.*, 1976, **41**, 1849
9. D. C. O. Salazar, D. O. Cowan, *J. Organomet. Chem.*, 1991, **408**, 227
10. P. Zanello, G. Opromolla, M. Herberhold, H. Brendel, *J. Organomet. Chem.*, 1994, **484**, 67
11. D. L. Compton, P. F. Brandt, T. B. Rauchfuss, D. F. Rosenbaum, C. F. Zukoski, *Chem. Mater.*, 1995, **7**, 2342
12. M. J. Brown, J. F. Corrigan, *J. Organomet. Chem.*, 2004, **689**, 2872
13. S. Kumar, S. K. Tripathi, H. B. Singh, G. Wolmershäuser, *J. Organomet. Chem.*, 2004, **689**, 3046.
14. S. Hartmann, R. F. Winter, T. Scheiring, M. Wanner, *J. Organomet. Chem.*, 2001, **637**, 240
15. M. R. Burgess, Ph.D. Thesis, University of Wales Swansea, 1999
16. V. C. Gibson, N. J. Long, C. K. Williams, M. Fontani and P. Zanello, *Dalton Trans.*, 2003, 3599
17. M. J. Brown and J. F. Corrigan, *J. Organomet. Chem.*, 2004, **689**, 2872
18. J. D. Carr, S. J. Coles, M. B. Hursthouse, M. E. Light, E. L. Munro, J. H. R. Tucker and J. Westwood, *Organometallics*, 2000, **19**, 3312
19. V. C. Gibson, N. J. Long, C. K. Williams, M. Fontani, P. Zanello, *J. Chem. Soc., Dalton Trans.*, 2003, 3599

20. J. B. Headridge, *Electrochemical Techniques for Inorganic Chemists*, Academic Press, USA, 1969

CHAPTER FIVE

Rhodium Complexes of Novel Ferrocenyl Chalcogenide Ligands

BACKGROUND, RESULTS AND DISCUSSION

5.1 Background

Not much work has been reported concerning rhodium complexes of organochalcogenide ligands. The literature summarized below will be covered in the order monodentate, bidentate and polydentate ligands.

5.1.1 Monodentate ligands

The reaction of Me_2E ($\text{E} = \text{Se}$ or Te) and $[\text{Rh}_3\text{RuH}(\text{CO})_{12}]$ yields $[\text{Rh}_3\text{RuH}(\text{CO})_9]_2(\text{EMe}_2)_3$. The structure of $[\text{Rh}_3\text{RuH}(\text{CO})_9]_2(\text{SeMe}_2)_3$ shows the Me_2Se ligands behave as bridging four-electron donors occupying all the axial positions on the two Rh_3 faces with Rh-Se bond lengths of 2.551(6) and 2.567(6) Å (Fig. 5.1).^{1,2}

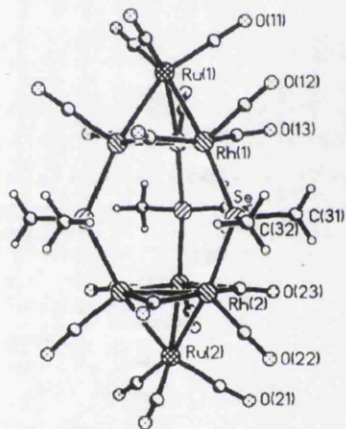


Fig. 5.1 Crystal structure of $[\text{Rh}_3\text{RuH}(\text{CO})_9]_2(\text{SeMe}_2)_3$

The addition of SeMe_2 , TeR_2 ($\text{R} = \text{Me}$ or Et) or $(\text{CH}_2)_4\text{Te}$ results in the substitution of one of the CO ligands in $[\text{Rh}_2(\text{C}_5\text{H}_5)_2(\mu\text{-CO})_2(\text{CF}_3\text{CCCF}_3)]$. The Rh-Te distance is 2.540(2) Å in $[\text{Rh}_2(\text{C}_5\text{H}_5)_2(\text{CO})(\text{CF}_3\text{CCCF}_3)\{(\text{CH}_2)_4\text{Te}\}]$ (Fig. 5.2).³

In the complexes $[\text{RhCl}_3\text{L}_3]$ ($\text{L} =$ telluracyclopentane or 1,3-dihydrobenzo[c]tellurophene), $[\text{Rh}(\eta^5\text{-C}_5\text{Me}_5)\text{L}][\text{CF}_3\text{SO}_3]_2$ and $[\text{Rh}(\eta^5\text{-C}_5\text{Me}_5)\text{Cl}_2\text{L}]$ ($\text{L} =$ 1,3-dihydrobenzo[c]tellurophene), L behaves as a monodentate ligand.⁴⁻⁷

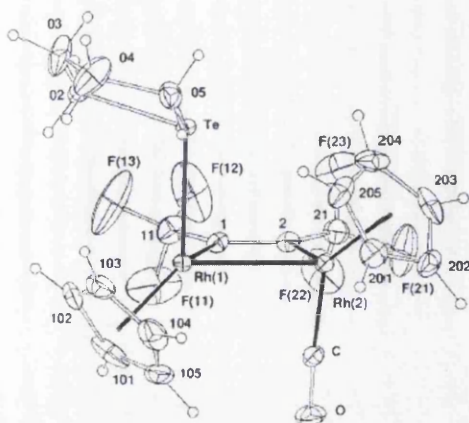


Fig. 5.2 Crystal structure of $[\text{Rh}_2(\text{C}_5\text{H}_5)_2(\text{CO})(\text{CF}_3\text{CCCF}_3)\{(\text{CH}_2)_4\text{Te}\}]$

5.1.2 Bidentate ligands

$[\text{PPh}_4][\text{RhCl}_4\text{L}]$, *trans*- $[\text{RhCl}_2\text{L}_2]\text{ClO}_4$, *cis*- $[\text{RhCl}_2\text{L}_2]\text{Cl}$ ($\text{L} = \text{MeSeCH}_2\text{CH}_2\text{SeMe}$) and *trans*- $[\text{RhCl}_2(\text{PhSeCH}_2\text{CH}_2\text{SePh})_2]\text{Cl}$ were synthesized; in the ^{77}Se NMR spectra of these compounds there is a large high frequency coordination shift.⁸

$[\text{RhCl}_2\text{L}_2]\text{PF}_6$ complexes ($\text{L} = \text{RTe}(\text{CH}_2)_3\text{TeR}$, $\text{R} = \text{Me}$ or Ph ; $\text{L} = o\text{-C}_6\text{H}_4(\text{TeMe})_2$) were confirmed by ^{125}Te NMR and UV-vis spectra to be *trans* isomers.⁹

Up to now, no crystal structure has been obtained for this kind of complexes.

5.1.3 Polydentate ligands

The tripodal ligand $\text{MeC}(\text{CH}_2\text{SeMe})_3$ may form the complex $[\text{RhL}_2](\text{PF}_6)_3$, which was inferred from one cluster of peaks in the mass spectrum corresponding to the $[\text{Rh}\{\text{MeC}(\text{CH}_2\text{SeMe})_3\}\text{-}\{\text{MeC}(\text{CH}_2\text{SeMe})_2(\text{CH}_2\text{Se})\}]^{2+}$ ion.¹⁰

With tripodal ligands, low oxidation state Rh(I) complexes $[\text{Rh}(\text{COD})\{\text{MeC}(\text{CH}_2\text{ER})_3\}]\text{PF}_6$ ($\text{E} = \text{Se}$, $\text{R} = \text{Me}$; $\text{E} = \text{Te}$, $\text{R} = \text{Me}$ or Ph) have been prepared. The crystal structures of $[\text{Rh}(\text{COD})\{\text{MeC}(\text{CH}_2\text{EMe})_3\}]\text{PF}_6$ ($\text{E} = \text{Se}$ or Te) reveal distorted square pyramidal geometries with the M-E bonds *trans* to COD significantly shorter than the axial M-E bond ($d(\text{Rh}-\text{Se})$: 2.479(2), 2.483(2), 2.635(2) Å; $d(\text{Rh}-\text{Te})$: 2.6226(8), 2.5786(8), 2.6924(7) Å) (Fig. 5.3). The Rh(III) complexes $[\text{Rh}(\eta^5\text{-C}_5\text{Me}_5)\{\text{MeC}(\text{CH}_2\text{ER})_3\}](\text{PF}_6)_2$ were synthesized, in which selenium acts as a stronger σ donor than tellurium.¹¹

The linear tridentate ligand, $\text{Te}\{(\text{CH}_2)_3\text{ER}\}_2$ ($\text{E} = \text{Te}$, $\text{R} = \text{Me}$ or Ph ; $\text{E} = \text{S}$, $\text{R} = \text{Me}$)^{12, 13}, can also form Rh(III) complexes $[\text{Rh}(\eta^5\text{-C}_5\text{Me}_5)\text{L}](\text{PF}_6)_2$. The Rh-Te bond

lengths are 2.6177(7), 2.6016(7), 2.6015(7) Å in $[\text{Rh}(\eta^5\text{-C}_5\text{Me}_5)\text{Te}\{(\text{CH}_2)_3\text{TePh}\}_2](\text{PF}_6)_2$ (Fig. 5.4).

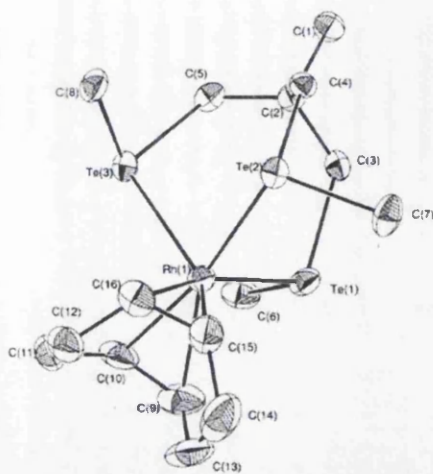


Fig. 5.3 Crystal structure of cation $[\text{Rh}(\text{COD})\{\text{MeC}(\text{CH}_2\text{TeMe})_3\}]^+$

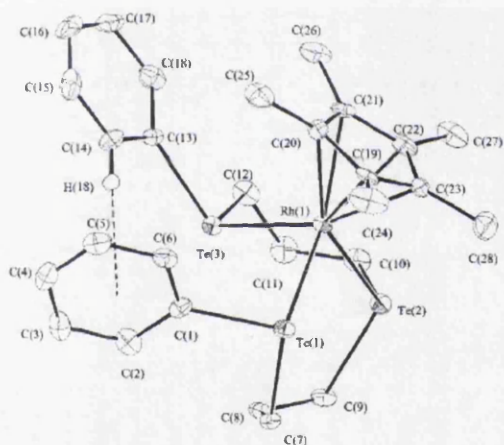


Fig. 5.4 Crystal structure of cation $[\text{Rh}(\eta^5\text{-C}_5\text{Me}_5)\text{Te}\{(\text{CH}_2)_3\text{TePh}\}_2]^+$

The Rh(III) complexes $[\text{RhX}_2\{[16]\text{aneSe}_4\}]\text{PF}_6$ (X = Cl or Br) were synthesized, and the *trans*-isomers are in the majority in DMF solution.¹⁴ The Rh-Se bond length is 2.456(1) and 2.461(1) Å in the $[\text{RhCl}_2\{[16]\text{aneSe}_4\}](\text{PF}_6)$. The analogue $[\text{RhCl}_2\{[8]\text{aneSe}_2\}_2]\text{PF}_6$ was also obtained.¹⁵

Several examples with mixed-donor ligands other than chalcogenide atoms were also reported which will not be included here.

In Chapter Three, the preparation and study of several series of palladium and platinum complexes of the ferrocenyl chalcogenide ligands was described. This work

was extended to analogous rhodium complexes. The synthesis, electronic spectroscopy and electrochemistry of rhodium complexes of ferrocenyl chalcogenide ligands are presented in the remaining of this chapter.

5.2 Rh complexes of $\text{FcE}(\text{CH}_2)_3\text{E}'\text{Fc}$ (E, E' = Se or Te)

5.2.1 Synthesis

The scheme used to synthesize $[\text{RhCl}_2\{\text{RE}(\text{CH}_2)_3\text{ER}\}_2]\text{PF}_6$ ⁹ was adopted here for the preparation of Rh(III) complexes of $\text{FcE}(\text{CH}_2)_3\text{E}'\text{Fc}$ (E, E' = Se or Te), and is illustrated below by the example of $[\text{RhCl}_2\{\text{FcSe}(\text{CH}_2)_3\text{SeFc}\}_2]\text{PF}_6$. The experimental details are given in Chapter Seven.

One equivalent of $\text{RhCl}_3 \cdot 3\text{H}_2\text{O}$ and two equivalents of $\text{FcSe}(\text{CH}_2)_3\text{SeFc}$ in ethanol (30 ml) were refluxed for 1 h; a little more than one equivalent of KPF_6 was then added and the mixture stirred at room temperature for another 1 h. The dark red precipitate was collected and washed with diethyl ether. The ES mass spectra showed an excellent match of the isotope pattern for the molecular ion unit that calculated for $[\text{RhCl}_2\{\text{FcSe}(\text{CH}_2)_3\text{SeFc}\}_2]^+$, and also confirmed the presence of PF_6^- .

No crystal suitable for X-ray analysis was obtained. The NMR spectra also show weak and broad features due to their large molecular weight of the complexes and their slow pyramidal inversion at room temperature.

5.2.2 Electronic spectra

UV-vis spectra are quite useful to distinguish *cis*- and *trans*- isomers of Rh complexes. The spectra of low-spin d^6 Rh(III) in an octahedral complexes contain two spin-allowed d-d transition bands: ${}^1\text{T}_{1g} \leftarrow {}^1\text{A}_{1g}$, and ${}^1\text{T}_{2g} \leftarrow {}^1\text{A}_{1g}$ (in the order of increasing energy), which are generally observed in the range 280-500 nm. The charge transfer bands are observed below 280 nm. In the dichloro complexes $[\text{RhCl}_2\text{L}_4]^+$, the intensity and wavenumbers of the d-d transitions are characteristic of the molecular geometry: (1) the lower symmetry *cis*- complexes (C_{2v} symmetry) exhibit significantly larger molar extinction coefficients than the *trans*- complexes (D_{4h} symmetry); (2) The d-d transitions in *cis*- complexes are observed at higher energy. The lower energy d-d transition is typically observed about 390 nm for the *cis*-complexes while that for the *trans*-complexes appears at about 440 nm. The higher energy d-d transition is observed about 290 nm for the *cis*-complexes and 340 nm for the *trans*-complexes.¹⁶⁻¹⁹

Table 5.1 lists the UV-vis data for three rhodium complexes of $\text{FcE}(\text{CH}_2)_3\text{E}'\text{Fc}$. Like their Pd or Pt analogues, these complexes give different spectra from the free ligands

(example shown in Fig. 5.5). The spectra display a similar pattern with two characteristic bands. There are new absorptions in the near ultraviolet region with high intensity around 340 nm. The lowest energy spin-allowed d-d band of the ferrocene unit in the compounds $\text{FcE}(\text{CH}_2)_3\text{E}'\text{Fc}$, at 440 nm ($\text{E} = \text{E}' = \text{Se}$) or 445 nm ($\text{E} = \text{Te}$; $\text{E}' = \text{Se}$ or Te), is obscured by a more intense absorption around 520 nm. If these two bands originate from d-d transitions, then these three complexes are *trans* geometric isomers. Compared to other Rh(III) *trans*-complexes, the two bands have a bathochromic shift and the molar extinction coefficients are larger. In the analogous complexes *trans*- $[\text{RhCl}_2\{\text{RTe}(\text{CH}_2)_3\text{TeR}\}]\text{PF}_6$ ($\text{R} = \text{Me}$ or Ph),⁹ there is only one d-d absorption band at around 480 nm with $\epsilon = 1000 \text{ dm}^3 \text{ mol}^{-1} \text{ cm}^{-1}$.

Table 5.1 UV-Vis data for compounds in $10^{-4} \text{ mol dm}^{-3} \text{ CH}_3\text{CN}$ solution

$\lambda_{\text{max}} / \text{nm}$ ($\epsilon / \text{dm}^3 \text{ mol}^{-1} \text{ cm}^{-1}$)

	λ_1	λ_2
$[\text{RhCl}_2\{\text{FcSe}(\text{CH}_2)_3\text{SeFc}\}_2]\text{PF}_6$	340 (25000)	535 (10000)
$[\text{RhCl}_2\{\text{FcSe}(\text{CH}_2)_3\text{TeFc}\}_2]\text{PF}_6$	345 (25500)	520 (11600)
$[\text{RhCl}_2\{\text{FcTe}(\text{CH}_2)_3\text{TeFc}\}_2]\text{PF}_6$	355 (27100)	510 (12200)

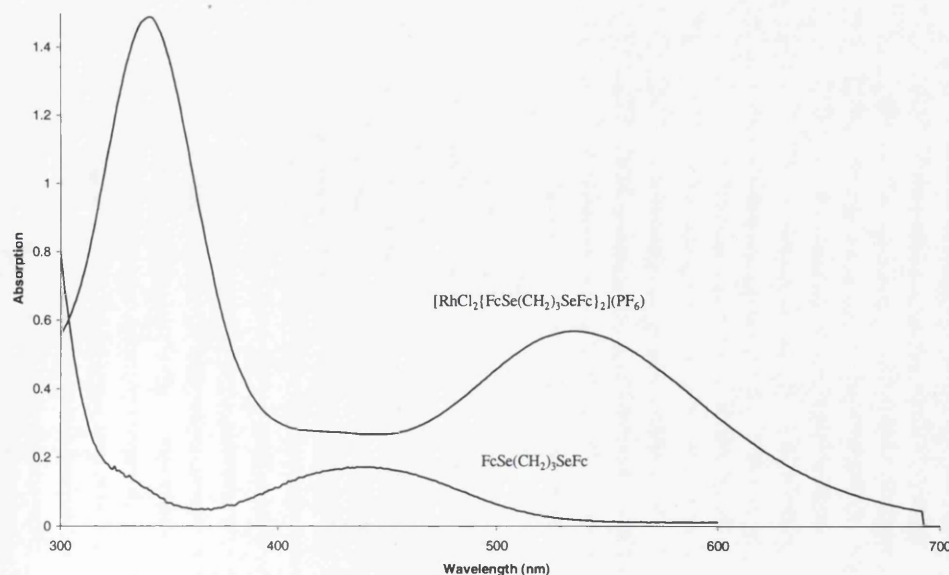


Fig. 5.5 UV-vis spectra of $\text{FcSe}(\text{CH}_2)_3\text{SeFc}$ and its Rh(III) complex in $10^{-4} \text{ mol dm}^{-3} \text{ CH}_3\text{CN}$ solution

5.2.3 Electrochemistry

Cyclic voltammetry (supplemented by differential pulse voltammetry where appropriate) was used to investigate the electrochemistry of the complexes in acetonitrile solution. The CV (Fig. 5.6) of $[\text{RhCl}_2\{\text{FcSe}(\text{CH}_2)_3\text{SeFc}\}_2]\text{PF}_6$ appears to show two waves but they are not well resolved. There are two peaks in the DPV (Fig. 5.7) at $E_p = 76$ and 303 mV (with respect to $\text{FcH}/[\text{FcH}]^+$); assuming that these correspond to the first and second ferrocenyl oxidations, $\Delta E_{1/2} = 227$ mV. The extent of electronic interaction between the two iron centres is thus between that exhibited by the palladium and platinum complexes (201 mV for $[\text{Pd}\{\text{FcSe}(\text{CH}_2)_3\text{SeFc}\}_2](\text{PF}_6)_2$ and 246 mV for $[\text{Pt}\{\text{FcSe}(\text{CH}_2)_3\text{SeFc}\}_2](\text{PF}_6)_2$). The lowest oxidation potential of the complex is also more positive than that of the “free” ligand, $\text{FcSe}(\text{CH}_2)_3\text{SeFc}$, just as it is for the Pd and Pt complexes.

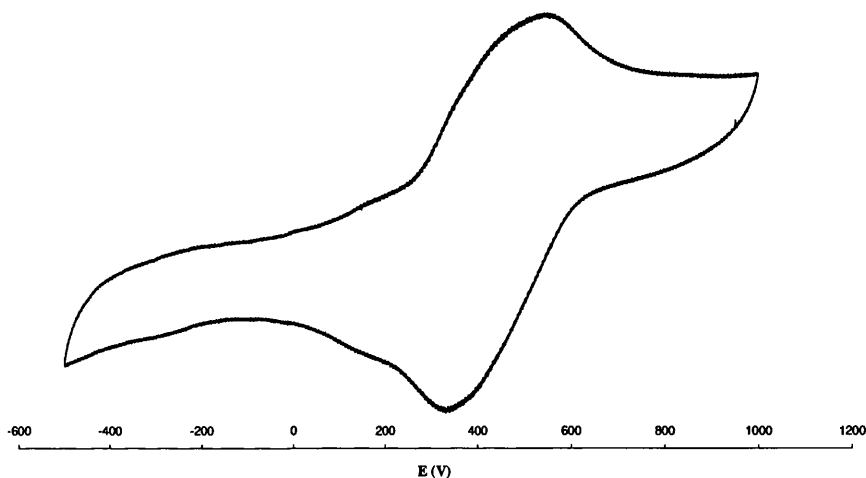


Fig. 5.6 CV of $[\text{RhCl}_2\{\text{FcSe}(\text{CH}_2)_3\text{SeFc}\}_2]\text{PF}_6$ in dry acetonitrile, 0.1 M $[\text{NBu}_4][\text{PF}_6]$ at a scan rate of 100 mV s^{-1}

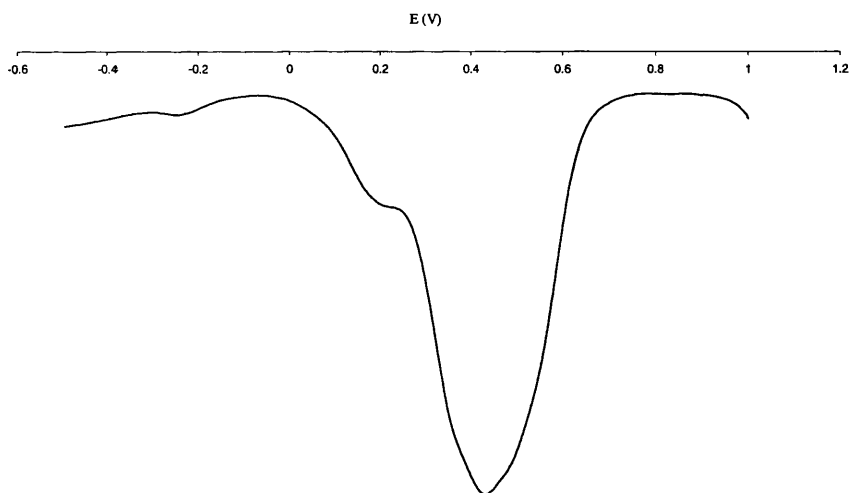


Fig. 5.7 DPV of $[\text{RhCl}_2\{\text{FcSe}(\text{CH}_2)_3\text{SeFc}\}_2]\text{PF}_6$ in dry acetonitrile, 0.1 M $[\text{NBu}_4][\text{PF}_6]$ at a scan rate of 100 mV s^{-1}

For $[\text{RhCl}_2\{\text{FcSe}(\text{CH}_2)_3\text{TeFc}\}_2]\text{PF}_6$, there are one quasi-reversible wave at $E_{1/2}(1) = 70 \text{ mV}$ ($|E_{\text{pa}} - E_{\text{pc}}| = 60 \text{ mV}$) and another at $E_{1/2}(2) = 297 \text{ mV}$ ($|E_{\text{pa}} - E_{\text{pc}}| = 197 \text{ mV}$), $\Delta E = 227 \text{ mV}$ (CV in Fig. 5.8 and DPV in Fig. 5.9). The change from $\text{FcSe}(\text{CH}_2)_3\text{SeFc}$ to $\text{FcSe}(\text{CH}_2)_3\text{TeFc}$ doesn't change the extent of electronic interaction between the two iron centres, which is larger than that in $[\text{M}\{\text{FcSe}(\text{CH}_2)_3\text{TeFc}\}_2](\text{PF}_6)_2$ (104 mV for $\text{M} = \text{Pd}$ and 101 mV for $\text{M} = \text{Pt}$).

The CV of $[\text{Rh}\{\text{FcTe}(\text{CH}_2)_3\text{TeFc}\}_2\text{Cl}_2]\text{PF}_6$ shows only one well resolved quasi-reversible wave at $E_{1/2} = 270 \text{ mV}$ ($|E_{\text{pa}} - E_{\text{pc}}| = 148 \text{ mV}$) (CV in Fig. 5.11 and DPV in Fig. 5.12). The oxidation potential is more positive than that in $[\text{M}\{\text{FcTe}(\text{CH}_2)_3\text{TeFc}\}_2](\text{PF}_6)_2$ ($\text{M} = \text{Pd}$, $E_{1/2} = 247 \text{ mV}$; $\text{M} = \text{Pt}$, $E_{1/2} = 205 \text{ mV}$).

Although there are no crystal structures' data, from the discussion in Chapter Four, we can predict that the through-bond $\text{Fe}\cdots\text{Fe}$ distances in $[\text{RhCl}_2\{\text{FcSe}(\text{CH}_2)_3\text{SeFc}\}_2]\text{PF}_6$ and $[\text{RhCl}_2\{\text{FcSe}(\text{CH}_2)_3\text{TeFc}\}_2]\text{PF}_6$ are shorter than 13.17 \AA to allow the interaction between the ferrocene moieties.

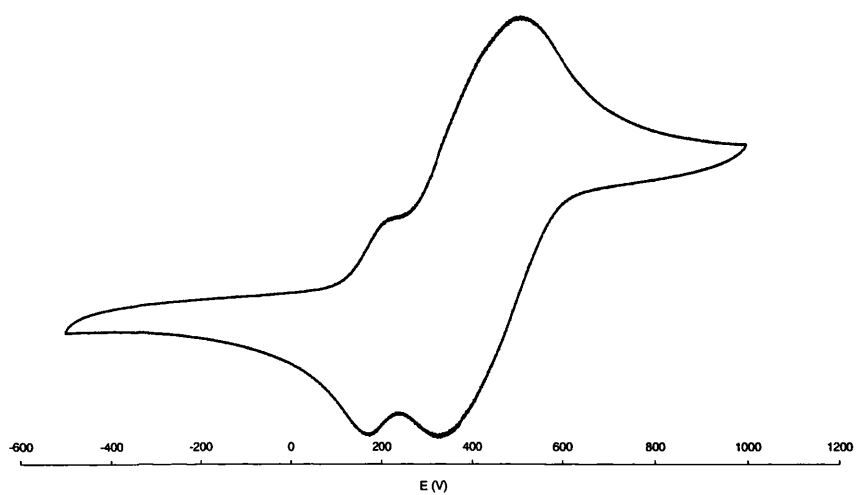


Fig. 5.8 CV of $[\text{RhCl}_2\{\text{FcSe}(\text{CH}_2)_3\text{TeFc}\}_2]\text{PF}_6$ in dry acetonitrile, 0.1 M $[\text{NBu}_4][\text{PF}_6]$ at a scan rate of 100 mV s^{-1}

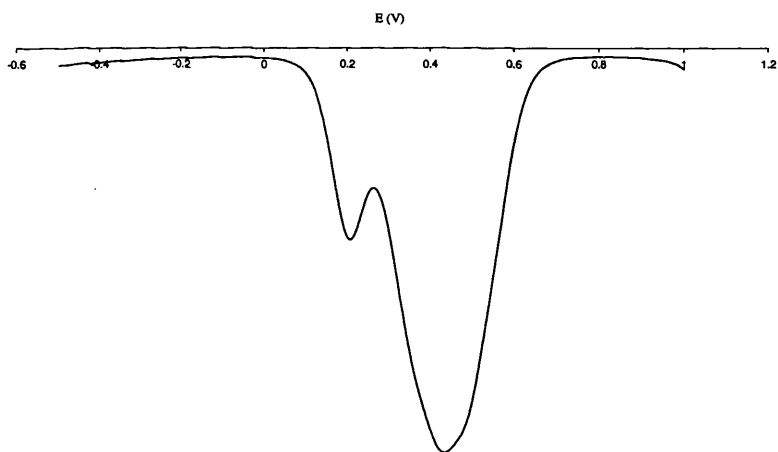


Fig. 5.9 DPV of $[\text{RhCl}_2\{\text{FcSe}(\text{CH}_2)_3\text{TeFc}\}_2]\text{PF}_6$ in dry acetonitrile, 0.1 M $[\text{NBu}_4][\text{PF}_6]$ at a scan rate of 100 mV s^{-1}

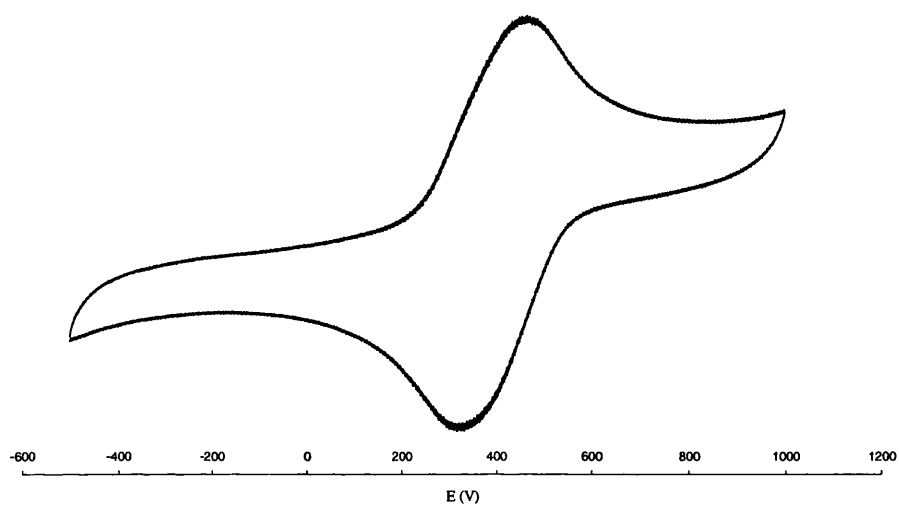


Fig. 5.10 CV of $[\text{RhCl}_2\{\text{FcTe}(\text{CH}_2)_3\text{TeFc}\}_2]\text{PF}_6$ in dry acetonitrile, 0.1 M $[\text{NBu}_4][\text{PF}_6]$ at a scan rate of 100 mV s^{-1}

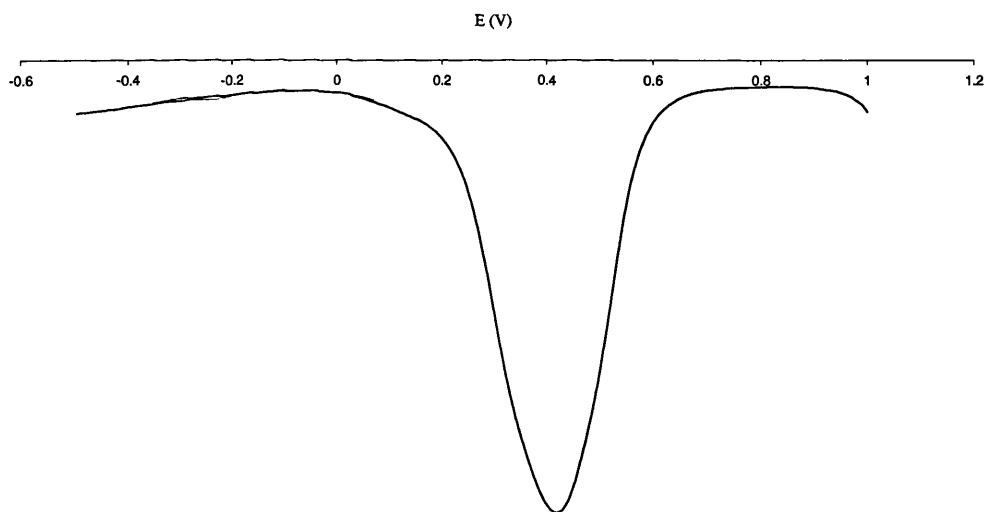


Fig. 5.11 DPV of $[\text{RhCl}_2\{\text{FcTe}(\text{CH}_2)_3\text{TeFc}\}_2]\text{PF}_6$ in dry acetonitrile, 0.1 M $[\text{NBu}_4][\text{PF}_6]$ at a scan rate of 100 mV s^{-1}

5.3 Other rhodium(III) complexes

The rhodium complexes of some other ferrocenyl chalcogenide ligands were also synthesized. But with the failure of obtaining good quality single crystals, this work was discontinued.

Rh(III) complexes of $\text{FcE}(\text{CH}_2)_n\text{E}'\text{Fc}$ ($n = 1, \text{E} = \text{E}' = \text{Se}$ or Te ; $n = 2, \text{E} = \text{E}' = \text{Se}$)

The general procedure used for the syntheses of all these complexes, was the same as that for $[\text{Rh}\{\text{FcSe}(\text{CH}_2)_3\text{SeFc}\}_2\text{Cl}_2]\text{PF}_6$. The experimental details are given in Chapter Seven.

The ES mass spectra showed an excellent match of the isotope pattern for the molecular ion unit that calculated for $[\text{RhCl}_2\{\text{FcE}(\text{CH}_2)_n\text{E}'\text{Fc}\}_2]^+$ and also confirmed the presence of PF_6^- .

Rh(III) complexes of $\text{MeC}(\text{CH}_2\text{EFC})_3$

The synthesis of $[\text{Rh}\{\text{MeC}(\text{CH}_2\text{SeFc})_3\}_2](\text{PF}_6)_3$ was performed as follows. One equivalent of $\text{RhCl}_3 \cdot 3\text{H}_2\text{O}$ and two equivalents of $\text{MeC}(\text{CH}_2\text{SeFc})_3$ in ethanol (30 ml) were refluxed for 1 h. Addition of more than three equivalents of KPF_6 gave a dark purple precipitate, which was collected by filtration and washed by diethyl ether. The ES mass spectra showed a molecular ion unit with the correct isotope pattern for $[\text{RhCl}_2\{\text{MeC}(\text{CH}_2\text{SeFc})_3\}_2]^+$ and confirmed the presence of PF_6^- . A similar result was obtained for $\text{MeC}(\text{CH}_2\text{TeFc})_3$. It appears that the tripodal ligand $\text{MeC}(\text{CH}_2\text{EFC})_3$ only behaves as a bidentate ligand, unlike its analogue $\text{MeC}(\text{CH}_2\text{SeR})_3$ ($\text{R} = \text{Me}$ or Ph),¹⁰ possibly due to the bulk of the ferrocenyl group.

5.4 References for Chapter Five

1. S. Rossi, J. Pursiainen, M. Ahlgren, T.A. Pakkanen, *J. Organomet. Chem.*, 1990, **391**, 403
2. S. Rossi, J. Pursiainen, T.A. Pakkanen, *J. Organomet. Chem.*, 1990, **397**, 81
3. M. Devery, R. S. Dickson, B. W. Skelton, A. H. White, *Organometallics*, 1999, **18**, 5292
4. T. Kemmitt, W. Levason, R. D. Oldroyd, M. Webster, *Polyhedron*, 1992, **11**, 2165
5. K. Badyal, W. R. McWhinnie, H. L. Chi, T. A. Hamor, *J. Chem. Soc., Dalton Trans.*, 1997, 1579
6. K. Badyal, W. R. McWhinnie, J. Homer, M. C. Perry, *J. Organomet. Chem.*, 1998, **555**, 279
7. W. Levason, G. Reid, V.-A. Tolhurst, *J. Chem. Soc., Dalton Trans.*, 1998, 3411
8. D. J. Gulliver, E. G. Hope, W. Levason, S. G. Murray, G. L. Marshall, *J. Chem. Soc., Dalton Trans.*, 1985, 1265
9. W. Levason, S. D. Orchard, G. Reid and V. A. Tolhurst, *J. Chem. Soc., Dalton Trans.*, 1999, 2071
10. W. Levason, S. D. Orchard, G. Reid, *Inorg. Chem.*, 2000, **39**, 3853
11. W. Levason, S. D. Orchard, G. Reid, *J. Chem. Soc., Dalton Trans.*, 2000, 2537
12. A. J. Barton, W. Levason, G. Reid, *Organometallics*, 2001, **20**, 3644
13. M. Hesford, W. Levason, S. D. Orchard, G. Reid, *J. Organomet. Chem.*, 2002, **649**, 214
14. P. F. Kelly, W. Levason, G. Reid, D. J. Williams, *J. Chem. Soc., Chem. Commun.*, 1993, 1716
15. W. Levason, J. J. Quik, G. Reid, *J. Chem. Soc., Dalton Trans.*, 1996, 3713
16. D. H. W. Carstens, G. A. Crosby, *J. Mol. Spectrosc.*, 1970, **34**, 113
17. A. J. Blake, G. Reid, M. Schröder, *J. Chem. Soc., Dalton Trans.*, 1989, 1675.
18. N. Goswami, R. Alberto, C. L. Barnes, S. Jurisson, *Inorg. Chem.*, 1996, **35**, 7546
19. A. M. Hill, W. Levason, S. R. Preece, M. Webster, *Polyhedron*, 1997, **16**, 1307

CHAPTER SIX

Miscellaneous Reactions

In this chapter, miscellaneous reactions attempted during my research work are presented. They were not explored further due to different reasons, such as low yields, instability of the compound *etc.*

6.1 Attempted reactions

Attempted reaction of [Cu(NCMe)₄](PF₆) and FcE(CH₂)₃EFc (E = Se or Te)

As there are several Cu(I) selenoether and telluroether complexes described in the literature¹, direct reaction between FcE(CH₂)₃EFc (E = Se or Te) and [Cu(NCMe)₄](PF₆) was attempted. The general procedure is illustrated below. The experimental details are given in Chapter Seven.

One equivalent of [Cu(NCMe)₄](PF₆) and two equivalents of FcSe(CH₂)₃SeFc were added to dry CH₂Cl₂. The solution was refluxed for 1 h and allowed to cool to room temperature. No obvious colour change was observed during the process. The mixture was reduced to 5 ml *in vacuo*, and diethyl ether (10 ml) was added to precipitate the product as a yellow powder. MS and NMR analytical results showed that this is just free ligand which may be due to the bulk of the ferrocenyl group inhibiting complexation to the first row transition metal.

Attempted reaction of HgX₂ and FcSe(CH₂)₃SeFc (X = Cl, I)

The Hg(II) reagents HgX₂ can react with macrocyclic chalcogen ligands.^{2,3} In the complexes obtained, the macrocycles always act as bidentate chelating ligands. A similar procedure was used for the attempted reactions between HgX₂ and FcSe(CH₂)₃SeFc.

One equivalent of HgI₂ in acetone was added to a CHCl₃ solution of FcSe(CH₂)₃SeFc. The mixture was refluxed for 24 h and allowed to cool to room temperature. The solution was reduced to 5 ml *in vacuo*, and diethyl ether was added to precipitate a yellow powder. NMR spectroscopy revealed the product to be free ligand.

The attempted reaction of HgCl₂ and FcSe(CH₂)₃SeFc also gave only free ligand.

It may be that the macrocyclic effect is required for the isolation of complexes of this type.

Attempted reaction of [Mo(CO)₃(NCMe)₃] and MeC(CH₂EFc)₃ (E = Se or Te)

As mentioned in Chapter One, although *fac*-[Mo(CO)₃{MeC(CH₂EMe)₃}] (E = Se or Te) can be synthesized, they are unstable in solution and decompose to

cis-[Mo(CO)₄{MeC(CH₂EMe)₃}₂].⁴ It was decided to attempt to react [Mo(CO)₃(NCMe)₃] and MeC(CH₂EFc)₃. The general procedure is illustrated below. The experimental details are given in Chapter Seven.

One equivalent of [Mo(CO)₆] was refluxed for 18 h in dry MeCN to give [Mo(CO)₃(NCMe)₃]. One equivalent of the ligand MeC(CH₂TeFc)₃ was added and the mixture stirred under nitrogen for a further 20 h. The solution was filtered and evaporated to dryness. The residue was dissolved in CH₂Cl₂ (5 ml), filtered and cold hexane added to yield a brown powder. The powder was collected, washed with cold hexane and dried under vacuum.

MALDI MS shows a good match of isotope pattern for the calculated isotope pattern for [Mo(CO)₃{MeC(CH₂TeMe)₃}] with that observed for the molecular ion. The IR spectrum shows two ν(CO) bands at 1921, 1817 cm⁻¹, but the compound decomposed quickly in solution.

The attempted reaction of [Mo(CO)₃(NCMe)₃] and MeC(CH₂SeFc)₃ yielded little product.

In view of the bulky ferrocenyl group and the instability of the complexes, this work was not explored further.

Attempted reaction of AgNO₃ and MeC(CH₂TeFc)₃

Self-assembly is an important topic in the supramolecular chemistry.⁵ With the aid of a suitable metal ion, a pre-designed structure can be successfully obtained. A trinuclear molecular capsule was assembled from a tripodal pyridyl ligand and three silver ions (Fig. 6.1).⁶ With this in mind, it was decided to try the reaction between AgNO₃ and MeC(CH₂TeFc)₃.

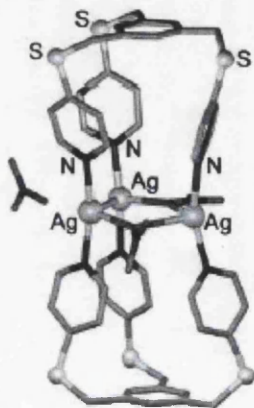


Fig. 6.1 Structure of a silver trinuclear molecular capsule

One equivalent of AgNO_3 in methanol/MeCN (2:1) was added to a dichloromethane solution of one equivalent of $\text{MeC}(\text{CH}_2\text{TeFc})_3$. Diethyl ether vapour was allowed to diffuse into the mixture to yield yellow crystals. ES mass spectrometry suggested the product was $[\text{Ag}\{\text{MeC}(\text{CH}_2\text{TeFc})_3\}_2]\text{NO}_3$, which may mean that $\text{MeC}(\text{CH}_2\text{TeFc})_3$ is not rigid enough to construct a trinuclear molecular capsule.

Attempted reaction of $[\text{RhCl}(\text{COD})]_2$ and $\text{MeC}(\text{CH}_2\text{EFc})_3$ ($E = \text{Se or Te}$)

Rh(I) complexes $[\text{Rh}(\text{COD})\{\text{MeC}(\text{CH}_2\text{ER})_3\}](\text{PF}_6)$ ($E = \text{Se, R = Me; E = Te, R = Me or Ph}$) have been prepared.⁷ It was decided to attempt to react $[\text{RhCl}(\text{COD})]_2$ and $\text{MeC}(\text{CH}_2\text{EFc})_3$. The general procedure is illustrated below. The experimental details are given in Chapter Seven.

The mixture of one equivalent of $[\text{RhCl}(\text{COD})]_2$, two equivalents of $\text{MeC}(\text{CH}_2\text{TeFc})_3$ and a little more than two equivalents of KPF_6 in CH_2Cl_2 was stirred at room temperature for 1 hour. The precipitated KCl was removed by filtration, the solvent volume reduced to 2 ml *in vacuo* and diethyl ether added (10 ml) to give a dark red product. MALDI mass spectrometry showed a cluster of peaks with the correct isotope pattern for $[\text{Rh}(\text{COD})\{\text{MeC}(\text{CH}_2\text{TeFc})_3\}](\text{PF}_6)$. The attempt to obtain single crystals suitable for crystallography failed.

The reaction $[\text{RhCl}(\text{COD})]_2$ and $\text{MeC}(\text{CH}_2\text{SeFc})_3$ also gave a dark red precipitate, but in quite low yield.

Attempted reaction of $[\text{Pd}_2(\text{NCMe})_6](\text{PF}_6)_2$ and $\text{FcSe}(\text{CH}_2)_3\text{Te}(\text{CH}_2)_3\text{SeFc}$

In Chapter Three, Pd(II) complexes of linear tridentate ligands was obtained with the formula $[\text{PdCIL}](\text{PF}_6)$. This suggests that if the starting reagent was changed to the Pd(I) compound $[\text{Pd}_2(\text{NCMe})_6](\text{PF}_6)_2$, the linear tridentate ligand may substitute MeCN to yield a dinuclear complex (Fig. 6.2). The procedure is illustrated below.

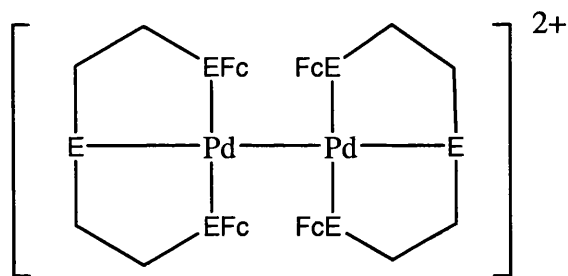


Fig. 6.2 Target dinuclear palladium complex

A dichloromethane solution of $\text{FcSe}(\text{CH}_2)_3\text{Te}(\text{CH}_2)_3\text{SeFc}$ (two equivalents) were added to an acetonitrile solution of $[\text{Pd}_2(\text{NCMe})_6](\text{PF}_6)_2$ (one equivalent). The mixture was stirred at room temperature for 24 h, the solvent volume reduced to 2 ml *in vacuo* and diethyl ether added (10 ml) to give a dark purple product. ES mass spectrometry showed a cluster of peaks at 973 and confirmed the presence of PF_6^- .

It appears that the target complex is unstable, either due to the weakness of the Pd-Pd bond or the bulk of the ferrocenyl group. No more work was done in this field.

Attempted reaction of Fc_2Te_2 and $[\text{W}(\text{CO})_5(\text{THF})]$

The reaction between $[\text{W}(\text{CO})_5\text{THF}]$ and Fc_2Se_2 yields the dinuclear complex $[\text{W}_2(\mu\text{-SeFc})_2(\text{CO})_8]$.⁸ The analogous reaction of Fc_2Te_2 with $[\text{W}(\text{CO})_5\text{THF}]$ was attempted.

Addition of Fc_2Te_2 to a solution of $[\text{W}(\text{CO})_5(\text{THF})]$ in THF at room temperature led immediately to a deepening of the colour from orange to dark red. After stirring overnight, the solution was reduced to dryness by evaporation of the solvent under reduced pressure, and the residue then extracted with hexane/toluene (1:1). The solution was filtered to remove a sticky black insoluble residue, and the solvent removed *in vacuo*. Thin layer chromatography revealed the presence of unreacted diferrocenyl ditelluride in addition to a new purple band assigned to the product. These could not be separated by column chromatography on SiO_2 .

NMR spectroscopy and mass spectrometry of the crude product showed that it was a complex mixture, and suggested that not only Te-C, but also Te-Te bond cleavage had taken place. Carrying out the reaction at low temperature ($-78\text{ }^\circ\text{C}$) did not significantly change the outcome.

6.2 References for Chapter Six

1. J. R. Black, W. Levason, *J. Chem. Soc., Dalton Trans.*, 1994, 3225
2. A. Mazouz, P. Meunier, M. M. Kubicki, B. Hanquet, R. Amardeil, C. Bornet, A. Zahidi, *J. Chem. Soc., Dalton Trans.*, 1997, 1043
3. S. C. Menon, H. B. Singh, R. P. Patel, S. K. Kulshreshtha, *J. Chem. Soc., Dalton Trans.*, 1996, 1203
4. A. J. Barton, J. Connolly, W. Levason, A. Media-Jalon, S. D. Orchard, G. Reid, *Polyhedron*, 2000, **19**, 1373
5. L. F. Lindoy and I. M. Atkinson, *Self-Assembly in Supramolecular Systems*, Ed. J. F. Stoddart, Royal Society of Chemistry, Cambridge, UK, 2000
6. D. J. Bray, L.-L. Liao, B. Antonioli, K. Gloe, L. F. Lindoy, J. C. McMurtrie, G. Wei, X.-Y. Zhang, *Dalton Trans.*, 2005, 2082
7. Levason, S. D. Orchard, G. Reid, *J. Chem. Soc. Dalton Trans.*, 2000, 2537
8. M. R. Burgess, Ph.D. Thesis, University of Wales Swansea, 1999

CHAPTER SEVEN

Experimental

7.1 General

All reactions were performed using standard Schlenk techniques and pre-dried solvents under an atmosphere of dinitrogen. All solvents were distilled from elemental alkali metal or Na/K alloy, except ethanol (which was degassed before use), acetonitrile and dichloromethane (which were distilled over calcium hydride). ^1H and ^{13}C NMR spectra: Bruker AC400; tetramethylsilane as internal standard. ^{77}Se and ^{125}Te NMR spectra: Bruker WM250; dimethyl selenide or dimethyl telluride as external standard. IR spectra: Perkin Elmer Spectrum One FT-IR Spectrometer. UV/Vis spectra: UNICAM UV 300 UV-visible Spectrometers in 1 cm quartz cells at room temperature.

Mass spectra were recorded by the EPSRC Mass Spectrometry Centre, using electron impact (EI), fast atom bombardment (FAB), positive ion electrospray (ES), matrix-assisted laser desorption/ionization (MALDI, DCTB: *trans*-2-[3-(4-*tert*-butylphenyl)-2-methylprop-2-enylidene]malononitrile as matrix, positive ionisation mode): m/z values have been rounded to the nearest integer or half-integer; assignments are based on isotopomers containing ^1H , ^{12}C , ^{19}F , ^{31}P , ^{35}Cl , ^{52}Cr , ^{56}Fe , ^{79}Br , ^{80}Se , ^{98}Mo , ^{130}Te , ^{103}Rh , ^{107}Ag , ^{106}Pd , ^{127}I , ^{184}W or ^{195}Pt ; expected isotope distribution patterns were observed.

Cyclic voltammetry (CV) and differential pulse voltammetry (DPV): Autolab PGSTAT30 potentiostat system; Pt working and auxiliary electrodes; Ag/Ag⁺ (0.01 M AgNO₃ in CH₃CN) as reference electrode; 0.1 M [NBu₄][PF₆] in CH₃CN (or in CH₂Cl₂ for carbonyl complexes) as supporting electrolyte; scan rates 100 mV s⁻¹ (CV), 72 mV s⁻¹ (DPV). Elemental analyses were performed by Butterworth Laboratories Ltd., Teddington, Middlesex, UK.

X-ray crystallography data collections were performed by Prof. M. D. Vaira (university of Florence, Italy) at room temperature with an Oxford Diffraction Xcalibur 3 CCD diffractometer and graphite-monochromated Mo-K α radiation ($\lambda = 0.71069$ Å). Intensity data sets were corrected for absorption by a multi-scan procedure.¹ The structures were solved by direct methods, with SIR-97,² and refined with SHELXL-97.³ All non-hydrogen atoms were refined anisotropically; hydrogens were in calculated positions, riding, each with a temperature factor linked to that of the respective carrier atom. For graphics ORTEP-3 was employed.⁴

Common laboratory reagents were purchased from commercial sources.

7.2 Preparation of starting materials

7.2.1 Fc₂E₂ (E = Se or Te)

Fc₂E₂ (E = Se, Te) were prepared from [Fe(η^5 -C₅H₅)₂] (FcH) *via* lithiation in THF with 0.9 equivalents of Li^tBu, treatment with selenium or tellurium, and air oxidation, in a minor modification of a literature procedure.^{5,6}

(FcSe)₂: A 1.6 M solution of ^tBuLi in pentane (6.25 ml, 10 mmol) was added slowly to a dry THF solution (30 ml) of ferrocene (2.24g, 12 mmol) at 0 °C. After 30 min, the solution was warmed to room temperature and stirred for another 30 min. Selenium powder (0.79 g, 10 mmol) was then added under a brisk flow of nitrogen gas and reacted for 1 h at room temperature. The mixture was then poured into a beaker and wet THF (10 ml) was added. The stirring was continued, normally for 1h to 1.5h, until the colour changed from dark red to orange. The solvent was removed by evaporation under reduced pressure. The residue was extracted with CH₂Cl₂. The filtered solution was evaporated to dryness, and then subjected to column chromatography on SiO₂. The unreacted ferrocene and a small amount of triselenoferrocenophane were eluted with hexane. Diferrocenyl diselenide was eluted with a 3:1 hexane: CH₂Cl₂ mixture, and obtained as an orange powder after evaporation of the solvent under reduced pressure. Yield 1.3g (50%).

¹H NMR (CDCl₃): 4.26 (C₅H₄, H₂₊₅, m, 2H), 4.22 (C₅H₄, H₃₊₄, m, 2H), 4.08 (C₅H₅, s, 5H).

¹³C NMR (CDCl₃): 75.77 (C₅H₄, C₂₊₅), 71.04 (C₅H₄, C₃₊₄), 69.76 (C₁), 69.64 (C₅H₅).

⁷⁷Se NMR (CDCl₃): 483.

(FcTe)₂: A 1.6 M solution of ^tBuLi in pentane (6.25 ml, 10 mmol) was added slowly to a dry THF solution (30 ml) of ferrocene (2.24g, 12 mmol) at 0 °C. After 30 min, the solution was warmed to room temperature and stirred for another 30 min. Tellurium powder (1.27 g, 10 mmol) was then added under a brisk flow of nitrogen gas and reacted for 1h at room temperature. The mixture was then poured into a beaker and wet THF (10 ml) was added. The stirring was continued, normally for 1h to 1.5h, until the colour changed from dark red to orange red. The solvent was removed by evaporation under reduced pressure. The residue was extracted with CH₂Cl₂. The filtered solution was evaporated to dryness, and then subjected to column chromatography on SiO₂. The unreacted ferrocene was eluted with hexane.

Diferrocenyl ditelluride was eluted with a 3:1 hexane: CH₂Cl₂ mixture, and obtained as a dark powder after evaporation of the solvent under reduced pressure. Yield 1.8g (60%).

¹H NMR (CDCl₃): 4.29 (C₅H₄, H₂₊₅, m, 2H), 4.20 (C₅H₄, H₃₊₄, m, 2H), 4.09 (C₅H₅, s, 5H).

¹³C NMR (CDCl₃): 79.36 (C₅H₄, C₂₊₅), 71.91 (C₅H₄, C₃₊₄), 69.72 (C₅H₅), 41.40(C₁).

¹²⁵Te NMR (CDCl₃): 381.

7.2.2 Fc₂E (E = Se or Te)

Diferrocenyl chalcogenides were synthesized by the Herberhold and Leitner's method,⁵ which is quite simple, but FcEEFc and FcEFc are difficult to separate. In order to obtain the pure product, a little more than two equivalents of FcLi were used. This resulted in consumption of all the FcEEFc reagent and pure FcEFc could be isolated by column chromatography.

FcSeFc: A 1.6 M solution of ^tBuLi in pentane (1.68 ml, 2.68 mmol) was added slowly to a dry THF solution (30 ml) of ferrocene (0.5 g, 2.68 mmol) at 0 °C. After 30 min, the solution was warmed to room temperature and stirred for another 30 min. Diferrocenyl diselenide (0.52 g, 1 mmol) was then added under a brisk flow of nitrogen gas and reacted for 1h at room temperature. The mixture was then poured into a beaker and wet THF (10 ml) was added. The stirring was continued, normally for 1h. The solvent was removed by evaporation under reduced pressure. The residue was extracted with CH₂Cl₂. The filtered solution was evaporated to dryness, and then subjected to column chromatography on SiO₂. The unreacted ferrocene was eluted with hexane. Diferrocenyl selenide was eluted with a 3:1 hexane: CH₂Cl₂ mixture, and obtained as an orange powder after evaporation of the solvent under reduced pressure. Yield 0.4 g (67%).

¹H NMR (CDCl₃): 4.24 (C₅H₄, H₂₊₅, m, 2H), 4.11 (C₅H₅, s, 5H), 4.08 (C₅H₄, H₃₊₄, m, 2H).

¹³C NMR (CDCl₃): 74.6 (C₅H₄, C₂₊₅), 69.8 (C₅H₄, C₃₊₄), 69.7(C₁), 69.7 (C₅H₅).

⁷⁷Se NMR (CDCl₃): 210.

FAB MS: 450 ([M]⁺, 100%), 265 ([FcSe]⁺, 18%).

FcTeFc, A 1.6 M solution of ^tBuLi in pentane (3.0 ml, 4.8 mmol) was added slowly to a dry THF solution (30 ml) of ferrocene (0.75 g, 4.8 mmol) at 0 °C. After 30 min, the solution was warmed to room temperature and stirred for another 30 min. Diferrocenyl ditelluride (1.0 g, 1.6 mmol) was then added under a brisk flow of nitrogen gas and reacted for 1h at room temperature. The mixture was then poured into a beaker and wet THF (10 ml) was added. The stirring was continued, normally for 1h. The solvent was removed by evaporation under reduced pressure. The residue was extracted with CH₂Cl₂. The extract was evaporated to dryness, and then subjected to column chromatography on SiO₂. Diferrocenyl ditelluride was eluted with a 3:1 hexane: CH₂Cl₂ mixture, and obtained as an orange powder after evaporation of the solvent under reduced pressure. Yield 0.7 g (57%).

¹H NMR (CDCl₃): 4.29 (C₅H₄, H₂₊₅, m, 2H), 4.10 (C₅H₄, H₃₊₄, m, 2H), 4.07 (C₅H₅, s, 5H).

¹³C NMR (CDCl₃): 78.9 (C₅H₄, C₂₊₅), 71.3 (C₅H₄, C₃₊₄), 69.6 (C₅H₅), 49.2 (C₁).

¹²⁵Te NMR (CDCl₃): 347.

FAB MS: 500 ([M]⁺, 95%), 315 ([FcTe]⁺, 100%).

7.2.3 fcSe₃

As mentioned in Chapter Two, all the 1,2,3-trichalcogena[3]ferrocenophane have been fully characterised. fcSe₃ was synthesized as described in the literature work with slight modification.⁷

A 1.6 M solution of ⁿBuLi in pentane (12.5 ml, 20 mmol) was added slowly to a dry THF solution (30 ml) of ferrocene (1.87 g, 10 mmol) at 0 °C. After 10 min, the solution was warmed to room temperature and stirred for another 2 h. Selenium powder (1.58 g, 20 mmol) was added under a brisk flow of nitrogen gas and reacted for 2 h at room temperature. Further selenium powder (0.79 g, 10 mmol) was then added and reacted for 1h at room temperature, then for 1h under air. The solvent was removed by evaporation under reduced pressure. The residue was extracted with CH₂Cl₂. The filtered solution was evaporated to dryness, and then subjected to column chromatography on SiO₂. The triselenoferrocenophane was eluted with hexane after the unreacted ferrocene, and obtained as an orange red powder after evaporation of the solvent under reduced pressure. Yield 2.1 g (50%).

¹H NMR (CDCl₃): 4.50-3.85 (C₅H₄, H₂₊₃₊₄₊₅, m, 2H).

^{13}C NMR (CDCl_3): 88.8 (C_1), 78.5, 71.2, 71.0, 69.9 (C_5H_4 , $\text{C}_{2+3+4+5}$).

7.2.4 $\text{MeC}(\text{CH}_2\text{Br})_3$

$\text{MeC}(\text{CH}_2\text{Br})_3$ was prepared by the literature route.⁸

Phosphorus tribromide (9.6 ml, 27.6g, 102 mmol) was added to 1,1,1-tris(hydroxymethyl)ethane (8.0 g, 67mmol) over 30 min. The mixture was then heated to 145 °C for 24 h. The reaction mixture was decomposed with 100 ml water, and extracted with toluene. The toluene solution was washed with sodium bicarbonate solution and then with water, dried over manganese sulphate, and concentrated *in vacuo* to give colourless oil. Yield 6.4 g (31%).

^1H NMR (CDCl_3): 3.50 (CH_2 , s, 6H), 1.30 (CH_3 , s, 3H).

^{13}C NMR (CDCl_3): 40.4 (CH_3C), 39.4 (CH_2), 22.0 (CH_3).

7.2.5 $\text{NCSeCH}_2\text{CH}_2\text{CH}_2\text{SeCN}$

1,3-Propanediyl diselenocyanate was synthesized as in the literature work with little modification.⁹

Solid potassium selenocyanate 6.86 g (0.048 mol) was added to 45 ml of dry acetone in a 250 mL three-neck flask equipped with a magnetic stirrer and condenser. After the mixture had been heated to 40 °C, 1,3-propanediyl dibromide (4.43 g, 0.022 mol) was added dropwise via syringe to the solution with constant stirring. Within 5 min, a white solid appeared in the reaction mixture, which was stirred for 2 h at 50 °C. The mixture was then allowed to cool, and the potassium bromide that had formed was removed by filtration. Removal of acetone under reduced pressure resulted in an orange oily residue. The oil was then dissolved in the minimum amount of diethyl ether, and placed at -20°C. The target compound crystallized as white needles. The product was filtered from the solution in air, washed with small amounts of cold diethyl ether, and dried under vacuum. The compound is quite smelly. Yield 2.90g (48%).

^1H NMR (CD_3COCD_3): 3.22 (SeCH_2 , m, 4H), 2.40 ($\text{CH}_2\text{CH}_2\text{CH}_2$, m, 2H)

^{13}C NMR (CD_3COCD_3): 103.2 (CN, $^1J_{\text{Se-C}} = 224$ Hz), 34.0 (CH_2 , $^2J_{\text{Se-C}} = 35.6$ Hz),
29.3 (CH_2 , $^1J_{\text{Se-C}} = 54.7$ Hz)

5.2.6 Other Starting Materials

[M(CO)₄(nbd)] (M = Cr or Mo) and [W(CO)₄(TMPDA)]

[M(CO)₄(nbd)] (M = Cr or Mo) and [W(CO)₄(TMPDA)] were synthesized by the literature routes.^{10, 11}

[MCl₂(PhCN)₂] (M = Pd or Pt)

[MCl₂(PhCN)₂] (M = Pd or Pt) were synthesized by the literature routes.¹²

[Cu(MeCN)₄](PF₆)

[Cu(MeCN)₄](PF₆) was synthesized by the literature route.¹³

[Rh(COD)Cl]₂

[Rh(COD)Cl]₂ was synthesized by the literature route.¹⁴

[Pd₂(NCMe)₆](PF₆)₂

[Pd₂(NCMe)₆](PF₆)₂ was synthesized by the literature route.¹⁵

[W(CO)₅(THF)]

[W(CO)₅(THF)] was synthesized by the literature route.¹⁶

7.3 Synthesis of new ferrocenyl chalcogenide ligands

7.3.1 FcE(CH₂)_nE'Fc (n = 1, E = E' = Se or Te; n = 2, E = E' = Se; n = 3, E, E' = Se or Te), FcE(CH₂)₃X (E = Se, X = Br or I; E = Te, X = Br)

The products were obtained as described in chapter two. Reaction details are given below.

FcSe(CH₂)₃SeFc and FcSe(CH₂)₃I: Fc₂Se₂ (0.527 g, 1 mmol) was dissolved in EtOH (50 ml), and the solution cooled to 0 °C. NaBH₄ (0.151 g, 4 mmol) was then added. After warming to room temperature and stirring for 2 h, the mixture became homogeneous. An ethanol solution of I(CH₂)₃I (3.1 ml, 4% v/v, 1 mmol) was added, and the mixture left to stir overnight. The solvent was removed by evaporation under reduced pressure. The residue was treated with water (25 ml) and extracted with CH₂Cl₂ (3 × 25 ml). The extract was dried over MgSO₄ and evaporated to dryness, then subjected to column chromatography on SiO₂. Elution with hexane/dichloromethane (3:1) produced two bands: the first contained FcSe(CH₂)₃I, an orange-yellow oil, yield 0.065 g (30%); the second contained FcSe(CH₂)₃SeFc, an orange-yellow solid, yield 0.128 g (45%). Carrying out this reaction under reflux led to the exclusive formation of FcSe(CH₂)₃SeFc, yield 70%. Elemental analysis calcd for C₂₃H₂₄Fe₂Se₂: C 48.46, H 4.24; found C 47.18, H 4.11. Spectroscopic data are summarised below:

FcSe(CH₂)₃I

¹H NMR (CDCl₃): 4.12 (C₅H₅, s, 5H), 4.14 (C₅H₄, H₃₊₄, m, 2H), 4.24 (C₅H₄, H₂₊₅, m, 2H), 3.17 (CH₂I, t, 2H, ³J_{H-H} = 8.8 Hz), 2.57 (SeCH₂, t, 2H, ³J_{H-H} = 8.8 Hz), 1.99 (CH₂CH₂CH₂, m, 2H).

¹³C NMR (CDCl₃): 75.2 (C₅H₄, C₂₊₅), 70.3 (C₅H₄, C₃₊₄), 70.2 (C₁), 69.8 (C₅H₅), 34.0 (CH₂CH₂CH₂), 30.1 (SeCH₂, ¹J_{Se-C} = 63.6 Hz), 6.7 (CH₂I).

⁷⁷Se NMR (CDCl₃): 185.

FAB MS: 434 (M⁺, 100%), 265 (FcSe⁺, 20%).

FcSe(CH₂)₃SeFc

$^1\text{H NMR}$ (CDCl_3): 4.19 (C_5H_4 , H_{2+5} , m, 2H), 4.11 (C_5H_4 , H_{3+4} , m, 2H), 4.10 (C_5H_5 , s, 5H), 2.54 (SeCH_2 , t, 4H, $^3J_{\text{H-H}} = 9.0$ Hz), 1.78 ($\text{CH}_2\text{CH}_2\text{CH}_2$, m, 2H).

$^{13}\text{C NMR}$ (CDCl_3): 74.3 (C_5H_4 , C_{2+5}), 69.2 (C_1), 68.7 (C_5H_4 , C_{3+4}), 68.3 (C_5H_5), 30.0 ($\text{CH}_2\text{CH}_2\text{CH}_2$), 28.0 (SeCH_2).

$^{77}\text{Se NMR}$ (CDCl_3): 188.

FAB MS: 572 (M^+ , 100%), 265 (FcSe^+ , 96%), 226 ($\text{FcCH}_2\text{CH}=\text{CH}_2^+$, 67%).

FcTe(CH₂)₃Br: Four equivalents of sodium borohydride (0.080 g, 2.02 mmol) were added to a 50 ml ethanol solution of diferrocenyl ditelluride (0.353 g, 0.51 mmol). After 1h, the mixture became a clear orange red solution. Then at 0°C, this solution was slowly transferred to a dilute ethanol solution (200 ml) containing excess α , ω -dibromopropane (1 ml). The reaction was allowed to continue for 2h, with the solution colour changing to yellow. The solvent was removed by evaporation under reduced pressure. The residue was treated with water (25 ml) and extracted with CH_2Cl_2 (3 \times 25 ml). The extract was dried over MgSO_4 and evaporated to dryness, then subjected to column chromatography on SiO_2 . Elution with hexane/dichloromethane (3:1) led to isolation of the product *FcTe(CH₂)₃Br* as an orange oil in high yield (0.355 g, 80%). *FcSe(CH₂)₃Br* was synthesized similarly. Spectroscopic data are summarised below:

FcSe(CH₂)₃Br

$^1\text{H NMR}$ (CDCl_3): 4.23 (C_5H_4 , H_{2+5} , m, 2H), 4.13 (C_5H_4 , H_{3+4} , m, 2H), 4.12 (C_5H_5 , s, 5H), 3.40 (CH_2Br , t, 2H, $^3J_{\text{H-H}} = 6.4$ Hz), 2.61 (SeCH_2 , t, 2H, $^3J_{\text{H-H}} = 7.2$ Hz), 2.01 ($\text{CH}_2\text{CH}_2\text{CH}_2$, m, 2H).

$^{13}\text{C NMR}$ (CDCl_3): 75.8 (C_5H_4 , C_{2+5}), not observed (C_1), 70.3 (C_5H_4 , C_{3+4}), 69.8 (C_5H_5), 33.6 (CH_2Br), 33.4 ($\text{CH}_2\text{CH}_2\text{CH}_2$), 27.8 (SeCH_2 , $^1J_{\text{Se-C}} = 63.3$ Hz).

$^{77}\text{Se NMR}$ (CDCl_3): 186.

EI/CI MS: 386 (M^+ , 45%), 265 (FcSe^+ , 100%).

FcTe(CH₂)₃Br

¹H NMR (CDCl₃): 4.28 (C₅H₄, H₂₊₅, m, 2H), 4.16 (C₅H₄, H₃₊₄, m, 2H), 4.09 (C₅H₅, s, 5H), 2.35 (CH₂Br, t, 2H, ³J_{H-H} = 8.3 Hz), 2.59 (TeCH₂, t, 2H, ³J_{H-H} = 6.3 Hz), 2.12 (CH₂CH₂CH₂, m, 2H).

¹³C NMR (CDCl₃): 79.9 (C₅H₄, C₂₊₅), 71.8 (C₅H₄, C₃₊₄), 69.7 (C₅H₅), 43.1 (C₁), 35.7 (CH₂Br), 35.1 (CH₂CH₂CH₂), 6.5 (FcTeCH₂).

¹²⁵Te NMR (CDCl₃): 299.

EI/CI MS: 436 (M⁺, 42%), 315 (FcTe⁺, 100%).

FcTe(CH₂)₃TeFc: Fc₂Te₂ (0.763 g, 1.14 mmol) was dissolved in EtOH (50 ml), and the solution cooled to 0 °C. NaBH₄ (0.173 g, 4.56 mmol) was then added. After warming to room temperature and stirring for 2 h, the mixture became homogeneous. An ethanol solution of I(CH₂)₃I (3.5 ml, 4% v/v, 1 mmol) was added, and the mixture left to stir overnight. The solvent was removed by evaporation under reduced pressure. The residue was treated with water (25 ml) and extracted with CH₂Cl₂ (3 × 25 ml). The extract was dried over MgSO₄ and evaporated to dryness, then subjected to column chromatography on SiO₂. Elution with hexane/dichloromethane (3:1) produced one band containing FcTe(CH₂)₃TeFc, a yellow solid, yield 0.46 g (60%). Elemental analysis calcd for C₂₃H₂₄Fe₂Te₂: C 41.40, H 3.62; found C 41.26, H 3.41. Spectroscopic data are summarised below:

¹H NMR (CDCl₃): 4.24 (C₅H₄, H₂₊₅, m, 2H), 4.13 (C₅H₄, H₃₊₄, m, 2H), 4.07 (C₅H₅, s, 5H), 2.53 (TeCH₂, t, 2H, ³J_{H-H} = 9.3 Hz), 1.95 (CH₂CH₂CH₂, m, 2H).

¹³C NMR (CDCl₃): 79.8 (C₅H₄, C₂₊₅), 71.6 (C₅H₄, C₃₊₄), 69.7 (C₅H₅), 43.7 (C₁, ¹J_{Te-C} = 304.4 Hz), 34.1 (CH₂CH₂CH₂), 11.2 (TeCH₂, ¹J_{Te-C} = 156.4 Hz).

¹²⁵Te NMR (CDCl₃): 295.

FAB MS: 668 (M⁺, 33%), 626 (FcTeTeFc, 10%), 399 (FcTe(CH₂)₆⁺, 100%)

FcSe(CH₂)₃TeFc: Fc₂Te₂ (0.182 g, 0.29 mmol) was dissolved in EtOH (50 ml), and the solution cooled to 0 °C. NaBH₄ (0.044 g, 1.16 mmol) was then added. After warming to room temperature and stirring for 2 h, the mixture became homogeneous. A THF solution of FcSe(CH₂)₃I (0.253 g, 0.584 mmol) was added, and the mixture left to stir overnight. The solvent was removed by evaporation under reduced

pressure. The residue was treated with water (25 ml) and extracted with CH_2Cl_2 (3 \times 25 ml). The extract was dried over MgSO_4 and evaporated to dryness, then subjected to column chromatography on SiO_2 . Elution with hexane/dichloromethane (3:1) produced $\text{FcSe}(\text{CH}_2)_3\text{TeFc}$, an orange-yellow solid, yield 0.325 g (90%). Elemental analysis calcd for $\text{C}_{23}\text{H}_{24}\text{Fe}_2\text{SeTe}$: C 44.65, H 3.91; found C 44.58, H 3.81. Spectroscopic data are summarised below:

$^1\text{H NMR}$ (CDCl_3): 4.24 (C_5H_4 , H_{2+5} , m, 2H), 4.18 (C_5H_4 , H_{2+5} , m, 2H), 4.13 (C_5H_4 , H_{3+4} , t, 2H), 4.10 (C_5H_4 , H_{3+4} , m, 2H), 4.10 (C_5H_5 , s, 5H), 4.07 (C_5H_5 , s, 5H), 2.54 (SeCH_2 , t, 2H, $^3J_{\text{H-H}} = 7.8$ Hz), 2.51 (TeCH_2 , t, 2H, $^3J_{\text{H-H}} = 7.3$ Hz), 1.87 ($\text{CH}_2\text{CH}_2\text{CH}_2$, m, 2H).

$^{13}\text{C NMR}$ (CDCl_3): 79.8 (C_5H_4 , C_{2+5}), 75.7 (C_5H_4 , C_{2+5}), 71.6 (C_5H_4 , C_{3+4}), 70.6 (SeC_1), 70.0 (C_5H_4 , C_{3+4}), 69.7 (C_5H_5), 69.6 (C_5H_5), 43.6 (TeC_1), 32.7 ($\text{CH}_2\text{CH}_2\text{CH}_2$), 31.7 (SeCH_2), 8.5 (TeCH_2).

$^{77}\text{Se NMR}$ (CDCl_3): 188 ($^4J_{\text{Se-Te}} = 11.72$ Hz).

$^{125}\text{Te NMR}$ (CDCl_3): 299.

FAB MS: 618 (M^+ , 43%), 315 (FcTe^+ , 85%), 265 (FcSe^+ , 99%), 226 ($\text{FcCH}_2\text{CH}=\text{CH}_2^+$, 100%).

FcSe(CH₂)₂SeFc: Similar as $\text{FcSe}(\text{CH}_2)_3\text{SeFc}$, using Fc_2Se_2 (0.52 g, 1 mmol), NaBH_4 (0.151 g, 4 mmol) and an ethanol solution of $\text{Br}(\text{CH}_2)_2\text{Br}$ (0.86 ml, 10% v/v, 1 mmol) to yield yellow solid $\text{FcSe}(\text{CH}_2)_2\text{SeFc}$, yield 0.278 g (50%). Spectroscopic data are summarised below:

$^1\text{H NMR}$ (CDCl_3): 4.19 (C_5H_4 , H_{2+5} , m, 2H), 4.11 (C_5H_4 , H_{3+4} , m, 2H), 4.09 (C_5H_5 , s, 5H), 2.71 (SeCH_2 , s, 4H).

$^{13}\text{C NMR}$ (CDCl_3): 75.7 (C_5H_4 , C_{2+5}), 73.6 (C_1), 70.1 (C_5H_4 , C_{3+4}), 69.7 (C_5H_5), 29.6 (SeCH_2 , $^1J_{\text{Se-C}} = 64.0$ Hz).

$^{77}\text{Se NMR}$ (CDCl_3): 232.

EI MS: 556 (M^+).

FcSeCH₂SeFc: Fc_2Se_2 (0.52 g, 1 mmol) was dissolved in EtOH (50 ml), and the solution cooled to 0 °C. NaBH_4 (0.151 g, 4 mmol) was then added. After warming to room temperature and stirring for 2 h, the mixture became homogeneous. ICH_2I (0.5 ml) was added, and the mixture left to stir overnight. The solvent was removed by evaporation under reduced pressure. The residue was treated with water (25 ml)

and extracted with CH_2Cl_2 (3 \times 25 ml). The extract was dried over MgSO_4 and evaporated to dryness, then subjected to column chromatography on SiO_2 . Elution with hexane/dichloromethane (3:1) produced $\text{FcSeCH}_2\text{SeFc}$, yield 0.49g (90%).

Spectroscopic data are summarised below:

$^1\text{H NMR}$ (CDCl_3): 4.27 (C_5H_4 , H_{2+5} , m, 2H), 4.14 (C_5H_4 , H_{3+4} , m, 2H), 4.10 (C_5H_5 , s, 5H), 3.61 (SeCH_2 , t, 2H, $^2J_{\text{Se-H}} = 7.8$ Hz);

$^{13}\text{C NMR}$ (CDCl_3): 75.5 (C_5H_4 , C_{2+5}), 72.1 (C_1 , $^1J_{\text{Se-C}} = 111$ Hz), 70.2 (C_5H_4 , C_{3+4}), 69.7 (C_5H_5), 24.4 (SeCH_2 , $^1J_{\text{Se-C}} = 85.6$ Hz).

$^{77}\text{Se NMR}$ (CDCl_3): 252.

FAB MS: 544 ($[\text{M}]^+$, 100%), 279 ($[\text{FcSeCH}_2]^+$, 74%), 265 ($[\text{FcSe}]^+$, 88%).

FcTeCH₂TeFc: Similar to $\text{FcSeCH}_2\text{SeFc}$, using Fc_2Te_2 (0.62 g, 1 mmol), NaBH_4 (0.151 g, 4 mmol) and ICH_2I (0.5 ml) to yield $\text{FcTeCH}_2\text{TeFc}$, yield 0.61g (90%).

Spectroscopic data are summarised below:

$^1\text{H NMR}$ (CDCl_3): 4.31 (C_5H_4 , H_{2+5} , m, 2H), 4.17 (C_5H_4 , H_{3+4} , m, 2H), 4.07 (C_5H_5 , s, 5H), 3.40 (TeCH_2 , t, 2H, $^2J_{\text{Te-H}} = 12.5$ Hz).

$^{13}\text{C NMR}$ (CDCl_3): 79.7 (C_5H_4 , C_{2+5}), 71.8 (C_5H_4 , C_{3+4}), 69.5 (C_5H_5), 48.1 (C_1), not observed (TeCH_2).

$^{125}\text{Te NMR}$ (CDCl_3): 413.

FAB MS: 644 ($[\text{M}]^+$, 35%), 315 ($[\text{FcTe}]^+$, 100%).

FcSe(CH₂)₄SeFc: Similar to $\text{FcSe}(\text{CH}_2)_3\text{SeFc}$, using Fc_2Se_2 (0.39 g, 0.75 mmol), NaBH_4 (0.121 g, 3.0 mmol) and an ethanol solution of $\text{I}(\text{CH}_2)_4\text{I}$ (2.5 ml, 4% v/v, 0.75 mmol). $\text{FcSe}(\text{CH}_2)_4\text{SeFc}$, an orange-yellow solid, yield 0.26 g (60%).

Spectroscopic data are summarised below:

$^1\text{H NMR}$ (CDCl_3): 4.24 (C_5H_4 , H_{2+5} , m, 4H), 4.16 (C_5H_4 , H_{3+4} , m, 4H), 4.12 (C_5H_5 , s, 10H), 2.48 (SeCH_2 , m, 4H), 1.57 (SeCH_2CH_2 , m, 4H).

$^{13}\text{C NMR}$ (CDCl_3): 75.7 (C_5H_4 , C_{2+5}), 71.4 (C_1), 70.2 (C_5H_4 , C_{3+4}), 69.9 (C_5H_5), 30.9 ($\text{CH}_2\text{CH}_2\text{CH}_2\text{CH}_2$), 29.4 (SeCH_2).

$^{77}\text{Se NMR}$ (CDCl_3): 193.

FAB MS: 586 ($[\text{M}]^+$, 30%), 265 ($[\text{FcSe}]^+$, 100%).

FcSe(CH₂)₅SeFc: Similar to $\text{FcSe}(\text{CH}_2)_3\text{SeFc}$, using Fc_2Se_2 (0.53 g, 1 mmol), NaBH_4 (0.151 g, 4 mmol) and an ethanol solution of $\text{I}(\text{CH}_2)_5\text{I}$ (3 ml, 4% v/v, 1

mmol). $\text{FcSe}(\text{CH}_2)_5\text{SeFc}$, an orange-yellow solid, yield 0.39 g (66%). Spectroscopic data are summarised below:

$^1\text{H NMR}$ (CDCl_3): 4.23 (C_5H_4 , H_{2+5} , m, 4H), 4.12 (C_5H_4 , H_{3+4} , m, 4H), 4.11 (C_5H_5 , s, 10H), 2.47 (SeCH_2 , m, 4H), 1.49-1.30 ($\text{CH}_2\text{CH}_2\text{CH}_2$, m, 4H+2H).

$^{13}\text{C NMR}$ (CDCl_3): 74.2 (C_5H_4 , C_{2+5}), 69.6 (C_1), 68.5 (C_5H_4 , C_{3+4}), 68.3 (C_5H_5), 28.9 & 28.5 ($\text{SeCH}_2\text{CH}_2\text{CH}_2$), 28.5 (SeCH_2).

$^{77}\text{Se NMR}$ (CDCl_3): 192.

FcSe(CH₂)₆SeFc: Similar to $\text{FcSe}(\text{CH}_2)_3\text{SeFc}$, using Fc_2Se_2 (0.527 g, 1 mmol), NaBH_4 (0.151 g, 4 mmol) and an ethanol solution of $\text{Br}(\text{CH}_2)_6\text{Br}$ (3 ml, 4% v/v, 1 mmol). Orange oil $\text{FcSe}(\text{CH}_2)_6\text{SeFc}$, yield 0.40 g (65%). Spectroscopic data are summarised below:

$^1\text{H NMR}$ (CDCl_3): 4.26 (C_5H_4 , H_{2+5} , m, 4H), 4.12 (C_5H_4 , H_{3+4} , m, 4H), 4.11 (C_5H_5 , s, 10H), 2.49 (SeCH_2 , t, 4H, $^3J_{\text{H-H}} = 7.2$ Hz), 1.49-1.23 ($\text{CH}_2\text{CH}_2\text{CH}_2$, m, 4H+2H).

$^{13}\text{C NMR}$ (CDCl_3): 75.6 (C_5H_4 , C_{2+5}), 69.2 (C_1), 70.0 (C_5H_4 , C_{3+4}), 69.7 (C_5H_5), 30.8 & 29.5 ($\text{SeCH}_2\text{CH}_2\text{CH}_2$), 30.1 (SeCH_2 , $^1J_{\text{Se-C}} = 59.8$ Hz).

FcTe(CH₂)₄TeFc: Similar to $\text{FcTe}(\text{CH}_2)_3\text{TeFc}$, using Fc_2Te_2 (0.623 g, 1 mmol), NaBH_4 (0.151 g, 4 mmol) and an ethanol solution of $\text{Br}(\text{CH}_2)_4\text{Br}$ (3.4 ml, 4% v/v, 1 mmol). Orange solid $\text{FcTe}(\text{CH}_2)_4\text{TeFc}$, yield 0.52g (75%). Spectroscopic data are summarised below:

$^1\text{H NMR}$ (CDCl_3): 4.27 (C_5H_4 , H_{2+5} , m, 4H), 4.13 (C_5H_4 , H_{3+4} , m, 4H), 4.08 (C_5H_5 , s, 10H), 2.50 (TeCH_2 , m, 4H), 1.60 (TeCH_2CH_2 , m, 4H).

$^{13}\text{C NMR}$ (CDCl_3): 79.6 (C_5H_4 , C_{2+5}), 71.3 (C_5H_4 , C_{3+4}), 69.6 (C_5H_5), 43.6 (C_1), 32.0, ($\text{CH}_2\text{CH}_2\text{CH}_2$), 34.2 ($\text{CH}_2\text{CH}_2\text{CH}_2$), 8.3 (TeCH_2 , $^1J_{\text{Te-C}} = 152$ Hz).

$^{125}\text{Te NMR}$ (CDCl_3): 302.

FcTe(CH₂)₆TeFc: Similar to $\text{FcTe}(\text{CH}_2)_3\text{TeFc}$, using Fc_2Te_2 (0.623 g, 1 mmol), NaBH_4 (0.151 g, 4 mmol) and an ethanol solution of $\text{Br}(\text{CH}_2)_6\text{Br}$ (3 ml, 4% v/v, 1 mmol). Orange oil $\text{FcTe}(\text{CH}_2)_6\text{TeFc}$, yield 0.57g (80%). Spectroscopic data are summarised below:

$^1\text{H NMR (CDCl}_3\text{)}$: 4.27 (C_5H_4 , H_{2+5} , m, 4H), 4.13 (C_5H_4 , H_{3+4} , m, 4H), 4.08 (C_5H_5 , s, 10H), 2.50 (TeCH_2 , t, 4H, $^3J_{\text{H-H}} = 7.2$ Hz), 1.58-1.21 ($\text{CH}_2\text{CH}_2\text{CH}_2$, m, 4H+2H).

$^{13}\text{C NMR (CDCl}_3\text{)}$: 79.7 (C_5H_4 , C_{2+5}), 71.5 (C_5H_4 , C_{3+4}), 69.7 (C_5H_5), 43.7 (C_1), 32.0, ($\text{CH}_2\text{CH}_2\text{CH}_2$), 31.4 ($\text{CH}_2\text{CH}_2\text{CH}_2$), 9.4 (TeCH_2 , $^1J_{\text{Te-C}} = 151$ Hz).

EI/CI MS: 714 ($[\text{M}]^+$, 30%), 399 ($[\text{FcTe}(\text{CH}_2)_6]^+$, 100%).

7.3.2 FcE(CH₂)₃E'(CH₂)₃EFc (E, E' = Se or Te)

FcSe(CH₂)₃Se(CH₂)₃SeFc was synthesized as follows: Se (0.055 g, 0.7 mmol) and NaBH₄ (0.05 g, 1.4 mmol) were refluxed in degassed ethanol (50 ml) under N₂ for 1 h to produce a clear solution. A THF solution of FcSe(CH₂)₃I (0.612 g, 1.4 mmol) or FcSe(CH₂)₃Br (0.544 g, 1.4 mmol) was then added, and the mixture was left to stir for 6 h. After removing the solvent by evaporation under reduced pressure, the residue was treated with water (25 ml) and then extracted with CH₂Cl₂ (25 ml × 3). The extract was dried over MgSO₄ and evaporated to dryness, then subjected to column chromatography on SiO₂. Elution with hexane/dichloromethane (3:1) produced four bands. The fourth band contained FcSe(CH₂)₃Se(CH₂)₃SeFc, a yellow powder with yield 0.269 g (55.7%).

FcSe(CH₂)₃Te(CH₂)₃SeFc was synthesized as above using Te instead of Se. Te (0.155 g, 1.24 mmol) and NaBH₄ (0.094 g, 2.48 mmol) were refluxed in degassed ethanol (50 ml) under N₂ for 1 h to produce a clear solution. A THF solution of FcSe(CH₂)₃I (1.096 g, 2.48 mmol) or FcSe(CH₂)₃Br (0.964 g, 2.48 mmol) was then added, and the mixture was left to stir for 6 h. After removing the solvent by evaporation under reduced pressure, the residue was treated with water (25 ml) and then extracted with CH₂Cl₂ (25 ml × 3). The extract was dried over MgSO₄ and evaporated to dryness, then subjected to column chromatography on SiO₂. Elution with hexane/dichloromethane (1:1) produced FcSe(CH₂)₃Te(CH₂)₃SeFc, a yellow powder with the yield 0.46 g (50%).

FcTe(CH₂)₃E(CH₂)₃TeFc (E = Se or Te) were synthesized similarly using FcTe(CH₂)₃Br instead of FcSe(CH₂)₃X (X = Br or I).

FcTe(CH₂)₃Se(CH₂)₃TeFc: Using Se (0.049 g, 0.62 mmol), NaBH₄ (0.047 g, 1.24 mmol) and a THF solution of FcTe(CH₂)₃Br (0.541g, 1.24 mmol). Elution with hexane/dichloromethane (1:1) produced FcTe(CH₂)₃Se(CH₂)₃TeFc, a yellow powder with yield 0.195 g (40%).

FcTe(CH₂)₃Te(CH₂)₃TeFc: Using Te (0.131 g, 1.02 mmol), NaBH₄ (0.079 g, 2.05 mmol) and a THF solution of FcTe(CH₂)₃Br (0.892 g, 2.05 mmol). Elution with hexane/dichloromethane (1:1) produced a band that contained FcTe(CH₂)₃Te(CH₂)₃TeFc, a yellow powder with yield 0.41g (48%).

Spectroscopic data are summarised below:

FcSe(CH₂)₃Se(CH₂)₃SeFc

¹H NMR (CDCl₃): 4.24 (C₅H₄, H₂₊₅, m, 4H), 4.13 (C₅H₄, H₃₊₄, m, 4H), 4.12 (C₅H₅, s, 10H), 2.56 (FcSeCH₂, t, 4H, ³J_{H-H} = 7.4 Hz), 2.48 (CH₂SeCH₂, t, 4H, ³J_{H-H} = 7.2 Hz), 1.82 (CH₂CH₂CH₂, m, 4H).

¹³C NMR (CDCl₃): 75.7 (C₅H₄, C₂₊₅), 70.9 (C₁), 70.2 (C₅H₄, C₃₊₄), 69.9 (C₅H₅), 31.4 (CH₂CH₂CH₂), 29.7 (FcSeCH₂), 23.8 (CH₂SeCH₂, ¹J_{C-Se} = 62 Hz).

⁷⁷Se NMR (CDCl₃): 190 (FcSe), 154 (CH₂SeCH₂).

FAB MS: 692 (M⁺, 53%), 265 (FcSe⁺, 100%).

FcSe(CH₂)₃Te(CH₂)₃SeFc

¹H NMR (CDCl₃): 4.23 (C₅H₄, H₂₊₅, m, 4H), 4.13 (C₅H₄, H₃₊₄, m, 4H), 4.12 (C₅H₅, s, 10H), 2.54 (SeCH₂, CH₂Te, m, 8H), 1.89 (CH₂CH₂CH₂, m, 4H).

¹³C NMR (CDCl₃): 75.7 (C₅H₄, C₂₊₅), 70.6 (C₁), 70.0 (C₅H₄, C₃₊₄), 69.8 (C₅H₅), 32.9 (CH₂CH₂CH₂), 31.8 (SeCH₂), 2.7 (CH₂Te, ¹J_{C-Te} = 156 Hz).

⁷⁷Se NMR (CDCl₃): 189.

¹²⁵Te NMR (CDCl₃): 228.

FAB MS: 738 (M⁺, 6%), 265 (FcSe⁺, 100%).

FcTe(CH₂)₃Se(CH₂)₃TeFc

¹H NMR (CDCl₃): 4.28 (C₅H₄, H₂₊₅, m, 4H), 4.14 (C₅H₄, H₃₊₄, m, 4H), 4.09 (C₅H₅, s, 10H), 2.57 (TeCH₂, m, 4H), 2.45 (CH₂Se, m, 4H), 1.91 (CH₂CH₂CH₂, m, 4H).

^{13}C NMR (CDCl_3): 78.3 (C_5H_4 , C_{2+5}), 70.2 (C_5H_4 , C_{3+4}), 68.2 (C_5H_5), 42.3 (C_1 , $^1J_{\text{C-Te}}$ = 304 Hz), 31.3 ($\text{CH}_2\text{CH}_2\text{CH}_2$), 24.6 (CH_2Se , $^1J_{\text{C-Se}}$ = 63 Hz), 7.4 (TeCH_2 , $^1J_{\text{C-Te}}$ = 158 Hz).

^{125}Te NMR (CDCl_3): 301.

^{77}Se NMR (CDCl_3): 151.

FAB MS: 790 (M^+ , 25%), 315 (FcTe^+ , 100%).

FcTe(CH₂)₃Te(CH₂)₃TeFc

^1H NMR (CDCl_3): 4.28 (C_5H_4 , H_{2+5} , m, 4H), 4.15 (C_5H_4 , H_{3+4} , m, 4H), 4.09 (C_5H_5 , s, 10H), 2.53 (FcTeCH_2 , CH_2TeCH_2 , m, 8H), 1.97 ($\text{CH}_2\text{CH}_2\text{CH}_2$, m, 4H).

^{13}C NMR (CDCl_3): 79.8 (C_5H_4 , C_{2+5}), 71.7 (C_5H_4 , C_{3+4}), 69.7 (C_5H_5), 43.8 (C_1 , $^1J_{\text{C-Te}}$ = 306 Hz), 34.3 ($\text{CH}_2\text{CH}_2\text{CH}_2$), 11.3 (FcTeCH_2 , $^1J_{\text{C-Te}}$ = 158 Hz), 5.4 (CH_2TeCH_2 , $^1J_{\text{C-Te}}$ = 156 Hz).

^{125}Te NMR (CDCl_3): 299 (FcTe , $^4J_{\text{Te-Te}}$ = 43 Hz), 233 (CH_2TeCH_2 , $^4J_{\text{Te-Te}}$ = 43 Hz).

FAB MS: 838 (M^+ , 8%), 315 (FcTe^+ , 58%).

7.3.3 $\text{CH}_3\text{C}(\text{CH}_2\text{EFc})_3$ (E = Se or Te)

$\text{MeC}(\text{CH}_2\text{SeFc})_3$ was prepared as follows: excess (FcSe)₂ (0.335 g, 0.64 mmol) was dissolved in EtOH (50 ml). NaBH_4 (0.096 g, 2.64 mmol) was then added at 0 °C; the mixture become homogeneous after stirring for 1 h at room temperature. $\text{MeC}(\text{CH}_2\text{Br})_3$ (0.066 g, 0.2 mmol) was then added. The solution was left to stir overnight at refluxing temperature, then the solvent was removed by evaporation under reduced pressure. The residue was treated with water (25 ml) and then extracted with CH_2Cl_2 (25 ml \times 3). The extract was dried over MgSO_4 and evaporated to dryness, then subjected to column chromatography on SiO_2 . Elution with hexane/dichloromethane (2:1) produced $\text{MeC}(\text{CH}_2\text{SeFc})_3$ as a yellow powder, yield 0.121 g (70%).

$\text{MeC}(\text{CH}_2\text{TeFc})_3$ was synthesized as above using Fc_2Te_2 instead of Fc_2Se_2 , using (FcTe)₂ (0.398 g, 0.64 mmol), NaBH_4 (0.096 g, 2.64 mmol) and $\text{MeC}(\text{CH}_2\text{Br})_3$ (0.066 g, 0.2 mmol). Elution with hexane/dichloromethane (2:1) produced $\text{MeC}(\text{CH}_2\text{TeFc})_3$ as a yellow powder, yield 0.165 g (82%).

Spectroscopic data are summarised below:

1,1,1-Tri(ferrocenylselenomethyl)ethane

$^1\text{H NMR}$ (CDCl_3): 4.23 (C_5H_4 , H_{2+5} , m, 6H), 4.10 (C_5H_4 , H_{3+4} , m, 6H), 4.09 (C_5H_5 , s, 15H), 2.73 (SeCH_2 , s, 6H), 0.94 (CH_3 , s, 3H).

$^{13}\text{C NMR}$ (CDCl_3): 75.6 (C_5H_4 , C_{2+5}), 72.7 (C_1), 70.0 (C_5H_4 , C_{3+4}), 69.8 (C_5H_5), 42.6 (SeCH_2 , $^1J_{\text{C-Se}} = 69$ Hz), 35.1 (CCH_3), 25.6 (CH_3).

$^{77}\text{Se NMR}$ (CDCl_3): 138.

MALDI MS: 862 (M^+).

1,1,1-Tri(ferrocenyltelluromethyl)ethane

$^1\text{H NMR}$ (CDCl_3): 4.25 (C_5H_4 , H_{2+5} , m, 6H), 4.13 (C_5H_4 , H_{3+4} , m, 6H), 4.06 (C_5H_5 , s, 15H), 2.78 (TeCH_2 , s, 6H), 1.00 (CH_3 , s, 3H).

$^{13}\text{C NMR}$ (CDCl_3): 79.9 (C_5H_4 , C_{2+5}), 71.6 (C_5H_4 , C_{3+4}), 69.6 (C_5H_5), 45.0 (C_1), 8.6 (TeCH_2), 38.8 (CCH_3), 26.9 (CH_3).

$^{125}\text{Te NMR}$ (CDCl_3): 216.

MALDI MS: 1008 (M^+).

7.3.4 $\text{FcE}(\text{CH}_2)_3\text{Se}(\text{CH}_2)_3\text{Se}(\text{CH}_2)_3\text{EFc}$ (E = Se or Te)

FcSe(CH₂)₃Se(CH₂)₃Se(CH₂)₃SeFc: NaBH_4 (0.064 g, 1.69 mmol) was added to an ethanol solution of $\text{NCSe}(\text{CH}_2)_3\text{SeCN}$ (0.212 g, 0.84 mmol) at 0 °C; the solution turned red in 5 minutes. Slowly warming to room temperature, the colour disappeared quickly, accompanying intense H_2 gas evolution. $\text{FcSe}(\text{CH}_2)_3\text{Br}$ (0.653 g, 0.84 mmol) in THF (5 ml) was then added slowly. The solution was left to stir overnight at room temperature. The solvent was removed by evaporation under reduced pressure. The residue was treated with water (25 ml) and then extracted with CH_2Cl_2 (25 ml \times 3). The extract was dried over MgSO_4 , evaporated to dryness, then subjected to column chromatography on SiO_2 . Elution with hexane/dichloromethane (1:3) produced $\text{FcSe}(\text{CH}_2)_3\text{Se}(\text{CH}_2)_3\text{Se}(\text{CH}_2)_3\text{SeFc}$ as an orange oil, yield 0.603 g (88%).

FcTe(CH₂)₃Se(CH₂)₃Se(CH₂)₃TeFc was synthesized similarly using $\text{FcTe}(\text{CH}_2)_3\text{Br}$ instead of $\text{FcSe}(\text{CH}_2)_3\text{Br}$: Using NaBH_4 (0.050 g, 1.32 mmol), an ethanol solution of $\text{NCSe}(\text{CH}_2)_3\text{SeCN}$ (0.167 g, 0.66 mmol) and $\text{FcTe}(\text{CH}_2)_3\text{Br}$ (0.575 g, 1.32 mmol).

Elution with hexane/dichloromethane (1:3) produced $\text{FcTe}(\text{CH}_2)_3\text{Se}(\text{CH}_2)_3\text{Se}(\text{CH}_2)_3\text{TeFc}$ as an orange oil, yield 0.577 g (97%).

Spectroscopic data are summarised below:

$\text{FcSe}(\text{CH}_2)_3\text{Se}(\text{CH}_2)_3\text{Se}(\text{CH}_2)_3\text{SeFc}$

$^1\text{H NMR}$ (CDCl_3): 4.24 (C_5H_4 , H_{2+5} , m, 4H), 4.13 (C_5H_4 , H_{3+4} , m, 4H), 4.12 (C_5H_5 , s, 10H), 2.58 (FcSeCH_2 , t, 4H, $^3J_{\text{H-H}} = 7.2$ Hz), 2.51 (CH_2SeCH_2 , m, 4H), 2.52 (CH_2SeCH_2 , m, 4H), 1.85 ($\text{CH}_2\text{CH}_2\text{CH}_2$, m, 6H).

$^{13}\text{C NMR}$ (CDCl_3): 75.7 (C_5H_4 , C_{2+5}), 70.5 (C_1), 70.1 (C_5H_4 , C_{3+4}), 69.8 (C_5H_5), 31.5 ($\text{CH}_2\text{CH}_2\text{CH}_2$), 31.4 ($\text{CH}_2\text{CH}_2\text{CH}_2$), 29.7 (FcSeCH_2 , $^1J_{\text{C-Se}} = 62$ Hz), 24.0 (CH_2SeCH_2 , $^1J_{\text{C-Se}} = 62$ Hz), 23.9 (CH_2SeCH_2 , $^1J_{\text{C-Se}} = 62$ Hz).

$^{77}\text{Se NMR}$ (CDCl_3): 153 (CH_2SeCH_2), 188 (FcSe).

EI MS : 814 (100%, M^+).

$\text{FcTe}(\text{CH}_2)_3\text{Se}(\text{CH}_2)_3\text{Se}(\text{CH}_2)_3\text{TeFc}$

$^1\text{H NMR}$ (CDCl_3): 4.28 (C_5H_4 , H_{2+5} , m, 4H), 4.15 (C_5H_4 , H_{3+4} , m, 4H), 4.09 (C_5H_5 , s, 10H), 2.99 (FcTeCH_2 , t, 4H, $^3J_{\text{H-H}} = 7.4$ Hz), 2.50 (CH_2SeCH_2 , t, 4H, $^3J_{\text{H-H}} = 7.4$ Hz), 2.49 (CH_2SeCH_2 , t, 4H, $^3J_{\text{H-H}} = 7.2$ Hz), 1.94-1.84 ($\text{CH}_2\text{CH}_2\text{CH}_2$, m, 6H)

$^{13}\text{C NMR}$ (CDCl_3): 79.8 (C_5H_4 , C_{2+5}), 71.7 (C_5H_4 , C_{3+4}), 69.7 (C_5H_5), 43.8 (C_1 , $^1J_{\text{C-Te}} = 304$ Hz), 32.8 ($\text{CH}_2\text{CH}_2\text{CH}_2$), 31.6 ($\text{CH}_2\text{CH}_2\text{CH}_2$), 26.2 (CH_2SeCH_2 , $^1J_{\text{C-Se}} = 62$ Hz), 24.1 (CH_2SeCH_2 , $^1J_{\text{C-Se}} = 62$ Hz), 8.9 (TeCH_2 , $^1J_{\text{C-Te}} = 158$ Hz).

$^{77}\text{Se NMR}$ (CDCl_3): 153.

$^{125}\text{Te NMR}$ (CDCl_3): 301.

EI MS : 910 (100%, M^+).

7.3.5 $\text{fc}[\text{Se}(\text{CH}_2)_3\text{Br}]_2$

fcSe_3 (0.422 g, 1 mmol) was dissolved in EtOH (100 ml); NaBH_4 (0.30 g, 8 mmol) was then added. After stirring for 2 h, the mixture became homogeneous. Excess $\text{Br}(\text{CH}_2)_3\text{Br}$ (1 ml) was added, and the mixture left to stir for 2 h. The solvent was removed by evaporation under reduced pressure. The residue was treated with water

(25 ml) and extracted with CH_2Cl_2 (3×25 ml). The extract was dried over MgSO_4 , evaporated to dryness, then subjected to column chromatography on SiO_2 . Eluting with hexane/dichloromethane (3:1), a small amount of orange red 1,5-diselena[5]ferrocenophane and the target product (0.293 g, 50%) were obtained sequentially. Spectroscopic data are summarised below:

$^1\text{H NMR}$ (CDCl_3): 4.24 (C_5H_4 , H_{2+5} , m, 4H), 4.17 (C_5H_4 , H_{3+4} , m, 4H), 3.40 (CH_2Br , t, 4H, $^3J_{\text{H-H}} = 6.4$ Hz), 2.63 (SeCH_2 , t, 4H, $^3J_{\text{H-H}} = 7.2$ Hz), 2.02 ($\text{CH}_2\text{CH}_2\text{CH}_2$, m, 4H).

$^{13}\text{C NMR}$ (CDCl_3): 77.0 (C_5H_4 , C_{2+5}), 71.7 (C_5H_4 , C_{3+4}), 71.3 (C_1), 33.4 (CH_2Br), 33.3 ($\text{CH}_2\text{CH}_2\text{CH}_2$), 27.8 (SeCH_2 , $^1J_{\text{Se-C}} = 63$ Hz).

EI/CI MS: 604 ($[\text{M}+\text{NH}_4]^+$), 586 ($[\text{M}]^+$).

7.3.6 difcSe₄

fcSe₃ (0.422 g, 1 mmol) was dissolved in EtOH (100 ml); NaBH_4 (0.30 g, 8 mmol) was then added. After stirring for 2 h, the mixture became homogeneous. fc[Se(CH_2)₃Br]₂ (0.586 g, 1 mmol) in THF (5 ml) was added, and the mixture left to stir for 24 h at room temperature. The solvent was removed by evaporation under reduced pressure. The residue was treated with water (25 ml) and extracted with CH_2Cl_2 (3×25 ml). The extract was dried over MgSO_4 , evaporated to dryness, then subjected to column chromatography on SiO_2 . The target product, a yellow solid (0.273g, 36%), was obtained by elution with hexane/dichloromethane (1:1). Spectroscopic data are summarised below:

$^1\text{H NMR}$ (CDCl_3): 4.29 (C_5H_4 , H_{2+5} , m, 8H), 4.21 (C_5H_4 , H_{3+4} , m, 8H), 2.95 (SeCH_2 , t, 8H, $^3J_{\text{H-H}} = 6.6$ Hz), 2.01 ($\text{CH}_2\text{CH}_2\text{CH}_2$, m, 4H).

$^{13}\text{C NMR}$ (CDCl_3): 75.5 (C_1), 74.6 (C_5H_4 , C_{2+5}), 70.5 (C_5H_4 , C_{3+4}), 29.4 ($\text{CH}_2\text{CH}_2\text{CH}_2$), 28.7 (SeCH_2 , $^1J_{\text{Se-C}} = 61$ Hz).

$^{77}\text{Se NMR}$ (CDCl_3): 170.

EI/CI MS: 771 ($[\text{M}+\text{H}]^+$), 770 ($[\text{M}]^+$, 100%).

7.3.7 fcSe₄

NaBH_4 (0.028 g, 0.19 mmol) was added to an ethanol solution of $\text{NCSe}(\text{CH}_2)_3\text{SeCN}$ (0.094 g, 0.374 mmol) at 0 °C; the solution turned red in 5 minutes. Slowly warming

to room temperature, the colour disappeared quickly, accompanying intense H₂ gas evolution. fc[Se(CH₂)₃Br]₂ (0.219 g, 0.374 mmol) in THF (5 ml) was then added slowly. The solution was left to stir at room temperature for 2 h. The solvent was removed by evaporation under reduced pressure. The residue was treated with water (25 ml) and then extracted with CH₂Cl₂ (25 ml × 3). The extract was dried over MgSO₄, evaporated to dryness, then subjected to column chromatography on SiO₂. Elution with hexane/dichloromethane (1:1) produced the target product as an orange solid, yield 0.136 g (58%). ¹H, ¹³C and ⁷⁷Se NMR spectra are shown in Figs. 7.1-7.4 and spectroscopic data are summarised below:

¹H NMR (CDCl₃): 4.20 (C₅H₄, H₂₊₅ and H₃₊₄, s, 8H), 2.86 (SeCH₂, m, 4H), 2.77 (SeCH₂, m, 4H), 2.65 (SeCH₂, m, 4H), 2.10 (SeCH₂CH₂CH₂Se, m, 2H), 1.99 (FcSeCH₂CH₂CH₂Se, m, 4H).

¹³C NMR (CDCl₃): 77.7 (C₁), 75.3 (C₅H₄, C₂₊₅), 70.4 (C₅H₄, C₃₊₄), 32.8 (SeCH₂CH₂CH₂Se), 31.1 (FcSeCH₂CH₂CH₂Se), 29.4 (SeCH₂, ¹J_{Se-C} = 61 Hz), 24.1 (SeCH₂, ¹J_{Se-C} = 61 Hz), 23.3 (SeCH₂, ¹J_{Se-C} = 61 Hz).

⁷⁷Se NMR (CDCl₃): 170, 161.

EI/CI MS: 629 ([M+H]⁺), 628 ([M]⁺, 50%).

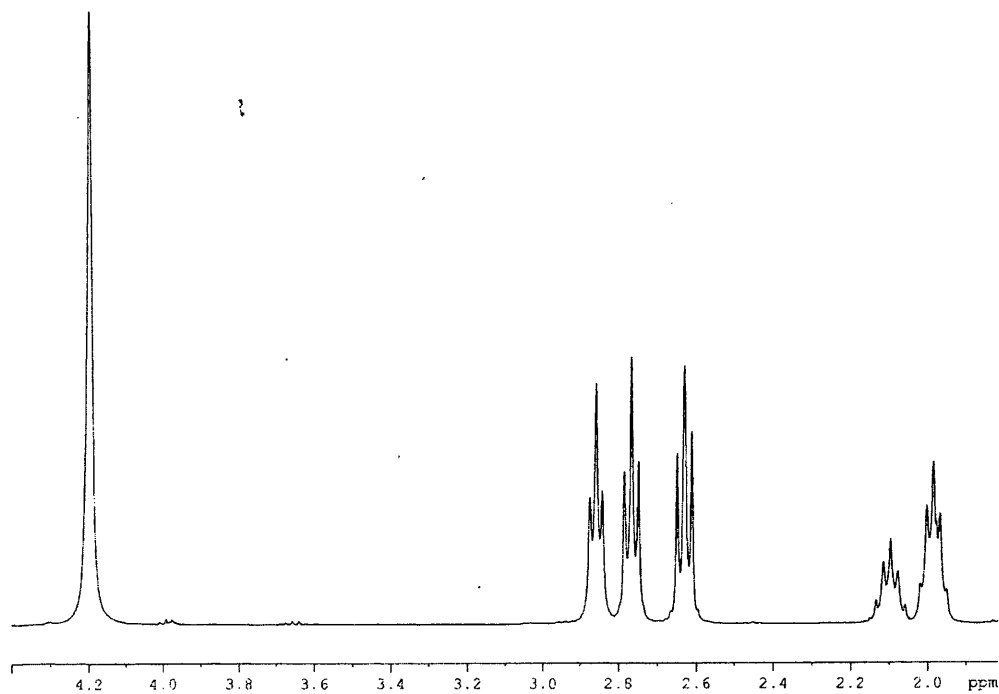


Fig. 7.1 ¹H NMR spectrum of fcSe₄ in CDCl₃ solution

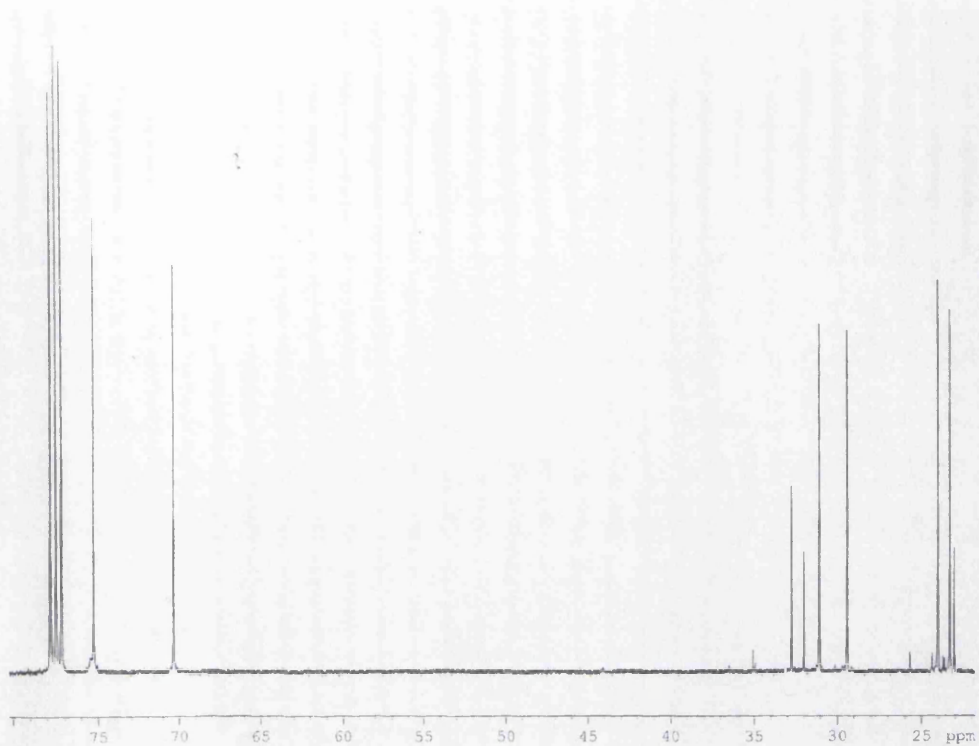


Fig. 7.2 ^{13}C NMR spectrum of fcSe_4 in CDCl_3 solution

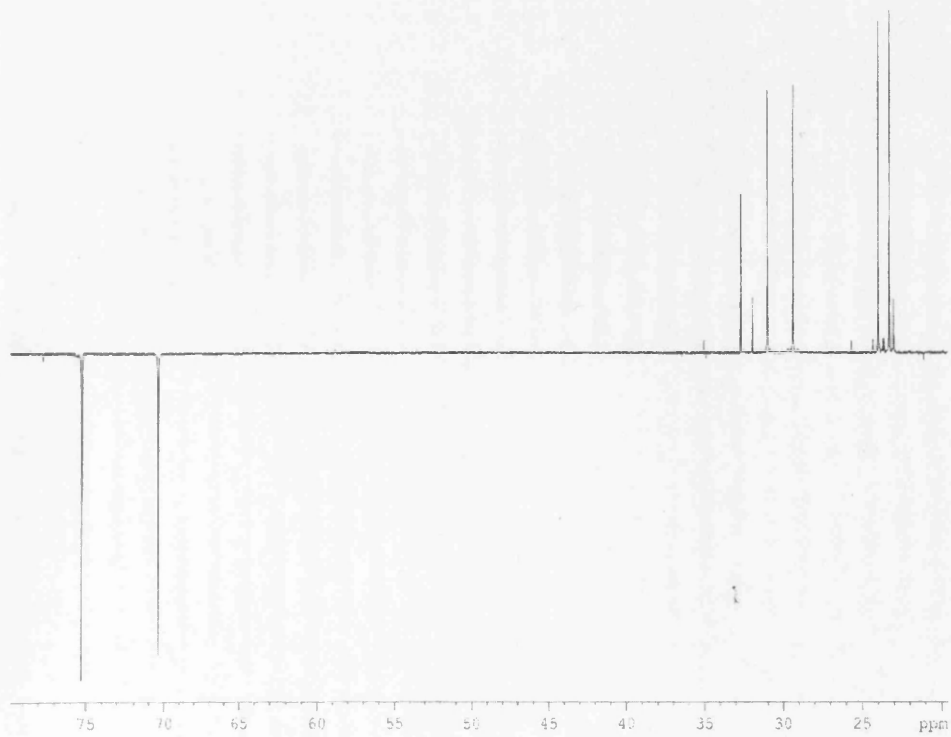


Fig. 7.3 ^{13}C DEPT NMR spectrum of fcSe_4 in CDCl_3 solution

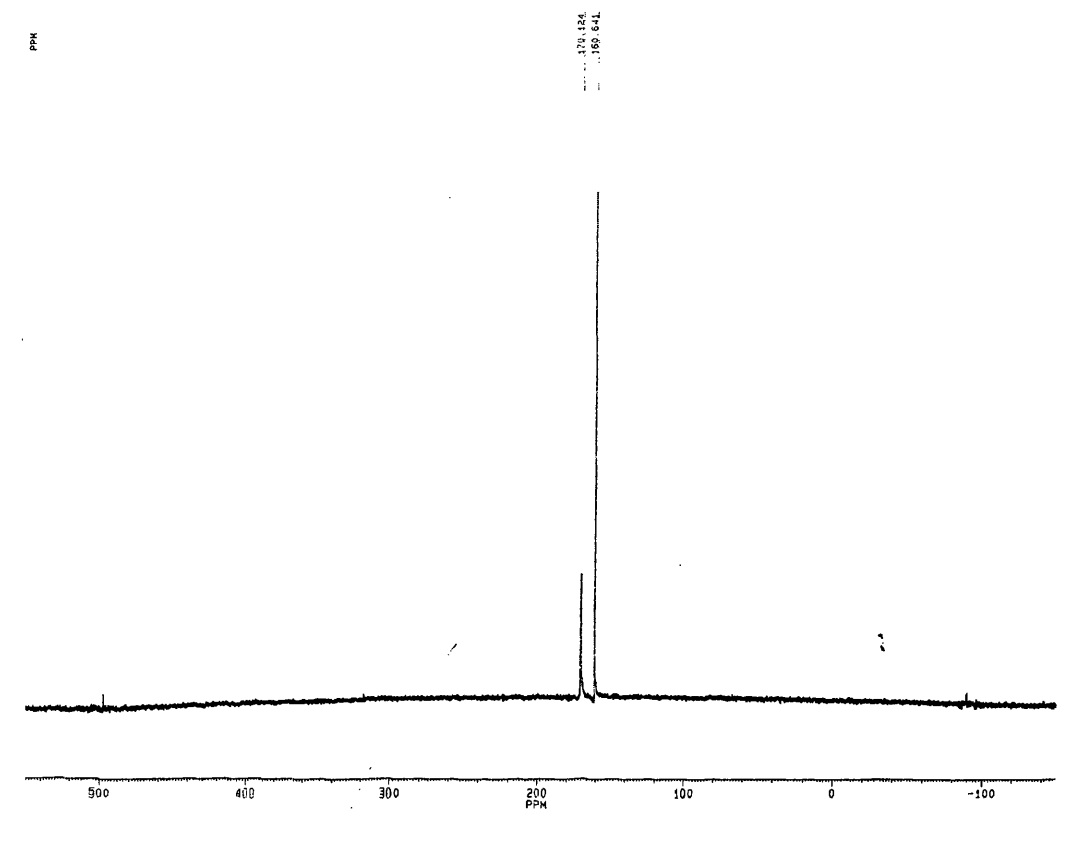


Fig. 7.4 ^{77}Se NMR spectrum of fcSe_4 in CDCl_3 solution

7.3.8 $\text{FcECH}_2\text{C}_6\text{H}_4\text{CH}_2\text{EFc}$ (E = Se or Te)

The synthetic scheme was similar to that for $\text{FcSe}(\text{CH}_2)_3\text{SeFc}$, with only changing from $\text{X}(\text{CH}_2)_3\text{X}$ to $\text{BrCH}_2\text{C}_6\text{H}_4\text{CH}_2\text{Br}$.

FcSeCH₂C₆H₄CH₂SeFc: Fc_2Se_2 (0.527 g, 1 mmol) was dissolved in EtOH (50 ml), and the solution cooled to 0 °C. NaBH_4 (0.156 g, 4 mmol) was then added. After warming to room temperature and stirring for 2 h, the mixture became homogeneous. A THF solution (5 ml) of $\text{BrCH}_2\text{C}_6\text{H}_4\text{CH}_2\text{Br}$ (0.264 g, 1 mmol) was added, and the mixture left to stir overnight. The solvent was removed by evaporation under reduced pressure. The residue was treated with water (25 ml) and extracted with CH_2Cl_2 (3 × 25 ml). The extract was dried over MgSO_4 and evaporated to dryness, then subjected to column chromatography on SiO_2 . Elution with

hexane/dichloromethane (2:1) led to isolation of the yellow product $\text{FcSeCH}_2\text{C}_6\text{H}_4\text{CH}_2\text{SeFc}$ (0.337g, 53%). Spectroscopic data are summarised below:

$^1\text{H NMR}$ (CDCl_3): 6.87 (C_6H_4 , s, 4H), 4.09 (C_5H_4 , H_{2+5} and H_{3+4} , s, 8H), 4.08 (C_5H_5 , s, 10H), 3.67 (SeCH_2 , s, 4H, $^2J_{\text{Se-H}} = 13.2$ Hz).

$^{13}\text{C NMR}$ (CDCl_3): 136.8 (C_6H_4 , C_{1+4}), 127.6 (C_6H_4 , $\text{C}_{2+3+5+6}$), 74.5 (C_5H_4 , C_{2+5}), 69.4 (C_5H_4 , C_1), 68.7 (C_5H_4 , C_{3+4}), 68.2 (C_5H_5), 32.3 (SeCH_2 , $^1J_{\text{Se-C}} = 58.4$ Hz).

$^{77}\text{Se NMR}$ (CDCl_3): 286.

EI/CI MS : 632 (M^+ , 50%), 450 ($\text{FcSeCH}_2\text{C}_6\text{H}_4\text{CH}_2\text{Se}^+$, 60%), 265 (FcSe^+ , 80%).

$\text{FcTeCH}_2\text{C}_6\text{H}_4\text{CH}_2\text{TeFc}$: synthesized as above using Fc_2Te_2 instead of Fc_2Se_2 . Using Fc_2Te_2 (0.623 g, 1 mmol), NaBH_4 (0.156 g, 4 mmol) and a THF solution (5 ml) of $\text{BrCH}_2\text{C}_6\text{H}_4\text{CH}_2\text{Br}$ (0.264 g, 1 mmol). Yellow product $\text{FcTeCH}_2\text{C}_6\text{H}_4\text{CH}_2\text{TeFc}$ was obtained with yield 0.47 g (64%). Spectroscopic data are summarised below:

$^1\text{H NMR}$ (CDCl_3): 6.80 (C_6H_4 , s, 4H), 4.16 (C_5H_4 , H_{2+5} , m, 4H), 4.13 (C_5H_4 , H_{3+4} , m, H), 4.05 (C_5H_5 , s, 10H), 3.84 (TeCH_2 , s, 4H, $^2J_{\text{Te-H}} = 28.8$ Hz).

$^{13}\text{C NMR}$ (CDCl_3): 139.3 (C_6H_4 , C_{1+4}), 128.6 (C_6H_4 , $\text{C}_{2+3+5+6}$), 80.0 (C_5H_4 , C_{2+5}), 71.8 (C_5H_4 , C_{3+4}), 69.6 (C_5H_5), 45.5 (C_5H_4 , C_1), 12.7 (TeCH_2 , $^1J_{\text{Te-C}} = 269$ Hz).

$^{125}\text{Te NMR}$ (CDCl_3): 496.

EI/CI MS : 730 (M^+).

7.3.9 difcSe₄-p-Xylene

fcSe_3 (0.422 g, 1 mmol) was dissolved in EtOH (100 ml); NaBH_4 (0.30 g, 8 mmol) was then added. After stirring for 2 h, the mixture became homogeneous. A THF solution (5 ml) of $\text{BrCH}_2\text{C}_6\text{H}_4\text{CH}_2\text{Br}$ (0.264 g, 1 mmol) was added, and the mixture left to stir overnight. The solvent was removed by evaporation under reduced pressure. The residue was treated with water (25 ml) and extracted with CH_2Cl_2 (3 \times 25 ml). The extract was dried over MgSO_4 , evaporated to dryness, then subjected to column chromatography on SiO_2 . The target product, a yellow solid (0.067g, 15%), was obtained by elution with hexane/dichloromethane (1:2). Spectroscopic data are summarised below:

^1H NMR (CDCl_3): 6.85 (C_6H_4 , s, 8H), 4.11 (C_5H_4 , H_{2+5} and H_{3+4} , m, 16H), 3.67 (SeCH_2 , m, 4H), 3.68 (SeCH_2 , m, 4H).

^{13}C NMR (CDCl_3): 138.4 (C_6H_4 , C_{1+4}), 129.1 (C_6H_4 , $\text{C}_{2+3+5+6}$), 76.0 (C_5H_4 , C_{2+5}), 71.6 (C_5H_4 , C_1), 69.8 (C_5H_4 , C_{3+4}), 33.7 (SeCH_2).

^{77}Se NMR (CDCl_3): 287.

EI/CI MS: 894 (M^+ , 10%)

7.4 Synthesis of transition metal complexes with ferrocenyl chalcogenide ligands

7.4.1 [M{FcE(CH₂)₃E'Fc}₂](PF₆)₂ (M = Pd or Pt; E, E' = Se or Te)

[Pd{FcSe(CH₂)₃SeFc}₂](PF₆)₂: PdCl₂ (11 mg, 0.062 mmol) was refluxed in MeCN (30 ml) for 2 h to give a yellow solution of [PdCl₂(NCMe)₂]. After cooling, TlPF₆ (43 mg, 0.123 mmol) was added and stirring continued for another 15 min. FcSe(CH₂)₃SeFc (70 mg, 0.123 mmol) in CH₂Cl₂ (5 ml) was then added, and the mixture stirred at room temperature for 24 h to give a blue liquid and a fine white precipitate of TlCl. The mixture was centrifuged to remove TlCl and reduced to 2 ml *in vacuo*. Diethyl ether (10 ml) was added to precipitate the product as a blue powder with yield is 75 mg (79%). Elemental analysis calcd for C₄₆H₄₈F₁₂Fe₄P₂PdSe₄: C 35.96, H 3.15; found: C 34.47, H 3.04%. ES MS: 1395 ([M-PF₆]⁺).

[Pt{FcSe(CH₂)₃SeFc}₂](PF₆)₂: PtCl₂ (24 mg, 0.09 mmol) was refluxed in MeCN (30 ml) for 2 h to give a yellow solution of [PtCl₂(NCMe)₂]. After cooling, TlPF₆ (64 mg, 0.18 mmol) was added and stirring continued for another 15 min. FcSe(CH₂)₃SeFc (140 mg, 0.18 mmol) in CH₂Cl₂ (5 ml) was then added, and the mixture stirred at room temperature for 48 h to give a red liquid and a fine white precipitate of TlCl. The mixture was centrifuged to remove TlCl and reduced to 2 ml *in vacuo*. Diethyl ether (10 ml) was added to precipitate the product as a peach powder with yield 114 mg (78%). Elemental analysis calcd for C₄₆H₄₈F₁₂Fe₄P₂PtSe₄: C 34.00, H 2.98; found: C 30.96, H 2.78%. ES MS: 1484 ([M-PF₆]⁺), 669.5 ([M-2PF₆]²⁺).

Other complexes are synthesized similarly.

[Pd{FcTe(CH₂)₃TeFc}₂](PF₆)₂: Using PdCl₂ (16 mg, 0.085 mmol), TlPF₆ (59 mg, 0.17 mmol) and FcTe(CH₂)₃TeFc (114 mg, 0.17 mmol) to yield the product as a cyan powder with yield 88 mg (60%). Elemental analysis calcd for C₄₆H₄₈F₁₂Fe₄P₂PdTe₄: C 31.92, H 2.80; found: C 27.78, H 2.59%. ES MS: 1575 ([M-PF₆]⁺).

$[Pt\{FcTe(CH_2)_3TeFc\}_2](PF_6)_2$: Using $PtCl_2$ (29 mg, 0.11 mmol), $TIPF_6$ (77 mg, 0.22 mmol) and $FcTe(CH_2)_3TeFc$ (148 mg, 0.22 mmol) to yield the product as a orange red powder with yield 103 mg (52%). Elemental analysis calcd for $C_{46}H_{48}F_{12}Fe_4P_2PtTe_4$: C 30.36, H 2.66; found: C 27.68, H 2.48%. ES MS: 1664 ($[M-PF_6]^+$), 759.5 ($[M-2PF_6]^{2+}$).

$[Pd\{FcSe(CH_2)_3TeFc\}_2](PF_6)_2$: Using $PdCl_2$ (17.8 mg, 0.095 mmol), $TIPF_6$ (66 mg, 0.19 mmol) and $FcSe(CH_2)_3TeFc$ (119 mg, 0.19 mmol) to yield the product as a dark blue powder with yield 100 mg (65%). Elemental analysis calcd for $C_{46}H_{48}F_{12}Fe_4P_2PdSe_2Te_2$: C 33.82, H 2.96; found: C 32.58, H 2.91%. ES MS: 1485 ($[M-PF_6]^+$), 670 ($[M-2PF_6]^{2+}$).

$[Pt\{FcSe(CH_2)_3TeFc\}_2](PF_6)_2$: Using $PtCl_2$ (21 mg, 0.09 mmol), $TIPF_6$ (63 mg, 0.18 mmol) and $FcSe(CH_2)_3TeFc$ (113 mg, 0.18 mmol) to yield the product as a red powder with yield 93 mg (60%). Elemental analysis calcd for $C_{46}H_{48}F_{12}Fe_4P_2PtSe_2Te_2$: C 32.08, H 2.81; found: C 30.10, H 2.58%. ES MS: 1574 ($[M-PF_6]^+$), 714.5 ($[M-2PF_6]^{2+}$).

7.4.2 $[MCl_2\{FcE(CH_2)_nEFc\}]$ (M = Pd or Pt, n = 1, E = Se or Te; M = Pt, n = 2, E = Se)

$[PdCl_2(FcSeCH_2SeFc)_2]$: A DCM solution (3 ml) of $FcSeCH_2SeFc$ (44 mg, 0.080 mmol) was placed in the bottom of a test tube (d = 5 mm). A MeCN solution (3 ml) of $[PdCl_2(NCPh)_2]$ (15 mg, 0.040 mmol) was then carefully layered onto the DCM solution surface. Cubic crystals suitable for single-crystal X-ray analysis were collected after one week (35 mg, 70%). Similar method was adopted for complexes below.

$[PtCl_2(FcSeCH_2SeFc)_2]$: Using $FcSeCH_2SeFc$ (56 mg, 0.10 mmol) and $[PtCl_2(NCPh)_2]$ (15 mg, 0.05 mmol). Orange red cubic crystals suitable for single-crystal X-ray analysis were collected after one week (57 mg, 84%).

$[PdCl_2(FcTeCH_2TeFc)]$: Using $FcTeCH_2TeFc$ (87 mg, 0.137 mmol) and $[PdCl_2(NCPh)_2]$ (52 mg, 0.137 mmol). Dark red rod crystals suitable for single-crystal X-ray analysis were collected after one week (95 mg, 85%).

$[PtCl_2(FcTeCH_2TeFc)]$: Using $FcTeCH_2TeFc$ (18 mg, 0.027 mmol) and $[PdCl_2(NCPh)_2]$ (20 mg, 0.027 mmol). Orange long column crystals suitable for single-crystal X-ray analysis were collected after one week (18 mg, 74%).

$[PdCl_2(FcSe(CH_2)_2SeFc)]$: Using $FcSeCH_2SeFc$ (21 mg, 0.040 mmol) and $[PdCl_2(NCPh)_2]$ (15 mg, 0.040 mmol). Dark red small plate crystals suitable for single-crystal X-ray analysis were collected after one week (18 mg, 60%).

7.4.3 $[M(CO)_4\{FcE(CH_2)_3E'Fc\}]$ ($M = Cr$ or W , $E = E' = Te$; $M = Mo$, $E, E' = Se$ or Te)

$[Cr(CO)_4\{FcTe(CH_2)_3TeFc\}]$: $[Cr(CO)_4(nbd)]$ (120 mg, 0.47 mmol) was dissolved in degassed toluene (40 ml) and the ligand $FcTe(CH_2)_3TeFc$ (318 mg, 0.47 mmol) added. The reaction mixture was stirred at 100 °C overnight and then the toluene removed *in vacuo*. The residue was dissolved in CH_2Cl_2 (5 ml), filtered and cold hexane added to yield a brown powder. The powder was collected, washed with cold hexane and dried under vacuum (156 mg, 40%).

$[Mo(CO)_4\{FcSe(CH_2)_3SeFc\}]$: $[Mo(CO)_4(nbd)]$ (195 mg, 0.65 mmol) was dissolved in degassed toluene (40 ml) and the ligand $FcSe(CH_2)_3SeFc$ (369 mg, 0.65 mmol) added. The reaction mixture was stirred at room temperature overnight and then the toluene removed *in vacuo*. The residue was dissolved in CH_2Cl_2 (5 ml), filtered and cold hexane added to yield a brown powder. The powder was collected, washed with cold hexane and dried under vacuum (156 mg, 31%).

$[Mo(CO)_4\{FcTe(CH_2)_3TeFc\}]$: Similar method as $[Mo(CO)_4\{FcSe(CH_2)_3SeFc\}]$, using $[Mo(CO)_4(nbd)]$ (60 mg, 0.2 mmol) and $FcTe(CH_2)_3TeFc$ (134 mg, 0.2 mmol) to obtain a yellow powder (140 mg, 80%).

$[Mo(CO)_4\{FcSe(CH_2)_3TeFc\}]$: Similar method as $[Mo(CO)_4\{FcSe(CH_2)_3SeFc\}]$, using $[Mo(CO)_4(nbd)]$ (109 mg, 0.363 mmol) and $FcSe(CH_2)_3TeFc$ (225 mg, 0.363 mmol) to obtain a brown powder (180 mg, 60%).

$[W(CO)_4\{FcTe(CH_2)_3TeFc\}]$: $[W(CO)_4(TMPDA)]$ (146 mg, 0.34 mmol) was dissolved in degassed toluene (40 ml) and the ligand $FcTe(CH_2)_3TeFc$ (230 mg, 0.34 mmol) added. The reaction mixture was stirred at 80 °C overnight and then the toluene removed *in vacuo*. The residue was dissolved in CH_2Cl_2 (5 ml), filtered and cold hexane added to yield a brown powder. The powder was collected, washed with cold hexane and dried under vacuum (173 mg, 53%).

Spectroscopic data for the above compounds are summarised below:

$[Cr(CO)_4\{FcTe(CH_2)_3TeFc\}]$

1H NMR (CD_2Cl_2): 4.55 (C_5H_4 , H_{2+5} , br, 4H), 4.29 (C_5H_4 , H_{3+4} , m, 4H), 4.18 (C_5H_5 , m, 10H), 2.85 ($TeCH_2$, br, 4H), 2.49 ($CH_2CH_2CH_2$, m, 4H).

^{13}C NMR (CD_2Cl_2): 207.6 (CO), 76.4, 76.3 (C_5H_4 , C_{2+5}), 72.7, 71.9 (C_5H_4 , C_{3+4}), 70.6 (C_5H_5), 47.1 (C_1), 26.3 ($CH_2CH_2CH_2$), 12.7 ($TeCH_2$, $^1J_{Te-C} = 156.4$ Hz).

^{125}Te NMR (CD_2Cl_2): 429.

FAB MS: 836 ($[M]^+$), 724 ($[M-4CO]^+$), 672 ($[M-Cr(CO)_4]^+$).

$[Mo(CO)_4\{FcSe(CH_2)_3SeFc\}]$

1H NMR (CD_2Cl_2): 5.24 (C_5H_4 , H_{2+5} , m, 4H), 4.27 (C_5H_4 , H_{3+4} , m, 4H), 4.25 (C_5H_5 , s, 10H), 2.80 ($SeCH_2$, t, br, 4H), 1.88 ($CH_2CH_2CH_2$, m, br, 2H).

^{13}C NMR ($CDCl_3$): 217.7, 209.5 (CO), 76.0 (C_5H_4 , C_{2+5}), 71.0 (C_1), 70.4 (C_5H_4 , C_{3+4}), 70.0 (C_5H_5), 36.6 ($CH_2CH_2CH_2$), 27.2 ($SeCH_2$).

^{77}Se NMR ($CDCl_3$): 176.

FAB MS: 782 ($[M]^+$), 572 ($[M-Mo(CO)_4]^+$).

$[Mo(CO)_4\{FcSe(CH_2)_3TeFc\}]$

1H NMR (CD_2Cl_2): 4.57, 4.47 (C_5H_4 , H_{2+5} , br, 4H), 4.37, 4.31 (C_5H_4 , H_{3+4} , br, 4H), 4.23, 4.20 (C_5H_5 , s, 10H), 2.77, 2.55 ($SeCH_2$, $TeCH_2$, br, 4H), 1.99-1.80 ($CH_2CH_2CH_2$, m, 2H).

^{13}C NMR (CD_2Cl_2): 217.8, 216.2, 210.9, 206.9 (CO), 77.8, 77.5, 76.7, 76.2 (C_5H_4 , C_{2+5}), 74.0, 73.0, 71.9, 71.3 (C_5H_4 , C_{3+4}), 70.7, 70.5, 70.3 (C_5H_5), 38.2 (TeC_1), 31.9, 30.9, 30.6 ($\text{CH}_2\text{CH}_2\text{CH}_2$), 27.8 (SeCH_2), 17.7, 12.7 (TeCH_2).

^{77}Se NMR (CD_2Cl_2): 175.

^{125}Te NMR (CD_2Cl_2): 337.

FAB MS: 832 ($[\text{M}]^+$).

$[\text{Mo}(\text{CO})_4\{\text{FcTe}(\text{CH}_2)_3\text{TeFc}\}]$

^1H NMR (CD_2Cl_2): 4.53, 4.50 (C_5H_4 , H_{2+5} , m, 4H), 4.33, 4.28 (C_5H_4 , H_{3+4} , m, 4H), 4.18 (C_5H_5 , s, 10H), 2.61, 2.43 (TeCH_2 , m, 4H), 1.66 ($\text{CH}_2\text{CH}_2\text{CH}_2$, m, 2H).

^{13}C NMR (CD_2Cl_2): 211.7, 216.6 (CO), 73.0 (C_5H_4 , C_{2+5}), 71.5 (C_5H_4 , C_{3+4}), 70.6 (C_5H_5), 47.6 (C_1), 27.5 ($\text{CH}_2\text{CH}_2\text{CH}_2$), 13.8 (TeCH_2).

^{125}Te NMR (CD_2Cl_2): 344.

FAB MS: 882 ($[\text{M}]^+$).

$[\text{W}(\text{CO})_4\{\text{FcTe}(\text{CH}_2)_3\text{TeFc}\}]$

^1H NMR (CD_2Cl_2): 4.42 (C_5H_4 , H_{2+5} , m, 4H), 4.17 (C_5H_4 , H_{3+4} , m, 4H), 4.05 (C_5H_5 , s, 10H), 2.65 (TeCH_2 , t, 4H, $^3J_{\text{H-H}} = 9$ Hz), 1.71 ($\text{CH}_2\text{CH}_2\text{CH}_2$, m, 2H).

^{13}C NMR (CD_2Cl_2): 204.7, 202.7 (CO), 77.6 (C_5H_4 , C_{2+5}), 69.9 (C_5H_4 , C_{3+4}), 68.6 (C_5H_5), 47.0 (C_1), 28.9 ($\text{CH}_2\text{CH}_2\text{CH}_2$), 12.9 (TeCH_2).

^{125}Te NMR (CD_2Cl_2): 272 ($^1J_{\text{Te-W}} = 74$ Hz), 269.

FAB MS: 968 ($[\text{M}]^+$), 940 ($[\text{M-CO}]^+$), 856 ($[\text{M-4CO}]^+$), 672 ($[\text{M-W}(\text{CO})_4]^+$).

7.4.4 $[\text{MCl}\{\text{FcE}(\text{CH}_2)_3\text{E}'(\text{CH}_2)_3\text{EFc}\}](\text{PF}_6)$ (M = Pd or Pt, E, E' = Se or Te)

$[\text{PdCl}\{\text{FcSe}(\text{CH}_2)_3\text{Se}(\text{CH}_2)_3\text{SeFc}\}](\text{PF}_6)$: PdCl_2 (58 mg, 0.326 mmol) was refluxed in MeCN (30 ml) for 2 h to give a yellow solution of $[\text{PdCl}_2(\text{NCMe})_2]$. After cooling, TIPF_6 (117 mg, 0.326 mmol) was added and stirring continued for another 15 min. $\text{FcSe}(\text{CH}_2)_3\text{Se}(\text{CH}_2)_3\text{SeFc}$ (225 mg, 0.326 mmol) in CH_2Cl_2 (5 ml) was then added, and the mixture stirred at room temperature for 24 h to give a purple blue liquid and

a fine white precipitate of TiCl_4 . The mixture was centrifuged to remove TiCl_4 and reduced to 2 ml *in vacuo*. Diethyl ether (10 ml) was added to precipitate the product as a blue powder, 0.24 g (88%).

$[\text{PtCl} \{ \text{FcSe}(\text{CH}_2)_3\text{Se}(\text{CH}_2)_3\text{SeFc} \}](\text{PF}_6)$: PtCl_2 (96 mg, 0.36 mmol) was refluxed in MeCN (30 ml) for 2 h to give a yellow solution of $[\text{PtCl}_2(\text{NCMe})_2]$. After cooling, TIPF_6 (130 mg, 0.36 mmol) was added and stirring continued for another 15 min. $\text{FcSe}(\text{CH}_2)_3\text{Se}(\text{CH}_2)_3\text{SeFc}$ (250 mg, 0.36 mmol) in CH_2Cl_2 (5 ml) was then added, and the mixture stirred at room temperature for 48 h to give a orange red liquid and a fine white precipitate of TiCl_4 . The mixture was centrifuged to remove TiCl_4 and reduced to 2 ml *in vacuo*. Diethyl ether (10 ml) was added to precipitate the product as a red powder, 0.20 g (60%).

Similar method was used to synthesize complexes below.

$[\text{PdCl} \{ \text{FcSe}(\text{CH}_2)_3\text{Te}(\text{CH}_2)_3\text{SeFc} \}](\text{PF}_6)$: Using PdCl_2 (60 mg, 0.34 mmol), TIPF_6 (120 mg, 0.326 mmol) and $\text{FcSe}(\text{CH}_2)_3\text{Te}(\text{CH}_2)_3\text{SeFc}$ (251 mg, 0.34 mmol) to yield a blue powder, 0.287 g (60%).

$[\text{PtCl} \{ \text{FcSe}(\text{CH}_2)_3\text{Te}(\text{CH}_2)_3\text{SeFc} \}](\text{PF}_6)$: Using PtCl_2 (91 mg, 0.34 mmol), TIPF_6 (118 mg, 0.34 mmol) and $\text{FcSe}(\text{CH}_2)_3\text{Te}(\text{CH}_2)_3\text{SeFc}$ (252 mg, 0.34 mmol) to yield a red powder, 0.28 g (85%).

$[\text{PdCl} \{ \text{FcTe}(\text{CH}_2)_3\text{Se}(\text{CH}_2)_3\text{TeFc} \}](\text{PF}_6)$: Using PdCl_2 (57 mg, 0.32 mmol), TIPF_6 (112 mg, 0.32 mmol) and $\text{FcTe}(\text{CH}_2)_3\text{Se}(\text{CH}_2)_3\text{TeFc}$ (250 mg, 0.32 mmol) to yield as a blue powder, 0.34 g (85%).

$[\text{PtCl} \{ \text{FcTe}(\text{CH}_2)_3\text{Se}(\text{CH}_2)_3\text{TeFc} \}](\text{PF}_6)$: Using PtCl_2 (40 mg, 0.15 mmol), TIPF_6 (53 mg, 0.15 mmol) and $\text{FcTe}(\text{CH}_2)_3\text{Se}(\text{CH}_2)_3\text{TeFc}$ (118 mg, 0.15 mmol) to yield a red powder, 0.13 g (85%).

$[\text{PdCl} \{ \text{FcTe}(\text{CH}_2)_3\text{Te}(\text{CH}_2)_3\text{TeFc} \}](\text{PF}_6)$: Using PdCl_2 (45 mg, 0.252 mmol), TIPF_6 (88 mg, 0.252 mmol) and $\text{FcTe}(\text{CH}_2)_3\text{Te}(\text{CH}_2)_3\text{TeFc}$ (211 mg, 0.252 mmol) to yield a dark blue powder, 0.198 g (80%).

$[PtCl\{FcTe(CH_2)_3Te(CH_2)_3TeFc\}](PF_6)$: Using $PtCl_2$ (51 mg, 0.192 mmol), $TIPF_6$ (67 mg, 0.192 mmol) and $FcTe(CH_2)_3Te(CH_2)_3TeFc$ (161 mg, 0.192 mmol) to yield a red powder, 0.15 g (90 %).

Spectroscopic data for the above compounds are summarised below:

$[PdCl\{FcSe(CH_2)_3Se(CH_2)_3SeFc\}]PF_6$

1H NMR (CD_3COCD_3): 4.79, 4.67 (C_5H_4 , H_{2+5} , m, 4H), 4.48, 4.46 (C_5H_4 , H_{3+4} , m, 4H), 4.37, 4.27 (C_5H_5 , s, 10H), 3.20-2.02 (CH_2 , br, 12H).

^{13}C NMR ($CDCl_3$): 76.0, 75.3 (C_5H_4 , C_{2+5}), 72.6 (C_5H_4 , C_{3+4}), 71.9 (C_5H_5), 72.2 (C_1), 33.5 ($CH_2CH_2CH_2$), 31.1 ($FcSeCH_2$), 26.4 (CH_2SeCH_2).

^{77}Se NMR (CD_3COCD_3): 227, 202.

ES MS: 835 ($[M-PF_6]^+$).

$[PtCl\{FcSe(CH_2)_3Se(CH_2)_3SeFc\}]PF_6$

1H NMR (CD_3CN): 4.99, 4.83 (C_5H_4 , H_{2+5} , m, 4H), 4.64, 4.48 (C_5H_4 , H_{3+4} , m, 4H), 4.53, 4.43 (C_5H_5 , s, 10H), 3.46 ($FcSeCH_2$, m, 4H), 3.23 (CH_2SeCH_2 , m, 4H), 2.77-2.20 ($CH_2CH_2CH_2$, br, 4H).

^{13}C NMR (CD_3CN): 74.6, 72.9, 72.5, 72.0 (C_5H_4 , C_{2+5} , C_{3+4}), 71.8, 71.7 (C_5H_5), 34.2 ($CH_2CH_2CH_2$), 30.8 ($FcSeCH_2$), 26.6, 26.4 (CH_2SeCH_2).

^{77}Se NMR (CD_3COCD_3): 220 ($^1J_{Pt-Se} = 388$ Hz), 200 ($^1J_{Pt-Se} = 268$ Hz).

ES MS: 924 ($[M-PF_6]^+$).

$[PdCl\{FcSe(CH_2)_3Te(CH_2)_3SeFc\}]PF_6$

1H NMR (CD_3CN): 4.70 (C_5H_4 , H_{2+5} , s, 4H), 4.64 (C_5H_4 , H_{3+4} , s, 4H), 4.54, 4.47 (C_5H_5 , s, 10H), 3.18, 3.02 ($FcSeCH_2$, broad, 4H), 2.93-2.81 (CH_2TeCH_2 , broad, 4H), 3.26-2.13 ($CH_2CH_2CH_2$, broad, 4H).

^{13}C NMR (CD_3CN): 73.8 (C_5H_4 , C_{2+5}), 70.1 (C_1), 71.0 (C_5H_4 , C_{3+4}), 70.3 (C_5H_5), 33.1 ($CH_2CH_2CH_2$), 25.8 ($FcSeCH_2$), 13.0 (CH_2TeCH_2).

^{77}Se NMR (CD_3CN): 195.

FAB MS: 885 ($[M-PF_6]^+$).

$[PtCl\{FcSe(CH_2)_3Te(CH_2)_3SeFc\}]PF_6$

^1H NMR (CD_3CN): 4.77 (C_5H_4 , H_{2+5} , s, 4H), 4.66 (C_5H_4 , H_{3+4} , s, 4H), 4.58, 4.49 (C_5H_5 , s, 10H), 3.29-3.23 (FcSeCH_2 , m, 4H), 3.04-2.89 (CH_2TeCH_2 , m, 4H), 2.81-2.75, 2.40-2.32 ($\text{CH}_2\text{CH}_2\text{CH}_2$, m, 4H).

^{13}C NMR (CD_3CN): 73.2 (C_5H_4 , C_{2+5}), 70.7 (C_1), 71.3, 70.9 (C_5H_4 , C_{3+4}), 70.2, 70.0 (C_5H_5), 33.8 ($\text{CH}_2\text{CH}_2\text{CH}_2$), 25.8 (FcSeCH_2), 11.0 (CH_2TeCH_2).

^{77}Se NMR (CD_3CN): 217 ($^1J_{\text{Pt-Se}} = 399$ Hz).

MALDI MS: 974 ($[\text{M-PF}_6]^+$).

$[\text{PdCl}\{\text{FcTe}(\text{CH}_2)_3\text{Se}(\text{CH}_2)_3\text{TeFc}\}]\text{PF}_6$

^1H NMR (CD_3CN): 4.73, 4.60, 4.59, 4.56 (C_5H_4 , H_{2+5} , H_{3+4} , br, 8H), 4.43, 4.42 (C_5H_5 , br, 10H), 3.03-2.70 (CH_2 , m, 4H),

^{13}C NMR (CD_3CN): 76.4, 74.1 (C_5H_4 , C_{2+5}), 71.9, 71.7 (C_5H_4 , C_{3+4}), 70.2, 70.0 (C_5H_5), 48.2 (C_1), 32.0, 31.7 ($\text{CH}_2\text{CH}_2\text{CH}_2$), 25.5 (CH_2SeCH_2), 17.0 (FcTeCH_2).

^{77}Se NMR (CD_3CN): 232, 226.

^{125}Te (CD_3CN): not resolved.

ES MS: 935 ($[\text{M-PF}_6]^+$).

$[\text{PtCl}\{\text{FcTe}(\text{CH}_2)_3\text{Se}(\text{CH}_2)_3\text{TeFc}\}]\text{PF}_6$

^1H NMR (CD_3CN): 4.82, 4.59, 4.58, 4.55 (C_5H_4 , H_{2+5} , H_{3+4} , m, 8H), 4.44, 4.43 (C_5H_5 , s, 10H), 3.07-2.83 (CH_2 , m, 12H).

^{13}C NMR (CD_3CN): 75.8, 74.0 (C_5H_4 , C_{2+5}), 72.2, 71.2 (C_5H_4 , C_{3+4}), 69.9, 69.8 (C_5H_5), 47.5 (C_1), 31.8 ($\text{CH}_2\text{CH}_2\text{CH}_2$), 25.7 (CH_2SeCH_2), 16.9 (FcTeCH_2).

^{77}Se NMR (CD_3CN): 204.4, 204.0 ($^1J_{\text{Pt-Se}} = 187$ Hz).

^{125}Te (CD_3CN): 356.7, 357.0 ($^1J_{\text{Pt-Te}} = 480$ Hz).

ES MS: 1024 ($[\text{M-PF}_6]^+$).

$[\text{PdCl}\{\text{FcTe}(\text{CH}_2)_3\text{Te}(\text{CH}_2)_3\text{TeFc}\}]\text{PF}_6$

^1H NMR (CD_3CN): 4.83, 4.64, 4.60, 4.56 (C_5H_4 , H_{2+5} , H_{3+4} , br, 8H), 4.42, 4.41 (C_5H_5 , s, 10H), 3.32 (FcTeCH_2 , br, 4H), 3.02 (CH_2TeCH_2 , m, 4H), 2.83 ($\text{CH}_2\text{CH}_2\text{CH}_2$, m, br, 4H).

^{13}C NMR (CD_3CN): 76.3, 74.0 (C_5H_4 , C_{2+5}), 71.9, 71.6 (C_5H_4 , C_{3+4}), 69.9 (C_5H_5), 40.6 (C_1), 27.0 ($\text{CH}_2\text{CH}_2\text{CH}_2$), 17.9, 17.4 (FcTeCH_2), 13.3, 14.7 (CH_2TeCH_2).

^{125}Te (CD_3CN): not resolved.

ES MS: 985 ($[\text{M-PF}_6]^+$).

$[\text{PtCl}\{\text{FcTe}(\text{CH}_2)_3\text{Te}(\text{CH}_2)_3\text{TeFc}\}]\text{PF}_6$

^1H NMR (CD_3CN): 4.78, 4.71, 4.69, 4.65 (C_5H_4 , H_{2+5} , H_{3+4} , br, 8H), 4.53, 4.51 (C_5H_5 , s, 10H), 3.21 (FcTeCH_2 , m, 4H), 2.94 (CH_2TeCH_2 , m, 4H), 2.30 ($\text{CH}_2\text{CH}_2\text{CH}_2$, br, 4H).

^{13}C NMR (CD_3CN): 75.9, 74.1 (C_5H_4 , C_{2+5}), 72.3, 71.3 (C_5H_4 , C_{3+4}), 69.9 (C_5H_5), 47.1 (C_1), 27.8, 27.0 ($\text{CH}_2\text{CH}_2\text{CH}_2$), 18.0, 17.3 (FcTeCH_2), 13.3, 13.0 (CH_2TeCH_2).

^{125}Te (CD_3CN): 369, 354 ($^1J_{\text{Pt-Te}} = 232$ Hz), 355 ($^1J_{\text{Pt-Te}} = 515$ Hz).

FAB MS: 1074 ($[\text{M-PF}_6]^+$).

7.4.5 $[\text{M}\{\text{FcE}(\text{CH}_2)_3\text{Se}(\text{CH}_2)_3\text{Se}(\text{CH}_2)_3\text{EFc}\}](\text{PF}_6)_2$ ($\text{M} = \text{Pd}$ or Pt , $\text{E} = \text{Se}$ or Te)

$[\text{Pd}\{\text{FcSe}(\text{CH}_2)_3\text{Se}(\text{CH}_2)_3\text{Se}(\text{CH}_2)_3\text{SeFc}\}](\text{PF}_6)_2$: PdCl_2 (131 mg, 0.74 mmol) was refluxed in MeCN (30 ml) for 2 h to give a yellow solution of $[\text{PdCl}_2(\text{NCMe})_2]$. After cooling, TIPF_6 (517 mg, 1.48 mmol) was added and stirring continued for another 15 min. $\text{FcSe}(\text{CH}_2)_3\text{Se}(\text{CH}_2)_3\text{Se}(\text{CH}_2)_3\text{SeFc}$ (603 mg, 0.74 mmol) in CH_2Cl_2 (5 ml) was then added, and the mixture stirred at room temperature for 24 h to give a blue liquid and a fine white precipitate of TiCl_4 . The mixture was centrifuged to remove TiCl_4 and reduced to 2 ml *in vacuo*. Diethyl ether (10 ml) was added to precipitate the product as a blue powder. Yield 0.61 g (68%). ES MS: 1067 ($[\text{M-PF}_6]^+$).

$[\text{Pt}\{\text{FcSe}(\text{CH}_2)_3\text{Se}(\text{CH}_2)_3\text{Se}(\text{CH}_2)_3\text{SeFc}\}](\text{PF}_6)_2$: PtCl_2 (110 mg, 0.41 mmol) was refluxed in MeCN (30 ml) for 2 h to give a yellow solution of $[\text{PtCl}_2(\text{NCMe})_2]$. After cooling, TIPF_6 (286 mg, 0.82 mmol) was added and stirring continued for another 15 min. $\text{FcSe}(\text{CH}_2)_3\text{Se}(\text{CH}_2)_3\text{Se}(\text{CH}_2)_3\text{SeFc}$ (335 mg, 0.41 mmol) in CH_2Cl_2 (5 ml) was then added, and the mixture stirred at room temperature for 48 h to give a

red liquid and a fine white precipitate of TlCl. The mixture was centrifuged to remove TlCl and reduced to 2 ml *in vacuo*. Diethyl ether (10 ml) was added to precipitate the product as a brick red sticky product. Yield 0.41 g (76%). ES MS: 1156 ([M-PF₆]⁺).

[Pd{FcTe(CH₂)₃Se(CH₂)₃Se(CH₂)₃TeFc}](PF₆)₂: Using PdCl₂ (62 mg, 0.35 mmol), TIPF₆ (245 mg, 0.70 mmol) and FcTe(CH₂)₃Se(CH₂)₃Se(CH₂)₃TeFc (318 mg, 0.35 mmol) to yield a blue powder. Yield 0.38 g (82%). ES MS: 1167 ([M-PF₆]⁺).

[Pt{FcTe(CH₂)₃Se(CH₂)₃Se(CH₂)₃TeFc}](PF₆)₂: Using PtCl₂ (60 mg, 0.226 mmol), TIPF₆ (158 mg, 0.45 mmol) and FcTe(CH₂)₃Se(CH₂)₃Se(CH₂)₃TeFc (205 mg, 0.226 mmol) to yield a red powder. Yield 0.22 g (68%). ES MS: 1256 ([M-PF₆]⁺).

7.4.6 [Pt₂Cl₂(FcSeCH₂C₆H₄CH₂SeFc)₃](PF₆)₂

[Pt₂Cl₂(FcSeCH₂C₆H₄CH₂SeFc)₃](PF₆)₂: PtCl₂ (62 mg, 0.23 mmol) was refluxed in MeCN (30 ml) for 2 h to give a yellow solution of [PdCl₂(NCMe)₂]. After cooling, TIPF₆ (165 mg, 0.46 mmol) was added and stirring continued for another 15 min. FcSeCH₂C₆H₄CH₂SeFc (150 mg, 0.47 mmol) in CH₂Cl₂ (5 ml) was then added, and the mixture stirred at room temperature for 48 h to give a red liquid and a fine white precipitate of TlCl. The mixture was centrifuged to remove TlCl and reduced to 2 ml *in vacuo*. Diethyl ether (10 ml) was added to precipitate the product as a red powder. Yield 0.254 g (80%). ES MS: 2507 ([M-PF₆]⁺), 1181 ([M-2PF₆]²⁺).

7.4.7 [M(difcSe₄)](PF₆)₂ (M = Pd or Pt)

[Pd(difcSe₄)](PF₆)₂: PdCl₂ (95 mg, 0.545 mmol) was refluxed in MeCN (30 ml) for 2 h to give a yellow solution of [PdCl₂(NCMe)₂]. After cooling, TIPF₆ (380 mg, 1.09 mmol) was added and stirring continued for another 15 min. difcSe₄ (420 mg, 0.545 mmol) in CH₂Cl₂ (5 ml) was then added, and the mixture stirred at room temperature for 24 h to give a purple blue liquid and a fine white precipitate of TlCl. The mixture was centrifuged to remove TlCl and reduced to 2 ml *in vacuo*. Diethyl ether (10 ml) was added to precipitate the product as a blue powder, 0.55 g (88%). Spectroscopic data are summarised below:

$^1\text{H NMR (CD}_3\text{COCD}_3\text{)}$: 5.41, 4.80, 4.60 (C_5H_4 , H_{2+5} , H_{3+4} , d, 16H), 3.93-2.57 (CH_2 , m, br, 12H).

$^{13}\text{C NMR (CD}_3\text{COCD}_3\text{)}$: 79.8, 79.4, 77.3, 76.4, 76.0, 75.8, 72.7, 72.5 (C_5H_4 , C_{2+5} , C_{3+4}), 66.5 (C_1), 36.7, 36.4 (SeCH_2), 27.2, 26.2 ($\text{CH}_2\text{CH}_2\text{CH}_2$).

$^{77}\text{Se NMR (CD}_3\text{COCD}_3\text{)}$: 292 (weak), 261 (strong).

ES MS: 1023 ($[\text{M-PF}_6]^+$).

$[\text{Pt}(\text{difcSe}_4)](\text{PF}_6)_2$: PtCl_2 (124 mg, 0.468 mmol) was refluxed in MeCN (30 ml) for 2 h to give a yellow solution of $[\text{PtCl}_2(\text{NCMe})_2]$. After cooling, TIPF_6 (328 mg, 0.936 mmol) was added and stirring continued for another 15 min. difcSe_4 (360 mg, 0.468 mmol) in CH_2Cl_2 (5 ml) was then added, and the mixture stirred at room temperature for 48 h to give a purple blue liquid and a fine white precipitate of TlCl . The mixture was centrifuged to remove TlCl and reduced to 2 ml *in vacuo*. Diethyl ether (10 ml) was added to precipitate the product as a pale red powder, 0.446 g (76%). Spectroscopic data are summarised below:

$^1\text{H NMR (CD}_3\text{COCD}_3\text{)}$: 5.47, 5.20, 4.92, 4.61 (C_5H_4 , H_{2+5} , H_{3+4} , d, 16H), 3.69-2.47 (CH_2 , m, br, 12H),

$^{13}\text{C NMR (CD}_3\text{COCD}_3\text{)}$: 77.3, 76.8, 75.5, 74.4, 74.1, 73.7, 71.8, 71.6 (C_5H_4 , C_{2+5} , C_{3+4}), 68.3 (C_1), 34.5, 34.0 (SeCH_2), 27.5, 27.3 ($\text{CH}_2\text{CH}_2\text{CH}_2$).

$^{77}\text{Se NMR (CD}_3\text{COCD}_3\text{)}$: 264 (weak), 242 (strong, $^1J_{\text{Pt-Se}} = 300 \text{ Hz}$).

ES MS: 1112 ($[\text{M-PF}_6]^+$).

7.4.8 $[\text{M}(\text{fcSe}_4)](\text{PF}_6)_2$

$[\text{Pd}(\text{fcSe}_4)](\text{PF}_6)_2$: Similar to $[\text{Pd}(\text{difcSe}_4)](\text{PF}_6)_2$, using PdCl_2 (104 mg, 0.59 mmol), TIPF_6 (412 mg, 1.18 mmol) and fcSe_4 (368 mg, 0.59 mmol) in CH_2Cl_2 (5 ml) to yield a blue powder, 0.36 g (60%). Spectroscopic data are summarised below:

$^1\text{H NMR (CD}_3\text{COCD}_3\text{)}$: 5.31, 5.20, 4.80, 4.60 (C_5H_4 , H_{2+5} , H_{3+4} , s, 4H), 3.56-2.46 (CH_2 , m, br, 18H).

$^{13}\text{C NMR (CD}_3\text{COCD}_3\text{)}$: 78.9, 77.9, 75.4, 72.7 (C_5H_4 , C_{2+5} , C_{3+4}), 74.2 (C_1), 36.1 ($\text{SeCH}_2\text{CH}_2\text{CH}_2\text{Se}$), 35.4 ($\text{FcSeCH}_2\text{CH}_2\text{CH}_2\text{Se}$), 30.0, 29.4, 26.2 (SeCH_2).

^{77}Se NMR (CD_3COCD_3): 256 (weak), 219 (weak), 215, 186.

ES MS: 881 ($[\text{M-PF}_6]^+$), 368 ($[\text{M-2PF}_6]^{2+}$).

$[\text{Pt}\{\text{fcSe}_4\}](\text{PF}_6)_2$: Similar to $[\text{Pt}(\text{difcSe}_4)](\text{PF}_6)_2$, using PtCl_2 (74 mg, 0.28 mmol), TlPF_6 (196 mg, 0.56 mmol) and fcSe_4 (176 mg, 0.28 mmol) in CH_2Cl_2 (5 ml) to yield a red powder, 0.186 g (63%). ^1H , ^{13}C and ^{77}Se NMR spectra are shown in Figs. 7.5-7.8 and spectroscopic data are summarised below:

^1H NMR (CD_3COCD_3): 5.31, 5.15, 4.83, 4.61 (C_5H_4 , H_{2+5} , H_{3+4} , s, 4H), 3.65-2.50 (CH_2 , m, br, 18H).

^{13}C NMR (CD_3COCD_3): 76.6, 75.7, 73.4, 71.5 (C_5H_4 , C_{2+5} , C_{3+4}), 68.4, 65.0 (C_1), 34.5, 34.0 ($\text{SeCH}_2\text{CH}_2\text{CH}_2\text{Se}$), 33.7, 32.6 ($\text{FcSeCH}_2\text{CH}_2\text{CH}_2\text{Se}$), 27.9, 26.1, 24.8 (SeCH_2).

^{77}Se NMR (CD_3COCD_3): 236 (weak, $^1J_{\text{Pt-Se}} = 348$ Hz), 215 ($^1J_{\text{Pt-Se}} = 388$ Hz), 194 (weak, $^1J_{\text{Pt-Se}} = 116$ Hz), 170 ($^1J_{\text{Pt-Se}} = 55$ Hz)

ES MS: 970 ($[\text{M-PF}_6]^+$).

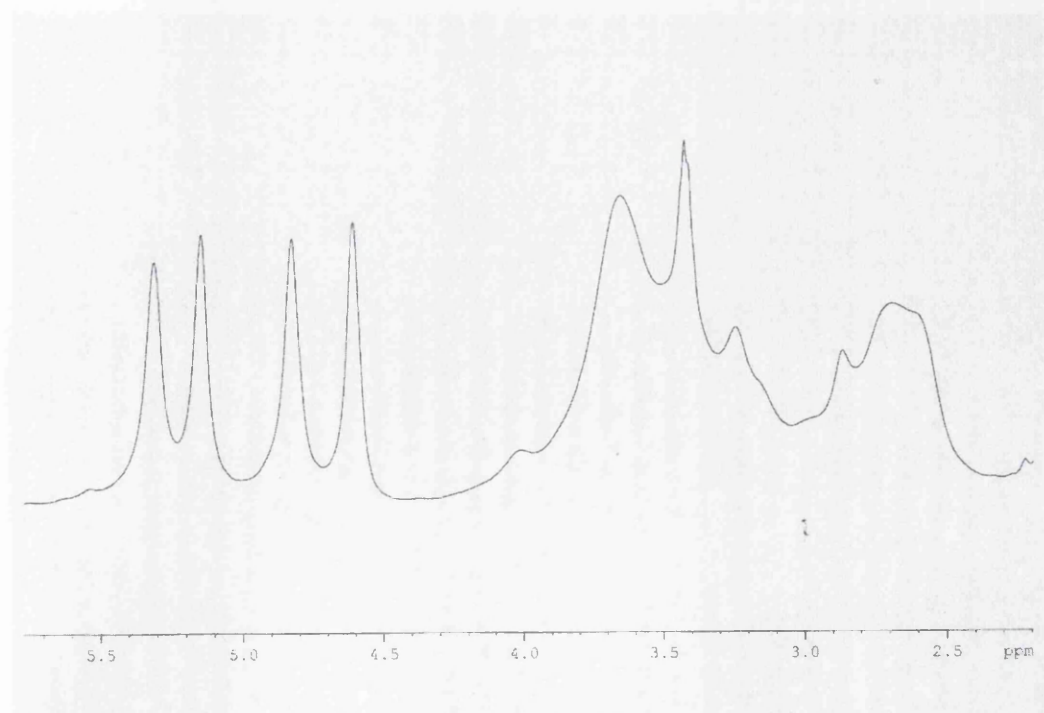


Fig. 7.5 ^1H NMR spectrum of $[\text{Pt}\{\text{fcSe}_4\}](\text{PF}_6)_2$ in CD_3COCD_3 solution

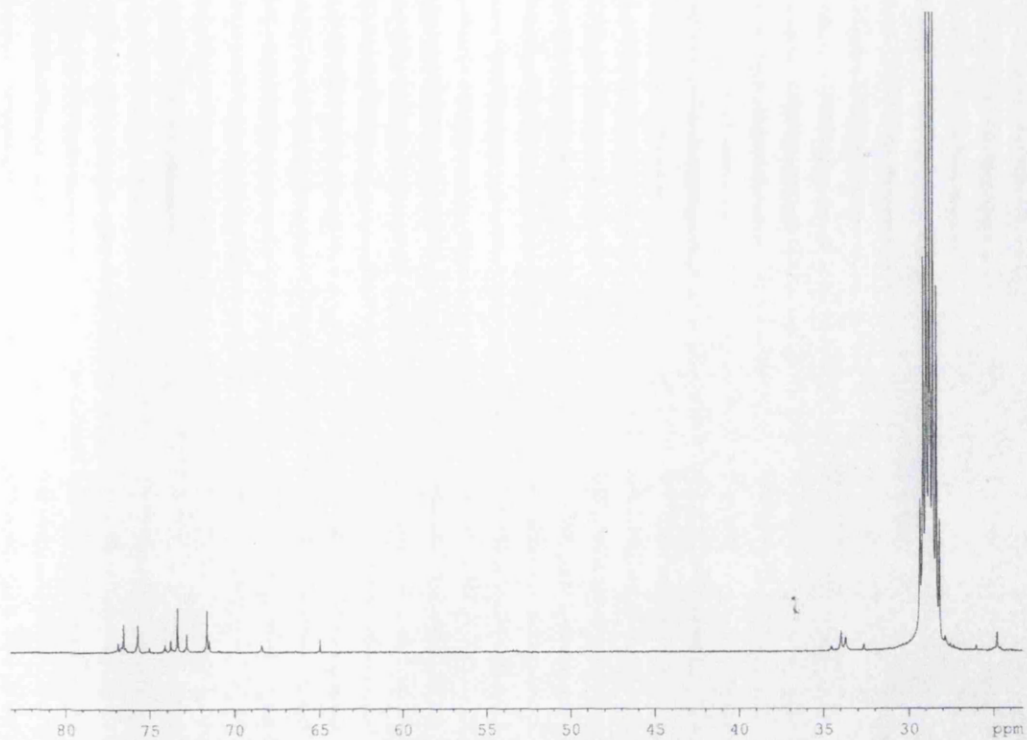


Fig. 7.6 ^{13}C NMR spectrum of $[\text{Pt}\{\text{fcSe}_4\}](\text{PF}_6)_2$ in CD_3COCD_3 solution

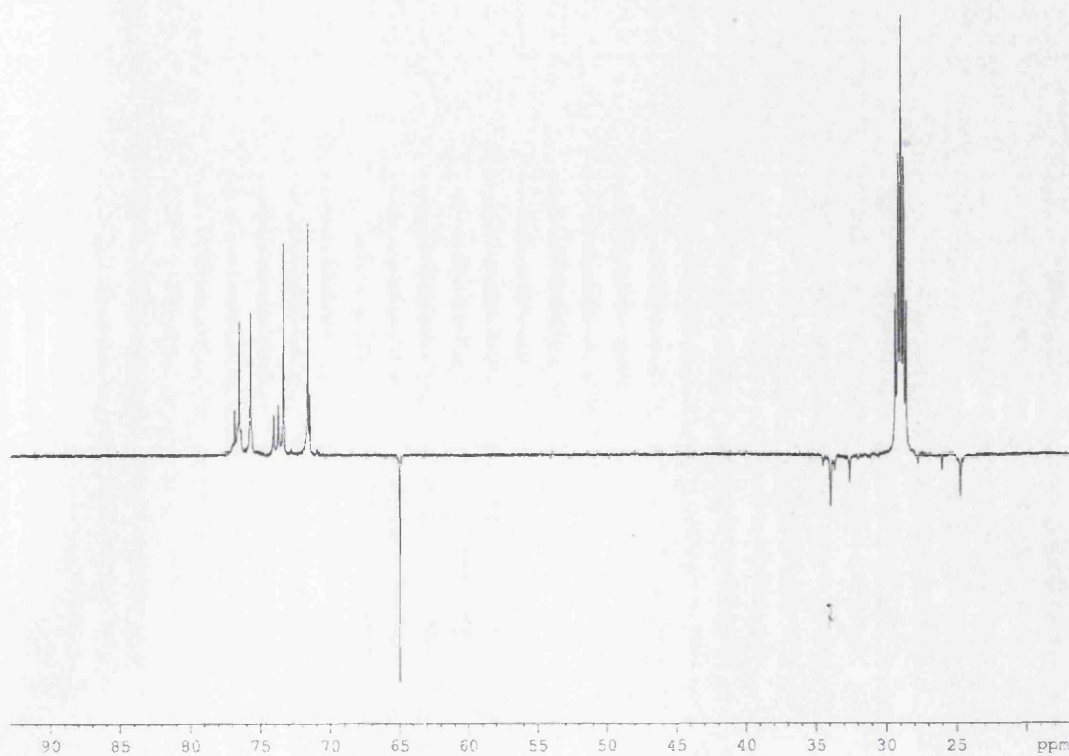


Fig. 7.7 ^{13}C DEPT NMR spectrum of $[\text{Pt}\{\text{fcSe}_4\}](\text{PF}_6)_2$ in CD_3COCD_3 solution

7.5 Rhodium complexes

$[RhCl_2\{FcSe(CH_2)_3SeFc\}_2]PF_6$: $RhCl_3 \cdot 3H_2O$ (21 mg, 0.105 mmol) and $FcSe(CH_2)_3SeFc$ (121 mg, 0.2 mmol) in ethanol (30 ml) were refluxed for 1 h; KPF_6 (24 mg, 0.13 mmol) was then added and the mixture stirred at room temperature for another 1 h. The dark red precipitate was collected and washed with diethyl ether. Yield: 90 mg (58%). ES MS: 1317 ($[M-PF_6]^+$).

$[RhCl_2\{FcTe(CH_2)_3TeFc\}_2]PF_6$ was prepared similarly: Using $RhCl_3 \cdot 3H_2O$ (45 mg, 0.217 mmol), $FcTe(CH_2)_3TeFc$ (290 mg, 0.435 mmol) and KPF_6 (74 mg, 0.4 mmol) to yield the dark red precipitate. Yield: 200 mg (56%). ES MS: 1497 ($[M-PF_6]^+$).

$[RhCl_2\{FcSe(CH_2)_3TeFc\}_2]PF_6$: was prepared similarly: Using $RhCl_3 \cdot 3H_2O$ (20 mg, 0.197 mmol), $FcSe(CH_2)_3TeFc$ (122 mg, 0.394 mmol) and KPF_6 (36.8 mg, 0.20 mmol) to yield the dark red precipitate. Yield: 139 mg (50%). ES MS: 1407 ($[M-PF_6]^+$).

$[RhCl_2\{FcSe(CH_2)_2SeFc\}_2]PF_6$: Using $RhCl_3 \cdot 3H_2O$ (36 mg, 0.17 mmol), $FcSe(CH_2)_2SeFc$ (187 mg, 0.34 mmol) and KPF_6 (63 mg, 0.34 mmol) to yield the purple precipitate. Yield: 145 mg (60%). ES MS: 1289 ($[M-PF_6]^+$).

$[RhCl_2\{FcSeCH_2SeFc\}_2]PF_6$ was synthesized similarly: Using $RhCl_3 \cdot 3H_2O$ (63 mg, 0.30 mmol), $FcSeCH_2SeFc$ (163 mg, 0.30 mmol) and KPF_6 (65 mg, 0.35 mmol) to yield the purple precipitate. Yield 0.264 g (70%). MALDI MS: 1261 ($[M-PF_6]^+$).

$[RhCl_2\{FcTeCH_2TeFc\}_2]PF_6$ was synthesized similarly: Using $RhCl_3 \cdot 3H_2O$ (21 mg, 0.10 mmol), $FcTeCH_2TeFc$ (64 mg, 0.10 mmol) and KPF_6 (21 mg, 0.10 mmol) to yield the purple precipitate. Yield 91 mg (63%). ES MS: 1351 ($[M-PF_6]^+$).

$[RhCl_2\{MeC(CH_2SeFc)_3\}_2]PF_6$: $RhCl_3 \cdot 3H_2O$ (27 mg, 0.13 mmol) and $MeC(CH_2SeFc)_3$ (224 mg, 0.26 mmol) in ethanol (30 ml) were refluxed for 1 h. Addition of KPF_6 (93 mg, 0.5 mmol) gave a dark purple precipitate, which was collected by filtration and washed by diethyl ether. Yield: 133 mg (50%). ES MS: 1901 ($[M-PF_6]^+$).

$[RhCl_2\{MeC(CH_2TeFc)_3\}_2](PF_6)$: $RhCl_3 \cdot 3H_2O$ (17 mg, 0.08 mmol) and $MeC(CH_2TeFc)_3$ (161 mg, 0.16 mmol) in ethanol (30 ml) were refluxed for 1 h. Addition of KPF_6 (20 mg, 0.11 mmol) gave a dark purple precipitate, which was collected by filtration and washed by diethyl ether. Yield: 157 mg (84%). ES MS: 2171 ($[M-PF_6]^+$).

7.6 Other attempted reactions

Attempted reaction of [Cu(NCMe)₄](PF₆) and FcSe(CH₂)₃SeFc: [Cu(MeCN)₄](PF₆) (0.079 g, 0.212 mmol) and FcSe(CH₂)₃SeFc (0.241 g, 0.423 mmol) were added to dry CH₂Cl₂ (30 ml). The solution was refluxed for 1 h and allowed to cool to room temperature. The mixture was reduced to 5 ml *in vacuo*, then diethyl ether (10 ml) was added to precipitate the product as a yellow powder. Yield: 0.38 g.

Attempted reaction of [Cu(NCMe)₄](PF₆) and FcTe(CH₂)₃TeFc: [Cu(NCMe)₄](PF₆) (0.084 g, 0.225 mmol) and FcTe(CH₂)₃TeFc (0.3 g, 0.45 mmol) were added to dry CH₂Cl₂ (30 ml). The solution was refluxed for 1 h and allowed to cool to room temperature. The mixture was reduced to 5 ml *in vacuo*, then diethyl ether (10 ml) was added to precipitate the product as a yellow powder. Yield: 0.24 g.

Attempted reaction of [Mo(CO)₃(NCMe)₃] and MeC(CH₂TeFc)₃: Mo(CO)₆ (0.05 g, 0.19 mmol) was added to dry degassed MeCN (30 ml) and the mixture was refluxed for 18 h to give [Mo(CO)₃(NCMe)₃]. The ligand MeC(CH₂TeFc)₃ (0.20 g, 0.2 mmol) was added and the mixture stirred under nitrogen for a further 20 h. The solvent was removed by evaporation under reduced pressure. The residue was dissolved in CH₂Cl₂ (5 ml), filtered and cold hexane added to yield a brown powder. The powder was collected, washed with cold hexane and dried under vacuum. Yield: 0.71 g (30%). MALDI MS: 1179 ([M]⁺). IR(ν (CO)): 1921, 1817 cm⁻¹.

Attempted reaction of [Mo(CO)₃(NCMe)₃] and MeC(CH₂SeFc)₃: Mo(CO)₆ (0.04 g, 0.15 mmol) was added to dry degassed MeCN (30 ml) and the mixture was refluxed for 18 h to give [Mo(CO)₃(NCMe)₃]. The ligand MeC(CH₂SeFc)₃ (0.13 g, 0.15 mmol) was added and the mixture stirred under nitrogen for a further 20 h. The solvent was removed by evaporation under reduced pressure. The residue was dissolved in CH₂Cl₂ (5 ml), filtered and cold hexane added to yield a brown powder with low yield.

Attempted reaction of [Mo(CO)₃(NCMe)₃] and FcSe(CH₂)₃Te(CH₂)₃SeFc: Mo(CO)₆ (0.089 g, 0.34 mmol) was added to dry degassed MeCN (30 ml) and the mixture was refluxed for 18 h to give [Mo(CO)₃(NCMe)₃]. The ligand FcSe(CH₂)₃Te(CH₂)₃SeFc

(0.25 g, 0.34 mmol) was added and the mixture stirred under nitrogen for a further 20 h. The solvent was removed by evaporation under reduced pressure. The residue was dissolved in CH₂Cl₂ (5 ml), filtered and cold hexane added to yield a brown powder. The powder was collected, washed with cold hexane and dried under vacuum with low yield

Attempted reaction of HgI₂ and FcSe(CH₂)₃SeFc: HgI₂ (0.114 g, 0.25 mmol) in acetone (20 ml) was added into FcSe(CH₂)₃SeFc (0.143 g, 0.25 mmol) in dry CHCl₃ (10 ml). The solution was refluxed for 24 h and allowed to cool to room temperature. The mixture was reduced to 5 ml *in vacuo*, the diethyl ether (10 ml) was added to precipitate a yellow powder. NMR spectrometry revealed the product to be free ligand.

Attempted reaction of HgCl₂ and FcSe(CH₂)₃SeFc: HgCl₂ (0.068 g, 0.25 mmol) in acetone (20 ml) was added into FcSe(CH₂)₃SeFc (0.143 g, 0.25 mmol) in dry CHCl₃ (10 ml). The solution was refluxed for 24h and cooled to room temperature. The mixture was reduced to 5 ml *in vacuo*, then diethyl ether (10 ml) was added to precipitate a yellow powder. NMR spectrometry revealed the product to be free ligand.

Attempted reaction of AgNO₃ and MeC(CH₂TeFc)₃: A solution of AgNO₃ (0.014 g, 0.08 mmol) in methanol/MeCN (2:1) (15 ml) was added to the solution of MeC(CH₂TeFc)₃ (0.08 g, 0.08 mmol) in dichloromethane (5 ml). Diethyl ether vapour was allowed to diffuse into the solvent to yield yellow crystals. ES mass spectrometry suggested that the product to be [Ag{MeC(CH₂TeFc)₃}₂]NO₃. ES MS: 2135 ([M]⁺).

Attempted reaction of [RhCl(COD)]₂ and MeC(CH₂SeFc)₃: [RhCl(COD)]₂ (43 mg, 0.086 mmol) was added to MeC(CH₂SeFc)₃ (148 mg, 0.172 mol) and KPF₆ (35 mg, 0.18 mmol) in CH₂Cl₂ (30 ml) and the mixture stirred at room temperature for 1 hour. The precipitated KCl was removed by filtration, the solvent volume reduced to 2 ml *in vacuo* and diethyl ether added (10 ml) to give a dark red precipitate in quite low yield.

*Attempted reaction of [RhCl(COD)]₂ and MeC(CH₂TeFc)₃: [RhCl(COD)]₂ (55 mg, 0.11 mmol) was added to MeC(CH₂TeFc)₃ (222 mg, 0.22 mol) and KPF₆ (44 mg, 0.24 mmol) in CH₂Cl₂ (30 ml) and the mixture stirred at room temperature for 1 hour. The precipitated KCl was removed by filtration, the solvent volume reduced to 2 ml *in vacuo* and diethyl ether added (10 ml) to give a dark red product with yield 0.236 g. MALDI mass spectrometry suggested that the product was [Rh(COD){MeC(CH₂TeFc)₃}(PF₆). MALDI MS: 1225 ([M]⁺).*

*Attempted reaction of [Pd₂(NCMe)₆](PF₆)₂ and FcSe(CH₂)₃Te(CH₂)₃SeFc: A dichloromethane solution (10 ml) of FcSe(CH₂)₃Te(CH₂)₃SeFc (284 mg, 0.38 mmol) was added to an acetonitrile solution (10 ml) of [Pd₂(NCMe)₆](PF₆)₂ (562 mg, 0.76 mmol). The mixture was stirred at room temperature for 24 h. The solvent volume was reduced to 2 ml *in vacuo* and diethyl ether added (10 ml) to give a dark purple product with yield 0.423 g. ES mass spectrometry a cluster of peaks at 973 and the presence of PF₆⁻.*

*Attempted reaction of Fc₂Te₂ and [W(CO)₅(THF)]: Addition of Fc₂Te₂ (180 mg, 0.29 mmol) to a solution of [W(CO)₅(THF)] (209 mg, 0.58 mmol) in THF (50 ml) at room temperature led immediately to a deepening of the colour from orange to dark red. After stirring overnight, the solution was reduced to dryness by evaporation of the solvent under reduced pressure, and the residue then extracted with hexane/toluene (1:1). The solution was filtered to remove a sticky black insoluble residue, and the solvent removed *in vacuo*. ES mass spectrometry suggested that the product was a mixture.*

7.7 References for Chapter Seven

1. G. M. Sheldrick, *SADABS, Program for Empirical Absorption Corrections*, University of Göttingen, Germany, 1986
2. A. Altomare, M. C. Burla, M. Camalli, G. Cascarano, C. Giacovazzo, A. Guagliardi, A. G. Moliterni, G. Polidori and R. Spagna, *J. Appl. Crystallogr.*, 1999, **32**, 115
3. G. M. Sheldrick, *SHELXL97, Program for Crystal Structure Refinement*, University of Göttingen, Göttingen, Germany, 1986
4. L. J. Farrugia, *J. Appl. Crystallogr.*, 1999, **32**, 837
5. M. Herberhold, P. Leitner, *J. Organomet. Chem.*, 1987, **336**, 153
6. G. Mugesh, A. Panda, H. B. Singh, N. S. Punekar, R. J. Butcher, *J. Am. Chem. Soc.*, 2001, **123**, 839
7. R. Broussier, A. Abdulla, B. Gautheron, *J. Organomet. Chem.*, 1987, **332**, 165
8. W. V. E. Doering, L. K. Levy, *J. Am. Chem. Soc.*, 1955, **77**, 509
9. C. M. Goldman, M. M. Olmstead, P. K. Mascharak, *Inorg. Chem.*, 1996, **35**, 2752
10. J. J. Eisch, R. B. King, *Organomet. Syn.*, 1965, **1**, 122
11. G. R. Dobson, G. C. Faber, *Inorg. Chim. Acta*, 1970, **4**, 87
12. R. J. Angelici, *Inorg. Synth.*, 1990, **28**, 60
13. R. J. Angelici, *Inorg. Synth.*, 1990, **28**, 68
14. G. Giodano and R. H. Crabtree, *Inorg. Synth.*, 1979, **19**, 218
15. D. J. Doonan, A. L. Balch, S. Z. Goldberg, R. Eisenberg, and J. S. Miller, *J. Am. Chem. Soc.*, 1975, **97**, 1961.
16. W. Strohmeier, F. J. Muller, *Chem. Ber.*, 1969, **102**, 3608